CARBON BIOGEOCHEMISTRY OF THE EASTERN BERING SEA SHELF

By

Jessica N. Cross

RECOMMENDED:

Dr. Richard Feely

Dr. Dean Stockwell

Dr. Thomas Weingartner

Dr. Terry Whitledge

Dr. Jeremy Mathis, Advisory Committee Chair

Dr. Brenda Konar
Head, Program, Marine Science and Limnology

APPROVED:

Dr. Michael Castellini
Dean, School of Fisheries and Ocean Sciences

Dr. John C. Eichelberger
Dean of the Graduate School

20 December 2013
Date

CARBON BIOGEOCHEMISTRY OF THE EASTERN BERING SEA SHELF

A

DISSERTATION

Presented to the Faculty

of the University of Alaska Fairbanks

in Partial Fulfillment of the Requirements

for the Degree of

DOCTOR OF PHILOSOPHY

By

Jessica N. Cross, B.S.

Fairbanks, Alaska

December 2013

Abstract

The uptake of anthropogenic carbon dioxide (CO_2) has caused perturbations to marine biogeochemistry in recent years, including decreasing ocean pH and carbonate mineral saturation states (Ω). Collectively termed ocean acidification (OA), these conditions hinder the growth of calcium carbonate shells and effectively reduce habitat for some marine calcifiers. Given that the Bering Sea is one of the world's most productive marine ecosystems and supports both commercial fishing industries and subsistence communities, it is integral to understand its susceptibility to OA.

Here, new observations of the organic and inorganic carbon systems are used to identify mechanisms leading to CO_2 accumulation and sub-regional enhancement of vulnerability to OA processes. Chapter 1 describes the state of knowledge of OA in this area, highlighting two regions where low Ω conditions are consistently observed: near the coast, and over the northern shelf. Chapter 2 describes net heterotrophic processes near the coast, in conjunction with low bottom water Ω. Chapter 3 examines this heterotrophy in more detail, showing that focused deposition of organic matter and its subsequent respiration. Chapters 4 and 5 focus on very low Ω values observed over the northern shelf. In combination with natural respiration processes, anthropogenic CO_2 was shown to cause low Ω and seasonal dissolution of carbonate minerals in Chapter 4. Chapter 5 illustrates how sea ice cover inhibits the flux of CO_2 from the surface ocean to the atmosphere, which raises the inventory of CO_2 in the water column.

These results are synthesized in Chapter 6. Low-Ω conditions and areas of carbonate mineral dissolution will continue to expand as anthropogenic CO_2 accumulates in shelf waters in the coming decades, further reducing viable habitat for key calcifiers. Model projections of future surface water conditions indicate that average Ω over the Bering Sea shelf will drop below the observed natural variability by 2100, with average conditions favoring carbonate mineral dissolution in surface waters by 2150. Presently, episodic events will cause regions of the Bering Sea to be undersaturated in Ω, which could have significant and cascading impacts throughout the Pacific-Arctic region.

Table of Contents

Page

Page

Page

List of Figures

Page

Page

List of Tables

Page

List of Appendices

Acknowledgements

"A single brain cell has no intelligence, but in company it can do extraordinary things."

--Jasper Fforde

During the development of this dissertation, it was my very good fortune to have good company. Between 2007 and 2012, the joint support of the National Science Foundation (NSF) and the North Pacific Research Board (NPRB) permitted wide-ranging collaborative research from over ninety different institutions through the Bering Sea Project. The opportunity to engage and experience the broad diversity of skills provided by the investigators in this program was a unique advantage for me as a student. I was strongly encouraged to envision how my detailed work might fit into a broader concept: a better understanding of the structure and function of the Bering Sea ecosystem, and the potential impacts of future changes. By emphasizing the value of diverse scientific interests, encouraging collaboration, and including an often-neglected human element in the project, the Bering Sea Project has shaped the way that I think about science. I thank both the leadership of NSF and NPRB and the Bering Sea Project Science Advisory Board for bringing this program to fruition. Specifically, I'm grateful for the supplementary funding provided by the U.S. Bureau of Ocean and Energy Management and Regulation, Alaska OCS Region and the Coastal Marine Institute at the University of Alaska Fairbanks that enabled my participation in this program.

My experience was greatly aided by numerous principle investigators in the project, many of whom appear as coauthors on the manuscripts contained in this volume. Drs. Carin Ashjian, Jackie Grebmeier, Carol Ladd, Mike Lomas, Brad Moran, Calvin Mordy, Dave Shull, and Phyllis Stabeno were all valuable teachers. I also gained a wealth of knowledge both in and out of the field from their technical staff, namely Ned Cokelet, Bill Floering, Nancy and Dave Kachel, Pat Kelley, Fred Menzia, Brandi Murphy, Dan Naber, and Eric Wisegarver. It was also a pleasure to engage with other graduate students during the project, and work closely with Matt Baumann and Maggie Esch. Maggie, no cruise is ever as much fun without you.

I'm also grateful for my numerous instructors at the University of Alaska Fairbanks, particularly for their patience with a chemist with next to no earth science knowledge but a demanding enthusiasm. Drs. Mark Johnson, Harper Simmons, and Ana Aguilar-Islas taught inspiring and indispensible courses after which I hope to model my own. I thank them for taking the time to teach well. I also found many willing teachers outside the community, including Drs. Nicholas Bates, Karen Frey, and Robert Byrne. Thank you for your willingness to work with early career scientists.

I would be capable of so much less if it were not for the exacting standards set by my advisory committee. Through Drs. Richard Feely, Dean Stockwell, Tom Weingartner and Terry Whitledge, I learned to see the innovation and creativity that developed our field and that is ultimately requisite for new progress. I thank each of them for their passion and encouragement.

Ultimately, I owe my greatest debt of gratitude to my advisory committee chair, Dr. Jeremy Mathis, whose support has been an incalculable privilege. His driving motivation afforded me opportunities to travel, speak, network, and collaborate. The team he assembled during my tenure in his lab—Kristen Shake, Stacey Reisdorph, Natalie Monacci, Dan Naber, and Dr. Wiley Evans—taught me the value of diverse scientific perspectives. Most of all, his commitment to serve his community, state, and country according to his greatest skill unequivocally demonstrated the value of scientific enquiry as human capital. I was willfully stubborn about it—I really wanted to believe in the ivory tower—but his insistent example has proven to me that the analytical mind is a national asset, and its value is determined by public service. There is a deserving world outside of academia. It is much more rewarding to engage it than not.

Jeremy, Tom, Terry, Dean, and Dick: through your example, I know more about science, leadership, and the pursuit of excellence than I can envision having learned on my own these past six years. The only way I can hope to repay you is through good stewardship of the education and skills you have leant to me.

Lastly, I thank my friends and family for their patient support through this endeavor. They variously and tirelessly talked me out of being frustrated and into creative

problem solving; into working through the weekends, but occasionally taking a day off; they fueled my enthusiasm and built my confidence. Most importantly, I learned from you to always remember that work is not only a privilege, but also a personal and social responsibility. I am proud to represent our family as our first female Ph.D.

Chapter 1:
Introduction

The southeastern Bering Sea shelf is one of the world's most highly productive marine ecosystems, supporting a diverse food web and nearly half of the annual U.S. fish landings. Because of the ecological and economic importance of the Bering Sea fisheries, several large-scale, interdisciplinary scientific research programs have studied the region in the past several decades, placing a particular emphasis on understanding mechanisms that influence patterns in upper trophic level productivity (McRoy et al., 1986; O'Connor et al., 1992; McRoy, 1993; Macklin, 1999; Stabeno and Hunt, 2002; Wiese et al., 2012; Harvey and Sigler, 2013). These successful efforts have employed what has become known as an ecosystem approach, which emphasizes coordinated study of regional physical, chemical, and ecological variability. These multidisciplinary programs have enabled the development of a detailed portrait of the regional biogeochemistry in the context of the local physical processes and biological communities.

The first systematic review of the Bering Sea carbon system synthesized several international data sets spanning the entire Bering Sea basin and associated North Pacific (Park et al., 1974). Taken together, these studies hinted at several driving mechanisms controlling large observed variability in carbon system parameters and influencing energy flow to upper trophic levels, including physical circulation processes (e.g., upwelling; eddy propagation; vertical overturning), seasonal variations in temperature and sea ice extent, and the biological pump. Following this effort, a commercially valuable species shift favoring large populations of walleye pollock prompted an interdisciplinary, multi-institutional international effort to understand the underpinnings of commercial fisheries, and to understand and manage potential future changes. The Processes and Resources of the Bering Sea Shelf (PROBES) Program significantly advanced the hydrographic and ecosystem understanding of the area, resulting in the classification of sub-regional spatial

domains (Coachman, 1986), each with differing characteristics in carbon cycle dynamics (Walsh and McRoy, 1986).

Subsequent studies like the Outer Continental Shelf Environmental Assessment Program (OCSEAP), the Inner Shelf Transfer and Recycling (ISHTAR) Program, Fisheries Oceanography Coordinated Investigations (FOCI), the Inner Front Program (IFP), and Southeastern Bering Sea Carrying Capacity (SEBSCC) Program expanded on the ideas developed during PROBES and have resulted in various confirmations and spatiotemporal refinement of the carbon cycle drivers hypothesized by Park et al. (1974). However, fundamental questions concerning the cycling of carbon in light of global environmental change remain. Most recently, the Bering Ecosystem Study (BEST) and Bering Sea Integrated Ecosystem Research Program (BSIERP) were jointly initiated in order to investigate the potential ecosystem perturbations that may result from global environmental change processes. The oceanic uptake of anthropogenic carbon dioxide (CO_2) in recent times has been shown to cause systematic perturbations to marine biogeochemistry, including reductions in pH and saturation states (Ω) of important biogenic carbonate minerals (e.g., Sabine et al., 2004; Orr et al., 2005; Sabine and Feely, 2007; Doney et al., 2009; Feely et al., 2009; Byrne et al., 2010). This process, termed ocean acidification (OA), reduces the suitable habitat for some marine calcifiers, and may have profound negative implications for the associated food webs (Buddemeier et al., 2004; Cooley et al., 2006; Fabry et al., 2008; Kuffner et al., 2008; Doney et al., 2009). Of particular concern is that these changes could cause some ecosystems to shift to a less economically viable state (Cooley and Doney, 2009; Branch et al., 2012; Cooley et al., 2012; Narita et al., 2012).

In Arctic and sub-Arctic areas, mixing processes and colder temperatures precondition the water column to have naturally lower pH and higher CO_2 concentrations than more temperate areas of the global ocean, indicating a stronger vulnerability to acidification processes. These conditions can be further exacerbated by the activity of the biological community through the Phytoplankton-Carbonate Saturation State (PhyCaSS) interaction. High rates of phytoplankton primary production facilitate substantial uptake

of CO_2 in surface waters, increasing Ω at the surface. However, the efficient vertical export and subsequent remineralization of this organic carbon causes CO_2 to accumulate in bottom waters, causing a divergent, decreasing trajectory in bottom water saturation states, and amplifying the effects of existing ocean acidification (Bates and Mathis, 2009).

Strong vertical fluxes of inorganic carbon in shallow shelf waters typical of the PhyCaSS interaction were identified on the southeastern Bering Sea shelf during early work (Park et al., 1974) and refined during the PROBES Program (Codispoti et al., 1982, 1986). The resulting regional vulnerability to OA processes was initially investigated by OCSEAP (Chen, 1993). These studies indicated that the Bering Sea shelf exhibits both strong preconditioning of pH and saturation states and intense primary production, indicating a high regional susceptibility to OA processes, although no shallow-water undersaturations ($\Omega < 1$) of carbonate minerals were observed (some undersaturations were evident in deeper waters off the shelf). Recent observations in this area have shown that seasonal carbonate mineral undersaturations have since developed (Mathis et al., 2011; Appendix A). While the ultimate appearance of these undersaturations were linked to net accumulation anthropogenic CO_2, the intensity and spatial variability of these conditions were strongly influenced by the regional buildup of CO_2 in bottom waters resulting from respiration processes (Mathis et al., 2011; Appendix A).

In the Bering Sea, several processes can influence the intensity of the respiration signal and the natural accumulation of CO_2 in bottom waters in addition to local production and PhyCaSS processes. Focused deposition of organic matter or respiration products generated during a bloom at a different location or contributed from another source, such as the region's two large river systems, may also increase the respiration signal in a given area. Additionally, the hydrographic structure of the Bering Sea shelf may create localized conditions more favorable for the retention of the respiration reaction products, facilitating the seasonal accumulation of CO_2 and the suppression of carbonate mineral saturation states.

Freshwater runoff in the Bering Sea is mainly contributed by two sources: the Yukon and Kuskokwim Rivers (Lisitsyn, 1969). The Yukon River Basin alone transports nearly 60 million tons of suspended sediments into the Bering Sea with ~200 km^3 water annually (Brabets et al., 2000; Striegl et al., 2005). Given the location of the river mouth, this substantial volume of discharge primarily affects the northern Bering Sea. However, recent work suggests that wind-driven transport can cause the advection of Yukon River water both to the south and west of the delta (Danielson et al., 2012).

In the Yukon River, concentrations of organic carbon are highest during spring, coinciding with peak river discharge. However, nearly all of the organic carbon that reaches the coastal margin is non-labile, a typical characteristic of many large drainage basins e.g., (Fernandes and Sicre, 2000; Dittmar and Kattner, 2003). It is therefore unlikely that Yukon River organic matter is remineralized in the Bering Sea. By contrast, Yukon River concentrations of CO_2 are relatively high in winter, resulting from the accumulation of respiration products generated during slower downstream transport (Park et al., 1974; Striegl et al., 2007). The contribution of these respiration products could affect CO_2 accumulation over the Bering Sea shelf, at least during this season. The spring freshet dilutes these concentrations, and most Yukon River discharge exhibits lower DIC concentrations than those typical of the coastal regions, acting instead to dilute the respiration signal at the nearshore during this part of the year.

The Kuskokwim River Basin is smaller than the Yukon (130,000 km^2 compared to 853,300 km^2) and contributes a much lower volume of water on the annual scale (34 km^3 compared to 200 km^3). Despite its smaller size, the location of the Kuskokwim River mouth is located near the central shelf and its discharge impacts a greater shelf area than the Yukon River (Feely and Calder, 1981). While there is a paucity of data for the Kuskokwim River, basin lithology links the two drainage basins (Gallant et al., 1995) and downstream processes should thus be similar. The shorter length of the Kuskokwim limits the amount of time for respiration processes to occur during downstream flow. This indicates that some organic matter contributed by this river system may be labile, and may be remineralized over the Bering Sea shelf.

Generally, river discharge is restricted to the nearshore region (Coastal Domain; 0-50 m isobaths) by the Inner Front, one of several well-resolved, semi-permanent frontal structures that govern the hydrographic regimes of the Bering Sea (Kinder and Coachman, 1978; Coachman and Charnell, 1979; Coachman, 1986; Kachel et al., 2002). Resultantly, it is unlikely that the addition of labile organic matter from the Kuskokwim River or respiration products from either river will affect more area of the shelf than the Coastal Domain.

The physical structure of the middle and outer regions of the Bering Sea enhances vulnerability to acidification effects in specific regional areas. For example, upwelling of naturally CO_2-rich subsurface water from the Bering Sea basin could enhance the baseline corrosivity of waters near the shelf break. Upwelling in the Bering Sea can be driven by topography, as near the Pribilof, Bering, and Zhemchug Canyons (Kelly and Hood, 1971; Stabeno and Van Meurs, 1999; Brodeur, 2001; Kinney et al., 2009); by instabilities in the Bering Slope Current, leading to on-shelf transport of waters by eddies (Park et al., 1974; Schumacher and Stabeno, 1994; Stabeno and Van Meurs, 1999; Mizobata and Saitoh, 2004); and by episodic, wind-driven upwelling events (Danielson et al., 2012). Similar to the processes that restrict the wider circulation of river discharge over the shelf, the wide semi-permanent Central Front also provides a barrier between the shelf break and the central shelf areas at approximately the 100 m isobath (Coachman, 1986), and most upwelled deeper waters are restricted to this area (Outer Domain; 250-100 m isobath).

Resultantly, the area between these two strong fronts (Middle Domain; 50-100 m isobaths) is relatively well protected from the penetration of outside water masses and currents. In the absence of prominent topographical features, the along- and cross-shelf flow through the Middle Domain is relatively weak compared to the other two regions, with tidal flows providing the dominant source of water mass transport and property diffusion (Coachman, 1986). As the shelf widens to the north, these flows become even weaker (Stabeno et al., 2010). Slow flushing times reduce the dilution of water properties, and the transport of heat, salt, and other dissolved constituents is easily

observed. This latter characteristic is particularly obvious in the formation of the Bering Sea cold pool, where wintertime cooling is preserved through most of the year in the subsurface layer of the Middle Domain by the rapid onset of stratification (Stabeno et al., 2002; Ladd and Stabeno, 2012).

Given that colder waters also more efficiently store CO_2, it is probable for this reason alone that the cold pool is highly susceptible to OA processes. However, other Middle Domain characteristics may also enhance the natural accumulation of CO_2. Unique processes at the Central Front, such as the upward penetration of sedimentary iron and regenerated nutrients, make the Middle Domain one of the most productive regions of the Bering Sea (e.g., Hurst et al., 2010). Because of the vertical stability of the water column in this region, vertical export of these high volumes of biomass is particularly efficient and the retention of respiration products is subsequently favored. This vulnerability may also be enhanced to the north (e.g., > 60°N), where flows are slowest (Stabeno et al., 2010) and longer sea ice persistence results in the coldest bottom-layer temperatures on the shelf (Stabeno et al., 2002).

Here, seasonal hydrography, new discrete measurements of dissolved organic and inorganic carbon (DOC and DIC, respectively) and total alkalinity (TA) during 2008, 2009, and 2010 collected during the BEST-BSIERP Bering Sea Project (bsierp.nprb.org), and other available carbon data records were synthesized to quantify the seasonal variability in the organic and inorganic carbon systems of the shelf and identify areas of seasonal CO_2 accumulation leading to enhanced susceptibility to OA processes. In the following chapters, the Coastal Domain and the northern Middle Domain appear repeatedly as areas of interest in the regional carbon cycle and the spatiotemporal moderation of Ω.

Related recent work documenting observed shallow-water undersaturations in the Bering Sea is presented in Appendices A and B. While slight undersaturations were observed seasonally near the coast in Appendix A, the most intense shallow-water undersaturations were observed in bottom waters over the northern middle shelf.

Appendix B highlights the role of anthropogenic CO_2 in the duration and timing of onset of undersaturations over the Southern Bering Sea shelf.

Chapter 2 investigates the seasonal net community production and surface layer accumulation of total organic carbon in the water column. Net heterotrophy was apparent near the coast in summer of 2009, indicating more organic matter had been respired here than had been locally produced. Additionally, a simple calculation showed that most marine-derived organic matter was not retained in the surface layer, but exported to depth. A more detailed carbon budget, linking the primary production, recycling, and surface layer lateral transport of organic carbon to vertical export production on the annual scale is presented in Chapter 3. Focused deposition of organic matter was again apparent near the coast. Lateral transport through the middle shelf bottom waters was notably lower than the outer shelf, indicating that carbon may be more efficiently retained in this region. Notably, this reduced transport coincided with the lowest observed carbonate mineral undersaturations over the middle shelf.

Chapter 4 presents a thorough investigation of the regional carbonate chemistry, indicating that carbonate minerals are dissolving in the areas where the duration and intensity of undersaturations are maximized by slow flushing times and efficient retention of respiration products. An investigation of the impacts of sea ice on sea-air exchanges of CO_2 in Chapter 5 adds to the understanding of this process, showing that the mechanical inhibition of gas exchange by the ice matrix forces the sequestration CO_2 in surface waters over the northern middle shelf, and enhances the baseline concentration of CO_2 in this region.

These results are synthesized in Chapter 6, highlighting the role of regional-scale hydrographic processes contributing to CO_2 accumulation in the Coastal Domain and the northern Middle Domain, and the production and maintenance of low carbonate mineral saturation states in the northern Middle Domain. This chapter also includes some speculation on the propagation of these effects through Bering Strait and the Chukchi Sea to the Arctic Ocean. A brief, first-order estimation is used to project the future of carbonate mineral saturation state suppression in the Bering Sea, based on the natural

vulnerabilities highlighted here.

1.0 References

Bates, N.R., Mathis, J.T., 2009. The Arctic Ocean marine carbon cycle: evaluation of air-sea CO_2 exchanges, ocean acidification impacts and potential feedbacks. Biogeosci. 6, 2433−2459.

Brabets, T.P., Wang, B., Meade, R.H., 2000. Environmental and hydrologic overview of the Yukon River Basin, Alaska and Canada. Water-Resources Investigations Report No. 99-4204. USGS, Anchorage, AK, 114 pp.

Branch, T.A., DeJoseph, B.M., Ray, L.J., Wagner, C.A., 2012. Impacts of ocean acidification on marine seafood. Tr. Ecol. Evol. 28(3), 178−186.

Brodeur, R.D., 2001. Habitat-specific distribution of Pacific ocean perch (*Sebastes alutus*) in Pribilof Canyon, Bering Sea. Cont. Shelf Res. 21(3), 207−224.

Buddemeier R.W., Kleypas, J.A., Aronson, R.B., 2004. Coral reefs and global climate change: potential contributions of climate change to stresses on coral reef ecosystems. Pew Center on Global Climate Change, Arlington, VA, 56 pp.

Byrne, R.H., Mecking, S., Feely, R.A., Liu, X., 2010. Direct observations of basin-wide acidification of the North Pacific Ocean. Geophys. Res. Lett. 37, L02601.

Chen, C.-T.A, 1993. Carbonate chemistry of the wintertime Bering Sea marginal ice zone. Cont. Shelf Res. 13(1), 67−87.

Coachman, L.K., Charnell, R.L., 1979. On lateral water mass interaction—A case study, Bristol Bay, Alaska. J. Phys. Oceanogr. 9(2), 278−297.

Coachman, L.K., 1986. Circulation, water masses, and fluxes on the southeastern Bering Sea shelf. Cont. Shelf Res. 5(1-2), 23−108.

Codispoti, L.A, Friederich, G.E., Iverson, R.L., Hood, D.W., 1982. Temporal changes in the inorganic carbon system of the southeastern Bering Sea during spring 1980. Nature. 296(5854), 242−245.

Codispoti, L.A., Friederich, G.E., Hood, D.W., 1986. Variability in the inorganic carbon system over the southeastern Bering Sea shelf during spring 1980 and spring-summer 1981. Cont. Shelf Res. 5(1-2), 133−160.

Cooley S., Kite-Powell, H., Doney, S., 2006. Ocean acidification's potential to alter global marine ecosystem services. Oceanogr. 22(4), 172−181.

Cooley, S.R., Doney, S.C., 2009. Anticipating ocean acidification's economic consequences for commercial fisheries. Env. Res. Lett. 4(2), 024007.

Cooley, S.R., Lucey, N., Kite-Powell, H., Doney, S.C., 2012. Nutrition and income from mollusks today imply vulnerability to ocean acidification tomorrow. Fish Fish. 12(2), 182−215.

Danielson, S., Hedstrom, K., Aagaard, K., Weingartner, T., Curchister, E., 2012. Wind-induced reorganization of the Bering shelf circulation. Geophys. Res. Lett. 39, L08601.

Dittmar, T., Kattner, G., 2003. The biogeochemistry of the river and shelf ecosystem of the Arctic Ocean: a review. Mar. Chem. 83, 103−120.

Doney, S.C., Fabry, V.J., Feely, R.A., Kleypas, J.A., 2009. Ocean acidification: the other CO_2 problem. Ann. Rev. Mar. Sci. 1(1), 169−192.

Fabry, V.J., Seibel, B.A., Feely, R.A., Orr, J.C., 2008. Impacts of ocean acidification on marine fauna and ecosystem processes. ICES J. Mar. Sci. 65(3), 414−432.

Feely, R.A., Calder, J., 1981. The distribution and elemental composition of suspended particulate matter in Norton Sound and the northeastern Bering Sea shelf: Implications for Mn and Zn recycling in coastal waters, in: Hood, D., Calder, J. (Eds.), The Eastern Bering Sea Shelf: Oceanography and Resources. U.S. Department of Commerce, Washington, D.C., pp. 321−337.

Feely, R.A., Doney, S.C., Cooley, S.R., 2009. Ocean acidification: present conditions and future changes in a high-CO_2 world. Oceanogr. 22(4), 36−47.

Fernandes, M.B., Sicre, M.-A., 2000. The importance of organic carbon inputs on Kara Sea shelves as revealed by *n*-alkanes, OC, and $\delta^{13}C$ values. Org. Geochem. 31, 363−374.

Gallant, A., Binnian, E., Omernik, J., Shasby, M.B., 1995. Ecoregions of Alaska. USGS Professional Paper No. 1567. U.S. Government Printing Office, Washington, D.C., 73 pp.

Harvey, R.H., Sigler, M.F., 2013. An introduction to the Bering Sea Project: Volume II. Deep Sea Res. II. 94, 2−6.

Hurst, M.P., Aguilar-Islas, A.M., Bruland, K.W., 2010. Iron in the southeastern Bering Sea: Elevated leachable particulate Fe in shelf bottom waters as an important source for surface waters. Cont. Shelf Res. 30(5), 467-480.

Kachel, N.B., Hunt Jr., G.L., Salo, S.A., Schumacher, J.D., Stabeno, P.J., Whitledge, T.E., 2002. Characteristics and variability of the inner front of the southeastern Bering Sea. Deep Sea Res. II. 49, 5889−5909.

Kelly, J.J., Hood, D.W., 1971. Carbon dioxide in the Pacific Ocean and Bering Sea: upwelling and mixing. J. Geophys. Res. 76(3), 745−752.

Kinder, T.H., Coachman, L.K., 1978. The front overlying the continental slope in the Eastern Bering Sea. J. Geophys. Res. 83(C9), 4551−4559.

Kinney, J.C., Maslowski, W., Okkonen, S., 2009. On the processes controlling shelf-basin exchange and outer shelf dynamics in the Bering Sea. Deep Sea Res. II. 56(17), 1351−1362.

Kuffner, I.B., Andersson, A.J., Jokiel, P.L., Rodgers, K.S., Mackenzie, F.T., 2008. Decreased abundance of crustose coralline algae due to ocean acidification. Nat. Geosci. 1(2), 114−117.

Ladd, C., Stabeno, P.J., 2012. Stratification on the Eastern Bering Sea shelf revisited. Deep Sea Res. II. 65-70, 72−83.

Lisitsyn, A.P., 1969. Recent Sedimentation in the Bering Sea. Bezrukov, P.L. (Transl). Israel Program for Scientific Translations, Jerusalem, 624 pp.

Macklin, S.A., (Ed.), 1999. Bering Sea FOCI Final Report. FOCI Report No. B356. National Technical Information Service, Springfield, VA, 173 pp.

Mathis, J.T., Cross, J.N., Bates, N.R., 2011. The role of ocean acidification in systemic carbonate mineral suppression in the Bering Sea. Geophys. Res. Lett. 38, L19602.

McRoy, C.P., 1993. ISHTAR, the project: an overview of Inner Shelf Transfer and Recycling in the Bering and Chukchi Seas. Cont. Shelf Res. 13(5-6), 473−479.

McRoy, C.P., Hood, D.W., Coachman, L.K., Walsh, J.J., Goering, J.J., 1986. Processes and resources of the Bering Sea shelf (PROBES): The development and accomplishments of the project. Cont. Shelf Res. 5(1-2), 5−21.

Mizobata, K., Saitoh, S., 2004. Variability of Bering Sea eddies and primary productivity along the shelf edge during 1998 − 2000 using satellite multisensory remote sensing. J. Mar. Syst. 50, 101−111.

Narita, D., Rehdanz, K., Tol, R.S.J., 2012. Economic costs of ocean acidification: a look into the impacts on global shellfish production. Clim. Ch. 113(3-4), 1049−1063.

O'Connor, H.J., Izrael, Y.A., Tsyban, A.V., Whitledge, T.E., McRoy, C.P., Coachman, L.K., 1992. Program on long-term ecological investigations of the Bering Sea and other Pacific Ocean ecosystems (BERPAC Program), in: Nagel, P.A. (Ed.), Results of the Third Joint U.S.-U.S.S.R. Bering and Chukchi Seas Expedition (BERPAC), Summer 1988. U.S. Fish and Wildlife Service, Washington, D.C., pp. 3−6.

Orr, J.C., Fabry, V.J., Aumont, O., Bopp, L., Doney, S.C., Feely, R.A., et al., 2005. Anthropogenic ocean acidification over the twenty-first century and its impact on calcifying organisms. Nature. 437(7059), 681−686.

Park, P.K., Gordon, L.I., Alvarez-Borrego, S., 1974. The carbon dioxide system of the Bering Sea, in: Hood, D., Kelley, E. (Eds.), Oceanography of the Bering Sea. University of Alaska Fairbanks Institute of Marine Science, Fairbanks, AK, pp. 107−147.

Sabine, C.L., Feely, R.A., 2007. The oceanic sink for carbon dioxide, in: Reay, D., Hewitt, N., Grace, J., Smith, K. (Eds.), Greenhouse Gas Sinks. CABI Publishing, Oxfordshire, U.K., pp. 31−49.

Sabine, C.L., Feely, R.A., Gruber, J., Key, R.M., Lee, K., Bullister, J.L., et al., 2004. The oceanic sink for anthropogenic CO_2. Science. 305(5682), 367−371.

Schumacher, J.D., Stabeno, P.J., 1994. Ubiquitous eddies of the eastern Bering Sea and their coincidence with concentrations of larval pollock. Fish. Oceanogr. 3(3), 182−190.

Stabeno, P.J., Van Meurs, P., 1999. Evidence of episodic on-shelf flow in the southeastern Bering Sea. J. Geophys. Res. 104(C12), 29715−29720.

Stabeno, P.J., Hunt Jr., G.L., 2002. Overview of the Inner Front and Southeast Bering Sea Carrying Capacity Programs. Deep Sea Res. II. 49, 6157−6168.

Stabeno, P.J., Kachel, N.B., Sullivan, M., Whitledge, T.E., 2002. Variability of physical and chemical characteristics along the 70 m isobath of the southeastern Bering Sea. Deep Sea Res. II. 49, 5931−5943.

Stabeno, P., Napp, J., Mordy, C., Whitledge, T., 2010. Factors influencing physical structure and lower trophic levels of the eastern Bering Sea shelf in 2004: Sea ice, tides, and winds. Progr. Oceanogr. 85, 180−196.

Striegl, R.G., Aiken, G.R., Dornblaser, M.M., Raymond, P.A., Wickland, K.P., 2005. A decrease in discharge-normalized DOC export by the Yukon River during summer through autumn. Geophys. Res Lett. 32, L21413.

Striegl, R.G., Dornblaser, M.M., Aiken, G.R., Wickland, K.P., Raymond, P.A., 2007. Carbon export and cycling by the Yukon, Tanana, and Porcupine rivers, Alaska, 2001 − 2005. Wat. Resour. Res. 43, W02411.

Walsh, J.J., McRoy, C.P., 1986. Ecosystem analysis in the southeastern Bering Sea. Cont. Shelf Res. 5(1-2), 259−288.

Wiese, F.K., Wiseman, W.J., Van Pelt, T.I., 2012. Bering Sea linkages. Deep Sea Res. II. 65-70, 2−5.

Chapter 2:

Hydrographic controls on net community production and total organic carbon distributions in the eastern Bering Sea[1]

2.0 Abstract

In order to assess spatial and temporal variability of net community production (NCP) in shelf areas of the eastern Bering Sea, seawater samples for dissolved inorganic carbon (DIC) and total organic carbon (TOC) were collected during BEST-BSIERP cruises in the spring, summer, and fall of 2009 and compared to prior measurements made in 2008. DIC and TOC data were used to estimate seasonal changes in rates of NCP and the balance of net autotrophy versus heterotrophy in different shelf areas. In 2009, springtime surface layer DIC concentrations were generally uniform across the shelf and averaged ~2100 μmoles kg^{-1}, although concentrations in northern shelf areas (under sea ice cover) were slightly higher (~2130 μmoles kg^{-1}). Subsequently, surface layer DIC (~1950 μmoles kg^{-1}) decreased significantly by summertime with the largest drawdown of DIC observed in the Middle Domain between 57° and 61°N. In this area, high NCP rates of up to 92 mmoles C m^{-2} d^{-1} were observed and higher than those reported in 2008. Comparing 2008 and 2009, the shelf-wide average drawdown of DIC in the upper 30 m between spring and summer was greater by ~16 μmoles kg^{-1}. In both spring and summer of 2008 and 2009, concentrations of TOC generally decreased from the coast. TOC concentrations were tightly coupled to salinity, particularly in spring, and largely influenced by the discharge of the Yukon and Kuskokwim Rivers. TOC accumulation between spring and summer was relatively small. In nearshore regions of the shelf, negative rates of NCP were indicative of net heterotrophy with remineralization of labile organic carbon from rivers likely contributing to the observed net respiration signal in

[1]Cross, J.N., Mathis, J.T., Bates, N.R., 2012. Hydrographic controls on net community production and total organic carbon distributions in the eastern Bering Sea. Deep Sea Res. II. 65-70, 98–109.

this region. In contrast, net heterotrophy was not observed in 2008, when river discharge rates were 30% lower (likely with lower river transport of TOC). While 2009 rates of production were higher outside the Coastal Domain than those observed in 2008, integrated annual production over the shelf was fairly comparable between the two years (2008: 103 Tg C yr^{-1}; 2009: 97.2 Tg C yr^{-1}). DOC accumulation in the surface layer was also equivalent between the two years (~12 μmoles kg^{-1}), and in both years shelf-wide export production was estimated to be ~75% of total NCP.

2.1 Introduction

Global climate change and recent fluctuations in sea ice extent have been linked to changes in the marine ecosystem of the Bering Sea shelf over the past several decades (e.g., Francis et al., 1998; Springer, 1998; Hollowed et al., 2001; Hunt et al., 2002; Schumacher et al., 2002; Overland and Stabeno, 2004; Grebmeier et al., 2006a; Rho and Whitledge, 2007; Bates et al., 2010; Mathis et al., 2010). Furthermore, Grebmeier et al. (2006b) suggested that the areas of the Bering Sea affected by these changes are expanding, with unknown consequences to carbon and nutrient biogeochemical cycling. While the effects of these physical and biogeochemical forces on the inorganic carbon cycle have been recently described (Mathis et al., 2010, 2011), there remains a paucity of data on the organic carbon cycle in the region. Most studies concerning organic carbon are focused on sedimentary oxygen consumption or export production rates, specifically for the purpose of describing the origins of sedimentary organic matter and pelagic-benthic coupling (e.g., Grebmeier et al., 1988; Grebmeier and McRoy, 1989; Fukuchi et al., 1993; Grebmeier 1993, Grebmeier et al., 1995; Grebmeier and Cooper, 1995; Grebmeier and Dunton, 2000; Cooper et al., 2002; Coyle and Pinchuk, 2002). However, only two studies on the water column content of organic carbon have been conducted previously (Agatova et al., 1999; Guo, et al., 2004), with the latter focused on the open-ocean western Bering Sea rather than the shelf. This critical lack of data leads to a significant gap in our understanding of carbon cycling and dynamics in the Bering Sea shelf, and predictability of responses to changes in the marine ecosystem.

Here we describe the spatio-temporal distribution and hydrographic control of total organic carbon (TOC) in 2008 and 2009 and compare dissolved inorganic carbon (DIC) concentrations and rates of net community production (NCP) in 2009 to those observed in 2008 (Mathis et al., 2010) over the Bering Sea shelf. Rates of NCP are determined at numerous locations over the broad shelf in the context of six "domains" defined by differing physical characteristics.

2.2 Study Area

In accordance with other studies, (e.g., Mathis et al., 2010; Lomas et al., 2012), the Bering Sea shelf was divided into three along-shelf domains divided by semi-permanent frontal structures (Coachman and Charnell, 1979; Coachman, 1986; Stabeno et al., 1999). The innermost front roughly overlies the 50 m isobath (Kachel et al., 2002), providing a barrier between the Coastal and Middle Domains (Figure 2.1). The Central Front is a broader transition zone between the 80 m and 100 m isobaths, and separates the Middle and Outer Domains (Coachman, 1986). The Shelf Break Front sequesters the waters of the Outer Domain from direct mixing with basin waters (Schumacher and Stabeno, 1998). The influence of sea ice on bottom temperatures distinguishes the northern shelf from the southern shelf at approximately 60°N (e.g., Wyllie-Escheveria and Wooster, 1998; Stabeno et al., 2002). Bathymetric features direct along-shelf flows to the north and west, although residence times are typically long (~three months; Coachman, 1986).

2.3 Methods

2.3.1 Sample Collection

Physical, chemical and biological measurements were made in the eastern Bering Sea from the following ships: (1) USCGC *Healy* during spring (April/May) and summer (July) of 2008 and spring (April/May) of 2009; (2) the R/V *Knorr* in Summer (June/July) of 2009, and; (3) NOAA ship *Miller Freeman* in Fall (September) of 2009. In 2008,

stations were occupied on three east-west transect (SL, MN and NP lines) lines and one north-south transect along the 70 m isobath (70M line; Figure 2.1), as previously described (Mathis et al., 2010). In 2009, the SL, MN, NP and 70M line transects were repeated in spring and summer. In fall, the NP line was replaced by the CN line. At the beginning of each spring cruise, sea ice cover was near 100% at all stations. Towards the end of the spring cruises, sea ice had diminished and the southern stations of the 70M line (<57°N) were ice-free when sampled in both years. During summer and fall of 2008 and 2009, the entire Bering Sea shelf was ice-free.

At each CTD/hydrocast station, water samples were collected for DIC, total alkalinity (TA), and TOC. Seawater samples for DIC/TA were drawn from Niskin bottles into pre-cleaned 300 mL borosilicate bottles. These samples were immediately poisoned with mercuric chloride ($HgCl_2$) to halt biological activity. Seawater for TOC samples was drawn from Niskin bottles into pre-conditioned, TOC-free 60 mL bottles and frozen to halt biological activity. All samples were shipped to shore-based laboratories for analysis.

2.3.2 Analytical Methods

DIC and TA samples were analyzed using a highly precise and accurate gas extraction/coulometric detection system (Bates, 2001; Mathis et al., 2010). The analytical system consists of a VINDTA 3C (Versatile Instrument for the Detection of Total Alkalinity; http://www.marianda.com) coupled to a CO_2 coulometer (model 5012; UIC Coulometrics). TA samples were determined by potentiometric titration using the VINDTA 3C. Routine analyses of Certified Reference Materials (CRMs, provided by A.G. Dickson, Scripps Institution of Oceanography) ensured that the accuracy of the DIC and TA measurements were within 0.1% (~2 μmoles kg^{-1}) and stable over time. The VINDTA 3C provides real-time corrections to DIC and TA values according to *in-situ* temperature, salinity, and phosphate and silicate concentrations. These hydrographic data were accessed through the EOL Bering Sea Project Data Archive for spring and summer of 2008 (Stabeno, 3-21-2011a, b) and 2009 (Stabeno, 3-21-2011c, d) and provided by NOAA-PMEL for fall of 2009 (Mordy, pers. comm.).

TOC (dissolved + suspended particulate organic carbon) samples were analyzed using the Shimadzu TOC-V/CSN system. Reference standards produced by the Hansell Certified Reference Material program were analyzed each day. Samples were systematically referenced to low-carbon water and deep and surface reference waters every sixth analysis. The between-day precision in DOC measurements was 1-2 μmoles kg^{-1} and long term accuracy was stable over time.

Net community production was calculated via the measurement of the net seasonal consumption of the photosynthetic reactant DIC, according to the method of Williams (1993) and adjusted for the influences of freshwater discharge and calcium carbonate formation according to our previous work (Mathis et al., 2010). In general, the addition of water with low concentrations of DIC (e.g., ice melt) to the surface layer dilutes DIC concentrations. Because NCP also decreases DIC concentrations in the upper 30 m, these dilutive influences can cause a false amplification of the NCP signal. Conversely, addition of high-DIC waters between spring and summer (e.g., river discharge) can cause a dampening of the NCP signal. Each of these effects can be corrected by normalizing DIC to a constant deep-water reference salinity (S = 35; Millero, 2008). Normalized DIC concentrations are denoted nDIC in this manuscript. The formation and dissolution of calcium carbonate ($CaCO_3$) can also cause changes in DIC. A correction for this affect can be applied by measuring seasonal changes in total alkalinity (TA) (Codispoti et al., 1986; Lee, 2001). Approximately half of the seasonal change in TA and nitrate content can be estimated to affect DIC concentrations, such that:

$$\Delta DIC_{Alk} = \frac{\left[\left(Alk_{\text{Summer (30m)}} - Alk_{\text{Spring (30m)}}\right) + \left(\left(NO_3\right)_{\text{Summer (30m)}} - \left(NO_3\right)_{\text{Spring (30m)}}\right)\right]}{2} \qquad \text{(Eq. 2.1)}$$

Nitrate values to complement our measured alkalinity samples were accessed at the EOL Bering Sea Project Data Archive and provided by Calvin Mordy at NOAA-PMEL. Therefore, our estimates of NCP are calculated according to the following equation,

modified from Williams (1993) such that NCP is the only significant process affecting DIC concentrations in the upper mixed layer:

$$NCP = nDIC_{\text{Summer (30 m)}} - nDIC_{\text{Spring (30 m)}} - \Delta DIC_{Alk} \quad \text{(Eq. 2.2)}$$

2.3.3 Assumptions and Caveats

Other sources of uncertainty in the NCP calculation do exist. The timing of sampling relative to the initiation of blooms can introduce additional error to NCP calculations if DIC measurements are made after the initiation or before the completion of the spring bloom. Additionally, there is a net advection from south to north over the shelf in the Bering Sea. However, effects from transport should be minimal as residence times over the Bering Sea shelf have been estimated to be on the order of three months, and longer in some regions (Coachman, 1986). All of our stations were reoccupied in less than 90 days, reducing the overestimations of NCP that could be caused by advective transport, but possibly missing late-season production. Air-sea CO_2 gas exchange and vertical diffusion also add DIC to the mixed layer at an increasing rate across the season, as productivity increases the gradient between concentrations of CO_2 in the atmosphere, surface ocean, and deeper waters. A previous study has shown that air-sea exchange can account for a ~10% underestimation of NCP in this region, while vertical diffusion caused a ~3% underestimation of NCP in the region (Mathis et al., 2010). Because of these caveats, we note that the rates of NCP estimated in this paper are likely conservative.

2.4 Results

2.4.1 Seasonal Variation of DIC in 2009

The seasonal variation of DIC in 2009 is presented in Figures 2.2 and 2.3. In spring, DIC concentrations were closely correlated with salinity and ranged from ~2000 μmoles kg^{-1} in the Coastal Domain to ~2400 μmoles kg^{-1} (Figure 2.2A) in offshore bottom waters (> 200 m). Concentrations were relatively uniform across the shelf,

averaging ~2100 μmoles kg^{-1} (Figure 2.3A), although northern regions (> 60°N) exhibited above average DIC concentrations (~2130 μmoles kg^{-1}; Figure 2.3A). Summertime DIC concentrations in 2009 ranged much more widely than spring concentrations (Figure 2.2B; ~1850 μmoles kg^{-1} in Middle Domain surface waters to ~2375 μmoles kg^{-1} in bottom waters off the shelf). In surface waters (< 30 m; SL line, Figure 2.3B; other lines, not shown), DIC concentrations were noticeably lower (~1950 μmoles kg^{-1}) across the shelf (Figure 2.3B). Low mixed layer concentrations were apparent in the Middle Domain along the SL, MN, and NP lines. Bottom water DIC concentrations in summer more closely matched springtime DIC concentrations, although noticeable increases occurred in bottom waters along the SL and MN lines, and clear maxima (~2300 μmoles kg^{-1}) appeared in bottom waters in the Inner and Middle Domains along the SL line (Figure 2.3B). In fall, DIC concentrations exhibited a smaller range than in summer (~1950 μmoles kg^{-1} in Middle Domain surface waters to 2350 μmoles kg^{-1} in bottom waters off the shelf of the CN line; Figure 2.2C). Surface layer concentrations were lower than in spring but higher than in summer in the Middle Domain and across the entire SL line (~2000 μmoles kg^{-1}; Figure 2.3C). Bottom water maxima (~2200 μmoles kg^{-1}) were apparent in the Outer Domain areas found along the CN, MN, and SL lines (Figure 2.3C).

2.4.2 Seasonal Variation of TOC in 2008 and 2009

In 2008 and 2009, TOC concentrations were closely coupled to salinity across the shelf. Between spring and summer, TOC concentrations increased over the shelf by approximately 12 μmoles kg^{-1} (Table 2.1), and by ~9 μmoles kg^{-1} between summer and fall of 2009. In spring, TOC concentrations ranged from ~55 μmoles kg^{-1} to ~100 μmoles kg^{-1} (Figure 2.4A, C). Concentrations were highest in the Coastal Domain and decreased with depth (Figure 2.5A, C). TOC concentrations peaked in the Coastal Domain along the MN line (~90 μmoles kg^{-1}). Minimum concentrations were seen in the bottom waters of the Outer Domain along the MN and NP lines. In the southern areas of the 70M line, TOC concentrations were higher than in northern shelf areas.

In summer, TOC concentrations ranged from 51 μmoles kg^{-1} to 127 μmoles kg^{-1} (Figure 2.4B, D). Maximum TOC concentrations were again observed in Coastal Domain surface waters along the MN and NP lines, and concentrations decreased offshore and with depth (Figure 2.5B, D). Minimum concentrations occurred in bottom waters off the shelf along the MN line. TOC concentrations in the mixed layer were ~85 μmoles kg^{-1}, whereas bottom water concentrations were ~5 μmoles kg^{-1} lower.

The high TOC concentrations observed in surface waters of the Coastal Domain in spring and summer were absent in fall (Figure 2.5E). TOC concentrations were still highest in these regions, but maxima decreased by ~9 μmoles kg^{-1} (Figure 2.4E). Minimum TOC concentrations (~60 μmoles kg^{-1}) were more widespread, occurring in the Outer and Middle Domain bottom waters of the MN and CN lines, and in the Outer Domain bottom waters of the SL line.

2.4.3 Spatial Distribution of Net Community Production in 2009

The low range of springtime DIC concentrations and lack of surface minima indicate that rates of NCP prior to our springtime station occupations were likely very low compared to the spring-summer transition. nDIC concentrations also showed a very well constrained range, confirming the minimal influence of early season productivity. In summer, subsurface chlorophyll maxima were observed at most locations at a depth of ~40 m (below the mixed layer) but the drawdown of DIC (e.g., Figure 2.3B) and nDIC (Table 2.2) was typically confined to the mixed layer (i.e., 0-30 m). nDIC concentrations had decreased by an average of ~106 μmoles kg^{-1} across the entire shelf by summertime but significant spatial variability was observed. In the southern Outer Domain and the northern and southern Middle Domains, nDIC drawdown typically was greater than > 100 μmoles kg^{-1}. In comparison, nDIC drawdown in the southern Coastal Domain was much lower, averaging ~23 μmoles kg^{-1}. In contrast to these regions, nDIC concentrations increased by ~15 μmoles kg^{-1} in the northern Coastal Domain, implying net heterotrophy rather than net autotrophy.

The calculated nDIC deficit between spring and summer was also corrected for the formation of $CaCO_3$, as discussed in Section 2.3.3. This correction was highly variable across the shelf and within each domain (Table 2.2). On average, $CaCO_3$ production increased the DIC deficit and raised our estimates of NCP in the northern regions of the Coastal and Middle Domains as well as in the southern Coastal Domain. In the southern Middle and southern Outer Domains, the DIC deficit was decreased and this lowered estimates of rate of NCP.

Negative rates of NCP were observed along the SL line (i.e., -6 mmoles C m^{-2} d^{-1}), MN line (-1 mmoles C m^{-2} d^{-1}) and the NP line (-11 mmoles C m^{-2} d^{-1}), indicating net heterotrophy in these areas (Figure 2.6). In contrast, positive values of NCP were observed in the Middle and Outer Domains, indicating a spring to summer period of net autotrophy (Figure 2.6). Some very high rates of NCP were observed in the Middle and Outer Domains in the vicinity of the Central Front on both the northern (85 mmoles C m^{-2} d^{-1}) and the southern shelf (92 mmoles C m^{-2} d^{-1}). However, average NCP rates in the Outer and Middle Domains were very similar (~50 mmoles C m^{-2} d^{-1}). Average NCP in the Coastal Domain was much lower (~7 mmoles C m^{-2} d^{-1} in the southern Coastal Domain and ~-11 mmoles C m^{-2} d^{-1} in the northern Coastal Domain. This difference in Coastal and Middle/Outer Domain productivity indicates a general off-shelf trend of increasing productivity. Neither a distinction nor trend between the northern and southern regions of the shelf was observed.

2.5 Discussion

2.5.1 Hydrographic Controls on TOC in 2008 and 2009

TOC dynamics over the shelf in spring and summer were fairly similar between the two years (Figure 2.5). Concentrations were consistently highest in summertime surface waters of the Coastal Domain, and decreased both offshore and with depth. However, one notable difference was observed: the range of TOC concentrations was greater in 2008 than in 2009. For example, minimum springtime concentrations were lower in 2008 by approximately 10 μmoles kg^{-1}, while maximum summertime

concentrations were ~10 μmoles kg^{-1} higher. Springtime sampling in 2008 was slightly earlier in the season than in 2009, and it is possible that the lower concentrations of TOC seen in offshore bottom waters over the shelf more accurately reflect wintertime conditions (Figure 2.5A). In contrast, the timing of sampling in summertime was similar in 2008 and 2009, suggesting that other factors must have caused the differences in spatial distribution of TOC maxima between the two years.

NCP and TOC were not well correlated over the shelf (Figure 2.7), and despite high rates of NCP in some regions, the accumulation of dissolved organic carbon (DOC) between seasons was relatively small in both 2008 and 2009 (Table 2.3). This suggests that DOC/TOC was a minor product of phytoplankton photosynthesis with a relatively large production of particulate organic carbon (POC) and subsequent vertical export to subsurface waters. If NCP = ΔTOC + POC_{exp} as suggested by Hansell and Carlson (1998), then the export of POC must have exceeded 80% of the calculated NCP for the region in most areas (Table 2.3). It should be noted that the calculation for POC_{exp} is an estimation only, and may include TOC that was exported laterally. Moran et al. (2012) measured much lower rates of export production in some areas in 2008 than we estimated with this calculation. However, in highly productive arctic and subarctic ecosystems, most annual phytoplankton production is seasonally exported rather than retained in the mixed layer. Gosselin et al. (1997) examined the fractionation of primary production between DOC and POC in the Arctic and found that 60-80% of total primary production was released as POC.

Our observations that NCP and TOC accumulation are uncoupled may indicate an allochthonous source of TOC to the shelf, and the high correlation between TOC and salinity we observed suggests that this source is likely river discharge, as in other coastal and coastal Arctic systems (Mantoura and Woodward, 1983; Kattner et al., 1999; Cauwet, 2002; Dittmar and Kattner, 2003; Hansell et al., 2004). USGS streamflow data show that maximal river discharge occurred during the same month in 2008 and 2009, with this peak in river flow coinciding with our summertime sampling in both years (USGS, 2010). However, the total rate and volume of discharge in 2009 was greater than

in 2008 (~30%; USGS, 2010). In keeping with these data, we observed higher summertime TOC concentrations offshore in 2009 than in 2008 (Figures 2.4D and 2.4B, respectively), although this still does not explain why TOC maxima were greater in 2008 than in 2009. It is possible that physical processes may have more effectively retained terrigenous TOC inshore of the Inner Front in 2008, while advection spread the TOC signal over a greater area of the shelf in 2009, resulting in relative dilution of 2009 values. Most organic matter discharged from high-latitude rivers is usually non-labile (Hansell et al., 1997; Mathis et al., 2007), so if we assume that all labile organic carbon discharged from rivers had been remineralized in 2008 and 2009, the lower TOC maxima in 2009 may also indicate a higher percentage of labile organic carbon discharged in 2009 relative to 2008.

2.5.2 Net Heterotrophy of the Coastal Domain

A negative rate of NCP (i.e. net heterotrophy) was observed in the Coastal Domain in 2009, as summertime concentrations of DIC had increased between spring and summer. This signal was not observed in 2008. While some productivity may have occurred within this region (i.e., Lomas et al., 2012; Moran et al., 2012), the drawdown of DIC due to primary production was masked by other processes that raised DIC concentrations between spring and summer. As discussed earlier, both atmospheric exchange and vertical diffusion can add DIC back into the mixed layer, dampening NCP signals. However, the Coastal Domain is typically a source of CO_2 to the atmosphere (Bates et al., 2010), indicating that atmospheric exchange in this case should have lowered DIC concentrations at the surface. Vertical diffusion may also have added DIC back into the surface layer, although we estimate that this should only have caused ~3% underestimation of NCP (Mathis et al., 2010). The timing of sampling could have contributed to the observed seasonal increase in DIC concentrations, suggesting that we observed low-DIC "post-bloom" concentrations in spring, and fall-like increases in summer. However, low concentrations of DIC relative to the rest of the shelf were not observed in the Coastal Domain in spring, indicating that it is unlikely that we missed the

spring bloom in this region. Therefore, another source must have contributed DIC to the surface layer of the Middle Domain in 2009.

Our previous work indicates that the primary control on inorganic carbon concentrations in the Coastal Domain is not biological productivity, but rather freshwater discharge (Mathis et al., 2011). Recall that peak outflow conditions corresponded to our summertime sampling, as stated in Section 2.5.1. Riverine organic carbon concentrations increase with rate and volume of discharge due to increased soil drainage, and peak outflows are typically associated with peak concentrations of organic carbon (Spitzy and Leenheer, 1991; Rember and Trefry, 2004; Striegl et al., 2005; Gueguen et al., 2006; Striegl et al., 2007). It then follows that the higher rate of discharge in 2009 would have delivered a higher total load of organic carbon over the shelf in 2009 relative to 2008.

A faster rate of discharge would have corresponded to a shorter time for remineralization during downstream flow and in nearshore estuaries, but this reduced remineralization may have been balanced by remineralization occurring within the Coastal Domain. While the spring freshet typically dilutes surface layer concentrations of DIC in the Coastal Domain (Striegl et al., 2007; Mathis et al., 2011), the net effect of the remineralization of the increased load of organic matter imparted by river discharge would have been to add more DIC to the Coastal Domain in 2009 relative to 2008. In addition, we earlier suggested that the percentage of organic carbon in this load may have been higher in 2009. Therefore, 2009 river discharge had higher total carbon content as well as a higher labile organic carbon content, and the combination of these two factors may have produced the net heterotrophic signal observed in the Coastal Domain.

2.5.3 Variability in NCP Between 2008 and 2009

Spatial distribution of NCP between 2008 and 2009 was very similar. In keeping with previous observations, Middle and Outer Domain NCP rates were higher than Coastal Domain rates in 2008 and 2009, and of a similar magnitude in both 2008 and 2009 (Table 2.4). Previous studies have indicated that increased depth relative to the

Coastal Domain permits strong seasonal stratification (Coachman, 1986), which contributes to the higher rates of productivity. Additionally, circulation patterns at the Central Front provide a near-continuous supply of iron and inorganic nitrogen to the surface layer (e.g. Springer et al., 1996) and limit the lateral dispersal of phytoplankton blooms, effectively confining these organisms within a regime idealized for productivity (Franks, 1992). The resultant high levels of spring and summer primary production span both the frontal system, portions of the Middle and Outer Domain, and the shelf break. This area has often been termed the "green belt" (e.g., Sorokin and Mikheev, 1979; Mackas et al., 1985; Coachman, 1986; Franks, 1992; Springer et al., 1996; Simpson and McRoy, 1999; McRoy et al., 2001; Okkonen et al., 2004;).

In both years, the lowest rates of NCP were observed in the Coastal Domain (Table 2.4). In this shallow region, the combination of this tidal energy with wind mixing completely overturns the water column and prevents consistent stratification even in summer (Coachman, 1986). This low stratification relative to the remainder of the shelf, in addition to nutrient limitation caused by isolation from high-nutrient basin waters (Sambrotto and Goering, 1983; Sambrotto et al., 1986; Whitledge et al., 1986; Springer and McRoy, 1993) prohibits extended periods of primary production despite high micronutrient availability relative to the remainder of the shelf (Aguilar-Islas et al., 2007; Hurst et al., 2010). This reduced volume of primary production has been previously observed to allow the dominance of other processes of biogeochemical modification (Mathis et al., 2011). This was particularly apparent in 2009, where higher river discharge resulted in a net heterotrophic signal that was not observed in 2008.

NCP extremes were noticeably higher in 2009 than in 2008. For example, maximum NCP rates were ~30 mmoles C m^{-2} d^{-1} greater in 2009, and minimum rates of production were ~20 mmoles C m^{-2} d^{-1} lower. Yet despite these localized variations, the total annual shelf-wide production in 2009 (~97.2 Tg C yr^{-1}) was very similar to production in 2008 (~103 Tg C yr^{-1}). These similarities may indicate that there is some consistency in the rate of NCP in years that are either "warm" or "cold" relative to the mean state. However, previous studies using this method of calculating NCP (including a

$CaCO_3$ correction) show that for the relatively warm years of 1980 and 1981 (Codispoti et al., 1982, 1986), NCP ranged from 14-23 mmoles C m^{-2} d^{-1} in 1980 and 100-200 mmoles C m^{-2} d^{-1} in 1981, a comparatively high degree of variability in "warm" years.

Additionally, our estimates show that large variation between "warm" and "cold" years makes it difficult to demonstrate changes in NCP rates in response to changes in physical and atmospheric drivers in the Bering Sea shelf region. If other studies are included (i.e., estimates of primary production or NCP from dissolved oxygen or nutrient changes), it is still difficult to demonstrate substantive differences in NCP between "warm" and "cold" years. For example, rates of NCP reported during a "cold" year in the early 1960s were estimated to be 217-667 mmoles C m^{-2} d^{-1} using oxygen modification (Ivenakov, 1961; Azova, 1964), while warm year production in 1992 was lower (i.e., 64 mmoles C m^{-2} d^{-1}; Sapozhnikov and Naletova, 1995). A comparison of these studies indicates that interannual variability of NCP in the Bering Sea could be very large (~2x; see Lomas et al., 2012), and that long-term trends may only be detected with longer time-series approaches or if there are substantial changes in rates of NCP.

2.6 Conclusions

In the spring and summer of 2008 and spring, summer and fall of 2009, spatio-temporal variability of TOC and NCP were measured for the eastern shelf of the Bering Sea. The unique hydrographic and biogeochemical characteristics that delineate each of the six domains found on the shelf dictate the character and magnitude of productivity in each zone. TOC concentrations over the shelf were primarily controlled by river discharge. Macronutrient concentrations are higher nearer the basin, while micronutrients are replete in coastal surface waters. The confluence of these occurs at the Central Front, and produces the highest rates of NCP in the region. Outer Domain NCP rates (54 mmoles C m^{-2} d^{-1}) were very similar to Middle Domain NCP rates (52 mmoles C m^{-2} d^{-1}), and were higher in 2009 than in 2008. The penetration of river waters with high inorganic carbon and labile organic carbon concentrations resulted in a net heterotrophic signal in the Coastal Domain (-11 mmoles C m^{-2} d^{-1}) in 2009. However, the estimated total

production of organic carbon over the entire shelf was comparable between the two years (2008: ~103 Tg C yr^{-1}; 2009: ~97.2 Tg C yr^{-1}; Table 2.4) and consistent with other measurements of production estimates across the shelf (e.g., Lomas et al., 2012).

In 2008 and 2009, production was highest through the Central Front, and generally lowest in nearshore regions. River discharge appeared to dominate the carbon cycle of the Coastal Domain, while biological production likely exerts more control in the Outer and Middle Domains. However, it will be important to monitor these spatial variations as well as the rates of production and the fate of organic matter as environmental conditions in this region continue to change. As shown in previous studies (e.g. Hunt and Stabeno, 2002; Hunt et al., 2002), changes in the timing and fate of the production could have dramatic consequences for both benthic and pelagic organisms.

2.7 Tables

Table 2.1 Seasonally averaged surface TOC concentrations (2008 – 2009). Seasonally averaged (upper 30 m) TOC concentrations in 2008 and 2009. NC: northern Coastal Domain; SC: southern Coastal Domain; NM: northern Middle Domain; SM: southern Middle Domain; SO: southern Outer Domain. Average values include data from across the entire shelf. Error listed is one standard deviation from the shelf wide mean.

		2008		2009		
Station	Domain	TOC Spring *μmoles kg^{-1}*	TOC Summer *μmoles kg^{-1}*	TOC Spring *μmoles kg^{-1}*	TOC Summer *μmoles kg^{-1}*	TOC Fall *μmoles kg^{-1}*
SL2	NC	82.3	83.0	87.3	94.2	78.7
SL4	NC	70.5	87.2	82.8	86.8	78.9
MN2	SC	92.4	116.0	80.6	92.0	78.7
MN3	SC	89.5	113.5	82.0	91.9	77.5
NP1	SC	79.1	85.6	89.6	99.1	--
SL7	NM	69.6	84.9	72.9	93.4	77.6
SL10	NM	76.4	83.0	69.3	87.9	76.6
SL13	NM	75.8	83.2	69.1	88.2	75.0
SL14	NM	66.1	80.6	69.3	85.2	76.4
70M43	NM	69.0	81.9	71.3	82.4	78.4
70M47	NM	68.5	83.3	69.3	85.6	76.9
70M51	NM	69.4	80.9	70.0	83.5	75.7
70M55	NM	69.1	83.4	70.6	90.6	77.4
MN5	SM	85.4	82.0	71.5	89.4	76.8
MN7	SM	73.8	81.7	70.5	88.8	75.7
NP4	SM	72.0	86.2	73.3	86.0	--
NP6	SM	71.8	81.6	72.3	84.5	--
NP8	SM	75.1	82.3	70.8	85.1	--
NP10	SM	70.6	79.5	71.2	82.3	--
70M1	SM	70.4	85.6	72.3	84.1	--
70M3	SM	70.8	85.4	71.6	84.2	73.4
70M5	SM	71.1	84.3	73.3	84.9	77.5
70M9	SM	71.0	84.1	74.3	84.4	78.3
70M13	SM	70.7	82.5	74.4	90.1	73.6
70M17	SM	70.4	82.3	72.7	88.6	77.7
70M25	SM	70.2	84.5	72.4	84.4	79.4
70M29	SM	70.3	83.4	72.2	84.7	75.4
70M35	SM	71.4	85.1	77.5	86.7	82.8
70M39	SM	72.7	83.3	72.8	82.6	82.5
MN11	SO	70.1	84.1	69.5	82.8	70.5
MN13	SO	66.1	82.2	69.4	75.5	68.9
MN15	SO	65.2	81.2	68.0	75.6	66.8
MN18	SO	65.6	80.0	66.1	79.1	65.1
MN20	SO	65.6	74.9	65.4	74.3	--
NP12	SO	75.2	79.6	70.4	80.1	--
NP15	SO	67.2	79.3	71.4	71.4	--
Avg.		72.5 ± 6.3	84.5 ± 7.8	73.0 ± 5.3	85.3 ± 5.7	76.0 ± 4.1

Table 2.2 Seasonally averaged NCP parameters (2009). Seasonally averaged (upper 30 m) nDIC concentration, nDIC deficit between spring and summer, calcium carbonate correction factor, rates of NCP based on seasonal drawdown of nDIC (NCP_{nDIC}) and rates of NCP based on seasonal drawdown of nDIC and corrected for the formation and dissolution of calcium carbonate minerals (NCP-$CaCO_3$) by station in 2009. Average values include data from across the entire shelf. Error listed is one standard deviation from the mean.

Stn.	Do.	Spring	nDIC spring	Summer	nDIC summer	Days	nDIC deficit	$CaCO_3$ corr.	NCP_{nDIC}	NCP - $CaCO_3$
			µmoles kg^{-1}		*µmoles kg^{-1}*		*µmoles kg^{-1}*	*µmoles kg^{-1}*	*mmoles C m^{-2} d^{-1}*	*mmoles C m^{-2} d^{-1}*
SL2	NC	18-Apr	2333	7-Jul	2357	80	-24	-7.8	-9.4	-6.3
SL4	NC	18-Apr	2325	7-Jul	2329	80	-4	-0.6	-1.4	-1.2
MN2	SC	7-Apr	2301	1-Jul	2306	85	-4	-4.8	-1.6	0.2
MN3	SC	7-Apr	2354	1-Jul	2301	85	53	-3.5	19.3	20.5
NP1	SC	20-Apr	2338	22-Jun	2328	63	10	-10.4	4.9	10.0
SL7	NM	16-Apr	2299	7-Jul	2218	82	81	-24.7	30.3	39.6
SL10	NM	16-Apr	2305	7-Jul	2213	82	92	-19.1	34.5	41.7
SL13	NM	15-Apr	2323	8-Jul	2175	84	148	-7.4	54.3	57.0
SL14	NM	15-Apr	2324	8-Jul	2174	84	150	-10.8	55.1	59.0
70M43	NM	7-May	2270	9-Jul	2145	63	125	10.8	61.3	56.0
70M47	NM	5-May	2305	9-Jul	2162	65	143	-2.0	67.9	68.8
70M51	NM	5-May	2323	9-Jul	2162	65	161	0.6	76.2	75.9
70M55	NM	5-May	2326	8-Jul	2161	64	165	-10.1	79.4	84.3
MN5	SM	8-Apr	2298	1-Jul	2243	84	55	-10.9	20.2	24.2
MN7	SM	9-Apr	2286	2-Jul	2123	84	163	-10.8	59.8	63.8
NP4	SM	21-Apr	2321	22-Jun	2267	62	54	-5.0	26.6	29.1
NP6	SM	21-Apr	2309	22-Jun	2160	62	149	-4.0	74.1	76.1
NP8	SM	22-Apr	2284	22-Jun	2108	61	176	-5.9	89.0	92.0
NP10	SM	22-Apr	2291	23-Jun	2186	62	105	4.0	52.3	50.3
70M1	SM	10-May	2280	12-Jul	2200	63	80	4.3	39.2	37.1
70M3	SM	10-May	2268	11-Jul	2133	62	136	2.6	67.5	66.2
70M5	SM	10-May	2276	11-Jul	2155	62	121	2.7	60.3	58.9
70M9	SM	9-May	2292	11-Jul	2317	63	-25	-1.8	-12.3	-11.4
70M13	SM	9-May	2285	11-Jul	2109	63	176	1.6	86.0	85.3
70M17	SM	9-May	2302	11-Jul	2136	63	166	5.1	81.3	78.8
70M25	SM	9-May	2301	10-Jul	2165	62	136	0.0	67.7	67.7
70M29	SM	8-May	2267	10-Jul	2204	63	63	1.8	31.0	30.1
70M35	SM	8-May	2301	10-Jul	2171	63	131	8.5	63.9	59.7
70M39	SM	7-May	2281	9-Jul	2146	63	134	8.4	65.8	61.7
MN11	SO	9-Apr	2285	2-Jul	2109	84	176	0.6	64.7	64.5
MN13	SO	10-Apr	2300	2-Jul	2155	83	145	9.2	54.0	50.5
MN15	SO	11-Apr	2266	3-Jul	2138	83	128	15.5	47.5	41.8
MN18	SO	11-Apr	2267	3-Jul	2157	83	110	5.5	40.7	38.7
MN20	SO	12-Apr	2279	4-Jul	2139	83	139	1.0	51.7	51.3
NP12	SO	24-Apr	2259	23-Jun	2123	60	136	-4.1	69.8	71.9
NP15	SO	23-Apr	2250	23-Jun	2170	61	81	-3.3	40.7	42.4
Average			2297 ± 24		2190 ± 70	71	106 ± 59		47.6 ± 27.5	48.2 ± 26.8

Table 2.3 Estimates of calculated export production (2008 – 2009). Estimates of calculated export production ($POC_{(exp)}$) at selected stations in Tg C yr^{-1} in 2008 and 2009. NC: northern Coastal Domain; SC: southern Coastal Domain; NM: northern Middle Domain; SM: southern Middle Domain; SO: southern Outer Domain. Error listed on domain averaged is one standard deviation from the mean. Blank values (--) in 2008 arise from unavailable NCP estimates for those stations. Blank values (--) in 2009 arise from negative NCP estimates.

		2008			2009		
Station	Domain	ΔnTOC *μmoles kg^{-1}*	$POC_{(exp)}$ *Tg C yr^{-1}*	$POC_{(exp)}$: NCP	ΔnTOC *μmoles kg^{-1}*	$POC_{(exp)}$ *Tg C yr^{-1}*	$POC_{(exp)}$: NCP
SL2	NC	5.3	14.5	107.2%	10.9	-16.1	--
SL4	NC	21.9	17.7	79.7%	6.7	-4.7	--
MN2	SC	--	--	--	14.0	-3.5	--
MN3	SC	26.2	6.6	69.0%	11.9	7.9	72.9%
NP1	SC	9.4	11.4	74.7%	12.0	-0.5	--
SL7	NM	19.0	15.1	94.1%	29.5	14.3	48.5%
SL10	NM	9.7	26.7	78.1%	25.3	18.6	60.0%
SL13	NM	10.0	13.1	66.5%	24.3	33.8	79.6%
SL14	NM	--	--	--	19.7	35.7	81.0%
70M43	NM	18.6	--	--	12.4	41.1	98.5%
70M47	NM	18.8	14.9	72.0%	19.8	43.6	85.0%
70M51	NM	--	--	--	16.1	51.1	90.4%
70M55	NM	20.0	29.7	85.3%	26.0	49.9	79.4%
MN5	SM	5.8	13.7	97.2%	22.1	10.1	50.0%
MN7	SM	1.4	16.0	182.9%	21.0	43.4	81.7%
NP4	SM	16.1	17.7	69.5%	14.6	16.2	66.7%
NP6	SM	--	--	--	14.7	55.6	87.8%
NP8	SM	--	--	--	16.8	67.0	87.5%
NP10	SM	10.1	22.7	71.7%	12.3	38.5	91.8%
70M1	SM	--	--	--	13.3	27.2	88.1%
70M3	SM	16.1	5.8	51.3%	14.4	50.2	91.1%
70M5	SM	--	--	--	13.9	44.4	90.5%
70M9	SM	--	--	--	11.6	-15.0	--
70M13	SM	14.0	15.2	80.9%	18.3	64.2	90.4%
70M17	SM	--	--	--	18.6	60.1	91.6%
70M25	SM	14.4	21.2	85.6%	13.8	50.7	89.9%
70M29	SM	11.9	24.2	89.5%	14.0	20.1	80.2%
70M35	SM	--	--	--	9.3	49.4	99.3%
70M39	SM	--	--	--	10.5	50.5	98.3%
MN11	SO	19.7	15.2	141.8%	15.3	33.7	91.7%
MN13	SO	20.2	20.6	117.4%	5.4	29.6	102.8%
MN15	SO	20.8	16.9	88.7%	7.2	25.6	107.3%
MN18	SO	17.2	20.7	81.3%	14.0	20.3	91.9%
MN20	SO	--	--	--	8.7	27.6	94.4%
NP12	SO	4.9	9.8	51.9%	10.4	36.8	89.7%
NP15	SO	--	--	--	0.1	23.2	95.9%
AVG	NC			93.5 ± 19.4 %			--
AVG	SC			71.8 ± 4.0 %			72.9 ± -- %
AVG	NM			79.2 ± 10.9 %			77.8 ± 16.1 %
AVG	SM			91.1 ± 39.7 %			85.7 ± 12.5 %
AVG	SO			96.2 ± 34.5 %			96.2 ± 6.4 %

Table 2.4 NCP and annual production of organic carbon (2008 – 2009). NCP (mmoles C m^{-2} d^{-1}) and annual production of organic carbon based on NCP-$CaCO_3$ (Tg C yr^{-1}) for each domain in 2008 and 2009. NCP estimates were based on calcium-carbonate corrected seasonal drawdown of nDIC (NCP-$CaCO_3$). NC: northern Coastal Domain; SC: southern Coastal Domain; NM: northern Middle Domain; SM: southern Middle Domain; SO: southern Outer Domain. Error listed is one standard deviation from the domain mean.

Do.	2008 NCP *mmoles C m^{-2} d^{-1}*	2009 NCP *mmoles C m^{-2} d^{-1}*	Area *m^2*	2008 NCP *Tg C yr^{-1}*	2009 NCP *Tg C yr^{-1}*
NC	17.5 ± 4	-11.4 ± 9	2.7×10^{11}	20.7 ± 5	-13.5 ± 11
SC	23.7 ± 7	7.8 ± 13	1.2×10^{11}	12.5 ± 4	4.1 ± 7
Total				33.1 ± 6	-9.4 ± 13
NM	36.7 ± 11	43.0 ± 36	1.7×10^{11}	27.4 ± 8	32.0 ± 27
SM	24.8 ± 10	52.3 ± 32	1.9×10^{11}	20.6 ± 8	43.6 ± 27
Total				48.0 ± 11	75.6 ± 38
SO	35.5 ± 6	54.4 ± 16	1.3×10^{11}	20.2 ± 3	31.0 ± 9

2.8 Figures

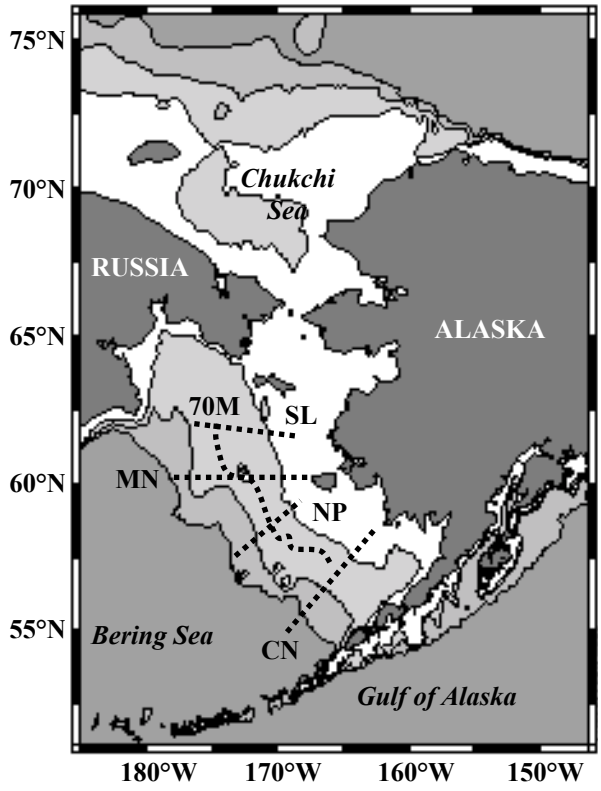

Figure 2.1 Map of the Bering and Chukchi Seas. Map of the Bering and Chukchi Seas, showing the locations of the five transect lines (SL, MN, NP, CN and 70M) in this study. Shading indicates bottom topography, with delineations at 50 m (Inner Front), 100 m (Central Front), and 250 m (Shelf Break Front).

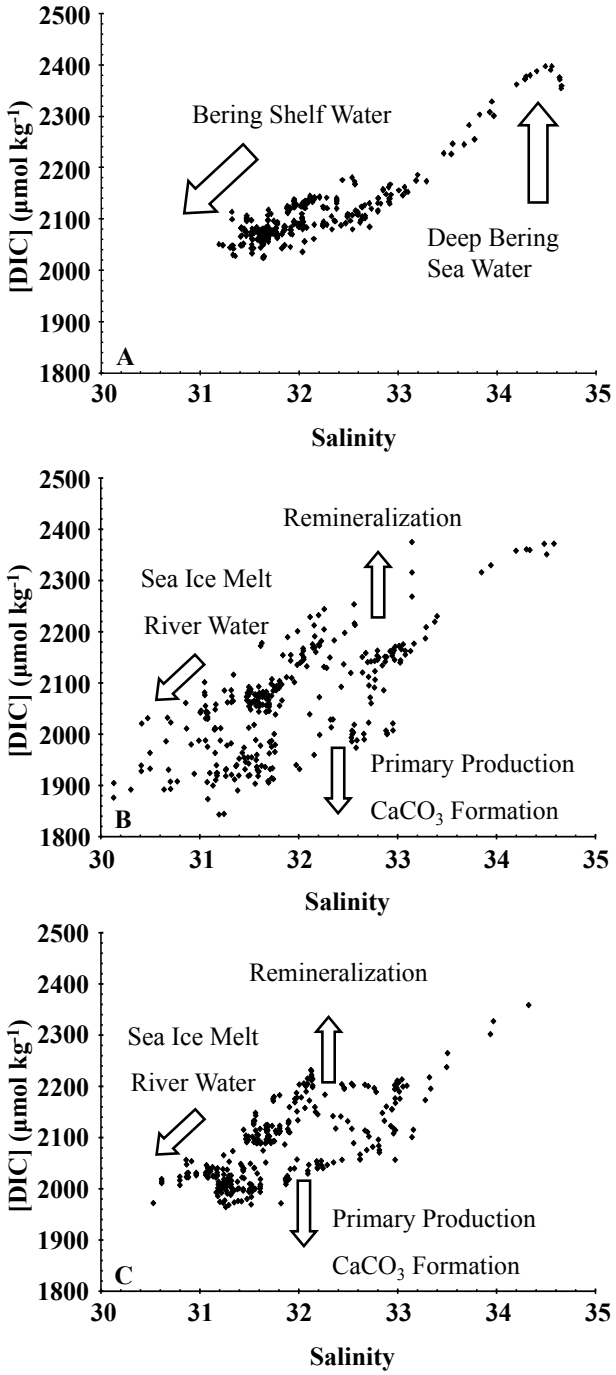

Figure 2.2 Seasonal DIC concentrations relative to salinity (2009). (A) Spring, 2009. (B) Summer, 2009. (C) Fall, 2009. Arrows show the direction of changes caused by freshwater inputs, sea ice melt, primary production, remineralization, and calcium carbonate formation.

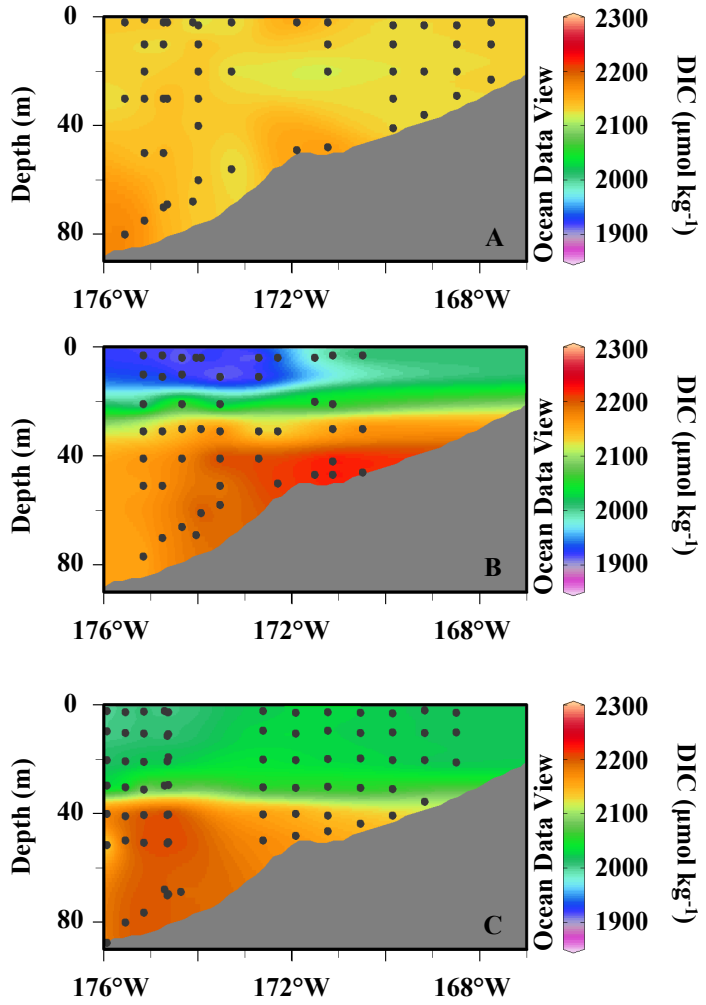

Figure 2.3 Seasonal DIC concentrations across the SL line (2009).

Seasonal DIC concentrations (µmoles kg^{-1}) across the SL line during 2009. (A) Spring, 2009. (B) Summer, 2009. (C) Fall, 2009.

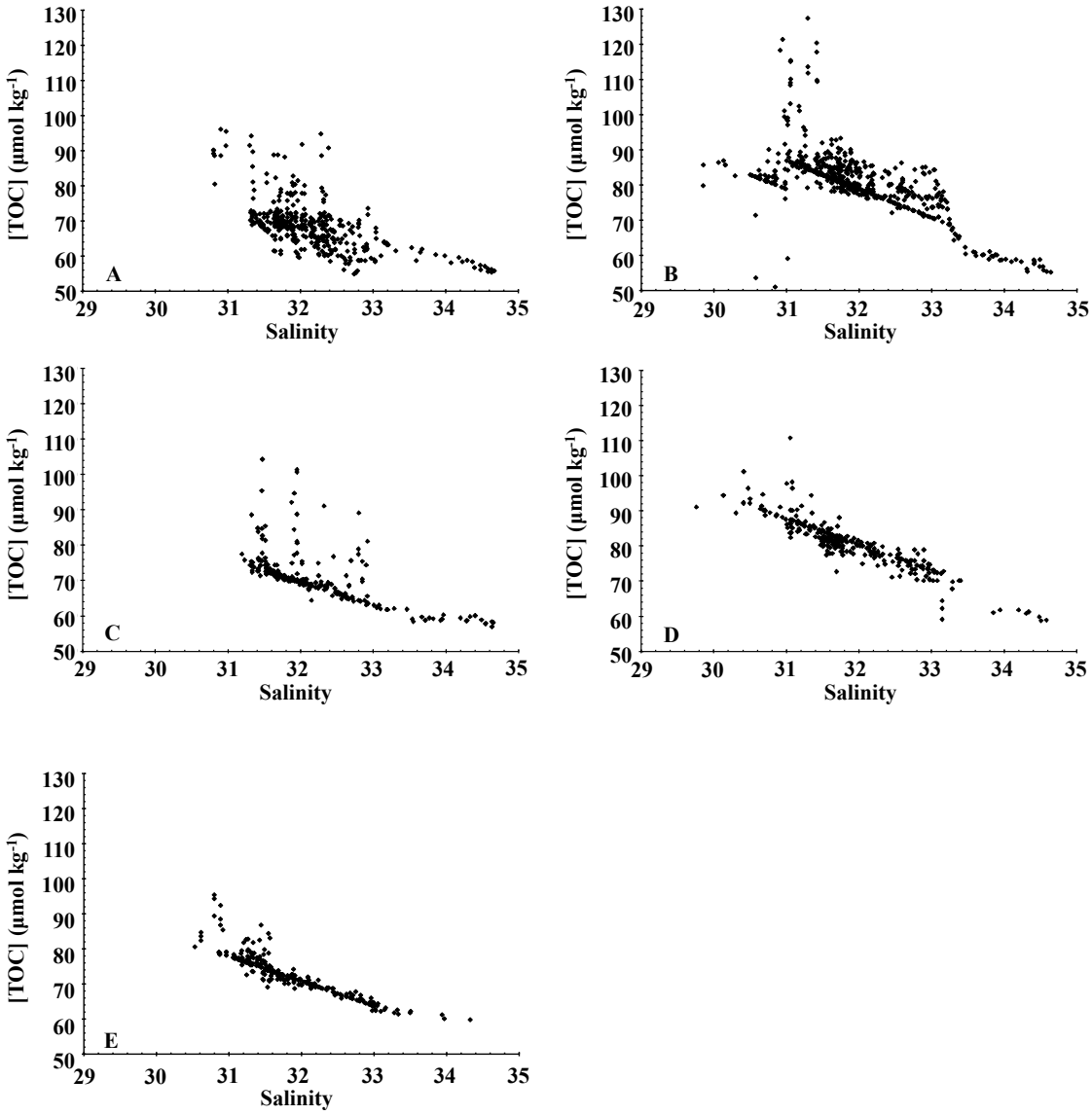

Figure 2.4 Seasonal TOC concentrations relative to salinity (2008 – 2009). Seasonal TOC concentrations (µmoles kg^{-1}) in 2008 and 2009 relative to salinity. TOC and salinity were well correlated in each season of both years. (A) Spring, 2008. (B) Summer, 2008. (C) Spring, 2009. (D) Summer, 2009. (E) Fall, 2009.

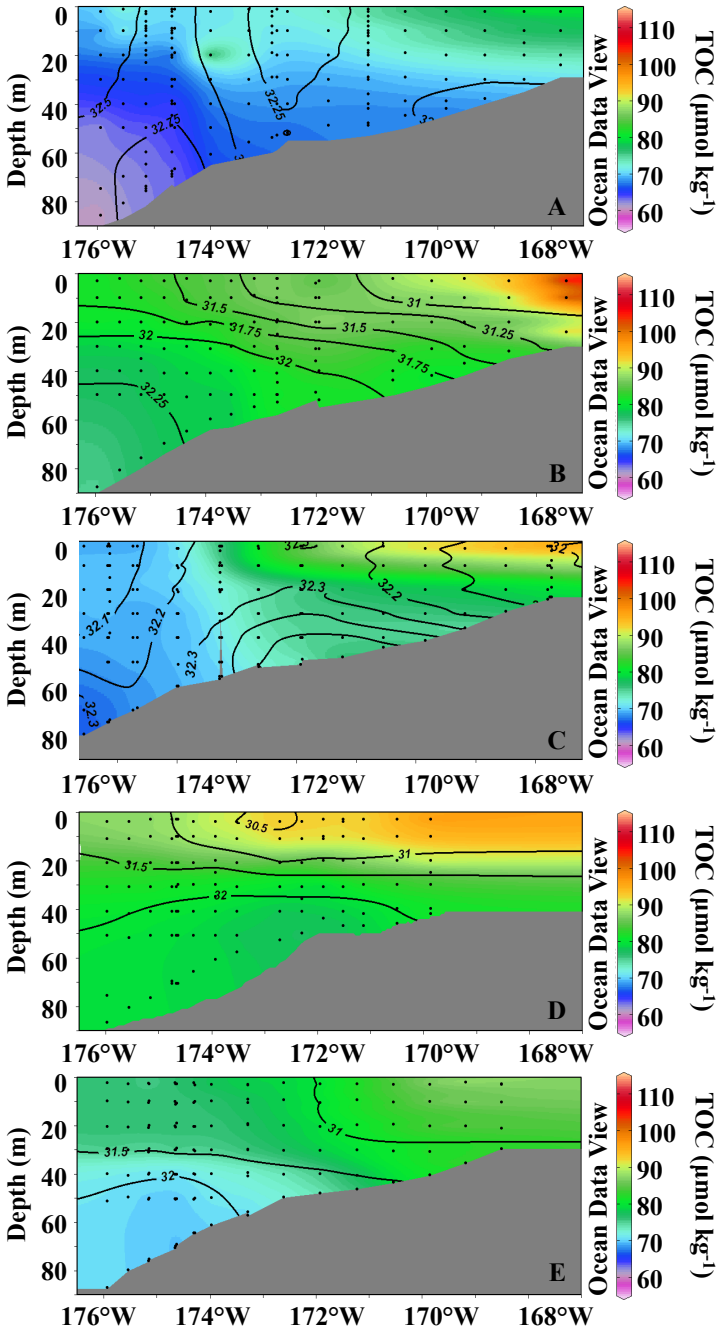

Figure 2.5 Seasonal TOC concentrations and salinity (SL line, 2008 – 2009). Seasonal TOC concentrations (µmoles kg^{-1} shading) and salinity (contour lines) across the SL line during 2008 and 2009. (A) Spring, 2008. (B) Summer, 2008. (C) Spring, 2009. (D) Summer, 2009. (E) Fall, 2009.

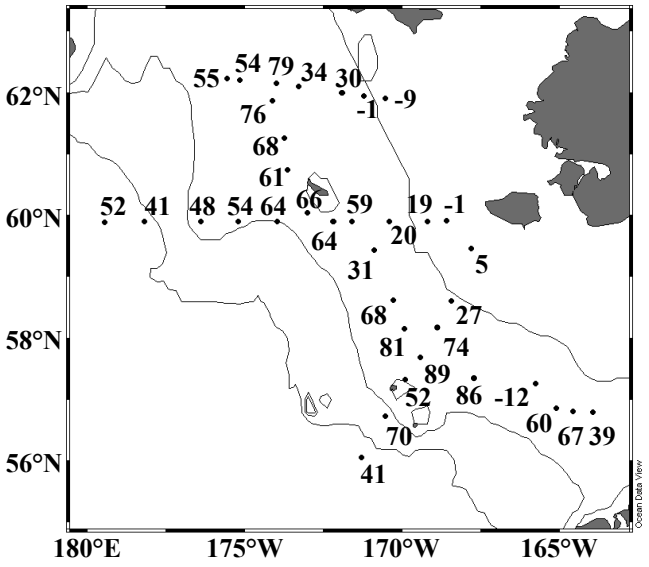

Figure 2.6 Net community production (2009). Net community production (mmoles C m^{-2} d^{-1}) based on the seasonal consumption of nDIC and corrected for the formation and dissolution of calcium carbonate minerals across the shelf.

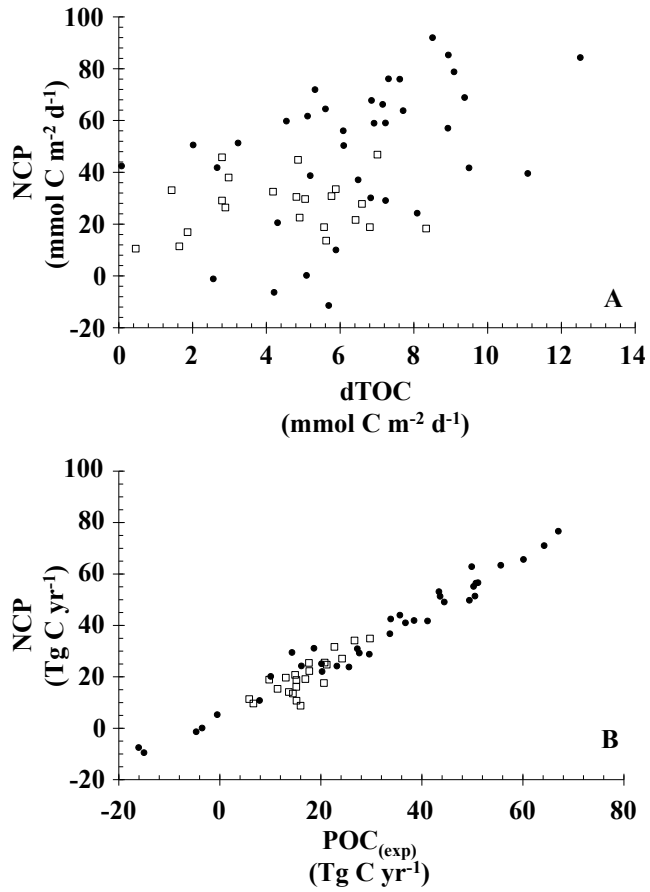

Figure 2.7 Relationship between NCP, TOC, and POC (2008 – 2009). (A) Relationship between NCP and accumulated TOC in the upper 30 m. (B) Approximated values for exported POC calculated as the difference between NCP and accumulated TOC. 2008 values are indicated by open boxes, while 2009 values are indicated by closed circles. In 2008 and 2009, there was no relationship between NCP and accumulated TOC (2008: $R^2 = 0.12$; 2009: $R^2 = 0\ .18$). By contrast, $POC_{(exp)}$ and NCP are strongly correlated in both years (2008: $R^2 = 0.70$; 2009: $R^2 = 0.97$).

2.9 Acknowledgements

The authors thank the officers and crew of the USCGC *Healy*, the R/V *Knorr*, and NOAA ship *Miller Freeman* for their work in supporting our science during multiple cruises. We also thank the hydrographic team from NOAA-PMEL for providing hydrographic data and assisting in sample collection, accessible through the EOL data archive supported by NSF and NOAA. Finally, we thank our colleagues in the BEST-BSIERP Project, supported by NSF and NPRB. This manuscript is BEST-BSIERP contribution no. 44. The work presented in this paper was supported by the U.S. Bureau of Ocean Energy Management and Regulation, Alaska OCS Region and the Coastal Marine Institute at the University of Alaska Fairbanks under Agreement M08AC12645. Statement of Work: Cross, J.N. Collected the samples in 2009, performed the analysis, generated the figures, and wrote the text. Mathis, J.T., and Bates, N.R., collected the samples in 2008 and provided guidance in manuscript preparation.

2.10 References

Agatova, A.I., Arzhanova, N.V., Torgunova, N.I., 1999. Organic matter of the Bering Sea, in: Louglin, T.R., Ohtani, K. (Eds.), Dynamics of the Bering Sea. University of Alaska-Fairbanks, Fairbanks, AK, pp. 261−283.

Aguilar-Islas, A.M., Hurst, M.P., Buck, K.N., Sohst, B., Smith, G.J., Lohan, M.C., et al., 2007. Micro- and macronutrients in the southeastern Bering Sea: Insight into iron-replete and iron-depleted regimes. Prog. Oceanogr. 73, 99–126.

Azova, N.V., 1964. Primary productivity of the Pribilof-Bristol area of the Bering Sea, in: Moiseev, P.A. (Ed.), Soviet Fisheries Investigations in the Northeastern Pacific, Part III. Pishchevaya Promyshlennost Publishing, Moscow, pp. 137–143.

Bates, N.R., 2001. Interannual variability of oceanic CO_2 and biogeochemical properties in the Western North Atlantic subtropical gyre. Deep Sea Res. II. 48, 1507–1528.

Bates, N.R., Mathis, J.T., Jeffries, M.A., 2010. Air-sea CO_2 fluxes on the Bering Sea shelf. Biogeosci. 7, 7271–7314.

Cauwet, G., 2002. DOM in the coastal zone, in: Hansell, D.A., Carlson, C.A. (Eds.), Biogeochemistry of Marine Dissolved Organic Matter. Academic Press, San Diego, CA, pp. 579–610.

Coachman, L.K., Charnell, R.L., 1979. On lateral water mass interaction–a case study, Bristol Bay, Alaska. J. Phys. Oceanogr. 9, 278–297.

Coachman, L.K., 1986. Circulation, water masses, and fluxes on the southeastern Bering Sea shelf. Cont. Shelf Res. 5, 23–108.

Codispoti, L.A., Friederich, G.E., Iverson, R.L., Hood, D.W., 1982. Temporal changes in the inorganic carbon system of the southeastern Bering Sea during spring 1980. Nature. 296, 242–245.

Codispoti, L.A., Friederich, G.E., Hood, D.W., 1986. Variability in the inorganic carbon system over the southeastern Bering Sea shelf during spring 1980 and spring-summer 1981. Cont. Shelf Res. 5(1-2), 133–160.

Cooper, L.W., Grebmeier, J.M., Larson, I.L., Egorov, V.G., Theodorakis, C., Kelly, H.P., et al., 2002. Seasonal variation in water column processes and sedimentation of organic materials in the St. Lawrence Island polynya region, Bering Sea. Mar. Ecol. Prog. Ser. 226, 13–26.

Coyle, K.O., Pinchuk, A.I., 2002. Climate-related differences in zooplankton density and growth on the inner shelf of the southeastern Bering Sea. Prog. Oceanogr. 55(1-2), 177–194.

Dittmar, T., Kattner, G., 2003. The biogeochemistry of the river and shelf ecosystem of the Arctic Ocean: a review. Mar. Chem. 83, 103–120.

Francis, R.C., Hare, S.R., Hollowed, A.B., Wooster, W.S., 1998. Effects of interdecadal climate variability on the oceanic ecosystems of the NE Pacific. Fish. Oceanogr. 7, 1–21.

Franks, P.J.S., 1992. Sink or swim: accumulation of biomass at fronts. Mar. Ecol. Prog. Ser. 82, 1–12.

Fukuchi M., Sasaki, H., Hattori, H., Matsuda, O., Tanimura, A., Handa, N., et al., 1993. Temporal variability of particulate flux in the northern Bering Sea. Cont. Shelf Res. 13, 693–704.

Gosselin, M., Levasseur, M., Wheeler, P.A., Horner, R.A., Booth, B.C., 1997. New measurements of phytoplankton and ice algal production in the Arctic Ocean. Deep Sea Res. II. 44(8), 1623–1644.

Grebmeier, J.M., 1993. The western Arctic shelf-basin interactions project. Arct. Res. U.S. 17, 24–36.

Grebmeier, J.M., McRoy, C.P., 1989. Pelagic-benthic coupling on the shelf of the northern Bering and Chukchi Seas III: Benthic food supply and carbon cycling. Mar. Ecol. Prog. Ser. 53, 79–91.

Grebmeier, J.M., Cooper, L.W., 1995. Influence of the St. Lawrence polynya on the Bering Sea benthos. J. Geophys. Res. 100, 4439–4460.

Grebmeier, J.M., Dunton, K.H., 2000. Benthic processes in the northern Bering/Chukchi Seas: Status and global change, in: Huntington, H.P. (Ed.), Impacts of Changes in

Sea Ice and Other Environmental Parameters in the Arctic. Marine Mammal Commission Workshop, Girdwood, AK, pp. 80–93.

Grebmeier, J.M., McRoy, C.P., Feder, H.M., 1988. Pelagic-benthic coupling on the shelf of the northern Bering and Chukchi Seas I: Food supply source and benthic biomass. Mar. Ecol. Prog. Ser. 48, 57–67.

Grebmeier, J.M., Overland, J.E., Moore, S.E., Farley, E.V., Carmack, E.C., Cooper, L.W., et al., 2006a. A major ecosystem shift in the Northern Bering Sea. Science. 311(5766), 1461–1464.

Grebmeier, J.M., Cooper, L.W., Feder, H.M., Sirenko, B.I., 2006b. Ecosystem dynamics of the Pacific-Influenced Northern Bering and Chukchi Seas in the Amerasian Arctic. Prog. Oceanogr. 71, 331–361.

Grebmeier, J.M., Smith Jr., W.O., Conover, R.B., 1995. Biological processes on Arctic continental shelves: ice-ocean-biotic interactions, in: Smith Jr., W.O., Grebmeier, J.M. (Eds.), Arctic Oceanography: Marginal Ice Zones and Continental Shelves. American Geophysical Union, Washington, D.C., pp. 231–261.

Gueguen, C., Guo, L., Wang, D., Tanaka, N., Hung, C.C., 2006. Chemical characteristics and origin of dissolved organic matter in the Yukon River. Biogeochem. 77, 139–155.

Guo, L., Tanaka, T., Wang, D., Tanaka, N., Murata, A., 2004. Distributions, speciation and stable isotope composition of organic matter in the southeastern Bering Sea. Mar. Chem. 91, 211–226.

Hansell, D.A., Carlson, C.A., 1998. Deep ocean gradients in dissolved organic carbon concentrations. Nature. 395, 263–266.

Hansell, D.A., Bates, N.R., Carlson, C.A., 1997. Predominantly vertical losses of carbon from the surface layer of the Equatorial Pacific Ocean. Nature. 386, 59–61.

Hansell, D.A., Kadko, D., Bates, N.R., 2004. Degradation of terrigenous dissolved organic carbon in the western Arctic Ocean. Science. 304, 858–861.

Hollowed, A.B., Hare, S.R., Wooster, W.S., 2001. Pacific basin climate variability and patterns of northeast Pacific marine fish production. Prog. Oceanogr. 49, 257–282.

Hunt Jr., G.L., Stabeno P.J., 2002. Climate change and the control of energy flow in the southeastern Bering Sea. Prog. Oceanogr. 55, 5–22.

Hunt Jr., G.L. Stabeno, P.J., Walters, G., Sinclair, E., Brodeur, R.D., Napp, J.M., et al., 2002. Climate change and control of the southeastern Bering Sea pelagic ecosystem. Deep Sea Res. II. 49(26), 5821–5853.

Hurst, M.P., Aguilar-Islas, A.M., Bruland, K.W., 2010. Iron in the southeastern Bering Sea: Elevated leachable particulate Fe in shelf bottom waters as an important source for surface waters. Cont. Shelf. Res. 30, 467–480.

Ivenakov, V.N., 1961. Primary production in the Bering Sea. Transl. Inst. Oceanol. Acad. Sci. U.S.S.R. 51, 36–56.

Kachel, N.B., Hunt Jr., G.L., Salo, S.A., Schumacher, J.D., Stabeno, P.J., Whitledge, T.E., 2002. Characteristics of the inner front of the southeastern Bering Sea. Deep Sea Res. II. 49, 5889–5909.

Kattner, G., Lobbes, J.M, Fitznar, H.P., Engbrodt, R., Nöthig, E.-M., Lara, R.J., 1999. Tracing dissolved organic substances and nutrients from the Lena River through the Laptev Sea (Arctic). Mar. Chem. 65, 25–39.

Lee, K., 2001. Global net community production estimated from the annual cycle of surface water total dissolved inorganic carbon. Limnol. Oceanogr. 46(6), 1287–1297.

Lomas, M.W., Moran, S.B., Casey, J.R., Bell, D.W., Tiahlo, M., Whitefield, J., et al., 2012. Spatial and seasonal variability of primary production on the Eastern Bering Sea shelf. Deep Sea Res. II. 65-70, 126−140.

Mackas, D.L., Denman, K.L., Abbott, M.K., 1985. Plankton patchiness: biology in the physical vernacular. Mar. Sci. Bull. 37, 652–674.

Mantoura, R.F.C., Woodward, E.M.S., 1983. Conservative behavior of riverine dissolved organic carbon in the Severen Estuary: Chemical and geochemical implications. Geochim. Cosmochim. Acta. 47, 1293–1309.

Mathis, J.T., Hansell, D.A., Kadko, D., Bates, N.R., Cooper, L.W., 2007. Determining net dissolved organic carbon production in the hydrographically complex western Arctic Ocean. Limnol. Oceanogr. 52(5), 1789–1799.

Mathis, J.T., Cross, J.N., Bates, N.R., Moran, S.B., Lomas, M.W., Stabeno, P.J., 2010. Seasonal distribution of dissolved inorganic carbon and net community production on the Bering Sea shelf. Biogeosci. 7, 1769–1787.

Mathis, J.T., Cross, J.N., Bates, N.R., 2011. The role of ocean acidification in systemic carbonate mineral suppression in the Bering Sea. Geophys. Res. Lett. 38, L19602.

McRoy, C., Whitledge, T.E., Springer, A.M., Simpson, E.P. 2001. The nitrate front in the Bering Sea: is this an iron curtain? Oral presentation abstract. http://www.aslo.org/meetings/aslomeetings.html.

Millero, F.J., 2008. The Marine Inorganic Carbon Cycle. Chem. Rev. 107, 308–341.

Moran, S.B., Lomas, M.W., Kelly, R.P., Gradinger, R., Granger, J., Iken, K., et al., 2012. Sea ice control of lower trophic carbon partitioning in the Eastern Bering Sea. Deep Sea Res. II. 65-70, 84−97.

Okkonen, S.R., Schmidt, G.M., Cokelet, E.D., Stabeno, P.J., 2004. Satellite and hydrographic observations of the Bering Sea 'Green Belt.' Deep Sea Res. II. 51, 1033–1051.

Overland, J.E., Stabeno, P.J., 2004. Is the climate of the Bering Sea warming and affecting the ecosystem? EOS Trans. Am. Geophys. Un. 85(33), 309.

Rember, R.D., Trefry, J.H., 2004. Increased concentrations of dissolved trace metals and organic carbon during snowmelt in rivers of the Alaskan Arctic. Geochim. Cosmochim. Acta. 68, 477–489.

Rho, T., Whitledge, T.E., 2007. Characteristics of seasonal and spatial variations of primary production over the southeastern Bering Sea shelf. Cont. Shelf Res. 27, 2556–2569.

Sambrotto, R.N., and Goering, J.J., 1983. Interannual variability of phytoplankton and zooplankton production on the southeast Bering Sea shelf, in: Wooster, W.S. (Ed.), From Year-to-Year: Interannual Variability of the Environment and Fisheries of the Gulf of Alaska and the Eastern Bering Sea. Washington State Sea Grant, Seattle, WA, pp. 161−177.

Sambrotto, R.N., Niebauer, H.J., Goering, J.J., Iverson, R.L., 1986. Relationships among vertical mixing, nitrate uptake, and phytoplankton growth during the spring bloom in the southeast Bering Sea middle shelf. Cont. Shelf. Res. 5, 161–198.

Sapozhnikov, V.V., Naletova, I.A., 1995. Studies of the biohydrochemical structure of the euphotic layer and primary production in the Bering Sea. Russ. Acad. Sci. Oceanol. 35(2), 189–196.

Schumacher, J.D. Stabeno, P.J., 1998. The continental shelf of the Bering Sea, in: The Sea. Vol. 11. John Wiley and Sons Inc., New York, NY, pp. 789–822.

Schumacher, J.D., Bond, N.A., Brodeur, R.D., Livingston, P.A., Napp, J.M., Stabeno, P.J., 2002. Climate changes in the southeastern Bering Sea and some consequences for biota, in: Hemple, G., Sherman K. (Eds.), Large Marine Ecosystems of the World: Trends in Exploitation, Protection and Research. Elsevier, Amsterdam, pp. 17–39.

Simpson, E., McRoy, C., 1999. Model evidence of a Bering Sea iron curtain. Oral presentation abstract. http://www.aslo.org/meetings/aslomeetings.html.

Sorokin, Y.I., Mikheev, V.N., 1979. Characteristics of the Peruvian upwelling ecosystem. Hydrobiol. 62, 165–189.

Spitzy, A., Leenheer, J., 1991. Dissolved organic carbon in rivers, in: Degens, E.T., Kempe, S., Richey, J.E. (Eds.), Biogeochemistry of Major World Rivers. Wiley Interscience, Chichester, U.K., pp. 213–232.

Springer, A.M., 1998. Is it all climate change? Why marine bird and mammal populations fluctuate in the North Pacific, in: Holloway, G., Muller, P., Henderson, D. (Eds.),

Biotic Impacts of Extratropical Climate Change in the Pacific. University of Hawaii at Manoa, Honolulu, HI, pp. 109–119.

Springer, A.M., McRoy, C.P., 1993. The paradox of food webs in the northern Bering Sea III: Patterns of primary production. Cont. Shelf Res. 13(5-6), 575−599.

Springer, A.M., McRoy, C.P., Flint, M.V., 1996. The Bering Sea Green Belt: shelf-edge processes and ecosystem production. Fish. Oceanogr. 5(3-4), 205–223.

Stabeno, P.J., Schumacher, J.D., Ohtani, K., 1999. The physical oceanography of the Bering Sea, in: Loughlin, T.R., Ohtani K. (Eds.), Dynamics of the Bering Sea: A Summary of Physical, Chemical, and Biological Characteristics, and a Synopsis of Research on the Bering Sea. North Pacific Marine Science Organization (PICES) University of Alaska Sea Grant, Fairbanks, AK, pp. 1–28.

Stabeno, P.J., Kachel, N.B., Sullivan, M., Whitledge, T.E., 2002. Variability of physical and chemical characteristics along the 70-m isobath of the southeastern Bering Sea. Deep Sea Res. II. 49, 5931–5943.

Stabeno, P.J., Sonnerup, R., Mordy, C.W., Whitledge, T.E., 3-21-2011a. HLY-08-02 CTD and Nutrient Data. Bering Sea Project Data Archive. http://data.eol.ucar.edu/codiac/dss/id=102.058.

Stabeno, P.J., Sonnerup, R., Mordy, C.W., Whitledge, T.E., 3-21-2011b. HLY-08-03 CTD and Nutrient Data. Bering Sea Project Data Archive. http://data.eol.ucar.edu/codiac/dss/id=102.059.

Stabeno, P.J., Sonnerup, R., Mordy, C.W., Whitledge, T.E., 3-21-2011c. HLY-09-02 CTD and Nutrient Data. Bering Sea Project Data Archive. http://data.eol.ucar.edu/codiac/dss/id=102.142.

Stabeno, P.J., Sonnerup, R., Mordy, C.W., Whitledge, T.E., 3-21-2011d. Knorr 195-10 2009 CTD and Nutrient Data. Bering Sea Project Data Archive. http://data.eol.ucar.edu/codiac/dss/id=102.198.

Striegl, R.G., Aiken, G.R., Dornblaser, M.M., Raymond, P.A., Wickland, K.P., 2005. A decrease in discharge-normalized DOC export by the Yukon River during summer through autumn. Geophys. Res. Lett. 32, L21413.

Striegl, R.G., Dornblaser, M.M., Aiken, G.R., Wickland, K.P., Raymond, P.A., 2007. Carbon export and cycling by the Yukon, Tanana, and Porcupine rivers, Alaska, 2001 – 2005. Water Resour. Res. 43, W02411.

USGS Streamflow Data, 2010. Hydrological Unit Code 19040805. Accessed November 2010. http://nwis.waterdata.usgs.gov.

Whitledge, T.E., Reeburgh, W.S., Walsh, J.J., 1986. Seasonal inorganic nitrogen distributions and dynamics in the southeastern Bering Sea. Cont. Shelf Res. 5, 109–132.

Williams, P.J., 1993. On the definition of phytoplankton production terms. ICES Mar. Sci. Symp. 197, 9–19.

Wyllie-Escheveria, T., Wooster, W.S., 1998. Year-to-year variations in Bering Sea ice cover and some consequences for fish distributions. Fish. Oceanogr. 7(2), 159–170.

Chapter 3:

Integrated assessment of the carbon budget in the southeastern Bering Sea[2]

3.0 Abstract

During the primary field program for the Bering Ecosystem Study (2008 – 2010), independent seasonal estimates of net primary production (*NPP*), net community production (*NCP*), vertical export production (C_{exp}), and benthic carbon consumption (*BCC*) were used to construct a shelf-wide carbon budget for the southeastern Bering Sea. Here, we quantify the production, utilization, and transport of *NPP* on the annual scale for the southeastern shelf region of the Bering Sea (spatially partitioned into Outer, Middle, and Coastal Domains). We observed that approximately 25% and 30% of *NPP* on the shelf is exported horizontally for the Middle and Outer Domains, respectively. This horizontal transport was the dominant mode of carbon export in the Outer Domain, exceeding C_{exp} by more than 30 g C m^{-2} yr^{-1} (99 g C m^{-2} yr^{-1} compared to 67 g C m^{-2} yr^{-1}, respectively). In the Middle Domain, C_{exp} was more prominent than lateral transport (65 g C m^{-2} yr^{-1} and 46 g C m^{-2} yr^{-1}, respectively), and vertically exported carbon was more efficiently recycled in this Domain than in the Outer Domain (53% and 32% of C_{exp} respectively). In the Coastal Domain of the southeastern Bering Sea shelf, lateral transport was a source of carbon to the bottom layer, with estimated input of carbon exceeding *NPP* by as much as 54 g C m^{-2} yr^{-1}. While the source of this additional carbon is unknown, one possible source is transport from the Middle Domain during wind events that induce coastal convergence. Overall, the combined carbon reservoir attributed to burial and transport in the Middle and Outer Domains is similar to a previous budget for this region, although some qualitative differences are apparent. The data presented here indicate a more pelagic character in the Outer Domain, and that the Middle Domain

---

[2]Cross, J.N., Mathis, J.T., Lomas M.W., Moran, S.B., Baumann, M.S., Shull, D.H., Mordy C.W., Ostendorf, M.L., Bates, N.R., Stabeno, P.J., and Grebmeier, J.M., 2013. Integrated assessment of the carbon budget in the southeastern Bering Sea. Deep Sea Res. II. In review.

carbon budget is only balanced when including processes occurring in the Coastal Domain.

3.1 Introduction

The southeastern Bering Sea is one of the most productive shelf areas of the global ocean, with daily rates of net primary production (*NPP*) during ice edge blooms exceeding ~10 g C m^{-2} d^{-1} under optimal growth conditions (Niebauer et al., 1995; Lomas et al., 2012). The fate of this production has significant consequences for the attendant food web and the energy provided by primary production sustains both pelagic and benthic commercial fisheries. However, varying physical and climatic conditions can favor energy accumulation in either the pelagic or the benthic compartments, with significant consequences for commercial populations (Hunt and Stabeno, 2002; Hunt et al., 2002; Hunt et al., 2011). Remineralization of detrital production in the subsurface water column and underlying sediments results in the seasonal accumulation of carbon dioxide (CO_2) in bottom waters, sharply reducing seawater pH during the highly productive spring-summer period (Mathis et al., 2011; Appendix A). This process increases the vulnerability to ocean acidification processes via the uptake of anthropogenic CO_2, and has been observed to result in undersaturation of important calcium carbonate ($CaCO_3$) minerals critical for shell-building organisms in both the Bering and Chukchi Seas (Bates et al., 2009; Mathis et al., 2011; Chapter 4).

Despite the importance of primary production for the Bering Sea ecosystem, some portions of the carbon cycle remain poorly understood. For example, a paucity of data from near-coastal regions has resulted in limited and often conflicting patterns in temporal variability and the balance of primary production and export (e.g., Lomas et al., 2012, Moran et al., 2012). Other aspects of the carbon cycle have only recently gained attention, such as microzooplankton herbivory and surface bacterial remineralization loops (Olson and Strom, 2002; Moran et al., 2012; Sherr et al., 2013; Stoecker et al., 2012a, b). Recent physical and biogeochemical data have also provided some evidence

that organic carbon losses due to lateral transport may be more complex than previously assumed (Danielson et al., 2012a, b; Baumann et al., 2013a, b).

In the last five years, oceanographic expeditions as part of the multidisciplinary Bering Ecosystem Study (BEST-BSIERP) project provided an opportunity to evaluate independent estimates of the various rate and budget components of the Bering Sea shelf carbon cycle as a whole, and thereby to examine some of these unresolved carbon sinks. In this study, we provide a synthesis of net primary production (*NPP*), net community production (*NCP*), export production (C_{exp}), and benthic carbon consumption (*BCC*) estimates to construct a budget for determining the fate of organic carbon production through heterotrophic utilization and transport across the southeastern Bering Sea shelf.

3.2. Methods

3.2.1 Sample Collection

Physical, chemical, and biological measurements for the water column and sediments were collected as part of the BEST-BSIERP project during the following cruises: USCGC *Healy* during spring (April/May) of 2008 and 2009, and summer (July) of 2008; R/V *Knorr* in summer (June/July) of 2009; and R/V *Thomas G. Thompson* during late spring (May/June) and early summer (June/July) of 2010. Hydrographic (CTD) stations were occupied along two east-west transect lines (i.e., NP and CN lines) and one north-south transect along the 70 m isobath (i.e., 70M) as well as in several regions of opportunity (Figure 3.1). Biological and sediment studies were conducted at a subset of these stations. At the beginning of each spring cruise, sea ice cover was near 100% at all stations except for the southern stations of the 70M line, which were ice-free when sampled during spring in all years. During spring of 2010, the timing of the occupation of some stations, as well as the spatial extent of sampling, was limited by the ice breaking capability of R/V *Thompson*. Some inshore stations were sampled later than usual during spring to allow for some sea ice melt. During summer observations, the entire Bering Sea shelf was ice-free for all years.

In order to facilitate a common spatial reference for the participants in the BEST-BSIERP project, the study region was divided into 16 standardized domains based on hydrographic structure, circulation patterns, and macrofaunal population distribution (Ortiz et al., 2012, Harvey and Sigler, 2013). Data included in this study were collected in BEST-BSIERP Region 4, which we denote as the southern Outer Domain; BEST-BSIERP Regions 3 and 6, which we denote as the southern Central Domain; and BEST-BSIERP Regions 2 and 7, which we denote as the southern Coastal Domain (Figure 3.1). Our domains comprise both the southern and the central portions of the eastern shelf according to the project definitions. However, a proviso to the definition of spatial domains is that the boundary between the southern and central shelves is included to provide a reference for the analysis of groundfish surveys and has no hydrographic or biogeochemical context. In the absence of a strong boundary between the southern and central shelves, we combined these two areas in our synthesis effort. This study thus assumes that the northern boundary between the southeastern and northeastern portions of the shelves is a cross-shelf jet occurring in the vicinity of Nunivak Island (Danielson et al., 2011; Ortiz et al., 2012). Near the shelf break, biological regimes in the vicinity of the Pribilof Islands also led to the distinction of an elliptical domain. Because of the unique processes occurring here, we have not included data collected in the Pribilof Domain (BEST-BSIERP Region 5).

After the seasonal data collected as described below was partitioned into domains, all available data within each domain was averaged. Error for each domain-specific seasonal measurement is one standard deviation from the mean. Standard compounding error was assumed for any calculations made from domain averages, such that total standard error was equal to the square root of the sum of the squares of error terms for the variables included in the calculation.

3.2.2 Sample Analysis

3.2.2.1 Water Column Rate Measurements

Net Primary Production (NPP). Samples for ^{14}C incubations were collected roughly every other day from depths approximating the ~1.5, ~5, ~9, ~17, ~33, ~55, and ~100 % light levels of surface incident photosynthetically active radiation (PAR) (Lomas et al., 2012). Light depths were determined by analysis of PAR profiles on the CTD downcast generated using an annually calibrated Biospherical Instruments PAR sensor. Net primary production (*NPP*) rates were calculated from the autotrophic incorporation of $NaH^{14}CO_3^-$ into particulate organic matter over a 24-hour simulated *in situ* incubation using the ratio of added radiocarbon to total inorganic carbon present (Parsons et al., 1984; Lomas et al., 2012). Daily volumetric rates of *NPP* were integrated to the deepest sample depth (i.e., ~1.5% light level) and corrected for passive incorporation of $NaH^{14}CO_3^-$ using a dark control and the total added activity for the profile measured at the start of the incubation.

Net Community Production. *NCP* was measured using the seasonal drawdown of the photosynthetic reactants dissolved inorganic carbon (DIC; NCP_{DIC}) and total inorganic nitrogen (nitrate + nitrite + ammonium or TIN; NCP_{TIN}) over the mixed layer depth (average = 30 m). Samples for DIC were taken at every hydrographic station along the MN and NP lines and every other station along the 70M line and analyzed according to the protocol of Mathis et al. (2010) and Chapter 2 using the VINDTA 3C system (MARIANDA Inc.). These samples were calibrated using certified reference material provided by A.G. Dickson (Scripps Institution of Oceanography) and normalized to a deep water reference salinity of 35. NCP estimates were corrected for precipitation of carbonate minerals (e.g., Lee, 2001; Mathis et al., 2010). Samples for nutrient analysis were syringe filtered using 0.45 μm cellulose acetate membranes, collected in 30 mL acid washed, high-density polyethylene bottles after three rinses, and analyzed shipboard within 1-12 hrs of collection. Nutrient analysis closely followed the WOCE-JGOFS standardization and analysis procedures specified by Gordon et al. (1994), including

reagent preparation, calibration of lab ware, preparation of primary and secondary standards, and corrections for blanks and refractive index.

NCP_{DIC} values were taken from Mathis et al. (2010) and Chapter 2 comprising measurements for both 2008 and 2009. Insufficient DIC observations in spring 2010 prevented the calculation of *NCP* for this year using inorganic carbon data. NCP_{TIN} calculations comprised data from all three years, and were performed as in Mordy et al. (2012), except that Mordy et al. only examined the middle shelf in 2008 and 2009. Data were converted from net nitrogen consumption to net carbon production via the Redfield Ratio (106 C : 16 N). While some older work has documented non-Redfieldian water column ratios of DIC : DIN, these perturbations were assumed to result from persistent denitrification processes, and did not necessarily imply non-Redfieldian phytoplankton uptake ratios (e.g., Codispoti et al., 1986). More recently, others have documented anomalous water column N : P ratios, resulting from increased phosphate demand during periods of rapid growth (Horak et al., 2013). Although unusually high phosphate content in particulate phytoplankton does not necessarily imply that C : N ratios should not conform to Redfieldian stoichiometry, some others have documented that low nitrate and high phosphate content relative to carbon content commonly co-occur in particulate phytoplankton (e.g., Martiny et al., 2013a, b). Here, we conform to the standard Redfieldian ratio, as utilized by Mordy et al. (2012).

Particulate Organic Carbon Export. Particulate organic carbon export (C_{exp}) flux was calculated using sediment trap POC mass, sediment trap ^{234}Th, and water column $^{234}Th/^{238}U$ disequilibrium, as described in Moran et al. (2012) and Baumann et al. (2013b). Surface tethered, free-floating sediment trap arrays were deployed in ice-free waters along the outer shelf and shelf break during spring and summer (n = spring and summer; 3 and 3 for 2008; 5 and 4 for 2009; 5 and 4 for 2010) (Baumann et al., 2013b). Briefly, sediment traps (4 per depth at depths of 25, 40, 50, 60 and 100 m) were filled with 0.4 μm pre-filtered, non-poisoned brine (S = ~85‰) to isolate swimmers from settling material and deployed for ~1 d. Upon recovery and after settling, traps were siphoned to the seawater brine interface indicated by the discontinuity between layers.

Traps were filtered onto a pre-combusted GF/F, sub-sampled (10 mm arc punch) for POC, and analyzed for ^{234}Th at sea.

Total (dissolved + particulate) ^{234}Th water column profiles were collected during each cruise throughout the shelf. ^{234}Th profiles were high resolution (~10 m) throughout the photic zone. Water column ^{234}Th samples were collected from CTD-rosette casts using the small volume (SV; 4 L) technique, in which ^{234}Th is extracted via co-precipitation with manganese oxide (MnO_2) (Benitez-Nelson et al., 2001; Buesseler et al., 2001). ^{234}Th contained on sediment trap and water column filter samples was quantified by the measurement of beta emissions of ^{234}mPa (Emax = 2.19 MeV; $t_{1/2}$ = 1.2 min) on a low-background beta detector (RISØ National Laboratory, Roskilde, Denmark; average detector efficiency: 44 ± 3%). ^{238}U activities were calculated from salinity according to the relationship ^{238}U (dpm L^{-1}) = salinity (‰) × 0.0708 (Chen et al., 1986). The 10 mm arc punch POC subsamples were dried, fumed with HCl, dried and analyzed for POC on a Carlo Erba-440 Elemental Analyzer (Exeter Analytical, Inc., North Chelmsford, MA, U.S.) (Pike and Moran, 1997).

3.2.2.2 Sedimentary Respiration Rates

Rates of sedimentary respiration were determined on intact sediment cores collected using an Ocean Instruments MC-800 eight-tube multicore. Up to three cores per station were incubated at near *in situ* temperatures for the determination of oxygen consumption rates. These were subcored using 8 cm diameter polycarbonate tubes. The cores were stored in the dark uncapped, for approximately 24 hours, after which they were sealed with silicone stoppers equipped with magnetic stirrers and connected reservoirs containing bottom water from the same stations. Overlying water was sampled from each core over a period of two to five days and dissolved oxygen concentrations were determined using a fiber-optic oxygen microsensor (PreSens Microx TX3), calibrated before and after each reading. Oxygen fluxes were corrected using an empirical formula ($y = 1.125x + 3.365$, where y is the corrected flux and x is the uncorrected flux) for the slow diffusion of oxygen from the silicone stoppers used during

incubations (Davenport et al., 2012). These fluxes were converted to benthic carbon consumption (*BCC*) via the Redfield Ratio of carbon to oxygen (106 C : 150 O_2; Anderson, 1995).

3.2.3 Carbon Mass Balance

While *NPP* and some carbon utilization and transport pathways were assessed through the BEST Program as described above (*NPP*; *NCP*; C_{exp}; *BCC*), these parameters do not directly account for every aspect of the carbon cycle. However, these measurements do enable the calculation of the major carbon pathways and reservoirs; in particular, lateral carbon transport, heterotrophic respiration, and carbon accumulation in upper trophic level biomass. A generalized schematic of these sources and sinks are given in Figure 3.2, separated into pelagic and benthic compartments.

3.2.3.1 Surface Layer Heterotrophic Respiration

There are two components to primary production: new production, which is composed of that portion of *NPP* that can be attributed to external nutrient inputs; and regenerated production, which is driven predominantly by the re-assimilation of nutrients generated by the heterotrophic consumption of organic matter (Dugdale and Goering, 1967; Platt et al., 1989; Williams, 1993). By contrast, *NCP* measures the balance of *NPP* and heterotrophic (R_H) respiration processes across a given time period, such that $NCP = NPP - R_H$ (Williams, 1993). Often, *NCP* measurements assume that macronutrient limitation facilitates the rapid re-assimilation of any regenerated nutrients, such *NCP* is conceptually equivalent to new production (e.g., Bates, 2006). Based on this assumption, the difference between *NPP* and *NCP* should be equal to regenerated production, with R_H occurring as a rapid intermediary step. During the early part of the production season, prior to the onset of extreme nutrient limitation, we assume that there is some lag in this process, and that only late-season regenerated production is perfectly efficient. Over the entire production season, we assume that the difference between *NPP* and *NCP* can be partitioned evenly between regenerated production and heterotrophic respiration.

3.2.3.2 Surface Layer Lateral Transport

The offset between independent measurements of *NCP* by the drawdown of two separate photosynthetic reactants allowed for the calculation of carbon removal by lateral transport under the assumption of Redfieldian C and N production. Previous studies (e.g., Mathis et al., 2010; Mordy et al., 2012; Chapter 2) have shown that NCP_{DIC} is generally greater than NCP_{TIN}. Errors in NCP_{DIC} due to diffusion and gas exchange and natural offsets produced by variations in the phytoplankton C : N ratio (Sambrotto, personal communication) are not large enough to account for this imbalance. Instead, we propose that NCP_{DIC} and NCP_{TIN} are not equal due to the lateral movement of water with differing DIC : TIN ratios during the production season.

Because TIN is a limiting factor in primary production on the Bering Sea shelf and is typically depleted to near-zero levels by summer despite any spatial variation in spring TIN stocks, lateral transport does not strongly affect NCP_{TIN} calculations. In short, all TIN is utilized everywhere over the shelf, so the contribution of lateral transport to NCP_{TIN} estimates is difficult to observe. In contrast, non-limiting photosynthetic reactants like DIC are not uniformly depleted to a standard level, and lateral transport can alter NCP_{DIC} calculations. Further, the effect of lateral transport is magnified relative to TIN. Redfieldian production causes DIC to vary nearly ten times more strongly than nitrate, and resulting contributions of lateral transport to NCP_{DIC} are much more obvious. The amount of carbon exported by lateral transport (T) from the upper 30 m can therefore be estimated by the difference in *NCP* measured by seasonal DIC drawdown and TIN drawdown, such that $NCP_{DIC} - NCP_{TIN} = T$.

In the Outer Domain, a paucity of NCP_{TIN} data prevented the direct calculation of a transport term. However, Baumann et al. (2013a) estimate that ~30% of total ^{234}Th production in the water column is exported off-shelf from the Outer and Middle Domains. In the absence of discrete measurements, as an upper estimate we apply this 30% lateral mass transport loss factor to the Outer Domain.

3.2.3.3. Surface Layer Retained Biomass

Direct measurement of export production allowed for the calculation of carbon retention at the surface layer by subtracting carbon losses from the initial *NPP* value, such that: $NPP - R_H - T - C_{exp}$ = Surface layer retained biomass. Previous studies have shown that dissolved organic carbon (DOC) and lower trophic level particulate organic carbon (POC) do not accumulate in the surface layer (e.g., Baumann et al., 2013b; Chapter 2). Therefore, any *NPP* unaccounted for by measured or assumed loss processes at the surface layer is likely not retained as part of the autotrophic carbon community, but rather is consumed and assimilated by higher trophic communities not included within the measured dissolved or particulate fraction.

3.2.3.4 Bottom Layer Carbon Partitioning

We address the fate of exported carbon in bottom waters in two ways. First, we account for losses to benthic carbon consumption as directly measured by *BCC*. Second, we provide an upper estimate of carbon burial through a regional measurement of the thorium focusing factor (*FF*) as reported by Baumann et al (2013a). *FF* describes the ratio of the inventory of ^{234}Th buried in the sediments relative to the water column deficit of ^{234}Th. While this is not a direct estimate of the carbon retention in the sediment, ^{234}Th is a particle reactive tracer, and can thus provide an upper-bound proxy for particulate carbon. By applying the percent *FF* of ^{234}Th in the sediments to C_{exp}, we can provide a first-order, upper estimate of carbon burial. *FF* estimates were not available for the Coastal Domain, which prevented the calculation of *B* in this region. Additional losses of C_{exp} occur through heterotrophic consumption in the water column and bottom layer lateral transport. Some carbon will also be retained as accumulated biomass in higher trophic levels. However, we were not able to isolate these carbon reservoirs for bottom waters based on the available data.

3.3 Results

3.3.1 Net Primary Production

25 seasonal estimates of *NPP* based on ^{14}C incubations integrated over the photic zone are available for the southeastern Bering Sea shelf, although the timing and spatial orientation of these estimates varied widely. In particular, only one *NPP* profile is available for the southern Outer Domain (Spring 2008). The southern Middle Domain exhibited the best coverage, with 20 profiles spanning both seasons of all three years. The southern inner shelf was not sampled during 2008, while a spring profile is available for 2009 and both spring and summer profiles are available for 2010. In both spring and summer, *NPP* was much higher in the Middle Domain (117.8 ± 259.3 mmoles C m^{-2} d^{-1} and 96.7 ± 153.4 mmoles C m^{-2} d^{-1}, respectively) than in the Coastal Domain (7.5 ± 1.2 mmoles C m^{-2} d^{-1} and 13.3 ± 8.2 mmoles C m^{-2} d^{-1}, respectively). Spring *NPP* was slightly higher than summer *NPP* for the Middle Domain on average, while *NPP* for the Coastal Domain was 75% higher than in spring.

3.3.2 Net Community Production

Because *NCP* requires two seasonal occupations to calculate a single rate of drawdown of dissolved gases or nutrients, only one seasonal estimate is available as a directly measured value for each year. However, most of the time period occurring between the seasonal occupations fell under the spring category. These *NCP* estimates are more a reflection of the seasonal drawdown of DIC and TIN integrated over the period of the spring bloom than the drawdown occurring over summer, and we denote these rates as typical of spring (Table 3.2).

Coverage of NCP_{DIC} over the shelf spanned all three domains. During spring of 2008 and 2009, DIC concentrations were nearly uniform throughout the water column and along each hydrographic section, indicating homogenized conditions typical of winter and preceding the spring bloom. DIC concentrations were drawn down as much as 176 μmoles kg^{-1} by summer (Mathis et al., 2010; Chapter 2), but varied spatially within each domain. At one station in the southern Middle Domain, DIC concentrations in the

upper 30 m were observed to increase between spring and summer. Some interannual variability was also observed. Coastal Domain NCP_{DIC} was higher in 2008 relative to 2009, while 2009 NCP_{DIC} was higher for the Middle and Outer Domains.

The greatest resolution for any single parameter in any single domain is provided by NCP_{TIN}. Approximately 33 seasonal profiles are available for the southern Coastal Domain and nearly 200 for the southern Middle Domain, although no seasonal estimates of NCP_{TIN} are available for the southern Outer Domain. Additionally, this parameter represents the best temporal resolution of any other parameter in the data set, with both spring and summer seasons sampled during all three years of the study.

Strong nutrient drawdown was observed between spring and summer station occupations, with substantial drawdown of bulk nutrient content integrated over the upper 30 m occurring by early to mid-May (Figure 3.3). The Middle Domain exhibited a much higher initial nutrient content (~200-500 mmoles DIN m^{-2}) than the Coastal Domain (~50-250 mmoles DIN m^{-2}). Additionally, low DIN concentrations were present in the water column through the summer season in the Middle Domain, while integrated values of DIN were substantially drawn down to < 50 mmoles DIN m^{-2} in the Coastal Domain. This spatial variation is typical of production in the Bering Sea. Limited macronutrient content (Sambrotto and Goering, 1983; Sambrotto et al., 1986; Whitledge et al., 1986; Springer and McRoy, 1993) but high micronutrient content (Aguilar-Islas et al., 2007; Hurst et al., 2010) of the Coastal Domain enables high rates of productivity in spring, but also facilitates faster and more complete drawdown of macronutrients. Prolonged productive periods are not typical of this domain relative to other areas of the shelf (Sambrotto et al., 1986; Whitledge et al., 1986; Springer and McRoy, 1993; Bond and Overland, 2005; Rho et al., 2005; Aguilar-Islas et al., 2007; Mathis et al., 2010). NCP_{TIN} was higher through the southern Middle Domain than in the southern Coastal Domain by a factor of two (20 ± 9 mmoles C m^{-2} d^{-1} and 10 ± 3 mmoles C m^{-2} d^{-1}, respectively).

3.3.3 Particulate Organic Carbon Export

In total, 96 seasonal estimates of C_{exp} were made between the three years of this study. The C_{exp} rates given in Table 3.2 are an average of all three methods used to calculate this parameter, although some variability between the methods was observed. In general, sediment trap POC fluxes from open water deployments showed an increase in C_{exp} between spring and summer, while POC export estimated from ^{234}Th deficits generally decreased between the two seasons. Note that the sediment trap measurements of POC export were made only at the shelf-slope edge whereas POC export fluxes were determined from water column measurements of the ^{234}Th deficit (Baumann et al., 2013a) taken over the entire shelf. In areas where both sediment trap data and ^{234}Th profiles were taken at the same geographic locations, these different techniques agree to within a factor of 1.5-2 for POC export fluxes (Baumann et al., 2013b). In general, we observed that C_{exp} decreased by 15-25% between spring and summer (Table 3.2). The magnitude of this decrease increased towards the coast, indicating a stronger or more rapid seasonal cycle in the Coastal Domain than in the Middle and Outer Domains. Rates of C_{exp} were similar between the Outer and Middle Domains (22 ± 12 mmoles C m^{-2} d^{-1} and 25 ± 11 mmoles C m^{-2} d^{-1}, respectively), while C_{exp} was higher in the Coastal Domain (32 ± 8 mmoles C m^{-2} d^{-1}), reflecting an increasing gradient towards the coast.

3.3.4 Benthic Carbon Consumption

Spring and summer estimates of benthic carbon consumption (*BCC*) are available for the Outer, Middle and Coastal Domains, comprising 26 total estimates. Most data are available for the Middle and Outer Domains, while only four samples are available for the Coastal Domain. In general, we observed that *BCC* increased towards the coast, although this gradient was much stronger during spring than during summer. Respiration rates were very similar across the entire shelf in the later production season, varying by 30% compared to the 75% variation observed in spring. A shelf-wide average shows that benthic respiration decreases between spring and summer, although there was some cross-shelf gradient in this parameter. Rates of *BCC* decreased strongly from spring to

summer in the Coastal Domain (~45%; Table 3.2), while these increased in the Outer Domain by an equivalent margin (~51%; Table 3.2). Benthic respiration was very similar between spring and summer for the Middle Domain (7.9 ± 4 mmoles C m^{-2} d^{-1} and 8.0 ± 4 mmoles C m^{-2} d^{-1}). However, the high respiration rate observed in the Coastal Domain in spring increased the average spring respiration rate over the shelf, contributing to a bias in the shelf-wide average towards the pattern of production observed in the Coastal Domain. Relative to other parameters, however, an 18% change occurring between the two seasons was minimal.

3.4 Discussion

3.4.1 An Annual Model for the Southeastern Bering Sea Carbon Cycle

Assuming that the SE Bering Sea carbon budget is imbalanced on the seasonal scale, it will be difficult to assess long-term imbalances due to losses of carbon to lateral transport using a seasonal resolution. To eliminate seasonal imbalances resulting from natural biogeochemical processes, it is therefore necessary to assess the budget on the annual scale. However, previous work has discussed the challenges facing synthesis efforts of biogeochemical data sets due to the heterogeneity of processes that occur over short time and space scales on the Bering Sea shelf (e.g., Lomas et al., 2012). Spatiotemporal variability is difficult to resolve given widespread station locations, spatially extensive regional domains, and infrequent samplings. An attempt to define an annual cycle of carbon production and utilization over the shelf using observational data is therefore problematic at best. Despite obvious spatial and temporal limitations, numerous other studies have provided evidence for generalized patterns of carbon modification over the shelf (see Table 3.1). For example, the literature record shows evidence from multiple perspectives that *NPP* peaks in spring, decreases in summer, and increases in fall (e.g., Sambrotto et al., 1986; Springer et al., 1996; Rho and Whitledge, 2007; Lomas et al., 2012; Moran et al., 2012; Mordy et al., 2012), although with regional variability.

Applying these emergent patterns to the observational data collected here provides an opportunity not only to fill in the gaps in our observational data and permit an analysis of this group as a whole, but also to consider the Bering Sea from a little-utilized annual perspective, and to test the validity of these annual patterns. Here, we approximate an annual carbon cycle by extrapolating seasonal measurements using previously observed or hypothesized patterns as a guide, and derive the resulting carbon mass balance. A detailed description of this approach and its application to this data set is described in Supplemental Section 1, and an illustration of this extrapolation and a brief description are given below.

In order to extrapolate our seasonal data, we assumed that the year was comprised of four 91.25-day seasons. Data were partitioned into these seasons according to the timing of cruises and the physical and biogeochemical cycles described in Table 3.1. In Figure 3.3A, we provide an illustration of the best generalized seasonal variation of our observed parameters presently allowed, normalized to the relative peak value for *NPP*. Data gaps were filled based on observed patterns, where possible, and otherwise using patterns observed in the literature.

As already mentioned, the literature record indicates that in primary production peaks in spring, decreases in summer, and increases again during autumn with the advent of seasonal storms, the breakdown of the seasonal thermocline and resulting convection that induce nutrient replenishment. Our observational data show that *NPP* followed this pattern in the Middle Domain, but not in the Coastal Domain. Limited data prevented an observation of temporal patterns in Outer Domain *NPP* (see Table 3.2). Based on the consistency of the pattern of production in the literature, we chose to extrapolate Outer Domain data according to the Middle Domain pattern. Coastal Domain data were allowed to vary as observed in spring and summer, with fall production extrapolated as an average of the two. Patterns for NCP_{DIC} and NCP_{TIN} are not available across multiple seasons, and we thus assumed that they would follow the pattern for *NPP*.

According to the literature and our data (see Table 3.2), C_{exp} increases with *NPP* at the onset of production, and then decreases linearly through the summer and fall

seasons. Our observations show that the Coastal Domain adhered to this pattern, but that C_{exp} in the Middle Domain was constant between spring and summer, and Outer Domain C_{exp} increased over this season. In both cases, fall rates of C_{exp} were assumed to decrease relative to summer, as has been observed in other areas (Buesseler, 1998). Due to a complete paucity of winter data, we assumed that previously well-established light and stratification constraints on primary production during this season resulted in negligible primary production (e.g., Niebauer et al., 1990; Springer et al., 1996; Ladd and Stabeno, 2012; Moran et al., 2012; Sigler et al., 2013), and therefore precluded subsequent carbon modification.

Where possible, the maximum amount of data were incorporated into this model to allow for naturally observed patterns, and seasonal variability that may differ among regions. For example, rates of *NPP* in active blooms were integrated over a 30-day period in order to minimize the effect of these extremely high rates over the entire season, with the remainder of *NPP* integrated over the remaining 61.25 days. Our data also indicate that benthic respiration does not vary seasonally, exhibiting a nearly constant background activity. During our spring surveys, most of the primary production had not reached the benthos although some respiration was evident (See Section 3.4; Table 3.2). We therefore incorporated this winter baseline rate of *BCC* into our model. Observations contradicting the average seasonal patterns for *NPP* and C_{exp} were also incorporated into the model, as previously described.

Without temporally continuous observations available for each parameter in a variety of locations within each domain, the illustration given in Figure 3.3A is beyond the reach of the data collected. At present, we are unable to assess any variation in rate across a season. Accordingly, our resolution of this seasonal cycle is given in Figure 3.3B, representing a first-order approximation of the annual cycle of production as allowed by the data collected.

3.4.2 Annual Mass Balance

The annual mass balance of carbon production and utilization is given in Table 3.3.and visually represented in Figure 3.4. *NPP*, our only listed carbon source, is given in black, while the various pelagic (green) and benthic (blue) sinks are indicated by the second series of bars. The benthic $R_H + T + Bio$ bulk term is indicated in white. The error given in each estimate in Table 3.3 is derived from the individual measurement error (Table 3.2). Standard compounding error was assumed for calculated variables, such that total standard error was equal to the square root of the sum of the squares of error terms for the variables included in the calculation.

In general, the carbon budgets for the Outer and Middle Domains were largely balanced even without distinguishing $R_H + T + Bio$ in the benthic compartment, although some differences were apparent in the internal partitioning of *NPP* between carbon sinks. In the Middle Domain, a greater proportion of *NPP* was exported vertically and remineralized more efficiently in the sedimentary compartment than in the Outer Domain. While surface layer lateral transport was similar between these two regions, lateral carbon transport was larger than vertical transport as a sink for carbon in the Outer Domain than in the Middle Domain. In the Coastal Domain, NCP_{DIC}, C_{exp} and *BCC* exceeded estimates of *NPP*, indicating a large organic carbon deficit in this region.

3.4.3 The Outer Domain Loses Carbon

The lateral mass transport terms given in Table 3.3 correspond well to other recent calculations, indicating that the estimates presented here are reasonable. Baumann et al. (2013a) provided an estimate of off-shelf export of POC of 19 mmoles C m^{-2} d^{-1}. An upper boundary to this estimate was also calculated by Baumann et al. (2013b) of 24 ± 35 mmoles C m^{-2} d^{-1}. Extrapolating these estimates according to the same pattern of seasonal change we attributed to C_{exp} here, this gives a range of annual transport between 50 and 66 g C m^{-2} yr^{-1}. Our calculated *T* value for the Middle Domain is somewhat lower than these mass estimates. Given that *T* could not be calculated for the Outer Domain, we scaled *T* in this region as 30% of *NPP*, as was estimated by Baumann et al. (2013a). The

discrete rate measurement range from Baumann et al. (2013b) is somewhat lower than what we projected in Table 3.3 for the Outer Domain. However, this range accounts only for westward lateral transport, while the estimate based on Baumann et al. (2013a) we show in Table 3.3 accounts for lateral transport in any horizontal direction out of the domain.

Lateral mass transport as %*NPP* is similar in the Outer and Middle Domains (Figure 3.5A, B). However, relative to other sinks for *NPP*, the significance of lateral mass transport is somewhat stronger in the Outer Domain than in the Middle Domain. In the Outer Domain, *T* occurs on approximately the same scale as R_H (Figure 3.5A). Both of these terms are larger than C_{exp}, indicating that organic carbon consumption in the surface layer and lateral mass transport are much more significant than vertical export and bottom water consumption of organic matter. In the Middle Domain, C_{exp} is the largest sink for *NPP*, indicating that vertical mass transport is more significant than lateral mass transport (Figure 3.5B).

The relative importance of transport in the Outer Domain may also be exhibited in bottom waters. Nearly identical *FF* result in similar percentages of C_{exp} lost to burial in each domain. Because *BCC* is so much stronger in the Middle Domain, a much smaller portion of C_{exp} is left over after utilization in this region (Figure 3.5C, D). As noted earlier, this bottom water remainder (hereafter referred to as *R*) should conceptually be split between R_H, *Bio*, and *T*. The smaller *R* for the Middle Domain may result from an insignificant contribution of benthic *T*. Long residence times exhibited by bottom waters in the Middle Domain (Coachman, 1986; Danielson et al., 2012b; Stabeno et al., 2012b) likely decrease the relative importance of *T* for the *R* term. The water column in the Outer Domain is much deeper than that for the Middle Domain, and residence times of bottom water for the Outer Domain are much shorter (Coachman, 1986). Based on this evidence, it is possible that a larger portion of *R* in this domain will be comprised of carbon lost to lateral mass transport occurring in the bottom layer of this region, and that the relative magnitude of this sink for *NPP* may account for the larger *R* in this domain.

3.4.4 The Coastal Domain Gains Carbon

Measured carbon utilization is greater than carbon production in the Coastal Domain. It is unlikely that this offset results from errors in C_{exp}. While it is possible that C_{exp} values may be influenced by sediment resuspension, there is a 1.5-2x agreement between sediment trap particulate matter and thorium profiles, implying that sediment resuspension may not be a significant concern (Moran et al., 2012; Baumann et al., 2013b). While a twofold difference can't explain the entire deficit, this error may account for much of it. However, the concurrent observation of NCP_{DIC} and *BCC* values are also greater than *NPP*, indicating that multiple sinks are greater than the estimated observed sources. Two possible solutions remain to balance the carbon budget: poor annual extrapolation of production data, or lateral mass transport of carbon into the system unresolved by NCP_{DIC} and NCP_{TIN}.

Lomas et al. (2012) observed that the annual spring bloom may be somewhat delayed relative to the rest of the shelf, with peak production occurring later. We even observed this pattern on average in our seasonal data (see Table 3.2). According to our extrapolation for data with both seasons, this merely switches the spring and summer seasons in this productivity pattern, as estimates of fall production are the average of spring and summer values. For errors in extrapolation to cover the Coastal Domain carbon deficit, our fall extrapolations are also too low, indicating then that spring production increases linearly through summer and fall. However, some measurements included in our annual extrapolation of *NPP* were based on a single spring station occupation, which would have underestimated annual productivity that peaks in summer. Without the single-season occupation data, *NPP* in this region would still be lower than NCP_{DIC}, C_{exp}, and *BCC*, indicating again that that compounding errors in our fall *NPP* extrapolation would be the source for this offset. However, nutrient limitation in later seasons is well established in the Bering Sea, and it is unlikely that fall production, even that stimulated by nutrient replenishment from persistent storms, would overwhelm peak productivity levels in nutrient-replete seasons.

While we cannot rule out that the large difference between *NPP* and C_{exp} is an artifact of the compounding of error during our calculations, there is some potential that this offset is caused by a supply of externally produced organic carbon to the Coastal Domain. As we have suggested with regards to NCP_{DIC}, input of preconditioned waters may be altering *BCC* and C_{exp} by delivering organic matter produced in other areas. In the Coastal Domain, lateral mass transport may be a source of carbon to this region, rather than a sink. In order to balance the offset between *NPP*, surface carbon utilization, lateral mass transport, and C_{exp}, an additional 66 g C m^{-2} yr^{-1}, or 7.92 Tg yr^{-1} is required for input into the southern Coastal Domain at minimum.

The most logical source of lateral mass transport of organic matter into the Coastal Domain are the Yukon and Kuskokwim Rivers, which contribute 234 km^3 of freshwater to the Coastal Domain annually (Appendix A). Previous work has indicated that the organic matter delivered to the shelf with these river waters can dramatically influence the carbon cycle of the Coastal Domain (Chapter 2; Appendix A). River data from the U.S. Geological Survey (USGS) indicate the combined organic matter discharge from these rivers is approximately ~1.27 Tg C yr^{-1}. Even under the extremely improbable assumption that all of this organic matter is delivered to the southern Coastal Domain, organic matter from rivers cannot provide an adequate supplement to support the observed benthic activity. Assuming an average total organic carbon (TOC) concentration of 65 μmoles kg^{-1} in the waters entering the Bering Sea from the north Pacific and using a volume transport from Unimak Pass into the Coastal Domain of 0.042 Sv (Kinney et al., 2009), we see that this source of carbon contributes another ~1.1 Tg C yr^{-1}, also a reservoir too small to cover the imbalance between C_{exp} and *NPP*.

An additional supply of organic matter to the southern Coastal Domain may be the southern Middle Domain. Our estimate of *T* for the Middle Domain indicates that ~8.74 Tg C yr^{-1} is exported laterally. This mass could easily support the benthic carbon demand occurring in the Coastal Domain. If the Middle Domain is the source of this excess organic matter, this would imply a significant focusing of dispersed production in this area similar to that observed over the northern shelf (Cooper et al., 2012). Recent

work suggests that during years exhibiting cold winters such as 2008 − 2010, enhanced northward flow occurring over the shelf results from an increased density gradient over the shelf due to greater volumes of ice production and brine rejection (Danielson et al., 2012b). Under these conditions, northerly winds cause coastal convergence and upwelling near the shelf break. If the effects of the cross-shelf density gradient and upwelling reach all the way to the coast, this convergence could deposit Middle Domain productivity in the Coastal Domain under the appropriate wind conditions and account for the missing carbon supply, and indicate that the Middle and Coastal Domains are balanced within 0.8 Tg C yr^{-1} when taken together.

3.4.5 Comparison with the Previous Bering Sea Carbon Budget

Rates of primary production on the Bering Sea shelf have been estimated since the early 1960s (Ivenakov, 1961; Azova, 1964), and several comprehensive reviews of the literature have been conducted each decade since the 1990's (e.g., Springer et al., 1996; Hunt et al., 2002; Mathis et al., 2010; Lomas et al. 2012). Because of the importance of the regional fisheries, these measurements are often discussed at an ecosystem level, with a particular emphasis on the energy provided to upper trophic levels and pelagic fish populations. The PROBES (Processes and Resources of the Bering Sea) Program developed a complete carbon budget based on the relative consumption of *NPP* by upper trophic levels. After accounting for heterotrophic energy requirements, Walsh and McRoy (1986) estimated that approximately 49% and 17% of annual *NPP* remained for transport and burial in the Outer and Middle Domains, respectively.

With the available data, it is possible to discretely calculate both a transport and a burial term for comparison. However, like the method of Walsh and McRoy (1986), this combined burial/transport remainder term can also be indirectly calculated by subtracting all heterotrophic carbon utilization terms (R_H, *Bio*, *BCC*) from *NPP*. For the BEST-BSIERP data set, these indirect remainder terms are higher than those calculated directly (Table 3.3). The difference between these two methods results from limited bottom water data, which prevents the partitioning of carbon between R_H, *T*, and *Bio* below 40 m. In

the direct calculation of the remainder term, any potential transport in bottom waters is ignored, and therefore the term is likely underestimated. In the indirect calculation of the remainder term, bottom water R_H and stored biomass is also ignored, resulting in an overestimation of the burial and transport term.

Of these two estimation methods, we suggest that the direct calculation is likely more accurate. Directly calculating the remainder term relies on fewer assumptions, and ignores only one carbon pool (bottom water *T*) while the indirect method ignores two (bottom water R_H and *Bio*). Considering that the transport velocities in bottom water are very small (Danielson et al., 2012a; Stabeno et al., 2012a, b), loss of carbon by lateral transport in bottom waters is likely also very small (e.g., Bacon et al., 1994), which substantially reduces the error generated by ignoring this term. In comparison, the carbon pools ignored by the indirect calculation of this remainder term are likely much larger. Water column respiration is nontrivial in bottom waters over the shelf (Mathis et al., 2011), and the magnitude of the R_H term, as well as the biomass stored by a sedimentary community that respires over the entire year, are likely larger in scale than bottom water transport.

Both our directly and indirectly calculated remainder terms are on the same order as those calculated by Walsh and McRoy (1986). Given the uncertainties inherent in these extrapolations and the wider spatial area covered here relative to PROBES, this is likely to be the best possible comparison. However, there are also qualitative differences between our data and those reported by Walsh and McRoy in the partitioning of carbon implied by these remainder terms. Our directly calculated remainder term is slightly smaller for the Outer Domain (Table 3.3). The data presented here indicate a larger portion of productivity and less vertical export than Walsh and McRoy (1986), but a smaller storage as biomass. Some of this additional productivity is accounted for by the addition of a carbon reservoir for heterotrophic respiration and the strong surface remineralization loop we have demonstrated here. While these remainder estimates may be lower than those calculated by Walsh and McRoy (1986), they also depict a more strongly pelagic system. This is illustrated in Figure 3.5, where the relative magnitude of

NPP compared to any benthic utilization or any pelagic utilization is very high. The extreme inherent variability in the Bering Sea makes it extremely difficult to document small long-term changes (Lomas et al., 2012). However, it is possible that the system has undergone a shift to a more strongly pelagic state in recent decades.

In the Middle Domain, Walsh and McRoy (1986) argued that despite a small, indirectly calculated B + T remainder, the carbon budget was likely balanced over this area. It was suggested that the remaining carbon was cycled through the bottom water and benthic system on the annual scale, and that the Middle Domain was a dominantly benthic carbon system. In fact, Figure 3.5 does indicate that carbon utilization and transport below 40 m is nearly twice as significant for this domain than for the Outer Domain (C_{exp} = 38% *NPP* and 20% *NPP* in the Middle and Outer Domains, respectively). Following vertical export of *NPP*, *BCC* by $\%C_{exp}$ is also much greater in the Middle Domain than in the Outer Domain (58% and 35%, respectively; Figure 3.5). However, surface layer utilization still dominates the modification of *NPP* in the Middle Domain ($R_H + T + Bio$ = 62% *NPP*), indicating that while the Middle Domain may have a stronger connection between surface production and benthic heterotrophy than the Outer Domain, it is still a predominantly pelagic system. We also demonstrate a qualitative loss of *NPP* to lateral mass transport and carbon burial.

Walsh and McRoy (1986) did not publish a carbon budget for the Coastal Domain, and the subsequent Inner Shelf Transfer and Recycling Program (ISHTAR) focused more on the northern Bering Sea shelf. Other previous work has indicated that the Coastal Domain of the northern shelf (> 60°N) can be net heterotrophic on the seasonal scale (Chapter 2), although the same study, and others, indicated that the southern Coastal Domain surface layer is net autotrophic on an annual scale (e.g., Mathis et al., 2010; Lomas et al., 2012). This carbon budget indicates that the southern Coastal Domain may be net heterotrophic on the annual scale when integrating over the full water column. We also suggest that the Coastal Domain may be a focusing center for carbon lost to transport from the Middle Domain.

3.4.6 Additional Questions

While this budget represents a first order estimate of the carbon budget in the SE Bering Sea, further questions also remain with respect to specific carbon biogeochemical processes. Given the demonstrated importance of lateral carbon transport and the dominance of heterotrophic processes at the coast, a better parameterization of both of these terms is essential to improving our understanding of the biological and biogeochemical cycles in the region. Given limited *NCP* data, our present model indicates that heterotrophic respiration in the surface layer maintains a constant ratio to *NPP* across the spring and summer seasons, although some variability has recently been inferred (Moran et al., 2012).

In the benthic compartment, our parameterization of benthic remineralization only accounts for aerobic pathways in the sediments. Other concurrent studies indicated that net denitrification over the entire Bering Sea shelf totals 5.2-6.2 Tg C yr^{-1} (Horak et al., 2013). Our study covers ~15% of the area of the Bering Sea shelf estimated by Horak et al. (2013), indicating that anaerobic respiration should account for 0.8-0.9 Tg C yr^{-1} over the southern Middle and Outer Domains. The combined *R* integrated over these domains is ~3 Tg C yr^{-1}. Correspondingly, the anaerobic signal estimated by Horak et al. (2013) accounts for ~25-30% of the combined Middle and Outer Domain *R* given in Table 3.3. Additional studies concerning the partitioning of *R* between anaerobic and aerobic sedimentary respiration, transport, and carbon stored as biomass could refine our understanding of bottom layer carbon cycling, especially in the Outer Domain where *R* accounts for nearly 40% of C_{exp} (Figure 3.5).

While the carbon imbalance in the Coastal Domain prevented the partitioning of carbon pools in this region, a better understanding of respiration processes could be particularly important. Focused deposition of laterally transported carbon may support the benthic community of the Coastal Domain relative to the pelagic community. However, the resulting net heterotrophy in this region due to bacterial remineralization processes could also induce a strong vulnerability to ocean acidification. While we have sufficient data in this region to make some statements about the potential importance of

laterally transported carbon to the Coastal Domain, it is clear that all carbon processes in this region require further study. Some of the conflicting temporal patterns in organic carbon production and the unbalanced budget may be resolved simply by better spatial and temporal resolution of data in this region.

While data gaps did not result in substantial carbon budgetary imbalances in the Outer Domain, limited spatial coverage of *NPP* may have skewed our results. While seasonal *NPP* rates for both spring and summer were observed to be highest in the Middle Domain, the highest rates of annual *NPP* were observed in the Outer Domain based on our annual extrapolation. However, this extrapolation was based on a single summer profile available for this region (Table 3.2). If a more highly resolved *NPP* value for the region were lower, this could adjust our surface layer carbon partitioning. Specifically, R_H and *Bio* would decrease, and C_{exp} and *T* would represent a larger proportion of *NPP* than indicated in Figure 3.5. Qualitatively, this would enhance our assessment that the Outer Domain loses carbon to lateral transport on the annual scale.

Across all domains, a better understanding of fall and winter processes could also provide a better basis for assembling future annual carbon budgets. Here, we have neglected water column autotrophy and heterotrophy in the winter season, although winter production (e.g., Miksis-Olds et al., 2013) and respiration (e.g., Chapter 5) have been observed in the Bering Sea. It has also been hypothesized that under-ice blooms during late winter and early spring may play a critical role in determining ecosystem dynamics in the following late spring and summer (Hunt and Stabeno, 2002). Understanding the contribution of winter processes should be a focus of any future process studies and synthesis efforts in the Bering Sea.

3.5 Conclusions

During the multi-disciplinary, multi-year field program executed by the Bering Ecosystem Study (BEST), independent sampling for net primary production (*NPP*), two types of net community production (*NCP*), export production (C_{exp}), and benthic carbon consumption (*BCC*) allowed for the first complete description of the annual carbon

budget of the Outer and Middle Domains of the southeastern Bering Sea shelf for the first time in over thirty years. From these discrete measurements, estimates of heterotrophic respiration, carbon stored as biomass, carbon burial in the sediments, and lateral mass transport were calculated to develop a carbon mass balance.

Specifically, we observed that more carbon is lost laterally in the Outer Domain than is exported vertically. A more efficient coupling between pelagic production and benthic utilization in the Middle Domain indicated a more balanced carbon budget. Unlike the Middle and Outer Domains, lateral mass transport was a source of carbon to the Coastal Domain. While the source of the organic carbon necessary to balance benthic utilization with organic carbon supply requires further study, focused deposition of Middle Domain *NPP* lost to transport could account for this imbalance. Relative to previous carbon budgets that indirectly calculated a percentage of *NPP* lost to transport and burial, this data set made it possible to directly calculate this sink. This direct method showed a similar, if somewhat smaller percentage of *NPP* lost to transport and burial in the Outer Domain (35% *NPP*, Table 3.3), and contradicted the previous assumption that the carbon budget was balanced in the Middle Domain by showing a 36% loss of *NPP* to transport and burial. However, taken in conjunction with the Coastal Domain, the combined carbon budget for both regions is fully balanced to within 1 Tg C yr^{-1}.
As environmental conditions continue to change, it will be important to monitor spatial variations in carbon cycle and to continue to pursue a better understanding of the Bering Sea carbon budget, particularly with regards to the Coastal Domain.

Some of the differences between this budget and Walsh and McRoy (1986) may have arisen due to the strong variability characteristic of the Bering Sea ecosystem. While striving for complete spatial resolution on short temporal scales is likely untenable, periodic synthesis efforts like the construction of carbon budgets may help to address some broad longer-term variability. For example, under expected future warming, TOC inputs from rivers will likely increase due to increased melting of permafrost and enhanced soil drainage (Striegl et al., 2005), which could strengthen the supply of organic matter to the benthos and increase net heterotrophic processes for the Coastal Domain.

Construction of carbon budgets could also help to assess expected changes in pelagic/benthic partitioning in the coming decades.

3.6 Tables

Table 3.1 Seasonality in the eastern Bering Sea. A seasonal description of the physical characteristics of the shelf, also showing a breakdown of field activity. June – Aug.: Summer. Sept. – Nov.: Fall. Dec. – Feb.: Winter. Mar. – May: Spring. Data from bolded cruises were included in this carbon budget in the seasons listed. Ship and program names are abbreviated as follows: Eastern Bering Sea (EBS) Groundfish Survey; R/V *Knorr* (KN); R/V *Thompson* (TN); USCGC *Healy* (HLY); Bering-Aleutian Salmon International Survey (BASIS); NOAA Ship *Miller Freeman* (MF); USCGC *Polar Sea* (PSEA).

Mo.	Physical Justification	2007	2008	2009	2010
June	0% Ice Cover; Appearance of N/S transition in middle domain due to solar insolation; weaker currents[l, m]	EBS Groundfish Survey	EBS Groundfish Survey	**KN195 (6/14 to 7/13);** EBS Groundfish Survey	**TN250 (6/16 to 7/14);** EBS Groundfish Survey
July	Wind direction switches to northeastward; variable wind strength; weaker currents; euphotic zone, elevated chlorophyll fluorescence, and oxygen supersaturation deeper than pycnocline; loss of nutrients in bottom layer; majority small phytoplankton; *NPP* declines[c, k, m]	EBS Groundfish Survey	**HLY0803 (7/1 to 7/31);** EBS Groundfish Survey	**KN195 (6/14 to 7/13);** EBS Groundfish Survey	**TN250 (6/16 to 7/14);** EBS Groundfish Survey
Aug.	Maximum annual Stratification Index (SI; J/m2; M2); variable wind strength; secondary freshet (glacial melt)[c, e, k]	BASIS Survey (8/15 to 10/8)			BASIS Survey (8/18 to 9/25)
Sept.	Maximum annual heat content; small fall bloom, incl. coccolithophores; wind direction E/SE; winds weak; deep mixing, remineralization, denitrification/anammox significant biogeochemical modifiers[d, h, l, k, l]	TN211 (9/25 to 10/11); BASIS Survey (8/15 to 10/8; 8/31 to 9/23); MF071 (9/17 to 9/30)	ME0823 (8/24 to 9/17); BASIS Survey (9/11 to 9/27)	MF0904b (9/22 to 10/13); BASIS Survey (8/26 to 9/14; 9/3 to 9/27)	BASIS Survey (8/18 to 9/25; 9/8 to 10/5)
Oct.	Stratification begins to erode; winds strengthen; flushing of central shelf begins[b, e, k]	TN211 (9/25 to 10/11); BASIS Survey (8/15 to 10/8)		MF0904b (9/22 to 10/13)	
Nov.	Ice formation begins; winds strong[k, l, m]				
Dec.	Ice covers northern shelf; winds strong; wind direction W/SW[k, l, m]				
Jan	Well-mixed water column (M4); winds strong; ice covers northern shelf; input of nutrient content to central shelf from Anadyr Water begins[c, k, m]				
Feb.	Winds strong; ice covers northern shelf[k, m]				
Mar.	Typical maximum ice extent; Winds strong; wind direction S/SW; under-ice bloom[j, k, m]		**HLY0801 (3/12 to 3/26)**	**HLY0901 (3/10 to 3/31)**	**PSEA 1001 (3/7 to 4/4)**
Apr.	Ice retreat begins; Ice-edge bloom; Winds begin to weaken; Depth-averaged temperature minimum[e, k, m]	HLY0701 (4/11 to 5/11); MF0706 (4/18 to 5/6)	**HLY0802 (3/27 to 5/5)**	**HLY0902 (4/1 to 5/11)**	
May	Rapid ice ablation; light availability increases; stratification sets up firmly; primary freshet (snow melt); weaker currents; widespread spring bloom; majority large phytoplankton; maximum rate *NPP*[a, c, e, f, g, j]	HLY0702 (5/16 to 6/18)		**HLY0902 (4/1 to 5/11)**	**TN249 (5/9 to 6/14)**

[a]Brabets et al., 2000; [b]Danielson et al., 2012b; [c]Dornblaser and Striegl, 2007; [d]Iida et al., 2012; [e]Ladd and Stabeno, 2012; [f]Lomas et al., 2012; [g]Moran et al., 2012; [h]Mordy et al., ; 2012; [i]Sigler et al., 2013; [j]Stabeno et al., 2001; [k]Stabeno et al., 2007; [l]Stabeno et al., 2012a; [m]Stabeno et al., 2012b

Table 3.2 Carbon production, utilization, and transport (2008 – 2010). Independently measured seasonal rates of carbon production, utilization and transport for the three domains of the southern shelf between 2008 and 2010 in mmoles C m^{-2} d^{-1}. *NPP* estimates of the southern Outer Domain are available only in summer, and include only one profile. *NCP* estimates are made between spring and summer. The measured rates are more heavily influenced by spring than summer dynamics, and are thus listed here as the spring rate. Subsequently, summer rates for *NCP* are not available. NCP_{TIN} was not measured in the southern Outer Domain. A focusing factor estimate from Baumann et al. (2013a) was not available for the Coastal Domain. Error listed is one standard deviation from the mean.

		southern Coastal Domain		**southern Middle Domain**		**southern Outer Domain**	
Parameter	**Abb.**	**Spring**	**Summer**	**Spring**	**Summer**	**Spring**	**Summer**
Net Primary Production	*NPP*	7.5 ± 1.2	13.3 ± 8.2	117.8 ± 259.3	96.7 ± 153.4	--	75.5 ± --
Net Community Production from DIC	NCP_{DIC}	15.8 ± 14.8	--	38.6 ± 33.5	--	45.0 ± 17.1	--
Net Community Production from TIN	NCP_{TN}	9.7 ± 2.8	--	20.2 ± 8.5	--	--	--
Export Production	C_{exp}	31.8 ± 7.6	23.8 ± 13.5	24.4 ± 11.3	19.9 ± 11.0	21.7 ± 12.1	22.4 ± 12.3
Focusing Factor	*FF*	--	--	0.3 ± 0.1	0.2 ± 0.1	0.3 ± 0.1	0.2 ± 0.2
Benthic Carbon Consumption	*BCC*	16.0 ± 1.8	8.8 ± 3.5	7.9 ± 3.8	8.0 ± 4.1	4.1 ± 0.8	6.2 ± 2.5

Table 3.3 Annual carbon budget for the Bering Sea shelf (2008 – 2010). The annual carbon budget mass balance for the three domains of the Bering Sea shelf based on the seasonal estimates from Table 3.2, in g C m^{-2} yr^{-1}. The abbreviation and measurement or calculation method for each parameter, as well as the water column layer over which it is valid, is also indicated. For measured parameters, the number of profiles contributing to the estimate is listed. For calculated parameters, the relative percent of *NPP* is also shown. The lateral transport term for the southern Outer Domain was calculated according to Baumann et al. (2013a). At bottom, remainder terms indicating percent loss of *NPP* to burial in the sediments or lateral mass transport were directly calculated by adding calculated burial and transport terms, and indirectly by accounting for all heterotrophic carbon requirements. The literature value for these estimates was calculated indirectly and taken from Walsh and McRoy (1986).

Parameter	Abbr.	Formula	Layer	southern Outer Domain		southern Middle Domain		southern Coastal Domain	
Net Primary Production	*NPP*	Measured	Upper 30 m	331 ± --	n = 1	172±72	n = 20	26 ± 15	n = 4
Net Community Production from DIC	NCP_{DIC}	Measured	Upper 30 m	111 ± 42	n = 22	95±83	n = 48	39 ± 36	n =14
Net Community Production from TIN	NCP_{TN}	Measured	Upper 30 m	--		50 ± 21	n = 193	24 ± 7	n = 33
Export Production	C_{exp}	Measured	40 m	67 ± 20	n = 55	65 ± 18	n = 35	80 ± 17	n = 6
Focusing Factor	*FF*	Measured	Sediment	0.28 ± 0.13	n = 20	0.26 ± 0.10	n = 27	--	
Benthic Carbon Consumption	*BCC*	Measured	Sediment	23 ± 7	n = 11	38 ± 19	n = 11	63 ± 12	n = 4
Heterotrophic Respiration	R_H	$0.5 \times NPP - NCP_{AVG}$	Upper 30 m	110 ± 21	*33% NPP*	50 ± 42	*29% NPP*	-3 ± 12	*-10% NPP*
Lateral Transport	*T*	$NCP_{DIC} - NCP_{TN}$	Upper 30 m	99 ± --	*30% NPP*	46 ± 85	*26% NPP*	15 ± 37	*56% NPP*
Carbon Stored as Biomass	*Bio*	$NPP - R_H - T - C_{exp}$	Upper 30 m	55 ± 29	*17% NPP*	12 ± 121	*7% NPP*	-66 ± 45	*-253% NPP*
Carbon Burial	*B*	$FF \times C_{exp}$	Sediment	19 ± 0	*6% NPP*	17 ± 0	*10% NPP*	--	
$R_H + T + Bio$	*R*	$C_{exp} - BCC - B$	Below 40 m	25 ± 22	*8% NPP*	10 ± 26	*6% NPP*	--	
Walsh Remainder (Indirect)		Literature	Full Water Column	49%		17% (0%)		--	
BEST Remainder (Direct)		$B + T$	Full Water Column	35%		36%		--	
BEST Remainder (Indirect)		$NPP - R_H - Bio - BCC$	Full Water Column	43%		42%		--	

3.7 Figures

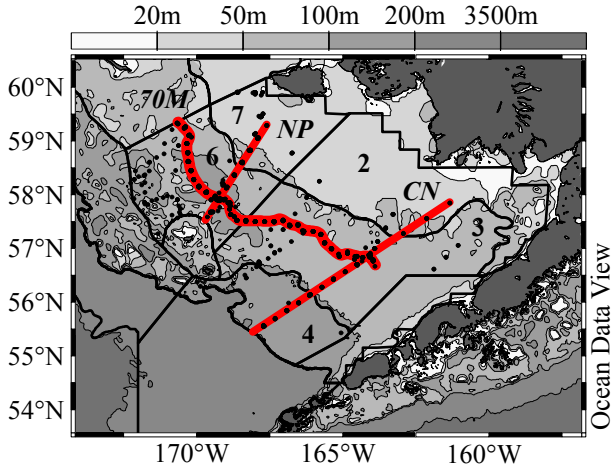

Figure 3.1 Map of the southeastern Bering Sea shelf. A map of the southeastern Bering Sea shelf indicating sampling locations (dots) and major regions as defined by the Bering Sea Project (numbered regions delineated with dark black outlines). Bathymetry is shaded according to depth. Repeat hydrographic lines include the CN Line, the MN Line, and the 70M Line, highlighted in red and labeled in italics.

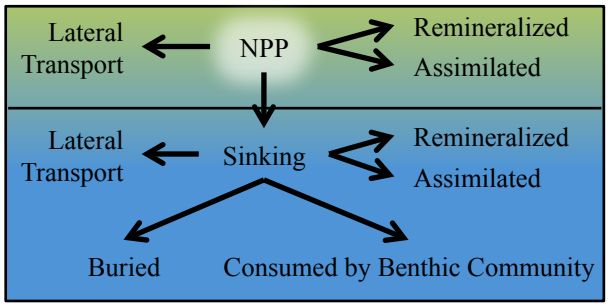

Figure 3.2 Budgetary components of the southeastern Bering Sea shelf carbon cycle. The pelagic compartment is shown in green and the benthic compartment is shown in blue. Arrows indicate sinks for the only organic carbon source parameterized in this budget, net primary production (*NPP*).

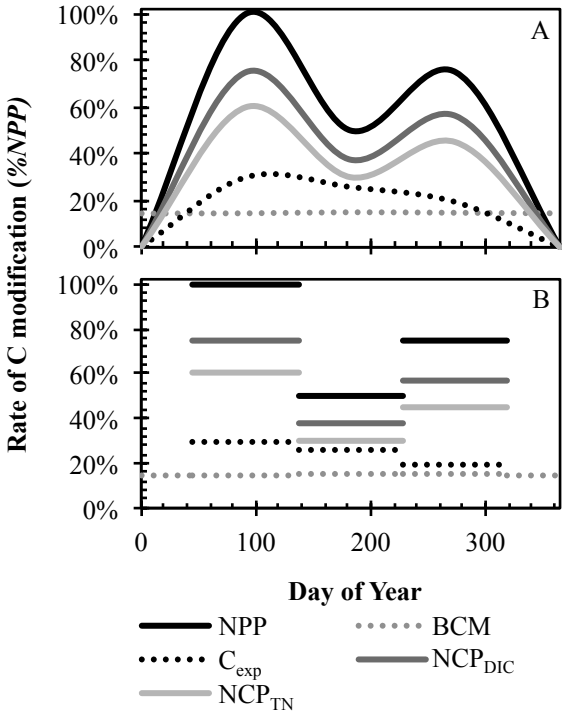

Figure 3.3 Normalized seasonal rate of carbon modification (2008 – 2010). The normalized rate of carbon modification occurring in each of the four seasons, relative to peak *NPP*. The highest rates of *NPP* typically occur in spring. (A) The generalized seasonal cycle determined through the literature record as indicated in Table 3.2, and our available measurements. (B) The annual extrapolation of seasonal measurements possible given the data sets included here. No rate variations within a particular season are included.

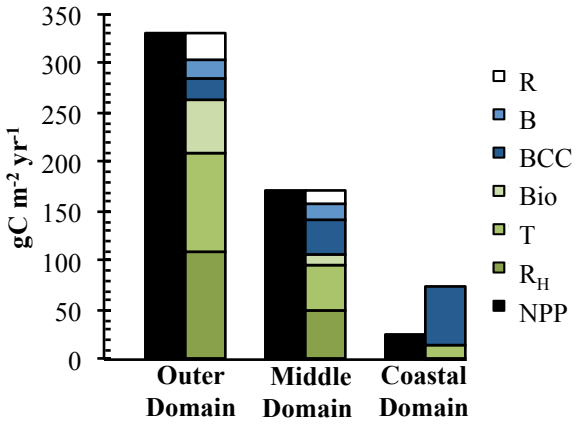

Figure 3.4 Carbon production, utilization, and transport (2008 – 2010). Carbon production, utilization and transport by g C m^{-2} yr^{-1} by each of the measured and calculated processes listed in Table 3. Production terms are indicated in black and grey, surface water sinks are indicated in green, bottom water carbon sinks are indicated in blue, and the total value of the indistinguishable bottom layer carbon sinks (*R,* where $R = R_H + T + Bio$ below 40 m) is indicated in white. This visualization highlights the increasing disconnect between *NPP* and carbon losses towards the Outer Domain, and the dominance of known carbon sinks (*BCC, T*) in excess of *NPP* in the Coastal Domain.

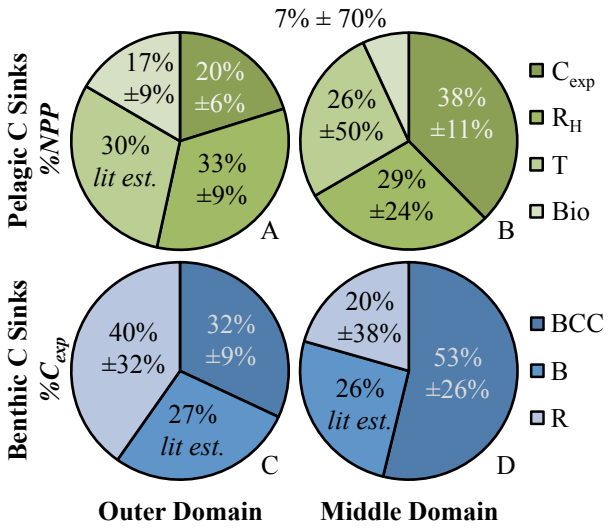

Figure 3.5 Pelagic and benthic carbon partitioning (2008 – 2010). (A) Pelagic sinks of *NPP* for the Outer Domain. (B). Pelagic sinks of *NPP* for the Middle Domain. (C) Benthic sinks of C_{exp} for the Outer Domain. (D) Benthic sinks of C_{exp} for the Middle Domain. Standard compounding error was assumed in the propagation of error terms from Table 3.3, except in cases where the values were estimated based on previous literature, indicated by *lit est*. In the benthic compartment, the *R* term is conceptually comprised of the bulk carbon modification by water column heterotrophy, carbon stored as biomass, and lateral transport. Partitioning among these sources was not possible with this data set.

3.8 Acknowledgements

The authors thank the officers and crew of USCGC *Healy*, R/V *Knorr*, and R/V *Thomas G. Thompson*, as well as Scott Hiller of SIO, Steve Roberts of UCAR, and the hydrographic team from NOAA-PMEL for their work in tirelessly supporting our science during multiple cruises. We also thank Ray Sambrotto for the provision of unpublished data for reference during this work. Lastly, we thank the Science Advisory Board, the data management team, and our colleagues in the BEST-BSIERP project, supported by NSF and NPRB. The synthesis presented in this paper was supported by the National

Science Foundation grants ARC-1107997 to JTM, ARC-0732359 and ARC-1106910 to MWL, ARC-0732680 to SBM, PLR-1107250 to CWM, and grant NPRB-B56 to SBM from the North Pacific Research Board. This publication was partially funded by the Joint Institute for the Study of the Atmosphere and Ocean (JISAO) under NOAA Cooperative Agreement NA10OAR4320148, and is contribution EcoFOCI-0808 to NOAA's Ecosystems and Fisheries-Oceanography Coordinated Investigations, contribution 2180 to JISAO, and contribution 3914 to NOAA's Pacific Marine Environmental Laboratory. This is BEST-BSIERP publication number XX. Statement of Work: Cross, J.N., designed the method of analysis, synthesized all available datasets, and prepared the manuscript for publication. Mathis, J.T., Lomas, M.W., and Moran, S.B., contributed datasets to the synthesis and provided guidance through manuscript preparation. Other coauthors contributed data to this synthesis effort.

3.9 References

Aguilar-Islas, A.M., Hurst, M.P., Buck, K.N., Sohst, B., Smith, G.J., Lohan, M.C., et al., 2007. Micro- and macronutrients in the southeastern Bering Sea: insight into iron-replete and iron-depleted regimes. Prog. Oceanogr. 73, 99–126.

Anderson, L.A., 1995. On the hydrogen and oxygen content of marine phytoplankton. Deep Sea Res. I. 42(9), 1675–1680.

Azova, N.V., 1964. Primary productivity of the Pribilof-Bristol area of the Bering Sea, in: Moiseev, P.A. (Ed.), Soviet Fisheries Investigations in the Northeastern Pacific, Part III. Pishchevaya Promyshlennost Publishing, Moscow, pp. 149–154.

Bacon, M.P., Belastock, R.A., Bothner, M.H., 1994. ^{210}Pb balance and implications for particle transport on the continental shelf, U.S. Middle Atlantic Bight. Deep Sea Res. II. 41(2-3), 511–535.

Bates, N.R., 2006. Air-sea CO_2 fluxes and the continental shelf pump of carbon in the Chukchi Sea adjacent to the Arctic Ocean. J. Geophys. Res. 111(C10), C10013.

Bates, N.R., Mathis, J.T., Cooper, L.W., 2009. Ocean acidification and biologically induced seasonality of carbonate mineral saturation states in the western Arctic Ocean. J. Geophys. Res. 114, C11007.

Baumann, M.S., Moran, S.B., Kelly, R.P., Lomas, M.W., Shull, D.H., 2013a. ^{234}Th balance and implications for seasonal particle retention in the eastern Bering Sea. Deep Sea Res. II. 94, 7–21.

Baumann, M.S., Moran, S.B., Kelly, R.P., Lomas, M.W., Bell, D.W., 2013b. Seasonal decoupling of organic carbon export and net primary production in relation to sea-ice at the shelf break of the eastern Bering Sea: implications for off-shelf carbon export. J. Geophys. Res. 118, 1–19.

Benitez-Nelson, C., Buesseler, K.O., Rutgers van der Loeff, M., Andrews, J., Ball, L., Crossin, G., et al., 2001. Testing a new small-volume technique for determining ^{234}Th in seawater. J. Radioanal. Nucl. Chem. 238(3), 795–799.

Bond, N.A., Overland, J.E., 2005. The importance of episodic weather events to the ecosystem of the Bering Sea shelf. Fish. Oceanogr. 14, 97–111.

Brabets, T.P., Wang, B., Meade, R.H., 2000. Environmental and hydrologic overview of the Yukon River Basin, Alaska, and Canada. Water Resources Investigations Report No. 99-4204. USGS, Anchorage, AK, 114 pp.

Buesseler, K.O., 1998. The decoupling of production and particulate export in the surface ocean. Glob. Biogeochem. Cycl. 12(2), 297–310.

Buesseler, K.O., Benitez-Nelson, C., Rutgers van der Loeff, M., Andrews, J., Ball, L., Crossin, G., et al., 2001. An intercomparison of small- and large-volume techniques for ^{234}Th in seawater. Mar. Chem. 74, 15–28.

Chen, J.H., Edwards, R.L., Wasserberg, G.J., 1986. ^{234}U and ^{232}Th in seawater. Earth Planet. Sci. Lett. 80(3-4), 241–251.

Coachman, L.K, 1986. Circulation, water masses, and fluxes on the southeastern Bering Sea shelf. Cont. Shelf Res. 5, 23–108.

Codispoti, L.A., Friederich, G.E., Hood, D.W., 1986. Variability in the inorganic carbon system over the southeastern Bering Sea shelf during spring 1980 and spring-summer 1981. Cont. Shelf Res. 5(1-2), 133–160.

Cooper, L.W., Janout, M.A., Frey, K.E., Pirtle-Levy, R., Guarinello, M.L., Grebmeier, J.M., et al., 2012. The relationship between sea-ice break-up, water mass variation, chlorophyll biomass, and sedimentation in the northern Bering Sea. Deep Sea Res. II. 65-70, 141–162.

Danielson, S., Eisner, L., Weingartner, T., Aagaard, K., 2011. Thermal and haline variability over the central Bering Sea shelf: Seasonal and interannual perspectives. Cont. Shelf Res. 31(6), 539–554.

Danielson, S., Hedstrom, K., Aagaard, K., Weingartner, T., Curchister, E., 2012a. Wind-induced reorganization of the Bering shelf circulation. Geophys. Res. Lett. 39(8), L08601.

Danielson, S., Weingartner, T., Aagaard, K., Zhang, J., Woodgate, R., 2012b. Circulation on the central Bering Sea shelf, July 2008 – July 2010. J. Geophys. Res. 117, C10003.

Davenport, E.S., Shull, D.H., and Devol, A.H., 2012. Roles of sorption and tube-dwelling benthos in the cycling of phosphorus in Bering Sea sediments. Deep Sea Res. II. 65-70, 163–172.

Dornblaser, M.M., Striegl, R.G., 2007. Nutrient (N, P) loads and yields at multiple scales and subbasin types in the Yukon River Basin, Alaska. J. Geophys. Res. 112, G04S57.

Dugdale, R.C., Goering, J.J., 1967. Uptake of new and regenerated forms of nitrogen in primary productivity. Limnol. Oceanogr. 12(2), 196–206.

Gordon, L.L., Jennings Jr., J.C., Ross, A.A., Krest, J.M., 1994. A suggested protocol for continuous flow automated analysis of seawater nutrients (phosphate, nitrate, nitrite, and silicic acid). Methods Manual No. 91-1. WOCE Hydrographic Program Office, Corvallis, OR, 55 pp.

Harvey, R.H., Sigler, M.F., 2013. An introduction to the Bering Sea Project: Volume II. Deep Sea Res. II. 94, 2−6.

Horak, R.E.A., Whitney, H., Shull, D.H., Mordy, C.W., Devol, A.H., 2013. The role of sediments in the Bering Sea shelf N cycle: Insights from measurements of benthic denitrification and benthic DIN fluxes. Deep Sea Res. II. 94, 95–105.

Hunt Jr., G.L., Stabeno, P.J., 2002. Climate change and the control of energy flow in the southeastern Bering Sea. Prog. Oceanogr. 55(1-2), 5–22.

Hunt Jr., G.L., Stabeno, P.J., Walters, G., Sinclair, E., Brodeur, R.D., Napp, J.M., et al., 2002. Climate change and control of the southeastern Bering Sea pelagic ecosystem. Deep Sea Res. II. 49, 5821–5853.

Hunt Jr., G.L., Coyle, K., Eisner, L., Farley, E.V., Heintz, R.A., Mueter, F., et al., 2011. Climate impacts on eastern Bering Sea food webs: a synthesis of new data and an assessment of the Oscillating Control Hypothesis. ICES J. Mar. Sci. 68(6), 1230–1243.

Hurst, M.P., Aguilar-Islas, A.M., Bruland, K.W., 2010. Iron in the southeastern Bering Sea: elevated leachable particulate Fe in shelf bottom waters as an important source for surface waters. Cont. Shelf Res. 30, 467–480.

Iida, T., Mizobata, K., Saitoh, S.-I., 2012. Interannual variability of coccolithophore *Emiliania huxleyi* blooms in response to changes in water column stability in the eastern Bering Sea. Cont. Shelf Res. 34, 7–17.

Ivenakov, V.N., 1961. Primary production in the Bering Sea. Transl. Inst. Oceanol. Acad. Sci. U.S.S.R. 51, 36–56.

Kinney, C.J., Maslowski, W., Okkonen, S., 2009. On the processes controlling shelf-basin exchange and outer shelf dynamics in the Bering Sea. Deep Sea Res. II. 56(17), 1351–1362.

Ladd, C., Stabeno, P.J., 2012. Stratification on the Eastern Bering Sea shelf revisited. Deep Sea Res. II. 65-70, 72–83.

Lee, K., 2001. Global net community production estimated from the annual cycle of surface water total dissolved inorganic carbon. Limnol. Oceangr. 46(6), 1287–1297.

Lomas, M.W., Moran, S.B., Casey, J.R., Bell, D.W., Tiahlo, M., Whitefield, J., et al., 2012. Spatial and seasonal variability of primary production on the Eastern Bering Sea Shelf. Deep Sea Res. II. 65-70, 126–140.

Martiny, A.C., Vrugt, J.A., Primeau, F.W., and Lomas, M.W., 2013a. Regional variation in the particulate organic carbon to nitrogen ratio in the surface ocean. Glob. Biogeochem. Cycl. 27, 723–731.

Martiny, A.C., Pham, C.T.A., Primeau, F.W., Vrugt, J.A., Moore, J.K., Levin, S.A., et al., 2013b. Strong latitudinal patterns in the elemental ratios of marine plankton and organic matter. Nat. Geosci. Lett. 6, 279−283.

Mathis, J.T., Cross, J.N., Bates, N.R., Moran, S.B., Lomas, M.W., Stabeno, P.J., 2010. Seasonal distribution of dissolved inorganic carbon and net community production on the Bering Sea shelf. Biogeosci. 7, 1769–1787.

Mathis, J.T., Cross, J.N., Bates, N.R., 2011. The role of ocean acidification in systemic carbonate mineral suppression in the Bering Sea. Geophys. Res. Lett. 19, 1–6.

Miksis-Olds, J.L., Stabeno, P.J., Napp, J.M., Pinchuk, A.E., Nystuen, J.A., Warren, J.D., et al., 2013. Ecosystem response to a temporary sea ice retreat in the Bering Sea: Winter 2009. Prog. Oceanogr. 111, 38–51.

Moran, S.B., Lomas, M.W., Kelly, R.P., Gradinger, R., Iken, K., Mathis, J.T., 2012. Seasonal succession of net primary productivity, particulate organic carbon export, and autotrophic community composition in the eastern Bering Sea. Deep Sea Res. II. 65-70, 84–97.

Mordy, C.W., Cokelet, E.D., Ladd, C., Menzia, F.A., Proctor, P., Stabeno, P.J., et al., 2012. Net community production on the middle shelf of the eastern Bering Sea. Deep Sea Res. II. 65-70, 110–125.

Niebauer, H.J., Alexander, V., Henrichs, S.M., 1995. A time-series study of the spring bloom at the Bering Sea ice edge I: Physical processes, chlorophyll, and nutrient chemistry. Cont. Shelf Res. 15, 1859–1878.

Niebauer, H.J., Alexander, V., Henrichs, S., 1990. Physical and biological oceanographic interaction in the spring bloom at the Bering Sea marginal ice edge zone. J. Geophys. Res. 95(C12), 22229–22241.

Olson, M., Strom, S., 2002. Phytoplankton growth, microzooplankton herbivory and community structure in the southeast Bering Sea: insight into the formation and

temporal persistence of an *Emiliania huxleyi* bloom. Deep Sea Res. II. 49(26), 5969–5990.

Ortiz, I., Wiese, F., and Grieg A., 2012. Marine regions of the eastern Bering Sea shelf. Accessed June 2012. http://bsierp.nprb.org/documents/BSIERP_Regions.doc.

Parsons, T., Maita, Y., Lalli, C., 1984. A Manual of Chemical and Biological Methods for Seawater Analysis. Pergamon Press, New York, NY, 184 pp.

Pike, S.M., Moran, S.B., 1997. Use of Poretics® 0.7 μm pore size glass fiber filters for determination of particulate organic carbon and nitrogen in seawater and freshwater. Mar. Chem. 57(3-4), 355–360.

Platt, T., Denman, D.L., Jassby, A.D., 1977. Modeling the productivity of phytoplankton, in: Goldberg, E.D. (Ed.), Ideas and Observations on Progress in the Study of the Sea. John Wiley, New York, NY, pp. 807–856.

Rho, T., Whitledge, T.E., 2007. Characteristics of seasonal and spatial variations of primary production over the southeastern Bering Sea shelf. Cont. Shelf Res. 27, 2556–2569.

Rho, T., Whitledge, T.E., Goering, J.J., 2005. Interannual variations of nutrients and primary production over the southeastern Bering Sea shelf during the spring of 1997, 1998, and 1999. Oceanol. (Engl. Transl.) 45, 376–390.

Sambrotto, R.N., Goering, J.J., 1983. Interannual variability of phytoplankton and zooplankton production on the southeast Bering Sea shelf, in: Wooster, W.S. (Ed.), From Year-to-Year: Interannual Variability of the Environment and Fisheries of the Gulf of Alaska and the Eastern Bering Sea. Washington State Sea Grant, Seattle, WA, pp. 161–177.

Sambrotto, R.N., Niebauer, H.J., Goering, J.J., Iverson, R.I., 1986. Relationships among vertical mixing, nitrate uptake, and phytoplankton growth during the spring bloom in the southeast Bering Sea middle shelf. Cont. Shelf Res. 5, 161–198.

Sherr, E.B., Sherr, B.F., Ross, C., 2013. Microzooplankton grazing impact in the Bering Sea during spring sea-ice conditions. Deep Sea Res. II. 94, 57–67.

Sigler, M.F., Stabeno, P.J., Eisner, L.B., Napp, J.M., Mueter, F.J., 2013. Spring and fall phytoplankton blooms in a productive subarctic ecosystem, the eastern Bering Sea, during 1995 – 2011. Deep Sea Res. II. In press.

Springer A.M., McRoy, C.P., 1993. The paradox of pelagic food webs in the northern Bering Sea III. Patterns of primary production. Cont. Shelf Res. 13, 575–599.

Springer, A.M., McRoy, C.P., Flint, M.V., 1996. The Bering Sea green belt: shelf-edge processes and ecosystem production. Fish. Oceanogr. 5(3-4), 205–223.

Stabeno, P.J., Bond, N.A., Kachel, N.B., Salo, S.A., Schumacher, J.D., 2001. On the temporal variability of the physical environment over the southeastern Bering Sea. Fish. Oceanogr. 10, 81–98.

Stabeno, P.J., Bond, N.A., Salo, S.A., 2007. On the recent warming of the Bering Sea shelf. Deep Sea Res. II. 54, 2599–2618.

Stabeno, P.J., Farley Jr., E.V., Kachel, N.B., Moore, S., Mordy, C.W., Napp, J.M., et al., 2012a. A comparison of the physics of the northern and southern shelves of the eastern Bering Sea and some implications for the ecosystem. Deep Sea Res. II. 65-70, 14–30.

Stabeno, P.J., Kachel, N.B., Moore, S.E., Napp, J.M., Sigler, M., Yamaguchi, A., et al., 2012b. Comparison of warm and cold years on the southeastern Bering Sea shelf and some implications for the ecosystem. Deep Sea Res. II. 65-70, 31–45.

Stoecker, D.K., Weigel, A.C., Goes, J.I., 2013a. Microzooplankton grazing in the Eastern Bering Sea in summer. Deep Sea Res. II. In press.

Stoecker, D.K., Weigel, A.C., Stockwell, D.A., Lomas, M.W., 2013b. Microzooplankton: Abundance, biomass, and contribution to chlorophyll in the eastern Bering Sea in summer. Deep Sea Res. II. In press.

Striegl, R.G., Aiken, G.R., Dornblaser, M.M., Raymond, P.A., Wickland, K.P., 2005. A decrease in discharge-normalized DOC export by the Yukon River during summer through autumn. Geophys. Res. Lett. 32, L21413.

Walsh, J.J., McRoy, C.P., 1986. Ecosystem analysis in the southeastern Bering Sea. Cont. Shelf Res. 5(1-2), 259–288.

Whitledge, T.E., Reeburgh, W.S., Walsh, J.J., 1986. Seasonal inorganic nitrogen distributions and dynamics in the southeastern Bering Sea. Cont. Shelf Res. 5, 109–132.

Williams, P.J., 1993. On the definition of phytoplankton production terms. ICES Mar. Sci. Symp. 197, 9–19.

Appendix 3.A Supplemental Section 1

In order to extrapolate our spring and summer data to the annual scale, we assumed that the four seasons as described in Table 3.1 each comprise 91.25 days and that the seasonal rates we observed comprised an average rate of change across the season. Based on a generally accepted pattern of seasonal carbon modification, we then designated a method for the extrapolation of seasonal data that was unavailable (e.g., fall data for each parameter; summer and fall data for parameters where only spring data were

available; spring and fall data for areas where only summer data were available). No data were extrapolated if no seasonal occupations were made in a given domain (e.g., NCP_{TIN}, outer shelf; Table 3.2).

The current perspective on spatiotemporal variability of production in the region emphasizes the localized nature of primary production occurring on different timescales, in different seasons, and different areas (e.g., Lomas et al., 2012). However, several generalized patterns have also been noted. Production rates are typically highest near the marginal ice zone, or ice edge blooms, while open water spring blooms typically exhibit a lower primary production rate (Moran et al., 2012). Sustained rates of high production into the summer season result from nutrient resupply at the shelf break (Springer et al., 1996), while nutrient resupply by storm-induced mixing over the shelf can augment summer and fall production (Sambrotto et al., 1986; Mordy et al., 2012).

While this pattern is probably typical of the Bering Sea shelf, the timing of onset and the magnitude of this cycle may differ spatially. For example, Lomas et al. (2012) observed that *NPP* in the Outer Domain decreased between spring and summer by 64% on average, while middle and Coastal Domain productivity strongly increased between the two seasons (352% and 338%, respectively). This indicates that the spring bloom during 2008 and 2009 was delayed in the shallower regions of the shelf relative to the Outer Domain. Additionally, the range of production observed at the shelf break in spring was higher than in the other two domains, indicating a spatial variation in the magnitude of production cycle.

In order to account for spatial variation in timing and magnitude of primary production, fall rates of *NPP* were assumed to be the average of spring and summer rates when both were available (middle domain, all three years; inner domain, 2010). Where only one season of data were available (Outer Domain, 2008; Coastal Domain, 2009), we adopted a generalized pattern of productivity. We assumed that spring *NPP* would be twice that of summer *NPP* and that fall production would again be the average of these two rates, or 75% of spring production. In each case winter production was assumed to be

negligible, as under-ice and ice-edge blooms are included in the spring season (Table 3.1).

Some of the variability in average regional primary production likely arises from the sampling of active bloom sites at the ice edge. Here, production values are very high, but likely subside on shorter timescales than 91.25 days. Where data from active phytoplankton bloom sites were incorporated into this analysis, blooms were identified as stations with integrated profile values with daily *NPP* rates greater than 100 mmoles C m^{-2} d^{-1}. These blooms were assumed to last 30 days, and samples collected outside of bloom sites were therefore integrated over the remaining 61.25 days of that season.

In order to extrapolate seasonal estimates of *NCP* from the spring values given, we assumed that the pattern in *NCP* would be equivalent to the pattern in *NPP*. Given that *NCP* estimates are conceptually equivalent to new production, an artifact of this approach is that any variation of *NPP* from the 0/1/0.5/0.75 seasonal cycle described above results from a simultaneous change in regenerated production and community respiration. Conceptually, it assumes that regenerated production would increase and the f-ratio decrease across the year as heterotrophic consumption facilitates the recycling of organic matter at the surface layer. Our data do show this pattern for both the Coastal and Middle Domains (Figure 3.A), although the magnitude of this change is dictated by the pattern we prescribed. If *NCP* does not decrease relative to *NPP* over time as we have assumed, the direction of this change may also be erroneous. However, a second artifact of this approach is that in areas where only one season of *NPP* data are available (e.g., Outer Domain), the f-ratio does not vary over time, and this is likely incorrect.

This variation in f-ratio due to increasing grazing pressures likely also affects C_{exp}. An increase in regenerated production enabled by an increase in respiration likely also signifies an increase in grazing pressure from this larger heterotrophic population. These grazers are likely assimilating an increasing amount of organic matter as well, reducing the overall proportion of C_{exp} over time. We therefore assumed that regardless of the pattern of production observed between spring and summer, increasing grazing pressure on a lower proportion of new production would reduce C_{exp}. Fall values of C_{exp}

were prescribed as 75% of summer C_{exp}. During winter, we assumed that the cessation of primary production would reduce C_{exp} to negligible levels.

Given that spring conditions in bottom waters were very cold, and that it was unlikely that organic material from the spring bloom had already reached the floor, it was likely that these respiration rates reflected the organic matter that had settled during the previous year and was slowly being oxidized. Therefore, winter rates of benthic respiration were assumed to be identical to the rates measured in spring. This indicates that the supply of organic matter is greater than the potential rate of consumption by the benthos, despite variations in community size, activity and structure throughout the year that could impose a seasonal cycle on benthic respiration. We therefore assumed that fall rates comprised an average of spring and summer rates. Relative to other parameters, benthic carbon consumption was nearly steady throughout the year.

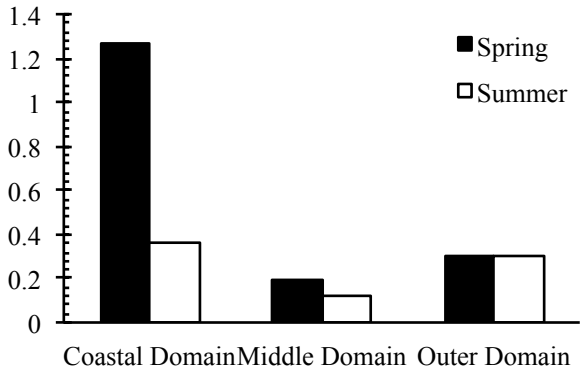

Figure 3.A Seasonal variability in f-ratio by domain (2008 – 2010). Black bars indicate spring estimates of the f-ratio, while white bars indicate summer estimates of the f-ratio.

Chapter 4:

Conservative and non-conservative variations of total alkalinity on the southeastern Bering Sea shelf[3]

4.0 Abstract

Recent observations of calcium carbonate ($CaCO_3$) mineral undersaturations on the Bering Sea shelf have prompted new interest in the physical and biological factors that control the inorganic carbon system in the region. Understanding of the dynamics that influence the spatio-temporal variability of total alkalinity (TA) – one major component of the seawater carbonate system – has been constrained by limited historical data collected across the shelf, and the consensus has been that TA is largely conservative. However, the recently documented undersaturated conditions have the potential to cause substantial non-conservative variability in TA in this region through the dissolution of carbonate minerals. In order to quantify the contribution of carbonate mineral precipitation and dissolution to variability in TA on the southeastern Bering Sea shelf, we examined seasonal observations of TA that were made between 2008 and 2010 as part of the BEST-BSIERP Bering Sea Project. Conservative influences accounted for most of the variability in TA concentrations, with well-constrained mixing dominating in spring and summer of 2008. Bering Shelf Water (BSW) contained a constant ratio of TA to salinity, while river discharge (RW) added TA relative to salinity at a predictable rate. Although substantial organic carbon production and denitrification can cause some non-conservative variation in TA concentrations (a maximum of ~15 μmoles kg SW^{-1} combined), carbonate mineral dissolution and precipitation were shown to be the most important processes responsible for non-conservative TA – salinity relationships. $CaCO_3$ uptake by the dominant pelagic phytoplankton calcifier (i.e., coccolithophores) was shown to alter TA concentrations by as much as 59 μmoles kg SW^{-1}. Evidence for

[3]Cross JN, Mathis JT, Bates NR, Byrne RH. Conservative and non-conservative variations of total alkalinity on the southeastern Bering Sea shelf. Mar. Chem. 2013;154:100–112.

shallow-water $CaCO_3$ mineral dissolution was also observed, which caused TA concentrations to increase by as much as 36 μmoles kg SW^{-1}. Therefore, contrary to our previous understanding, the non-conservative physico-biogeochemical factors observed in this study play an important role in controlling the ocean carbon cycle of the Bering Sea shelf.

4.1 Introduction

Over the past several decades, the physical and biological characteristics of the Bering Sea shelf have undergone a considerable transition associated with such factors as warming and enhanced sea ice loss. This subarctic region is highly sensitive to climate change (e.g., Napp and Hunt, 2001), with a variety of ecosystem-level effects resulting from these perturbations already observed. For example, rising importance of temperate taxa coupled with a decline in Arctic components has been observed in the pelagic community (e.g., Stabeno et al., 1999; Stockwell et al., 2001; Hunt et al., 2002; Macklin et al., 2002; Bond et al., 2003; Overland and Stabeno, 2004; Grebmeier et al., 2006). Continued changes are expected in the coming decades (Schumacher and Alexander, 1999; Stabeno et al., 1999; Hunt and Stabeno, 2002; Schumacher et al., 2003; Stabeno et al., 2012a, b) including warming of the shelf (Schumacher et al., 2003; Stabeno et al., 2006, 2012b), which may have potentially profound impacts on the southeastern Bering Sea ecosystem (Stabeno et al., 2012a).

The ocean carbon cycle of the Bering Sea shelf has also undergone some notable changes during the past decades. Recent studies have documented the occurrence of seasonal calcium carbonate ($CaCO_3$) mineral undersaturations in bottom waters over the shelf (Mathis et al., 2011; Appendix A), similar to seasonal occurrences in the western Arctic Ocean (e.g. Bates and Mathis, 2009). Such seasonal $CaCO_3$ mineral undersaturations in bottom waters result from the synergistic combination of ocean acidification due to ocean uptake of anthropogenic CO_2 from the atmosphere and seasonal physico-biogeochemical coupling that can suppress or enhance the saturation state (Ω) for $CaCO_3$ minerals (Bates and Mathis, 2009; Bates et al., 2012; Appendix A).

These undersaturated conditions may hinder the production and maintenance of carbonate shells and tests in both pelagic and benthic organisms (Fabry et al., 2009), with unknown consequences for the regional ecosystem and commercially valuable fisheries.

Observations of the change in TA concentrations over time have permitted the direct quantification of carbonate mineral dissolution in other areas of undersaturation (Andersson et al., 2007; Chen, 1993). These approaches assume that TA concentrations in excess of those predicted by a known conservative relationship between TA and salinity are caused by carbonate mineral dissolution. In previous studies of Bering Sea waters, TA was assumed to be a conservative parameter (Chen et al., 1985; Chen, 1993; Murata and Takizawa, 2002; Merico et al., 2006; Mathis et al., 2011; Appendix A), indicating that this approach may be appropriate for observations of seasonal production of TA and quantification of pH-mediated carbonate mineral dissolution in this area. However, complex mixing scenarios, wide spatial variability, and intense biogeochemical modification are common on the Bering Sea shelf and could complicate the calculation of non-conservative TA variability.

In order to assess the degree to which carbonate mineral precipitation and dissolution impacts the carbon system of the Bering Sea shelf, we explore the factors that control both conservative and non-conservative variations in TA across the eastern Bering Sea through seasonal measurements of the carbonate system between 2008 and 2010. We will demonstrate that the relationship between TA and salinity can be highly variable, and that even conservative processes can result in poorly constrained mixing relationships between TA and salinity. However, in cases where conservative mixing relationships are predictable, it is clear that both non-conservative carbonate mineral precipitation and dissolution mediate TA concentrations over the shelf. In addition to expected non-conservative variations in TA resulting from biogenic carbonate mineral precipitation and deep-water carbonate mineral dissolution, we also observed evidence for pH-mediated, shallow-water carbonate mineral dissolution during the fall of 2009.

4.2 Hydrographic Structure of the Bering Sea

Identification of non-conservative variations in TA is dependent on the ability to predict a baseline TA concentration, usually determined through discrete, close relationships between TA and salinity in differing water masses (e.g., Bates et al., 1996; Friis et al., 2003; Andersson et al., 2007; Cai et al., 2010a). On the eastern Bering Sea shelf, there are at least three unique water masses distinguishable by stable oxygen isotopes ($\delta^{18}O$; Weingartner, Danielson, and Aagaard, unpublished data; Figure 4.1). High density deep water from the adjacent Bering Sea basin, traditionally known as Anadyr Water (AW) exhibits $\delta^{18}O$ values near zero; low-density river water (RW) has a very light isotopic signature (strongly negative $\delta^{18}O$**;** Bering shelf water (BSW) exhibits a moderate density and $\delta^{18}O$ value. All are considered unique end-members. However, BSW $\delta^{18}O$ can be highly variable due to isotopic fractionation processes occurring during the freezing and melt of sea ice. Heavier isotopes are favored by the ice matrix (O'Neill, 1968) and thus ice melt exhibits a positive $\delta^{18}O$, while brine-influenced seawater exhibits a slightly more negative $\delta^{18}O$ (small vector, Figure 4.1).

The relative contributions of each of these end-members to the water mass over the shelf vary seasonally. During winter, homogenization of most chemical parameters occurs beneath the ice (Figure 4.2A), and BSW dominates nearly the entire shelf. The contributions of each of the other water-masses increase through spring and reach their maximum prominence in summer or fall. The Yukon and Kuskokwim Rivers contribute a large volume (~234 km^3) of freshwater to the shelf each year (Feely et al., 1981; Brabets et al., 2000; Striegl et al., 2005, Stabeno et al., 2006; Striegl et al., 2007). RW fractions reach their maximum after the spring freshet (May; Brabets et al., 2000; Dornblaser and Striegl, 2007; USGS NWIS, 2012). Although ice retreat can begin as early as February (Stabeno et al., 2001; Stabeno et al., 2012a), rapid onset of ice ablation usually occurs in May (Figure 4.2B). With the onset of heating through intense solar insolation and the weakening of surface currents, BSW is strongly partitioned through both salinity and temperature stratification by August (Ladd and Stabeno, 2012; Figure 4.2C). Upwelling of AW along the shelf break occurs most often during October through April under the

influence of southeasterly winds, although some on-shelf flow as a result of this wind forcing can occur during the more stratified summer months (Danielson et al., 2012).

The spatial extent of the contribution of AW and RW and the consequent mixing with BSW are defined by the hydrographic structure of the shelf (Figure 4.2), indicating that conservative mixing relationships should vary spatially as well as temporally. Circulation patterns and frontal structures divide the shelf into three along-shelf domains. The Coastal Domain is bounded by the coastline and Inner Front, which is typically located at the 50 m isobath (Kachel et al., 2002). RW plumes are typically restricted to this domain (Feely and Cline, 1976; Belkin and Cornillon, 2005; Danielson et al., 2006; Figure 4.2B, C). This area is shallow enough that the combination of wind and tidal mixing completely overturns the water column in most cases (Coachman, 1986; Stabeno et al., 2006), helping to thoroughly mix RW and BSW. However, rapid RW discharge can cause some stratification in this region during summer.

As the shelf deepens seaward of the Inner Front, separation of a wind-mixed surface layer and a tidally mixed bottom layer leads to the formation of a two-layer system that is most distinct during summer (Coachman, 1986; Stabeno et al., 2006; Figure 4.2C). Long residence times caused by slow along-shelf flow (Coachman, 1986, 1993; Overland and Roach, 1987, Stabeno et al., 1999) combined with the onset of stratification result in the isolation of cold, brine-influenced remnant winter waters near the bottom during this time (Ladd and Stabeno, 2012; Stabeno et al., 2012a, b; Zhang et al., 2012; Figure 4.2C). This seasonal partitioning is ultimately the source of the strong variability in BSW (small vector, Figure 4.1).

Located near the 100 m isobath, the Central Front is a broad transition between the Middle and Outer Domains. The Outer Domain is also bounded on the seaward side by the shelf-break front (250 m). This front isolates the Outer Domain from the deep basin waters of the Bering Sea (Coachman, 1986; Stabeno et al., 2006), although some penetration of basin waters into the Outer Domain can occur via upwelling events driven by eddies, shoaling topography, funneling of water through submarine canyons, and wind forcing. These effects are most common during the summer and fall (Coachman, 1982,

1986; Nihoul et al., 1993; Schumacher and Stabeno, 1998; Stabeno and van Meurs, 1999; Mizobata and Saitoh, 2004; Danielson et al., 2011, 2012).

4.3 Methods

4.3.1 Cruise Information and Water Column Sampling

As part of the BEST-BSIERP Bering Sea Project (NSF and NPRB; bsierp.nprb.org), measurements of TA and dissolved inorganic carbon (DIC) were made in the eastern Bering Sea from USCGC *Healy* during spring (April/May) of 2008, summer (July) of 2008, and spring (April/May) of 2009; R/V *Knorr* in summer (June/July) of 2009; NOAA ship *Miller Freeman* in fall (September) of 2009; and R/V *Thomas G. Thompson* in late spring (May/June) and summer (June/July) of 2010. Stations were occupied on several east-west transect lines (MN, SL, and NP, Figure 4.3) and one north-south transect along the 70 m isobath (70M, Figure 4.3). At the beginning of each spring cruise, sea ice cover was near 100% at all stations with the exception of stations at the southern end of the 70M line and some minor leads, particularly around the islands. During summer and fall of all three years, the entire Bering Sea shelf was ice-free. Discrete observations of DIC and TA, as well as calculations of seasonal NCP and saturation state data for the 2008 and 2009 cruises have been previously reported (Mathis et al., 2010, 2011; Chapter 2; Appendix A). Additional numerous publications associated with the BEST-BSIERP Bering Sea Project are available through two special issue volumes of Deep Sea-Research II (volume 65; second volume in press), with third and possible fourth volumes in preparation.

4.3.2 Analytical Methods

At each CTD/hydrocast station, seawater samples were analyzed for salinity and inorganic nutrients (nitrate, phosphate, silicate, etc.) by the NOAA Eco-Foci group (Gordon et al., 1994). Conductivity-temperature-depth samples were collected on downcasts with a Seabird Electronics 911-plus system using dual temperature and conductivity sensors. Seawater samples for dissolved inorganic carbon (DIC) and TA

were drawn from Niskin bottles into pre-cleaned ~300 mL borosilicate bottles and poisoned with mercuric chloride ($HgCl_2$) to halt biological activity. Ice core samples were processed according to the method of Appendix A. Samples were analyzed using a precise and accurate gas extraction/coulometric detection system (Bates, 2001). The analytical system consists of a VINDTA 3C (Versatile Instrument for the Detection of Total Alkalinity) coupled to a CO_2 coulometer. TA samples were determined by potentiometric titration using the VINDTA 3C. Routine analyses of Certified Reference Materials (CRMs, provided by A.G. Dickson, Scripps Institution of Oceanography) ensured that the accuracy of the DIC and TA measurements was within 0.08% (~2.0 μmoles kg SW^{-1}) and stable over time. Carbonate parameters (e.g., pH, $CaCO_3$ Ω for calcite (Ω_C) and aragonite (Ω_A) were calculated with CO2SYS version 1.05 from DIC, TA, temperature, salinity, phosphate, and silicate data using the thermodynamic model of Lewis and Wallace (1998) as updated by Robbins et al. (2010), using the borate dissociation constant of Dickson (1990); the silicate and phosphate dissociation constants listed by Dickson et al. (2007); the carbonic acid dissociation constants of Mehrbach et al. (1973) as refit by Dickson and Millero (1987); and the CO_2 solubility equations of Weiss (1974). At similar standards of measurement precision to those given here, the error in the calculation of saturation states is typically 0.10 units (Dickson, 2010; Hydes et al., 2010). The CO2SYS macro does not introduce any additional error beyond that of the empirical constants and laboratory data utilized (Lewis and Wallace, 1998).

4.3.3 USGS Data Sets

Two data sets from the USGS provided information about the Yukon and Kuskokwim Rivers. Historical stream flow and TA data were accessed through the National Water Information System (waterdata.usgs.gov/ak/nwis). The National Stream Quality Accounting Network provided frequent measurements of TA for the Yukon River (downloaded at: water.usgs.gov/nasquan). River data came from the closest available site to the river outlets; i.e., Yukon River samples included in this study were taken at USGS Site 15565447 (Pilot Station), and Kuskokwim River samples were taken

at USGS Site 15304000 (Crooked Creek). USGS measurements of TA were converted from an incremental titration of filtered water for mg $CaCO_3$ L^{-1} (USGS data parameter code 39086).

4.3.4 Data Visualization

Satellite True-Color images were created from Modis Aqua Level 0 files, which were downloaded from NASA's ocean color website (oceancolor.gsfc.nasa.gov) and processed using SeaDAS, a software package available through the same site. Graphics for this work were generated with Ocean Data View (Schlitzer, R., Ocean Data View, http://odv.awi.de, 2012). Interpolation of discrete observational data for the purposes of data visualization was generated according to the program's VG Gridding algorithm.

4.4 Results and Discussion

4.4.1 Conservative Variability in TA Concentrations

Conservative variability in TA concentrations is traditionally identified through confirmation that the ratio of salinity and TA (Specific Alkalinity (SA); Koczy, 1953) is constant within discrete water masses. However, conservative processes such as precipitation and evaporation can cause some SA variability even within discrete water masses. In order to "correct" variability in SA across a discrete water mass related to precipitation and evaporation, such as we might observe in the seasonal partitioning of BSW, a normalization can be performed relative to a reference salinity, such that: $nTA = TA / S \times S_{Ref}$ (Millero et al., 1998). In most cases, this equalizes the ratio of SA across a water mass with a variable salinity, and confirms that the change in alkalinity relative to salinity is conservative. However, application of this traditional method to regions that contain an increasing fraction of fresh water with a non-zero concentration of TA results in an ever-increasing normalized TA, such that nAlk at $S = 0$ is infinite. Assuming linear mixing between a two end-member system, this traditional method can be modified to accommodate a zero-salinity end-member with non-zero TA concentration (Friis et al., 2003), such that:

$$TA = TA_0 + b \quad \text{(Eq. 4.1)}$$

where TA_0 is the end-member TA concentration of river discharge, b is the slope of the regression line, and S is the salinity of the sample. The slope of this regression line can itself be predicted:

$$b = \frac{TA_1 - TA_0}{\Delta S} \quad \text{(Eq. 4.2)}$$

where TA_1 and TA_0 are the TA concentrations of the two end-members, and ΔS is the salinity difference between the end-members. Conversely, observing the slope and y-intercept of non-normalized, linearly changing TA concentrations can identify TA_0.

In order to identify conservative variability in TA concentrations in the Bering Sea, we used a combination of these two approaches. Figure 4.4 shows the relationship between TA and salinity for spring (Figure 4.4A) and summer (Figure 4.4B) of 2008 overlaid on isolines of constant SA. During both seasons of this year, a large portion of the mid-salinity data followed the 68 μmoles kg SW^{-1} S^{-1} isoline very closely, indicating that these data are all functionally derived from the same water mass. Given the salinity, we identified this water mass as BSW. However, this was the only area of constant SA we observed for this data set, indicating that while other water masses exist on the Bering Shelf, these data only represent areas of mixing between BSW and the other water masses. In particular, we were able to identify conservative influences of RW and some conservative variation in BSW due to sea ice formation and melt, which we discuss in Sections 4.1.1 and 4.1.2. However, conservative variability was not clear at higher salinities, indicating complex processes were occurring during mixing between AW and BSW, which we discuss in Section 4.1.3.

4.4.1.1 Conservative Mixing Between BSW and RW

In waters with lower salinities, we observed a linear deviation from the 68 μmoles kg SW^{-1} S^{-1} isoline during spring of 2008 (Figure 4.4A) along the central 70M line. Previous works (Mordy et al., 2012; Stabeno et al., 2012a) have identified this as a coastal water mass that was advected towards the center of the 70M line during this

season, and likely contains the influences of river discharge. In this two end-member mixing scenario, we can employ the Friis method described above to determine the end-member concentration of TA in RW. A regression of this portion of these data (low salinity waters along the central 70M line; rms = 0.21 μmoles kg SW^{-1}) indicated that the water mass had an end-member concentration of 1244 μmoles kg SW^{-1} at zero salinity. In summer, deviation of TA concentrations from the 68 μmoles kg SW^{-1} S^{-1} isoline gradually increased as salinity decreased. The resulting curvature indicated that the end-member concentration of TA in river waters gradually increased. Correspondingly, long-term data records from the USGS NASQUAN and NWIS data sets (Figure 4.5) also indicate that river TA reaches a minimum during the peak of the spring freshet (May), and gradually increases as flow slackens slightly through the summer months.

4.4.1.2 The Conservative Influences of Sea Ice Formation and Melt

Ideally, sea ice melt end-members can be assumed to have near-zero values of TA and salinity (e.g., Cai et al., 2010a). In such a case, BSW samples affected by sea ice melt would produce salinity and TA relationships with constant SA, identical to that of BSW, all the way to the origin. However, recent observations (e.g., Rysgaard et al., 2007, 2009, 2011) suggest that chemical processes occurring during ice formation partition TA between brine and solid ice, which may cause the SA of brine- or melt-influenced BSW to change. During ice formation, rejection of solute-rich brine contributes to very high $CaCO_3$ supersaturations and subsequent precipitation of $CaCO_3$ crystals (Assur, 1960; Rysgaard et al., 2007; Dieckmann et al., 2008; Fransson et al., 2009; Rysgaard et al., 2009; Dieckmann et al., 2010; Rysgaard 2011, 2012a, b; Nomura et al., 2013) in brine prior to drainage from the ice matrix. These precipitates collect in the ice matrix rather than flush with rejected brine (e.g., Jones and Coote, 1981; Killawee et al 1998; Papadimitriou et al., 2004; Rysgaard et al., 2007; Dieckmann et al., 2008). Because these precipitates dissolve when strong Ω supersaturations are diluted by ice ablation during the melt process, the TA of sea ice melt-waters is higher than the TA of sea ice brine (Rysgaard et al., 2007; Nedashovsky et al., 2009; Rysgaard et al., 2009, 2012a, b; Geilfus

et al., 2013), directly opposing the trend in salinity. While sea ice melt-water may have lower TA relative to shelf waters, the TA is elevated relative to its salinity. In some cases, this high-SA ice melt water consequently increases the buffering capacity of surface waters, decreasing surface layer pCO_2 (Rysgaard et al., 2012a).

Our observations indicated that the TA of individual core sections varies widely (Table 4.1). Some cores consistently exhibited a higher SA than BSW through each 10 cm core section (e.g., core numbers 39914 and 33916; Table 4.1) while others exhibited a consistently lower SA through the entire core, except in the bottom core sections (core numbers 39911 and 39918). Some cores exhibited no trend in SA with core depth (e.g., core numbers 39931, 39917). On average, the SA of our ice core samples (70 μmoles kg SW^{-1} S^{-1}) was higher than the average SA of BSW (68 μmoles kg SW^{-1} S^{-1}), which is consistent with the theoretical principle of TA retention in ice. However, strong variability inhibits a statistical differentiation between the SA of our ice core sections and BSW.

From a mixing standpoint, sea ice melt obviously impacts the interaction between BSW and river waters. The triangular distribution of TA and S at the low-salinity end of the summer of 2008 data (Figure 4.4B) provided evidence for a three end-member interaction (Cai et al., 2010a). This pattern indicates that a third water mass with a lower S and SA is mixing with all river-influenced BSW samples, causing a systematic lowering of SA across a range of low salinities. The only known possibility for this third water mass is low-salinity BSW, or a very similar water mass with slightly higher SA due to TA retention in sea ice.

4.4.1.3 The Influences of Anadyr Water

During spring of 2008 (Figure 4.4A), the relationship of TA and salinity showed a distinct bend at ~2300 μmoles kg SW^{-1}, where TA began to increase relative to salinity towards higher salinities. This salinity break was also observed during summer of 2008 (Figure 4.4B), and was apparent across the entire data record (Figure 4.4C). The linearity of this deviation suggests conservative mixing with another water mass of different SA,

similar to the linear deviation from constant SA created by mixing with river water at lower salinities during spring of 2008. This high-salinity water mass was located in deep waters off the shelf break, and thus likely represented the influences of AW. However, AW and BSW are ultimately derived from the same source; while the density of AW changes relative to BSW, the isotopic signature of both water masses remains similar (Figure 4.1), indicating that only conservative processes separate these two water masses. Additionally, both AW and BSW are derived from North Pacific Deep Water (NPDW, Stabeno et al., 2006); deep inflow of NPDW supplies the deep Bering Sea basin, while upwelled NPDW supplies the surface flows in the Gulf of Alaska and Bering Sea shelf. Therefore, we expect that the SA in these two water masses should be very similar, and that the large deviation in SA we observed in higher salinity deep waters indicated non-conservative addition of TA. It is possible that SA in these deep waters may not follow salinity exactly as particulate carbonates dissolve in low pH conditions typical of deep waters and gradually increase TA concentrations relative to salinity. We discuss this further in Section 4.2.3.

4.4.2 Non-conservative Variability in TA Concentrations.

While conservative mixing dominated variations in TA during spring and summer of 2008, Figure 4.4C shows that considerable non-conservative variability in SA can occur interannually. During 2009 and 2010, the absence of clear mixing relationships indicates that conservative processes were not apparent. While it is likely that much of this variability resulted from unresolved mixing relationships between multiple end-members, non-conservative modification of TA concentrations can be magnified in highly productive coastal systems (Hydes et al., 2010). In particular, the accumulation of organic carbon, denitrification, and carbonate mineral precipitation and dissolution can all cause some non-conservative perturbation to TA concentrations in extreme cases. During 2009 and 2010, production rates were highly magnified in some areas of the Bering Sea shelf relative to 2008 (e.g., Lomas et al., 2012; Chapter 2). Rather than unconstrained mixing, it is possible that the highly variable TA and SA observed during

the latter years of our field program resulted from the influence of these production-associated non-conservative processes. In order to specifically isolate the non-conservative influences of carbonate mineral precipitation and dissolution, we first calculated and corrected for any perturbation to TA concentrations caused by denitrification and organic carbon accumulation.

4.4.2.1 Organic Carbon Accumulation

TA is defined by the titration of all weak bases in solution with H^+. The presence of negatively charged surface groups on phytoplankton and bacterial cells can functionally increase the concentration of the weak bases that contribute to TA (Brewer and Goldman, 1976; Kim et al., 2006, 2009). While high concentrations of organic carbon can be observed, especially during ice edge blooms (e.g., Niebauer et al., 1995), this organic carbon is rapidly exported (Moran et al., 2012; Baumann et al., 2013; Chapter 3), and little retention in the water column has been observed (Chapter 2). What little TOC is found in the water column increases linearly with decreasing salinity (Chapter 2), and is assumed to be terrestrially derived. Thus, any addition of TA that is caused by TOC contribution from rivers is likely accounted for in our estimates of the river water end-member concentration of TA, causing TA to be slightly higher in these samples. While the exact contribution of organic carbon to TA concentrations varies by phytoplankton species composition, average estimates indicate that 200 μmoles POC kg SW^{-1} contributes between 3 and 5 μmoles TA kg SW^{-1} (Kim et al., 2006, 2009). In the Bering Sea, concentrations of TOC (which includes both the dissolved and particulate pools of organic carbon) are usually below 100 μmoles kg SW^{-1}, although concentrations can peak at 130 μmoles kg SW^{-1} (Chapter 2). Therefore, the maximum potential perturbation to TA was less than 3 μmoles TA kg SW^{-1}.

4.4.2.2 Denitrification

Anaerobic remineralization processes like denitrification and sulfate reduction can also impact TA concentrations, provided that the products of these reactions are

permanently lost (Hu and Cai, 2011). The utilization of one mole of sulfate during sulfate reduction will generate approximately two moles of TA, while denitrification will generate approximately one mole of TA for every mole of nitrogen denitrified (Chen and Wang, 1999). Some studies have estimated that in continental margin systems, anaerobic TA production can be significant across the global oceans (Chen, 2002; Thomas et al., 2009). Sedimentary denitrification has been shown to impact the entire water column in the Bering Sea, producing nitrate deficits in all seasons and across all domains (Granger et al., 2011; Mordy et al., 2012). A regional parameterization of the relationship between dissolved inorganic nitrogen (DIN) and phosphate indicates that on average, the DIN : phosphate residual (N**) can be calculated such that $N^{**} = DIN - (PO_4 \times 15.5) + 5.9$. According to this relationship, we observed that Bering Sea waters were denitrified by ~4 ± 3.5 μmoles NO_3 kg SW^{-1} across all seasons in all years, although values as low as -15 μmoles kg SW^{-1} were also observed. As stated above, if the products of this reaction were permanently lost, denitrification would have produced an average perturbation of ~4 μmoles kg SW^{-1} TA.

4.4.2.3 Carbonate Mineral Precipitation and Dissolution

Processes affecting $CaCO_3$ mineral precipitation and dissolution, as sinks and sources of TA, produce stronger non-conservative TA behavior relative to salinity compared to both TOC accumulation and denitrification (e.g., Brewer et al., 1975; Brewer and Goldman, 1976; Millero et al., 1998; Cai, 2003; Cai et al., 2010a, b). For example, non-conservative TA depletions of 25 – 30 μmoles kg SW^{-1} have resulted from the surface layer activity of coccolithophores (Bates et al., 1996), a calcifying haptophyte algae that produces liths of $CaCO_3$. Small populations of the coccolithophore *Emiliania huxleyi* have been observed in the Bering Sea since 1997 (Overland et al., 2001; Stabeno et al., 2001; Stockwell et al., 2001; Merico et al., 2003, 2004; Iida et al., 2012) with varying extent and frequency. Additionally, undersaturations of carbonate minerals have been observed in this region, which thermodynamically favor the dissolution of carbonate minerals and should non-conservatively increase water column TA concentrations.

Together, these two processes have the potential to cause the largest non-conservative perturbations to TA concentrations in the Bering Sea, and may help to explain some of the variability observed in TA concentrations where organic carbon accumulation and denitrification did not.

In order to isolate the effects of carbonate mineral precipitation on TA variation, corrections for both TOC accumulation and denitrification were applied to these data. Measured TOC concentrations were multiplied by 0.025, the maximum ratio of POC : TA perturbation observed by Kim et al. (2006), and subtracted from TA concentrations. The DIN residual of each sample was calculated according to Mordy et al., (2010). Given that negative DIN residuals indicate denitrification and correspond to TA addition, these values were then added to TA concentrations. Overall, the corrected TA (TA_C) concentrations were defined such that:

$$TA_C = TA_{Observed} - 0.025 \times TOC + DIN - (PO_4 \times 15.5) + 5.9 \quad \text{(Eq. 4.3)}$$

Below, we examine three particular cases of carbonate mineral precipitation and dissolution. Given the strong spatial variability in conservative relationships between TA and S, we allowed conservative variability in TA concentrations to vary for each case. To identify regional conservative TA variability, a linear regression between TA_C and salinity was performed on samples along the same hydrographic line, but outside the region of strongest TA variability (e.g., linear mixing relationships between TA_C and S in subsurface waters help to identify activity of coccolithophores in overlying surface waters). Therefore, any deviations relative to the regional conservative mixing regression line highlight the regional contributions of carbonate mineral precipitation and dissolution.

Coccolithophore production. During fall of 2009, we observed a large reduction in TA_C in surface waters along the middle shelf (e.g., 70M line; Figure 4.6). These reductions in TA concentrations were restricted to the Middle Domain, with one area of particularly intense drawdown observed near the intersection of the MN and 70M lines at ~60°N, and another farther south along the 70M line ~57.3°N (Figure 4.6). TrueColor Satellite images provided by SeaWifs Reprocessing (Feldman and McClain, Ocean Color

Web, 2012; Figure 4.7) for September 21 and October 8 showed distinctive blue-green colors indicative of the light reflectance by detached coccoliths (e.g., Suykens et al., 2010). These areas corresponded to the two identified locations of TA drawdown: one near the intersection of the 70M and MN lines just southwest of St. Matthew Island (SMI, Figure 4.7A); and another northwest of St. Paul Island (SPI, Figure 4.7B; also see Figure 4.3 for reference). A linear regression of TA_C and salinity of sub-surface water along the 70M line (rms = 3.7 μmoles kg SW^{-1}; $R^2 = 0.90$; bold black line, Figure 4.8) indicated that TA_C concentrations were drawn down by as much as 59 μmoles kg SW^{-1}, similar to other studies of coccolithophore blooms (e.g., 49 μmoles kg SW^{-1}; Harlay et al., 2010; Suykens et al., 2010; Harlay et al., 2011). This non-conservative depletion accounted for ~60% of the total depletion of TA occurring between seasons (maximally 101 μmoles kg SW^{-1}), indicating that non-conservative carbonate mineral precipitation can exert as much control over TA concentrations as conservative controls.

Carbonate Mineral Dissolution in Anadyr Water. As discussed earlier, we suggested that the SA of BSW and AW should be similar, if not identical, and suggested that the change in SA observed at high salinities was indicative of carbonate mineral dissolution rather than conservative mixing between AW and BSW. Figure 4.9A shows the variation in Ω_C with depth, indicating that the saturation horizon occurs at ~250 m. Each sample indicating an elevated SA at the higher salinities was taken below this depth, which also indicated that carbonate mineral dissolution should have impacted each of these samples and increased SA. Therefore, in order to calculate the excess TA in AW, we assumed that conservative influences would produce a TA_C of 68 × S, as the SA of BSW was 68 μmoles kg SW^{-1} S^{-1}.

Carbonate mineral dissolution in AW has been previously estimated in the Bering Sea at 45 μmoles $CaCO_3$ kg^{-1} SW^{-1} (Chen, 1993). Given that the dissolution of 1 μmole of $CaCO_3$ generates 2 mEq TA, we estimated $CaCO_3$ dissolution in our samples such that: $\Delta CaCO_3 = 0.5 \times (TA_C - 68 \times S)$. Overall, we obtained a similar value to Chen (1993) of ~40 μmoles kg SW^{-1} dissolved $CaCO_3$ in our deepest AW samples (Figure 4.9B). Further, we also observed that dissolved $CaCO_3$ was evident at approximately the same

depth as the calcite saturation horizon (Ω_C = 1; ~250 m, Figure 4.9A), confirming that all AW is likely affected by carbonate mineral dissolution. Our observed calcite saturation horizon was somewhat shallower than that observed by Chen (400 m; 1993), which could indicate the upward migration of the saturation horizon due to anthropogenic CO_2 inputs (e.g., Feely and Chen, 1982; Byrne et al., 2010; Feely et al., 2012).

Shallow-water carbonate mineral dissolution. Surface waters are typically supersaturated with respect to aragonite and calcite, and no shallow-water undersaturations were noted by Chen (1993). However, in recent years, undersaturations for both aragonite and calcite have been documented in the bottom waters of the Bering Sea shelf, as shallow as 40 m from the surface during the summer and fall of 2009 (Mathis et al., 2011; Appendix A). In most cases, these undersaturations can be slight ($CaCO_3$ Ω = 0.9), requiring as much as three years to dissolve carbonate minerals. Later in the season, increases in CO_2 from the respiration of exported organic carbon (e.g., Mathis et al., 2010, 2011; Appendix A) can generate $CaCO_3$ Ω low enough to force rapid carbonate mineral dissolution. For example, Ω_A as low as 0.51 has been observed in some areas of the shelf (Mathis et al., 2011; Appendix A).

Although observed $CaCO_3$ Ω in the Bering Sea is in some cases very low, the amount of resulting carbonate mineral dissolution depends on both the intensity and the duration of undersaturation events. At the lowest observed undersaturations, the time required for complete dissolution of available aragonitic solids (τ) is approximately five days of sustained undersaturation, assuming a reaction order of n = 1 and k_{CaCO_3} of 0.38 (Hales and Emerson, 1997):

$$\tau = \frac{1}{k_{CaCO_3}(1-\Omega)^n} = 5.26 \text{ days} \qquad \text{(Eq. 4.4)}$$

The corresponding Ω_C at this site was 0.80, requiring 13 days of persistent undersaturation for complete dissolution of available calcitic solids. Given that this value of k_{CaCO_3} was calculated based on laboratory data (Keir, 1980 as refit by Hales and Emerson, 1997) rather than *in-situ* sediment data, we assumed that this timescale was more indicative of the dissolution of carbonate solids suspended in the water column (as

by strong tidal resuspension). While conditions favoring carbonate mineral dissolution are often enhanced in sedimentary environments by metabolic processes (e.g., Suykens et al., 2011), direct measurement of the rates of sedimentary dissolution of carbonates indicates that sedimentary dissolution can be much slower than theoretical predictions (e.g., τ = 20,000 days at Ω = 0.5). Several authors have speculated that this discrepancy is possibly influenced by diffusive transport from the sediment surface, physicochemical reaction inhibition such as refractory biofilms, and larger area-to-volume ratios of carbonate mineral solids (Dreybrodt et al., 1996; Hales and Emerson, 1997; Morse and Arvidson, 2002). These influences may be reduced for suspended solids.

Continuous observations from moored sensors have indicated that Ω_A values of 0.5 emerge as early as July and persist for at least five months, with continuing undersaturation likely following the end of the data record (Appendix B). Relative to the time required for carbonate mineral dissolution in the Bering Sea, the duration of undersaturations provides sufficient time not only for partial but also for complete dissolution of available aragonite minerals using the reaction order and k_{CaCO_3} from Hales and Emerson (1997). To the authors' knowledge, no previous or current estimates of the suspended or sedimentary aragonite and calcite concentrations are available for this region. These data not only suggest that some dissolution of $CaCO_3$ is occurring over the Bering Sea shelf, and should affect TA concentrations, but that aragonite may be totally absent from surface sediments in this region. In this case, any carbonate mineral dissolution observed in this location would result from the advection of suspended aragonite solids, or the vertical export of seasonally produced aragonite solids from the surface. To precisely determine spatiotemporal variation of calcite and aragonite solid concentrations in surface sediments would require additional data.

In our Bering Sea data set, the lowest observed Ω occurred in fall of 2009 along the seaward edge of the SL line (see Figure 4.3 for reference). While continuous moored observations of carbonate parameters are not available for this location, seasonal samplings show that bottom waters at the seaward end of the line were undersaturated during the first seasonal occupation during spring of that year (mid April; Figure 4.10A),

persisted through summer (mid June; Figure 4.10B), and were again observed in fall (early October; Figure 4.10C). These consistent observations of low Ω_A in this area indicated that undersaturations likely persisted for at least these five months. During spring, near-bottom Ω_A values were as low as 0.61 at the seaward end of this line, and decreased through fall to 0.58 at the same site. At an Ω_A of 0.61, only seven days are required to dissolve available suspended aragonite minerals, while five months of undersaturations at this value were observed, providing ample time for carbonate mineral dissolution.

Along the SL line, we also observed excess TA_C relative to that expected from conservative mixing. Figure 4.11 shows the relationship of TA_C and salinity during fall of 2009. A regression of TA_C and S data from the inshore six stations of the SL line indicated well-constrained conservative mixing (rms = 4.57 μmoles kg SW^{-1}, $R^2 = 0.92$; bold black line, Figure 4.11). Relative to this conservative mixing, excess TA_C and therefore dissolved $CaCO_3$ were observed both in undersaturated bottom waters and the overlying surface waters (warm colors, Figure 4.12). While this penetration of dissolved $CaCO_3$ to the surface may suggest the dissolved carbonate is related to a separate water mass, we do not find evidence of a second water mass in the relationship of TA and S, and suggest that the excess TA_C and dissolved carbonate in the surface layer are derived from upward penetration of excess alkalinity from carbonate mineral dissolution in bottom waters.

Previous work (Mathis et al., 2011; Appendix A) has shown that the undersaturations observed in the Bering Sea are the result of a synergistic combination of natural carbonate mineral suppression and additional forcing from anthropogenic CO_2 ($CO_{2(Anth)}$) providing evidence that all seasonal undersaturations in this region are the result of $CO_{2(Anth)}$. It was hypothesized that as $CO_{2(Anth)}$ continues to accumulate in shelf waters, persistent undersaturations will first appear near the bottom, where CO_2 concentrations are naturally higher. During each of our seasonal occupations of the shelf between the spring of 2009 and the summer of 2010, we observed undersaturations of

aragonite in bottom waters at the seaward end of the SL line. This indicates that anthropogenic CO_2 may have produced the hypothesized persistent undersaturations.

In order to determine whether any of these undersaturations are natural, we can subtract the concentration of $CO_{2(Anth)}$ from the total CO_2 content of our samples and recalculate $CaCO_3$ Ω, following the example of Bates and Mathis (2009). While calculating the anthropogenic CO_2 content of shallow waters in the Bering Sea is difficult, previous work has estimated that the shelf waters were entirely saturated with ~45 μmoles excess CO_2 kg SW^{-1} in 1983 (Chen, 1993). Removal of this CO_2 from the water column does result in supersaturations of aragonite during the spring and summer of 2009 and 2010. However, an additional 25 – 30 μmoles kg SW^{-1} CO_2 must be removed in order to produce supersaturations during fall of 2009. With a known rate of CO_2 absorption, we can estimate the amount of carbonate that was absorbed between the observations made by Chen (1993) and the start of our field program in 2008. Recently, the rate of absorption of anthropogenic CO_2 was constrained in the subpolar North Pacific between 1999 and 2006 (Sea of Okhotsk; 44°N, 155°E; Watanabe et al., 2011) as 0.86 ± 0.12 μmoles kg SW^{-1} yr^{-1}. Extrapolating this rate linearly across the 25 years between Chen (1993) and our observations indicated that an additional 21.5 μmoles $CO_{2(Anth)}$ kg SW^{-1} has been absorbed by the Bering Sea, resulting in an overall estimate of ~66.5 μmoles $CO_{2(Anth)}$ kg SW^{-1}, which should be present in our 2008 – 2010 samples.

Based on this estimate of $CO_{2(Anth)}$, we conclude that all aragonite undersaturations in spring and summer and all calcite undersaturations in fall resulted from the additional presence of $CO_{2(Anth)}$. An additional 11 μmoles kg SW^{-1} anthropogenic CO_2 would be required to completely reproduce undersaturations of aragonite in fall. While this indicates that some carbonate mineral dissolution resulting from natural carbonate mineral undersaturations is possible during the fall season, we emphasize that the persistence of undersaturated conditions is substantially prolonged by $CO_{2(Anth)}$ and most of the carbonate mineral dissolution results from $CO_{2(Anth)}$. The dissolved $CaCO_3$ and excess TA_C calculated here provides the first evidence that ocean acidification is causing carbonate mineral dissolution in the Bering Sea.

This could have important implications on both the regional and the global scale. Increasing carbonate dissolution on the Bering Shelf could have potentially disruptive consequences for the regional ecosystem, as many calcifying marine species (Long et al., 2013a, b) are present in this ecosystem and provide critical links in the regional food web (Andersson et al., 2008; Boveng et al., 2008; Fabry et al., 2008, 2009; Chilton et al., 2010). Additionally, the transport of dissolved $CaCO_3$ from areas of local shallow-water carbonate mineral dissolution has been observed to have global importance (Friis et al., 2006). Flushing of newly dissolved free carbonate ions in BSW through Bering Strait (Macdonald et al., 2002; Kadko and Swart, 2004; Cooper et al., 2008) could provide a potential sink for excess CO_2 in the Arctic Ocean halocline (Chen, 1993). As excess CO_2 in the waters of shallow subarctic seas continues to increase, soluble carbonate phases (e.g., aragonite, high-Mg calcite) are expected to respond rapidly, providing an initial buffer against rising acidity (Morse et al., 2006) over the next several centuries.

4.5 Conclusions

We used seasonal samples taken during 2008 – 2010 to present the first thorough description of non-conservative processes affecting the spatio-temporal variations in TA concentrations over the Bering Sea shelf. During spring and summer of 2008, conservative mixing dominated much of the observed variability in TA concentrations. A constant ratio of TA : S was found across much of the shelf in both spring and summer indicating a variable but stable water mass, identified as BSW. Between the seasons, we found that freshwater discharge from rivers gradually contributed increasing amounts of TA to the shelf relative to salinity. During 2009 and 2010, mixing relationships were more spatially variable. However, along isolated transects, we did observe some conservative mixing.

Non-conservative variability in TA concentrations was found to be as important in determining seasonal changes in TA concentrations as conservative variations. Non-conservative variability resulting from organic carbon accumulation and denitrification was on average ~5 μmoles kg SW^{-1}, although these perturbations were as high as 15

μmoles kg SW^{-1} in some cases. By contrast, TA perturbations due to carbonate mineral precipitation and dissolution were much higher. We observed that biogenic carbonate mineral precipitation from a fall coccolithophore bloom in 2009 removed as much as 59 μmoles TA kg SW^{-1} relative to conservative mixing. Carbonate mineral dissolution in deep waters caused the highest deviations from expected mixing relationships, adding as much as 101 μmoles TA kg SW^{-1} from the dissolution of $CaCO_3$. We also observed some shallow-water carbonate mineral dissolution over the shelf, resulting from prolonged carbonate mineral undersaturations. In the most undersaturated areas of the shelf we observed as much as ~44 μmoles kg SW^{-1} of excess TA, corresponding to the dissolution of more than 20 μmoles kg SW^{-1} of $CaCO_3$ minerals. Given an estimate of ~66.5 μmoles kg SW^{-1} $CO_{2(Anth)}$, we observed that all undersaturations of aragonite during spring and summer and all calcite undersaturations in fall are caused by $CO_{2(Anth)}$, while natural respiration processes over the Bering Sea shelf are capable of producing seasonal aragonite undersaturations in fall. Given that the intensity and especially the duration of undersaturation events are prolonged by $CO_{2(Anth)}$, these observations constitute the first definitive evidence of shallow-water carbonate mineral dissolution as a result of ocean acidification in the Bering Sea.

Given the strong physico-biogeochemical variability of TA concentrations in this system, significant attention must be paid to TA parameterizations in the development of models and future projections of changes in the Bering Sea inorganic carbon system, such as the rate of dissolution of carbonate minerals, and the potential short- and long-term sinks of $CO_{2(Anth)}$. While some variations of the relationship between TA concentrations and S may be predictable, if not linear, we have shown here that salinity alone cannot be used as a proxy for TA in this system. In the Bering Sea, it is likely that TA concentrations vary not only as a function of salinity, but also as a function of marine calcification, shallow-water undersaturations, and other, minor processes.

4.6 Tables

Table 4.1 Ice core salinity, TA, and SA (2008). Salinity, TA (μmoles kg SW^{-1}) and SA (μmoles TA kg SW^{-1} S^{-1}) for 10 cm ice core sections collected from various regions across the shelf during spring of 2008. While the overall average SA for ice core sections is higher than that for BSW, strong variability prevents a statistical differentiation of these two water sources to the Bering Shelf.

Ice Core	Depth *cm*	salinity	TA *μmoles kg SW^{-1}*	SA *μmoles kg SW^{-1} S^{-1}*
39908	0-10	7.6	404	53.5
39908	20-30	4.8	415	87.5
39908	30-40	4.7	206	44.2
39908	50-60	5.6	282	50.8
39908	60-70	7.5	328	43.7
39909	0-10	6.7	561	84.4
39909	10-20	5.2	391	75.2
39909	20-30	3.7	267	73.1
39909	30-40	4.3	354	82.4
39909	40-50	6.2	387	62.5
39909	50-55	6.6	718	108.8
39911	0-10	6.0	380	63.3
39911	10-20	5.0	230	46.0
39911	20-30	6.0	214	35.6
39911	30-40	10.0	549	54.9
39911	40-50	14.2	1085	76.4
39914	0-10	6.7	563	84.5
39914	10-20	4.6	360	78.3
39914	30-40	7.4	703	95.0
39916	0-10	7.0	527	75.2
39916	10-20	6.1	431	70.7
39917	0-10	7.2	537	74.6
39917	10-20	4.5	307	68.2
39917	20-30	5.7	239	42.0
39917	30-40	8.8	308	35.0
39917	40-50	4.5	434	96.3
39917	50-60	5.1	760	149.0
39917	60-70	6.4	560	87.4
39917	70-80	7.4	506	68.3
39918	0-10	6.1	270	44.0
39918	10-20	5.4	318	58.8
39918	20-30	7.0	398	56.8
39918	30-40	9.9	725	73.2
39919	10-20	5.7	328	57.5
39919	20-30	3.3	229	69.3
39919	30-40	4.8	499	104.0
39919	40-50	6.3	362	57.4
39931	0-10	6.7	534	80.2
39931	10-20	4.6	331	71.9
39931	20-30	6.1	362	59.4
39931	30-40	7.4	484	65.4
39932	0-10	4.5	373	82.9
39932	10-20	5.4	374	69.3
39932	30-40	4.2	307	73.1
39932	40-50	5.1	280	55.0
AVERAGE ± 1 SD		**6.2 ± 1.9**	**426 ± 174**	**69.9 ± 21.1**

4.7 Figures.

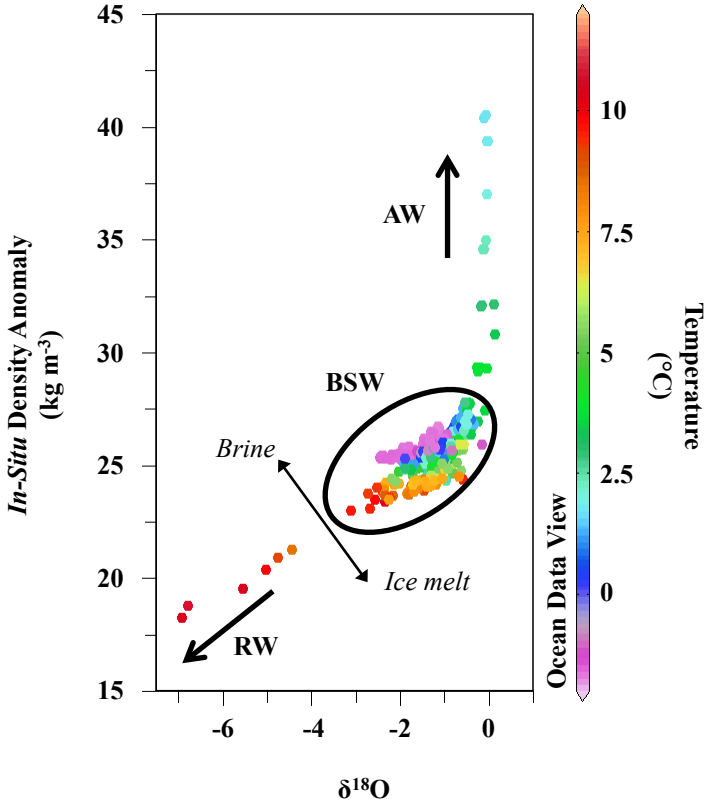

Figure 4.1 Water masses of the Bering Sea shelf. Three distinct groupings of water are apparent: low-density river discharge, with a strongly negative isotopic signature; variable Bering Shelf Water discharge, with mid-range density and slightly negative isotopic signature; and Anadyr Water from the deep basin, with a high density and a near-zero isotopic signature. The influences of ice formation and retreat provide a strong stratification of Bering Shelf water, with some stratification between denser bottom waters influenced by brine, and surface waters freshened by ice melt and heated by solar insolation. Data were provided by Weingartner, Danielson and Aagaard, from an unpublished data set.

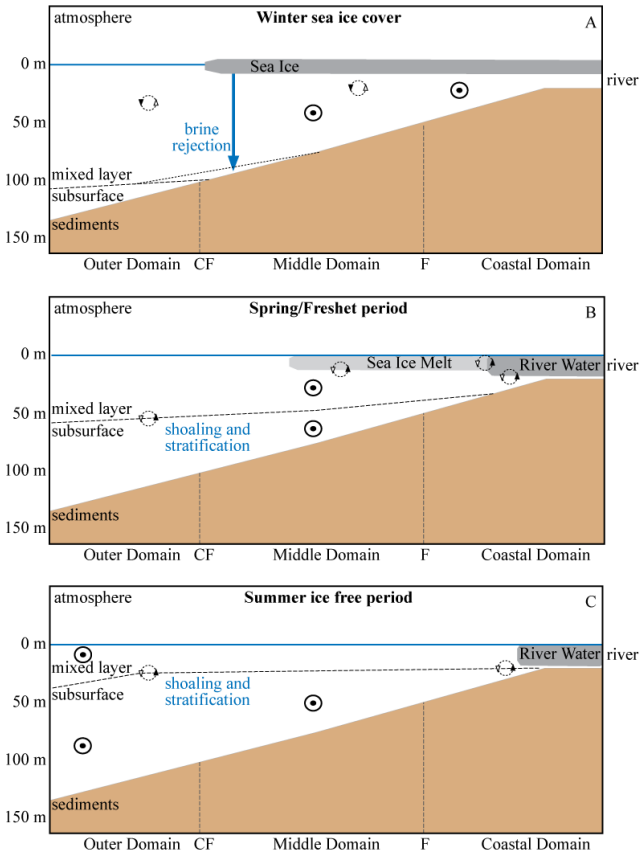

Figure 4.2 Seasonal circulation and hydrographic structure of the Bering Sea shelf. Black bull's-eyes denote along-shelf transport, while cycles denote mixing between water masses or layers. CF denotes the Central Front, dividing the Outer and Middle Domains. IF denotes the Inner Front, dividing the Middle and Coastal Domains. (A) During the winter season, homogenization of the water column occurs beneath sea ice cover. Shelf water is the prevalent water mass, although brine rejection does increase the density of some bottom waters. (B) During spring, ice melt and the terrestrial freshet both contribute significant volumes of fresh water to the surface layer. Salinity-driven stratification begins to isolate surface shelf waters from bottom shelf waters. (C) During summer, thermal stratification further isolates the surface shelf waters from bottom waters. The sea ice melt water fraction is lost due to mixing and export, while some river discharge remains apparent. Size reduced from original full-page printing.

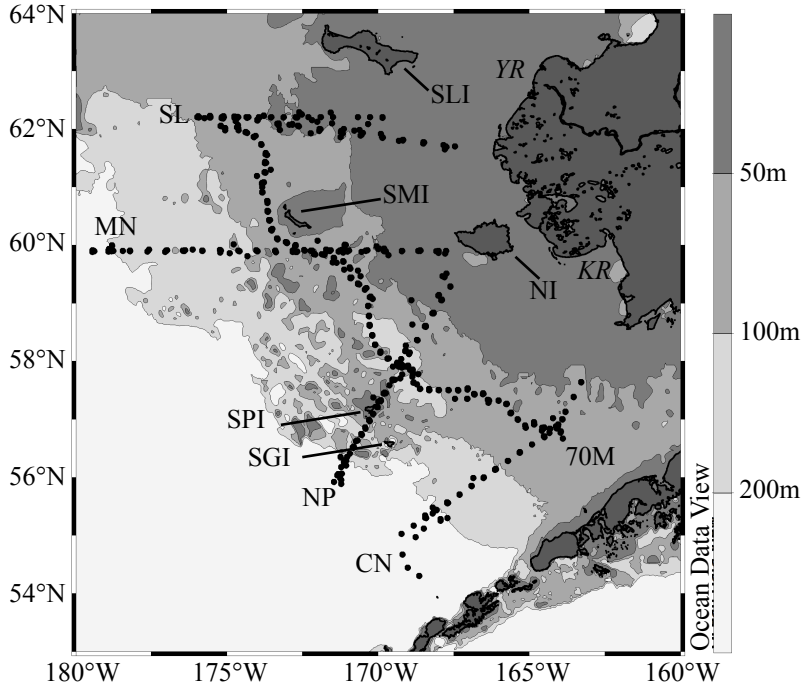

Figure 4.3 Map of sampling areas in the eastern Bering Sea (2008 – 2010). The five major hydrographic lines discussed in this paper are: the SL line (cross-shelf, north); the MN line (cross-shelf, Middle Domain); the NP line (cross-shelf, south); the CN line (cross-shelf, far south); and the 70M line (along-shelf, Middle Domain). Bathymetric color shading roughly corresponds to the three major domains on the Bering Sea shelf: the Coastal Domain (dark gray, 0-50 m); the Middle Domain (medium gray, 50-100 m); the Outer Domain (light gray, 100-200 m). Also indicated are the major islands: St. Lawrence Island (SLI), St. Matthew Island (SMI), Nunivak Island (NI), and the Pribilof Islands (St. Paul (SPI) and St. George (SGI)). The Yukon and Kuskokwim River outlets are also indicated in italics (*YR* and *KR*, respectively).

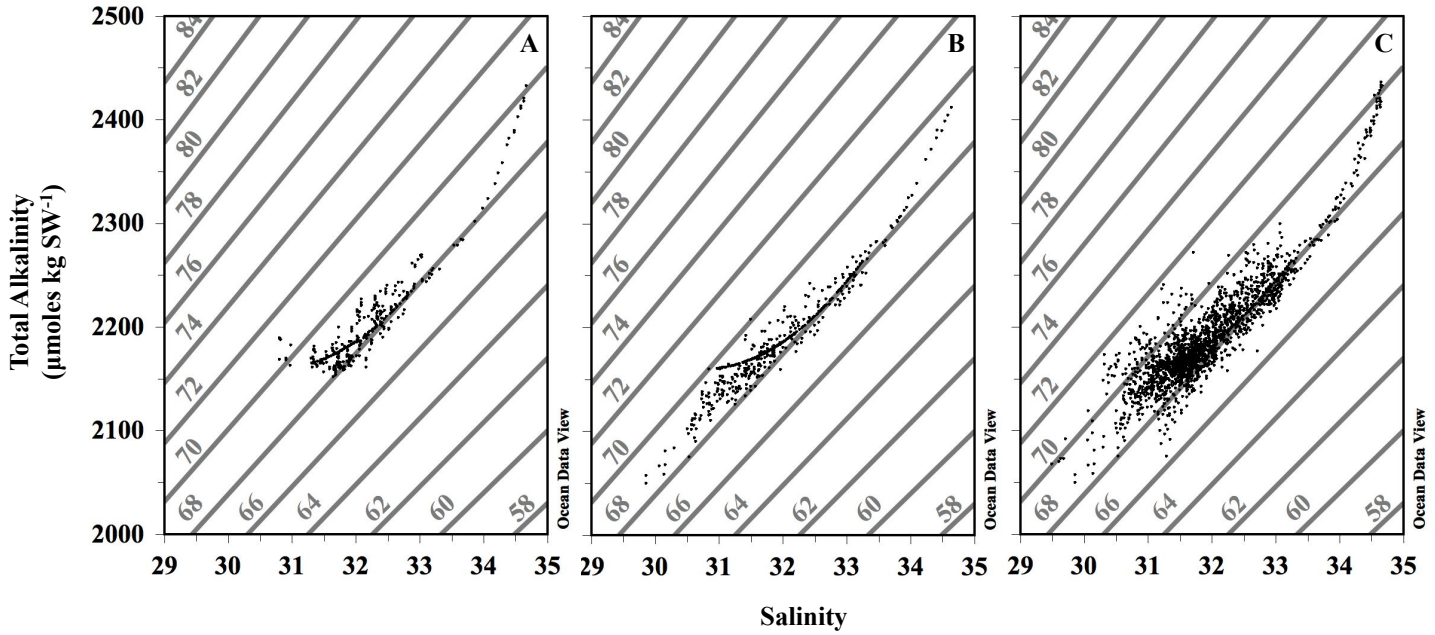

Figure 4.4 Distribution of TA versus salinity (2008 – 2010). Distribution of TA (µmoles kg SW^{-1}) versus salinity. (A) Spring 2008. (B) Summer 2008. (C) Entire data record, 2008 – 2010. Lines of constant SA (µmoles TA kg SW^{-1} S^{-1}) are drawn in the background for reference.

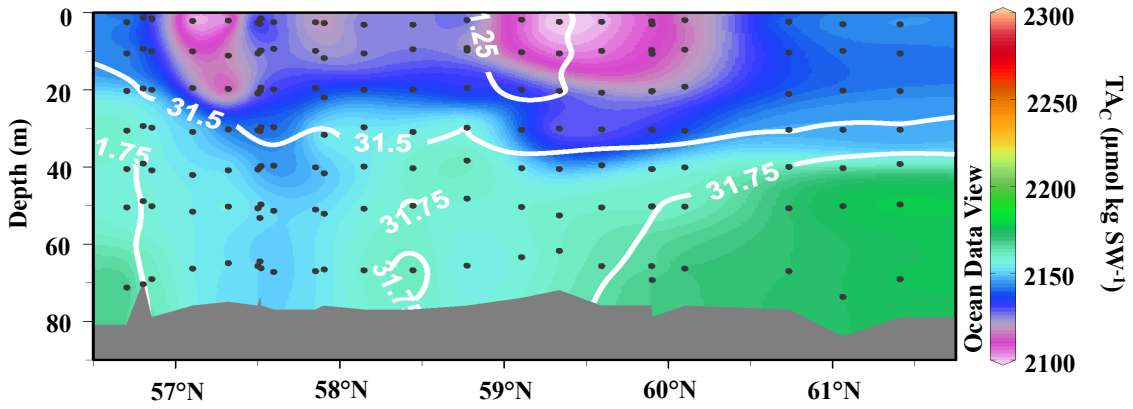

Figure 4.6 Variation of TA_C and salinity (70M line, Fall 2009). Variation of TA_C (color shading; µmoles kg SW^{-1}) and salinity (contour lines) across the 70M line during the fall of 2009. Areas of low TA in a freshened surface layer are not entirely related to conservative mixing, indicating as much as 59 µmoles kg^{-1} of non-conservative drawdown due to coccolithophore production (See also Figures 4.7, 4.8).

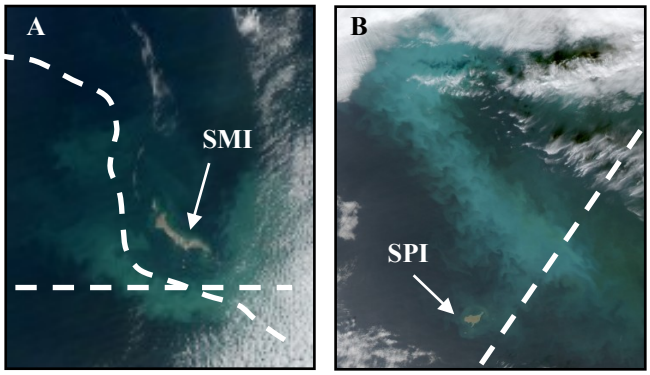

Figure 4.7 Satellite True-Color imagery of the 2009 coccolithophore bloom. (A) St. Matthew Island (SMI). (B) St. Paul Island (SPI). The blue-green coloration is caused by the light reflectance of detached coccoliths. Images courtesy of Feldman and McClain, Ocean Color Web, SeaWiFS Reprocessing. Approximate cruise tracks are indicated by white dashed lines.

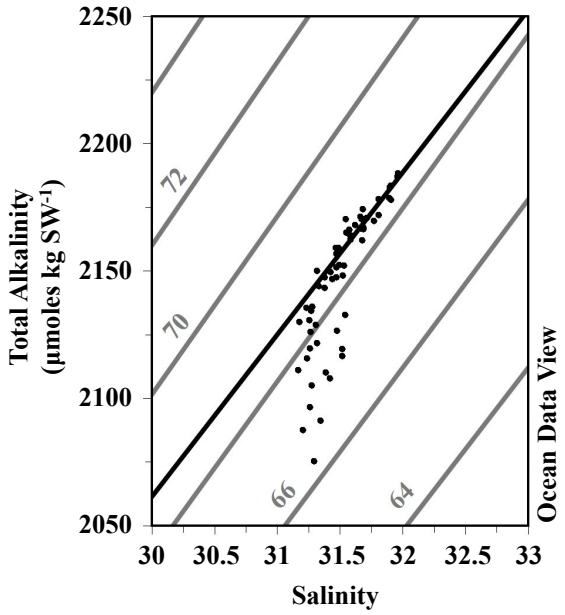

Figure 4.8 Relationship of TA and salinity (70M line, Fall 2009). The relationship of TA concentrations (µmoles kg SW^{-1}) and salinity along the 70M line during the fall of 2009. The bold black line indicates a regression of sub-surface data (rms = 3.70 µmoles kg SW^{-1}; $R^2 = 0.90$). The drawdown of TA and salinity relative to this line indicates biogenic uptake of TA. Lightweight black lines in the background indicate lines of constant SA (µmoles TA kg SW^{-1} S^{-1}) for reference.

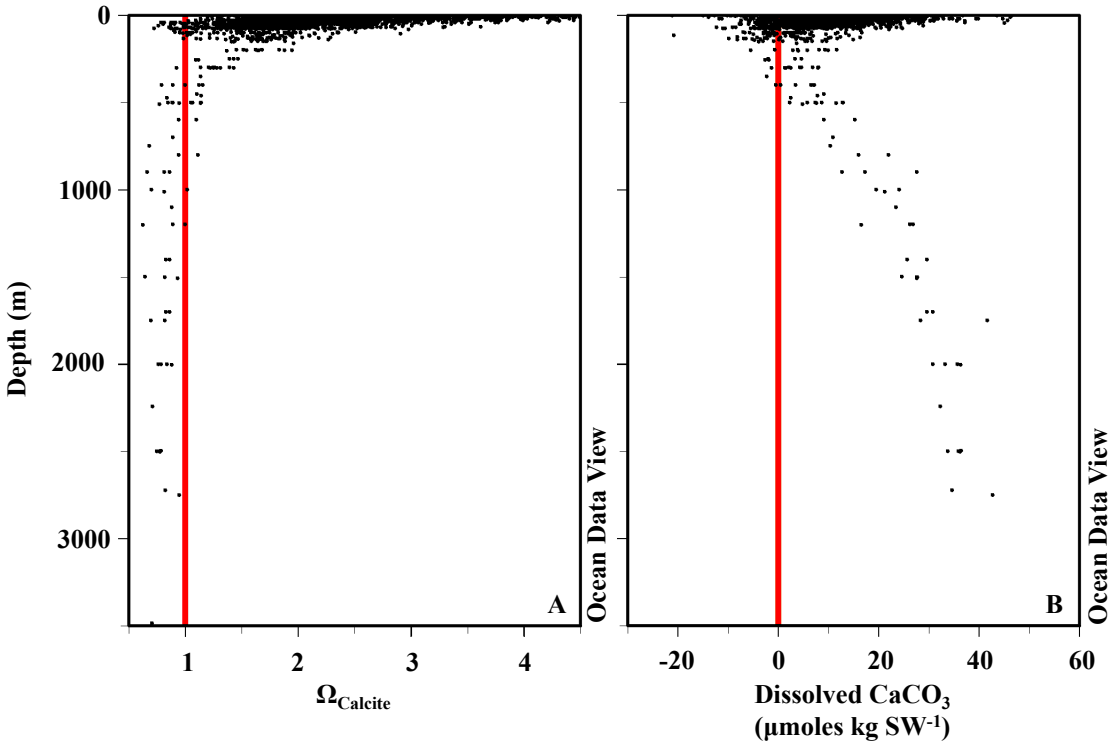

Figure 4.9 The appearance of the calcite saturation horizon and dissolved $CaCO_3$. (A) The depth of the calcite saturation horizon. (B) the appearance of dissolved $CaCO_3$ (µmoles kg SW^{-1}) as calculated according to Chen (1993). Dissolved $CaCO_3$ increases with depth below the saturation horizon (~250 m), while calcite undersaturations remain fairly constant indicating increasing effects of carbonate mineral dissolution with depth.

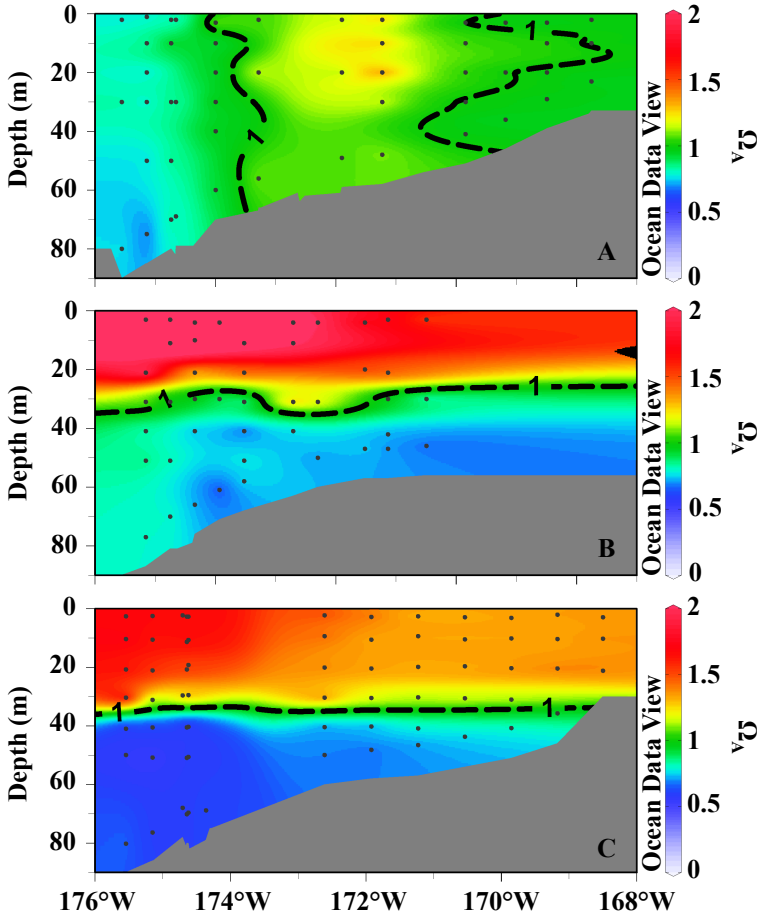

Figure 4.10 Seasonal variation aragonite saturation states (SL line, 2009). The saturation state of aragonite (color shading) along the SL line. (A) Spring, 2009. (B) Summer, 2009. (C) Fall , 2009. The dashed black line indicates the aragonite saturation horizon ($\Omega_A = 1$). Undersaturations were observed on the outer shelf during all three seasonal occupations.

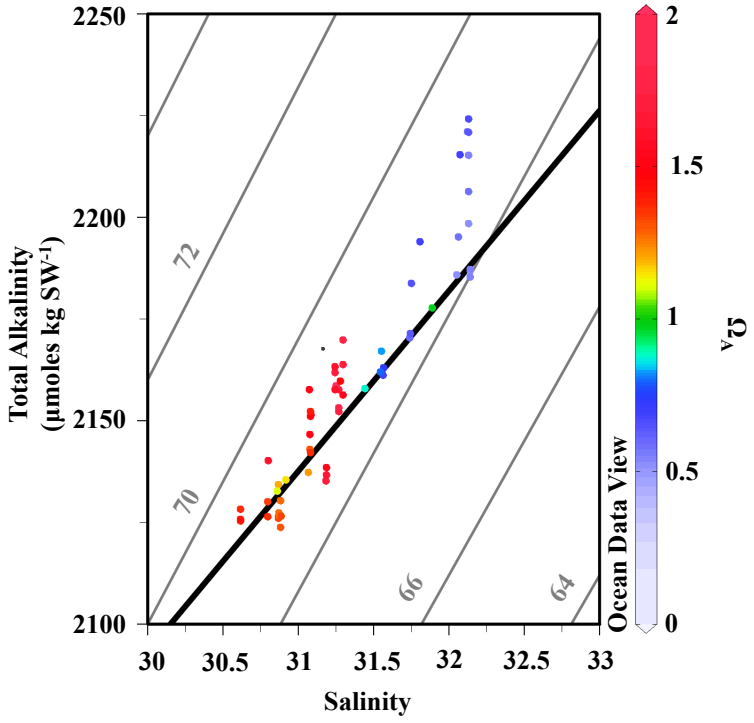

Figure 4.11 Relationship of TA_C and salinity (SL line, Fall 2009). Color shading indicates the saturation state of aragonite. A regression of TA_C and salinity from the inshore six stations along this line indicated conservative mixing (rms = 4.57 µmoles kg SW^{-1}, R^2 = 0.92; bold black line). Relative to this regression, excess TA was observed in undersaturated bottom waters (cool colors) and the overlying surface water (also see Figure 4.12). Lines of constant SA (µmoles TA kg SW^{-1} S^{-1}) are given in the background for reference.

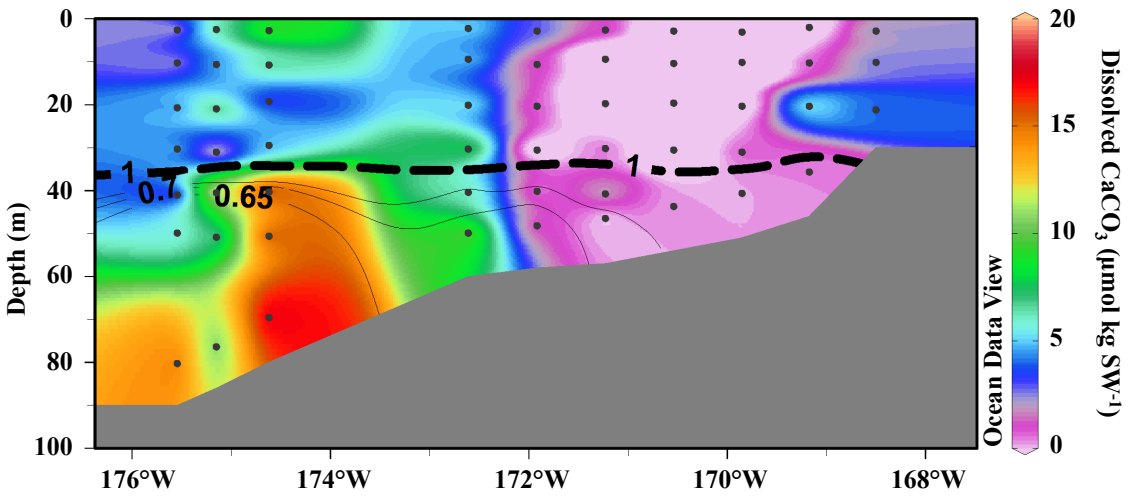

Figure 4.12 Dissolved $CaCO_3$ and aragonite undersaturations (SL line, Fall 2009). Dissolved $CaCO_3$ (µmoles kg^{-1}; color shading) and undersaturations of aragonite (contour lines) along the SL line during fall of 2009. The bold, dashed black line indicates the aragonite saturation horizon. The absence of dissolved $CaCO_3$ at the nearshore indicates conservative mixing in this region. The dissolved $CaCO_3$ observed at the westward end of the line in undersaturated waters indicates the first evidence of the impacts of ocean acidification on carbonate minerals in this region.

4.8 Acknowledgements

The authors thank the officers and crew of USCGC *Healy*, R/V *Knorr*, R/V *Thomas G. Thompson* and NOAA ship *Miller Freeman*, as well as Scott Hiller of SIO, Steve Roberts of UCAR, and the hydrographic team from NOAA-PMEL for their work in tirelessly supporting our science during multiple cruises. Statement of Work: Cross, J.N., collected samples in 2009 and 2010, performed the analysis, and prepared the manuscript for publication. Mathis, J.T., and Bates, N.R., contributed data to the effort and provided guidance during manuscript preparation. Byrne, R.H., provided guidance during manuscript preparation as an expert in carbonate mineral dissolution studies.

4.9 References.

Andersson AJ, Bates NR, Mackenzie FT. Dissolution of carbonate sediments under rising pCO_2 and ocean acidification: observations from Devil's Hole, Bermuda. Aquat Geochem 2007;13:237–64.

Andersson AJ, Mackenzie FT, Bates NR. Life on the margin: implications of ocean acidification on Mg-calcite, high latitude and cold-water marine calcifiers. Mar Ecol-Prog Ser 2008;373:265–73.

Assur A. Composition of sea ice and its tensile strength. Willamette: U.S. Army Snow, Ice, and Permafrost Research Establishment, Corps of Engineers; 1960. p. 106–38.

Bates NR. Interannual variability of oceanic CO_2 and biogeochemical properties in the western North Atlantic subtropical gyre. Deep Sea Res II 2001;48(8-9):1507–28.

Bates NR, Mathis JT. The Arctic Ocean marine carbon cycle: evaluation of air-sea CO_2 exchanges, ocean acidification impacts and potential feedbacks. Biogeosci 2009;6:2433–59.

Bates NR, Michaels AF, Knap AH. Alkalinity changes in the Sargasso Sea: geochemical evidence of calcification. Mar Chem 1996;51:347–58.

Bates NR, Orchowska MI, Garley R, Mathis, JT. Seasonal calcium carbonate undersaturation in shelf waters of the Western Arctic Ocean; how biological processes exacerbate the impact of ocean acidification. Biogeosci Disc 2012;9:14255–90.

Baumann MS, Moran SB, Kelly RP, Lomas MW, Shull DH. ^{234}Th balance and implications for seasonal particle retention in the eastern Bering Sea. Deep Sea Res II. 2013;94:7–21.

Belkin IM, Cornillon PC. Bering Sea thermal fronts from Pathfinder data: Seasonal and interannual variability. Phys Oceangr. 2005;3(1):6–20.

Bond NA, Overland JE, Spillane M, Stabeno P. Recent shifts in the state of the North Pacific. Geophys Res Lett 2003;30(23):2183.

Boveng PL, Bengtson JL, Buckley TW, Cameron MF, Dahle SP, Megrey BA, et al. Status review of the Ribbon Seal (*Histriophoca fasciata*). Report No. NMFS-AFSC-191. Seattle: U.S. Department of Commerce, NOAA, National Marine Fisheries Service, Alaska Fisheries Science Center; 2008.

Brabets TP, Wang B, Meade RH. Environmental and hydrologic overview of the Yukon River Basin, Alaska and Canada. Water-Resources Invenstigations Report No. 99–4204. Anchorage: USGS; 2000.

Brewer PG, Goldman JC. Alkalinity changes generated by phytoplankton growth. Limnol Oceanogr 1976;21(1):108–17.

Brewer PG, Wong GTF, Bacon MP, Spencer DW. An oceanic calcium problem? Earth Planet Sci Lett 1975;26:81–87.

Byrne RH, Mecking S, Feely RA, Liu X. Direct observations of basin-wide acidification of the North Pacific Ocean Geophys Res Lett 2010;37:L02601.

Cai W-J. Riverine inorganic carbon flux and rate of biological uptake in the Mississippi River plume. Geophys Res Lett 2003;30(2):1032.

Cai W-J, Hu X, Huang WJ, Jiang L-Q, Wang Y, Peng T-H, et al. Alkalinity distribution in the western North Atlantic Ocean margins. J Geophys Res 2010a;115:C08014.

Cai W-J, Chen L, Chen B, Gao Z, Lee SH, Chen J, et al. Decrease in the CO_2 uptake capacity in an ice-free Arctic Ocean basin. Science 2010b;329:556–59.

Chen C-TA. Carbonate chemistry of the wintertime Bering Sea marginal ice zone. Cont Shelf Res 1993;13(1):67–87.

Chen C-TA. Shelf- vs. dissolution-generated alkalinity above the chemical lysocline. Deep Sea Res II 2002;49:5365–75.

Chen C-TA, Wang S-L. Carbon, alkalinity, and nutrient budgets on the East China Sea continental shelf. J Geophys Res 1999;104:20675–86.

Chen C-TA, Wei C-L, Rodman MR. Carbonate chemistry of the Bering Sea. Report No. DOE/EV/10611-5. Washington, D.C.: U.S. Department of Energy, Office of Energy Research, Office of Basic Energy Sciences, Carbon Dioxide Research Division; 1985.

Chilton EA, Swiney K, Munk E, Foy RJ. 2010 Ecosystem consideration indicators for Bering Sea and Aleutian Islands tanner and king crab species. Kodiak (AK): U.S. Department of Commerce, NOAA, National Marine Fisheries Service, Alaska Fisheries Science Center; 2011.

Coachman LK. Flow convergence over a broad, flat continental shelf. Cont Shelf Res 1982;1:1–14.

Coachman LK. Circulation, water masses, and fluxes on the southeastern Bering Sea shelf. Cont Shelf Res 1986;5:23–108.

Coachman LK. On the flow field in the Chirikov Basin. Cont Shelf Res 1993;13:481–508.

Cooper LW, McClelland JW, Holmes RM, Raymond PA, Gibson JJ, Guay CK, et al. Flow-weighted values of runoff tracers ($\delta^{18}O$, DOC, Ba, alkalinity) from the six largest Arctic rivers. Geophys Res Lett 2008;35:L18606.

Danielson S, Aagaard K, Weingartner T, Martin S, Winsor P, Gawarkiewicz G, et al. The St. Lawrence Island polynya and the Bering shelf circulation: New observations that test the models. J Geophys Res 2006;111:C09023.

Danielson S, Eisner L, Weingartner T, Aagaard K. Thermal and haline variability over the central Bering Sea shelf: Seasonal and interannual perspectives. Cont Shelf Res 2011;31(6):539–54.

Danielson S, Hedstrom K, Aagaard K, Weingartner T, Curchitser E. Wind-induced reorganization of the Bering shelf circulation. Geophys Res Lett 2012;39:L08601.

Dickson AG. Thermodynamics of the dissolution of boric acid in synthetic seawater from 273.15 to 318.15 K. Deep Sea Res A 1990;37(5):755–66.

Dickson AG. The carbon dioxide system in sea water: equilibrium chemistry and measurements. In: Riebesell U, Fabry VJ, Hansson L, Gattuso, J-P, editors. Guide for best practices in ocean acidification research and data reporting. Luxemborg: Publications Office of the European Union; 2010. p. 17–39.

Dickson AG, Millero FJ. A comparison of the equilibrium constants for the dissociation of carbonic acid in seawater media. Deep Sea Res A 1987;34(10):1733–43.

Dickson AG, Sabine CL, Christian JR, editors. Guide to Best Practices for Ocean CO_2 Measurements. Sidney (BC): North Pacific Marine Science Organization; 2007.

Dieckmann GS, Hebrke G, Papadimitriou S, Göttlicher J, Steininger R, Kennedy H, et al. Calcium carbonate as ikaite crystals in Arctic sea-ice. Geophys Res Lett 2008;35:L08501.

Dieckmann GS, Nehrke G, Uhlig C, Göttlicher J, Gerland S, Granskog MA, et al. Brief communication: Ikaite ($CaCO_3 \bullet 6H_2O$) discovered in Arctic sea ice. Cyrosph Disc 2010;4:153–61.

Dornblaser MM, Striegl RG. Nutrient (N, P) loads and yields at multiple scales and sub-basin types in the Yukon River Basin, Alaska. J Geophys Res 2007;112:G04S57.

Dreybrodt W, Lauckner J, Svensson U, Buhmann D. The kinetics of the reaction $CO_2 + H_2O \rightarrow H^+ + HCO_3^-$ as one of the rate limiting steps for the dissolution of calcite in the system H_2O-CO_2-$CaCO_3$. Geochim Cosmochim Ac 1996;60:3375–81.

Fabry VJ, Seibel BA, Feely RA, Orr JC. Impacts of ocean acidification on marine fauna and ecosystem processes. ICES J Mar Sci 2008;65:414–32.

Fabry VJ, McClintock JB, Mathis JT, Grebmeier JM. Ocean acidification at high latitudes: the bellwether. Oceanography 2009;22(4):160–71.

Feely RA, Cline JD. Distribution, composition and transport of suspended particulate matter in the Gulf of Alaska and southeastern Bering Shelf. Geology 1976;12:409–84.

Feely RA, Chen C-T. The effect of excess CO_2 on the calculated calcite and aragonite saturation horizons in the northeast Pacific. Geophys Res Lett 1982;9:1294–7.

Feely RA, Massoth GJ, Paulson AJ. The distribution and elemental composition of suspended particulate matter in Norton Sound and the northeastern Bering Sea

shelf: Implications for Mn and Zn recycling in coastal waters. In: Hood DW, Calder JA, editors. The Eastern Bering Sea Shelf: Oceanography and Resources. Washington, D.C.: U.S. Department of Commerce; 1981. p. 321–337.

Feely RA, Sabine CL, Byrne RH, Millero FJ, Dickson AG, Wanninkhof R, et al. Decadal changes in the aragonite and calcite saturation state of the Pacific Ocean. Glob Biogeochem Cy 2012;26:GB3001.

Feldman GC, McClain CR. Ocean Color Web, SeaWIFS Reprocessing, [Internet]. Kuring N, Bailey SW, Eds. Greenbelt (MD); NASA Goddard Space Flight Center, cited 2012 July 10. Available from: http://oceancolor.gsfc.nasa.gov/.

Fransson A, Chierici M, Nojiri Y. New insights into the spatial variability of the surface water carbon dioxide in varying sea ice concentrations in the Arctic Ocean. Cont Shelf Res 2009;29:1317–28.

Friis K, Körtzinger A, Wallace DWR. The salinity normalization of marine inorganic carbon chemistry data. Geophys Res Lett 2003;30(2):1085.

Friis K, Najjar RG, Follows MJ, Dutkiewicz S. Possible overestimation of shallow-depth carbonate dissolution in the ocean. Glob Biogeochem Cy 2006;20(4):GB4019.

Geilfus N-X, Carnat G, Dieckmann GS, Halden N, Nehrke G, Papakyriakou T, et al. First estimates of the contribution of $CaCO_3$ precipitation to the release of CO_2 to the atmosphere during young sea-ice growth. J Geophys Res 2013;118:244–55.

Gordon, LL, Jennings Jr. JC, Ross AA, Krest JM. A suggested protocol for continuous flow automated analysis of seawater nutrients (phosphate, nitrate, nitrite, and silicic acid), Methods Manual No. 91-1. Corvallis, OR: WOCE Hydrographic Program Office; 1994.

Granger J, Prokopenko MG, Sigman DM, Mordy CW, Morse ZM, Morales LV, et al. Coupled nitrification-denitrification in sediments of the eastern Bering Sea shelf leads to ^{15}N enrichment of fixed N in shelf waters. J Geophys Res 2011;116:C11006.

Grebmeier JM, Overland JE, Moore SE, Farley EV, Carmack EC, Cooper LW, et al. A major ecosystem shift in the Northern Bering Sea. Science. 2006;311(5766):1461–4.

Hales B, Emerson S. Evidence in support of first-order dissolution kinetics of calcite in seawater. Earth Plan Sci Lett 1997;148:317–27.

Harlay J, Borges AV, Van Der Zee C, Delille B, Godoi RHM, Schiettecatte L-S, et al. Biogeochemical study of a coccolithophorid bloom in the northern Bay of Biscay (NE Atlantic Ocean) in June 2004. Prog Oceanogr 2010;86:317–36.

Harlay J, Chou L, De Bodt C, Van Oostende N, Piontek J, Suykens K, et al. Biogeochemistry and carbon mass balance of a coccolithophore bloom in the northern Bay of Biscay (June 2006). Deep Sea Res I 2011;58:111–27.

Hu X, Cai W-J. An assessment of ocean margin anaerobic processes on the oceanic alkalinity budget. Glob Biogeochem Cy 2001;25:GB3003.

Hunt Jr. GL, Stabeno PJ. Climate change and the control of energy flow in the southeastern Bering Sea. Prog Oceanogr 2002;55:5–22.

Hunt Jr. GL, Stabeno PJ, Walters G, Sinclair E, Brodeur RD, Napp JM, et al. Climate change and control of the southeastern Bering Sea pelagic ecosystem. Deep Sea Res II 2002;49:5821–63.

Hydes DJ, Loucaides S, Tyrrell T. Report on a desk study to identify likely sources of error in the measurements of carbonate system parameters and related calculations, particularly with respect to coastal waters and ocean acidification experiments. Report No. 83. Southampton (UK): National Oceanography Center Southampton; 2010.

Iida T, Mizobata K, Saitoh S-I. Interannual variability of coccolithophore *Emliania huxleyi* blooms in response to changes in water column stability in the eastern Bering Sea. Cont Shelf Res 2012;34:7–17.

Jones EP, Coote AR. Oceanic CO_2 produced by the precipitation of $CaCO_3$ from brines in sea ice. J Geophys Res 1981;86(C11):11041–43.

Kachel NB, Hunt G, Salo SA, Schumacher JD, Stabeno PJ, Whitledge TE. Characteristics of the inner front of the southeastern Bering Sea. Deep Sea Res II 2002;49:5889–909.

Kadko D, Swart S. The source of the high heat and freshwater content of the upper ocean at the SHEBA site in the Beaufort Sea in 1997. J Geophys Res 2004;109(C1):C01022.

Keir RS. The dissolution kinetics of biogenic calcium carbonates in seawater. Geochim Cosmochim Ac 1980;44:241–52.

Killawee JA, Fairchild IJ, Tison J-L, Janssens L, Lorrain R. Segregation of solutes and gasses in experimental freezing of dilute solutions: Implications for natural glacial systems. Geochim Cosmochim Ac 1998;62:3637–55.

Kim H-C, Lee K, Choy W. Contribution of phytoplankton and bacterial cells to the measured alkalinity of seawater. Limnol Oceanogr 2006;51(1):331–8.

Kim H-C, Lee K. Significant contribution of dissolved organic matter to seawater alkalinity. Geophys Res Lett 2009;36:L20603.

Koczy FF. The specific alkalinity. Deep Sea Res 1953;3(4):279–88.

Ladd C, Stabeno PJ. Stratification on the Eastern Bering Sea shelf revisited. Deep Sea Res II 2012;65-70:72–83.

Lewis ER, Wallace DWR. Program developed for CO_2 system calculations. Report No. BNL-61827. Oak Ridge (TN): U.S. Department of Energy, Oak Ridge National Laboratory, Carbon Dioxide Information Analysis Center; 1998.

Lomas MW, Moran SB, Casey JR, Bell DW, Tiahlo M, Whitefield J, et al. Spatial and seasonal variability of primary production on the Eastern Bering Sea shelf. Deep Sea Res II 2012;65-70:126–40.

Long WC, Swiney KM, Harris C., Page HN, Foy RJ. Effects of ocean acidification on juvenile Red King Crab (*Paralithodes camtschaticus*) and Tanner Crab (*Chinoecetes bairdi*) growth, condition, calcification, and survival. PLoS ONE 2013a;e60959.

Long WC, Swiney KM, Foy RJ. Effects of ocean acidification on the embryos and larvae of red king crab, *Paralithodes camtschaticus*. Mar Poll Bull 2013b;69(1-2):38–47.

MacDonald RW, McLaughlin FA, and Carmack EC. Fresh water and its sources during the SHEBA drift in the Canada Basin of the Arctic Ocean. Deep Sea Res I 2002;49:1769–85.

Macklin SA, Hunt Jr. GL, Overland JE. Collaborative research on the pelagic ecosystem of the southeastern Bering Sea shelf. Deep Sea Res II 2002;49(26):5813–19.

Mathis JT, Cross JN, Bates NR, Moran SB, Lomas MW, Stabeno PJ. Seasonal distribution of dissolved inorganic carbon and net community production on the Bering Sea shelf. Biogeosci 2010;7:1769–87.

Mathis JT, Cross JN, Bates NR. The role of ocean acidification in systemic carbonate mineral suppression in the Bering Sea. Geophys Res Lett 2011;38:L19602.

Mehrbach C, Culberson CH, Hawley JE, Pytkowicz RM. Measurement of the apparent dissociation constants of carbonic acid in seawater at atmospheric pressure. Limnol Oceanogr 1973;50:101–11.

Merico A, Tyrrell T, Brown CW, Groom SB, Miller PI. Analysis of satellite imagery for *Emiliania huxleyi* blooms in the Bering Sea before 1997. Geophys Res Lett 2003;30(6):1337–40.

Merico A, Tyrrell T, Lessard EJ, Oguz T, Stabeno PJ, Zeeman SI, et al. Modelling phytoplankton succession on the Bering Sea shelf: role of climate influences and trophic interactions in generating *Emiliania huxleyi* blooms 1997 – 2000. Deep Sea Res II 2004;51:1803–26.

Merico A, Tyrrell T, Cokacar T. Is there any relationship between phytoplankton seasonal dynamics and the carbonate system? J Mar Syst 2006;59(1-2):120–42.

Millero FJ, Lee K, Roche MP. Distribution of alkalinity in the surface waters of the major oceans. Mar Chem 1998;60:111–30.

Mizobata K, Saitoh S-I. Variability of Bering Sea eddies and primary productivity along the shelf edge during 1998–2000 using satellite multi-sensor remote sensing. J Mar Syst 2004;50(1-2):101–11.

Moran SB, Lomas MW, Kelly RP, Gradinger R, Iken K, Mathis JT. Seasonal succession of net primary productivity, particulate organic carbon export, and autotrophic community composition in the eastern Bering Sea. Deep Sea Res II 2012;65-70:84–97.

Mordy CW, Eisner LB, Proctor P, Stabeno PJ, Devol AH, Shull DH, et al. Temporary uncoupling of the marine nitrogen cycle: accumulation of nitrite on the Bering Sea shelf. Mar Chem 2010;121:157–66.

Mordy CW, Cokelet ED, Ladd C, Menzia FA, Proctor P, Stabeno PJ, et al. Net community production on the middle shelf of the eastern Bering Sea. Deep Sea Res II 2012;65-70:110–25.

Morse JW, Arvidson RS. The dissolution kinetics of major sedimentary carbonate minerals. Earth Sci Rev 2002;58:51–84.

Morse JW, Andersson AJ, Mackenzie FT. Initial responses of carbonate-rich shelf sediments to rising atmospheric pCO_2 and "ocean acidification": Role of high Mg-calcites. Geochim Cosmoquim Ac 2006;70:5814–30.

Murata A, Takizawa T. Impact of a coccolithophorid bloom on the CO_2 system in surface waters of the eastern Bering Sea shelf. Geophys Res Lett 2002;29:1547–51.

Napp JM, Hunt Jr. GL. Anomalous conditions in the southeastern Bering Sea 1997: linkages among climate, weather, ocean and biology. Fish Oceanogr 2001;10(1):61–8.

National Water Information System (NWIS) [Internet]. Hydrological Unit Code 19040805, Site Codes 15304000 (Kuskokwim River at Crooked Creek) and 15565447 (Yukon River at Pilot Station), Wallops Island (VA); U.S. Department of the Interior, cited 2012 Feb 28. Available from: http://nwis.waterdata.usgs.gov/nwis.

National Stream Quality Accounting Network (NASQUAN) [Internet]. Hydrological Unit Code 109040805, Site Code 15565447 (Yukon River at Pilot Station), Reston (VA); U.S. Department of the Interior, USGS, cited 2012 Feb 28. Available from: water.usgs.gov/nasquan.

Nedashovsky AP, Khvedynich SV, Petovsky TV. The effect of sea-ice growth on air-sea CO_2 flux in a tank experiment. Tellus 2009;58(B):418–26.

Niebauer, HJ, Alexander V, Henrichs SM. A time-series study of the spring bloom at the Bering Sea ice edge I. Physical processes, chlorophyll and nutrient chemistry. Cont Shelf Res 1995;15(15):1859–77.

Nihoul JC-J, Adam P, Brasseur P, Deleersnijder E, Djenidi S, Haus J. Three-dimensional general circulation model of the northern Bering Sea's summer ecohydrodynamics. Cont Shelf Res 1993;13(5-6):509–42.

Nomura D, Assmy P, Nehrke G. Granskog MA, Fischer M, Dieckmann GS, et al. Characterization of ikaite ($CaCO_3 \cdot 6H_2O$) crystals in first-year Arctic sea ice north of Svalbard. Ann Glaciol 2013;54(62):125–31.

O'Neill JR. Hydrogen and oxygen isotope fractionation between ice and water. J Phys Chem 1968;72:3683–4.

Overland JE, Roach AT. Northward flow in the Bering and Chukchi seas. J Geophys Res 1987;92:7097–105.

Overland JE, Stabeno PJ. Is the climate of the Bering Sea warming and affecting the ecosystem? Eos T Am Geophys Un 2004;85(33):309.

Overland JE, Bond NA, Adams JM. North Pacific atmospheric and SST anomalies in 1997: links to ENSO? Fish Oceanogr 2001;10:81–98.

Papadimitriou S, Kennedy H, Kattner G, Dieckmann GS, Thomas DN. Experimental evidence for carbonate precipitation and CO_2 degassing during sea ice formation. Geochim Cosmochim Ac 2004;68:1749–61.

Robbins LL, Hansen ME, Kleypas JA, Meylan SC. CO2calc – A user-friendly seawater carbon calculator for Windows, Max OS X, and iOS (iPhone). Report No. 2010-1280. Reston (VA): U.S. Department of the Interior, USGS; 2010.

Rysgaard S, Glud RN, Sejr MK, Bendtsen J, Christensen PB. Inorganic carbon transport during sea ice growth and decay: A carbon pump in polar seas. J Geophys Res 2007;112:C03016.

Rysgaard S, Bendtsen J, Pedersen LT, Ramlov H, Glud RN. Increased CO_2 uptake due to sea ice growth and decay in the Nordic Seas. J Geophys Res 2009;114:C09011.

Rysgaard S, Bendtsen J, Delille B, Dieckmann GS, Glud RN, Kennedy H, et al. Sea ice contribution to the air-sea CO_2 exchange in the Arctic and Southern Oceans. Tellus 2011;63(B):823–30.

Rysgaard S, Glud RN, Lennert K, Cooper M, Halden N, Leakey RJG, et al. Ikaite crystals in melting sea ice–implications for pCO_2 and pH levels in Arctic surface waters. Cryosph 2012a;6:901–8.

Rysgaard S, Søgaard DH, Cooper M, Pućko M, Lennert K, Papakyriakou TN, et al. Ikaite crystal distribution in Arctic winter sea ice and implications for CO_2 system dynamics. Cryosph Disc 2012b;6:5037–68.

Schlitzer R. Ocean Data View [Internet]. Ver. 4.5.0. Bremerhaven; Alfred Wegener Institute, cited 2012 May. Available from: http://odv.awi.de.

Schumacher JD, Stabeno PJ. Continental shelf of the Bering Sea. In: Brink KH, Robinson AR, editors. The Sea. Vol. 11. New York: John Wiley and Sons, Inc.; 1998. p. 789–822.

Schumacher JD, Alexander V. Variability and role of the physical environment in the Bering Sea ecosystem. In: Loughlin TR, Ohtani K, editors. Dynamics of the Bering Sea. Fairbanks (AK): University of Alaska Sea Grant; 1999. p. 147–160.

Schumacher JD, Bond NA, Brodeur RD, Livingston PA, Napp JM, Stabeno PJ. Climate changes in the southeastern Bering Sea and some consequences for biota. In: Hemple G, Sherman K, editors. Large marine ecosystems of the world: Trends in exploitation, Protection, and Research. Amsterdam: Elsevier; 2003. p. 17–40.

Stabeno PJ, van Meurs P. Evidence of episodic on-shelf flow in the southeastern Bering Sea. J Geophys Res 1999;104(C12):29715–20.

Stabeno PJ, Schumacher JD, Ohtani K. The physical oceanography of the Bering Sea. In: Loughlin TR, Ohtani K, editors. Dynamics of the Bering Sea. Fairbanks (AK): University of Alaska Sea Grant; 1999. p. 1–28.

Stabeno PJ, Bond NA, Kachel NB, Salo SA, Schumacher JD. On the temporal variability of the physical environment over the southeastern Bering Sea. Fish Oceanogr 2001;10(1):81–98.

Stabeno PJ, Hunt Jr. GL, Napp JM, Schumacher JD. Physical forcing of ecosystem dynamics on the Bering Sea shelf. In: Robinson AR, Brink KH, editors. The Sea. Vol. 14. New York: John Wiley and Sons; 2006. p. 1177–1212.

Stabeno PJ, Farley Jr. EV, Kachel NB Moore S, Mordy CW, Napp JM, et al. A comparison of the physics of the northern and southern shelves of the eastern Bering Sea and some implications for the ecosystem. Deep Sea Res II 2012a;65-70:14–30.

Stabeno PJ, Kachel NB, Moore SE, Napp JM, Sigler M, Yamaguchi A, et al. Comparison of warm and cold years on the southeastern Bering Sea shelf and some implications for the ecosystem. Deep Sea Res II. 2012b;65-70:31–45.

Stockwell DA, Whitledge TE, Zeeman SI, Coyle KO, Napp JM, Brodeur RD, et al. Anomalous conditions in the south-eastern Bering Sea, 1997: Nutrients, phytoplankton, and zooplankton. Fish Oceanogr 2001;10:99–116.

Striegl RG, Aiken GR, Dornblaser MM, Raymond PA, Wickland KP. A decrease in discharge-normalized DOC export by the Yukon River during summer through autumn. Geophys Res Lett 2005;32:L21413.

Striegl RG, Dornblaser MM, Aiken GR, Wickland KP, Raymond PA. Carbon export and cycling by the Yukon, Tanana, and Porcupine Rivers, Alaska, 2001 – 2005. Water Resour Res 2007;43:W02411.

Suykens K, Delille B, Chou L, DeBodt C, Harley J, Borges AV. Dissolved inorganic carbon dynamics and air-sea carbon dioxide fluxes during coccolithophore blooms in the Northwest European continental margin (northern Bay of Biscay). Glob Biogeochem Cy 2010;24:GB3022.

Suykens K, Schmidt S, Delille B, Harlay J, Chou L, De Bodt C, et al. Benthic remineralization in the northwest European continental margin (northern Bay of Biscay). Cont Shelf Res 2011;31:644–58.

Thomas H, Schiettecatte L-S, Suykens K, Kone YJM, Shadwick EH, Prowe AEF, et al. Enhanced ocean carbon storage from anaerobic alkalinity generation in coastal sediments. Biogeosci 2009;6:267–74.

Watanabe YW, Chiba T, Tanaka T. Recent change in the oceanic uptake rate of anthropogenic carbon in the North Pacific subpolar region determined using a carbon-13 time series. J Geophys Res 2011;116:C02006.

Weiss RF. Carbon dioxide in water and seawater: The solubility of a non-ideal gas. Mar Chem 1974;2:203–15.

Zhang J, Woodgate R, Mangiameli S. Towards seasonal prediction of the distribution and extent of cold bottom waters on the Bering Sea shelf. Deep Sea Res II 2012;65-70:58–71.

Chapter 5:

Sea-air CO_2 fluxes in the Bering Sea: New insights into late-season dynamics on an ice-covered continental shelf[4]

5.0 Abstract.

Between 2008 and 2012, assessments of three-month climatologies of sea ice cover and sea-air CO_2 fluxes in the Bering Sea showed that inhibition of potential CO_2 efflux by ice-cover resulted in an increase of the estimated annual Bering Sea shelf CO_2 sink from -6.9 ± 6.2 Tg C yr^{-1} to -9.4 ± 5.0 Tg C yr^{-1} (Tg = 10^{12} g), or by ~26%. The largest observed CO_2 effluxes occurred over the southern shelf, where sea ice coverage was minimal. Accounting for unrestricted late-season CO_2 efflux from ice-free areas rendered the ice-adjusted annual sea-air CO_2 flux for the Bering Sea weaker than in previous estimates. In the coming decades, warming sea surface temperatures and climate-driven ice retreat are expected to decrease the size of this CO_2 sink by reducing the inhibition of outgassing. These processes may be characteristic of other shallow, highly productive seasonal ice regimes, such as the Chukchi Sea.

5.1 Introduction.

The southeastern Bering Sea shelf (SEBS) exhibits the largest annual advance and retreat of seasonal sea ice in high latitude marginal seas (~1700 km latitudinally) [*Walsh and Johnson*, 1979]. The annual sea ice cycle creates differing physical regimes across the northern and southern regions of the continental shelf [*Stabeno et al.,* 2002, 2012a], with ice-affected waters exhibiting colder temperatures, a differing pycnocline, and clear marine ecosystem differences compared to the ice-free areas of the southern shelf.

---

[4]Cross, J. N., J. T. Mathis, K. E. Frey, C. E. Cosca, S. L. Danielson, N. R. Bates, R. A. Feely, T. Takahashi, and W. Evans (2013), Sea-air CO_2 fluxes in the Bering Sea: New insights into late-season dynamics on an ice-covered continental shelf, J. Geophys. Res., in review.

Whereas the impact of sea ice on shaping the physical environment and ecosystems of the SEBS is well known [*Hunt et al.,* 2002; *Stabeno et al.,* 2010; *Hunt et al.,* 2011; *Cooper et al.,* 2013], a paucity of autumn, winter, and early spring data has limited our understanding of the impact of ice on sea-air exchange of carbon dioxide (CO_2) in the region. Consequently, late season sea-air CO_2 fluxes are typically ignored under the assumption that ice cover causes complete mechanical inhibition of sea-air exchange during these times [*Bates et al.,* 2011], although spatially and seasonally variable ice cover [*Stabeno et al.,* 2012b] could provide ample opportunities for exchange. Further, these potential fluxes could be quite large, given that enhancement of exchange rates has been observed during periods of ice formation [*Else et al.,* 2011, *Miller et al.,* 2011]. CO_2 produced by late-season respiration processes has also been shown to accumulate in ice-covered waters [*Semiletov*, 1999; *Semiletov et al.,* 2004], potentially resulting in rapid outgassing upon ice retreat.

Recently, the spatiotemporal resolution of data for the entire SEBS has significantly increased through collection of new records of CO_2 partial pressure (pCO_2) data from underway flow-through systems on several vessels, along with over a dozen large-scale repeat hydrography surveys and the first deployment of moored autonomous carbon sensors in the region [Appendix B] (Figure 5.1). Here, we synthesized surface seawater data collected during 21 cruises over a five year period with reconstructed atmospheric pCO_2, climatological winds, and passive microwave-derived sea ice concentration data to generate a seasonal climatology of sea-air CO_2 fluxes. This approach quantifies late season sea-air CO_2 flux at high resolution (~12 km^2) and constrains the impacts of sea ice for the first time in this geographic region.

5.2 Methods

An expansive data set of surface water pCO_2 was compiled from a variety of sources, with over 53,000 measurements spanning the five year period from 2008 through 2012 (Figure 5.1), including: (1) continuous direct measurements of surface water pCO_2 from underway systems were obtained aboard the USCGC *Healy* by the Lamont Doherty

Earth Observatory (LDEO) Carbon Group (data available at http://www.ldeo.columbia.edu/res/pi/CO2/), and by National Oceanic and Atmospheric Administration (NOAA) researchers aboard the NOAA Ship *Oscar Dyson*; (2) a continuous five month record from May to October 2011 of autonomously collected surface pCO_2 data from the M2 mooring site by Mathis *et al*. [Appendix B]; and (3) previously published pCO_2 data calculated from discrete dissolved inorganic carbon (DIC) and total alkalinity (TA) samples collected by researchers at the University of Alaska, Fairbanks during the Bering Sea Project (2008–2010; bsierp.nprb.org) [*Bates et al*., 2011; *Mathis et al.,* 2011; Chapter 4; Appendix A].

Limited observations in January, February, and March reduced the maximum temporal resolution for complete annual coverage to three-month averaging, which corresponded well to seasonal scaling. To focus on sea ice processes, these seasons were grouped around periods of mean five-year (2008 – 2012) maximum and minimum ice extent (February – April and August – October, respectively), with the remaining three-month periods indicating periods of ice advance (November – January) and ice retreat (May – July). These "ice seasons" were determined using a five-year (2008 – 2012) mean ice edge as indicated by a 15% standard presence/absence ice cover threshold of daily gridded passive microwave ice concentration data from the National Snow and Ice Data Center (NSIDC) [*Cavalieri et al.*, 2013].

Surface water pCO_2 data were combined with a time/space co-located atmospheric pCO_2 product described in detail by Evans and Mathis [2013] to calculate sea-minus-air pCO_2 differences (ΔpCO_2). This treatment implicitly captures secular increases in both seawater and atmospheric pCO_2 [*Evans and Mathis,* 2013]. CO_2 solubility was calculated from ancillary measurements of sea surface temperature (SST) and sea surface salinity (SSS) using the relationship from Weiss [1974] corrected for seawater density. ΔpCO_2, SST, SSS, and CO_2 solubility data for each three-month season were averaged within 0.1° latitude by 0.2° longitude grid cells, creating seasonal climatologies of each parameter.

These products were coupled with seasonally averaged piston velocities calculated using the wind speed parameterization from Ho *et al*. [2011] and monthly second moments of wind speed from the Scatterometer Climatology of Ocean Winds (SCOW) [*Risien and Chelton,* 2008]. The SCOW data are 0.25° latitude by 0.25° longitude, have a 30 km land mask, and include coverage that is limited to south of 62.5°N. As such, pixels that lacked wind data were filled with margin-wide averages. The final product is a seasonal climatology of sea-air CO_2 fluxes (F_{CO_2}) at 0.1° latitude by 0.2° longitude resolution across the SEBS.

Recent work has suggested that there can be significant fluxes of CO_2 through ice [*Delille et al.,* 2007; *Else et al.,* 2008; *Mucci et al.,* 2010; *Nomura et al.,* 2010; *Miller et al.,* 2011; *Rysgaard et al.,* 2011], and that some ice-associated waters (e.g., polynyas) can exhibit enhanced gas transfer velocities relative to open water conditions [*Else et al.,* 2011]. However, use of standard methods for estimating gas transfer in ice-rich environments can be problematic, and correction factors applied to some of the above data sets have indicated more typical gas transfer velocities [e.g., *Lauvset et al.,* 2011]. Given that the community agreement on methods of measurement of gas transfer through ice is still evolving, and that typical patterns and controls of ocean-ice-atmosphere gas transfer are not yet understood (broadly discussed by Vancoppenolle *et al*. [2013]), it is not presently possible to broadly estimate these effects. For grid cells with five-year mean ice presence, we assumed ice cover caused the complete mechanical inhibition of gas exchange, damping F_{CO_2} to zero. This approach describes the maximum impact of ice on annual F_{CO_2}. Gas transfer through the ice matrix and gas transfer through small-scale open-water areas generated by continuous ice deformation (leads, polynyas, grain boundaries and micro-cracks, Takahashi *et al*. [2009]) likely reduce total influence of ice on gas exchange relative to this upper-bound estimate.

In order to constrain the influence of biogeochemical processes on F_{CO_2}, ΔpCO_2 climatologies for each season were reconstructed using surface water pCO_2 values normalized to the 2008–2012 mean annual SST from the equation of Takahashi *et al*.

[2002], such that $\left(pCO_2 \text{ at } T_{mean}\right) = \left(pCO_2 \text{ at } T_{obs}\right) \times e^{[0.0423\ (T_{mean} - T_{obs})]}$, and Extended Reconstructed Sea Surface Temperature (ERSST) data (http://www.ncdc.noaa.gov/ersst/; Figure 5.1). This calculation removes localized effects of seasonal warming and cooling on ΔpCO_2 values. Remaining variability in normalized-ΔpCO_2 ($n\Delta pCO_2$) has been shown to closely follow NCP and biological processes in the Bering Sea, with only minor contributions from changes in alkalinity and vertical mixing [*Bates et al.,* 2011]. As a result, $n\Delta pCO_2$ was assumed to indicate the influences of biological production and respiration, while $\Delta pCO_2 - n\Delta pCO_2$ was assumed to indicate the influences of temperature.

5.3 Results and Discussion

5.3.1 Observations

5.3.1.1 Ice Formation and Advance: Nov. – Jan.

Most of the northern shelf and inshore portions of the southern shelf of the Bering Sea exhibited ice presence during the December – January season (Figure 5.2A-C), corresponding to previously observed trends [*Stabeno et al.,* 2007, 2012b]. ΔpCO_2 ranged from -67 to +204 µatm (Figure 5.2A). Deviation between ΔpCO_2 and $n\Delta pCO_2$ as great as 86 µatm occurred over the northern shelf, highlighting the opposing effects of cooling (cool colors, Figure 5.2A) and respiration (warm colors, Figure 5.2B). While respiration typically dominated fluxes, cooling could have induced CO_2 influx in the absence of ice. $n\Delta pCO_2$ as low as -20 µatm also indicate the effects of production in limited areas over the central shelf. Although these areas were ice covered, under-ice and ice-algal production are not uncommon in the Bering Sea (e.g., Jin *et al*. [2007], Gradinger [2009], Miksis-Olds *et al*. [2013]).

In open water areas, mean F_{CO_2} was +21.2 mmoles C m^{-2} d^{-1} (n = 213; SD = 11.0 mmoles C m^{-2} d^{-1}; Figure 5.2C). Late-season respiration and any potential winter F_{CO_2} are typically ignored when calculating annual fluxes, assumed to be completely inhibited by ice cover (e.g., Bates *et al*. [2011]). The climatological ice edge calculated here shows

that a substantial open-water area was strongly influenced by respiration (Figure 5.2B), and indicates that respiration-driven return of CO_2 to the atmosphere can have a significant impact on annual CO_2 flux estimates from this region. Other studies have shown that these CO_2 fluxes could be enhanced during periods of ice formation and advance [*Else et al.,* 2011], indicating that these fluxes may be even more prominent than estimated here.

5.3.1.2 Maximum Ice Extent: Feb. – Apr.

The five-year seasonal mean ice edge calculated here (Figure 5.2D-F) covered most of the southern shelf, although the southern outer shelf remained ice-free in accordance with previously observed patterns (e.g., cold years; Stabeno *et al*. [2012b]; Miksis-Olds *et al*. [2013]). During this season, cooling processes reduced ΔpCO_2 by an average of 71.6 μatm (n = 73; SD = 16.0 μatm) across the entire shelf, inducing net negative ΔpCO_2 south of 60°N (Figure 5.2D). Respiration processes raised ΔpCO_2 over the entire shelf, except immediately near the ice edge (Figure 5.2E), and resulted in net positive ΔpCO_2 over the northern shelf. However, ice cover in these areas was assumed to reduce overall fluxes to zero (Figure 5.2F). Limited data from an open water area near the Aleutian Islands indicated negative F_{CO_2} (-8.7 ± 5.7 mmoles C m^{-2} d^{-1}; n = 25) resulting from cool SSTs.

5.3.1.3 Ice Retreat: May – July

The 2008–2012 average ice edge for May-July showed a typical complete retreat of ice from the southern areas of the SEBS [*Pease,* 1980; *Niebauer et al.,* 1990] (Figure 5.1; Figure 5.2G-I). Westward-dominating currents [*Stabeno et al.,* 2012b] and the St. Lawrence Island polynya also aided ice breakup in the western areas of the northern SEBS. Counter-intuitively, melting ice maintains SSTs to the south that are cooler than the annual average although warmer than the preceding season, and cooling processes did lower ΔpCO_2 in this area. The northern shelf, by contrast, has a much lower average annual SST (see Figure 5.1) and slight warming raised SSTs above the annual average,

causing increases in ΔpCO_2. In shallower coastal areas, this warming was strong enough to produce net positive ΔpCO_2 (Figure 5.2G) despite the onset of the spring bloom, indicated by uniformly negative $n\Delta pCO_2$ data (Figure 5.2H). Despite the variable effects of temperature, phytoplankton production maintained F_{CO_2} rates that were predominantly negative (-15.8 mmoles C m^{-2} d^{-1}; n = 1151; SD = 7.1 8 mmoles C m^{-2} d^{-1}; Figure 5.2I).

5.3.1.4 Open Water: Aug. – Oct.

During 2008 – 2012, the entire SEBS was ice-free during this season (Figure 5.2J-L). Warming above mean annual SST over the entire shelf raised ΔpCO_2 by 39.6 µatm (n = 679; SD = 15.2 µatm), producing net positive values in shallow coastal regions (Figure 5.2J). Production continued to dominate $n\Delta pCO_2$ values (Figure 5.2K), particularly along the shelf break. This region is typically referred to as the "Green Belt" [*Springer et al.,* 1996] for the high summer rates of production consistently observed. By contrast, overall macronutrient stocks are typically lower near shore and nutrient exhaustion slows primary production in the late season [*Sambrotto et al.,* 1986; *Lomas et al.,* 2012]. Correspondingly, we observed $n\Delta pCO_2$ values close to zero in some of these areas. Low $n\Delta pCO_2$ values were also observed over the central shelf, perhaps resulting from coccolithophore production [*Harlay et al.,* 2011; *Iida et al.,* 2012]. Overall, we observed warming-driven efflux (Figure 5.2L) in areas where $n\Delta pCO_2$ values were lower, and production-driven influx in other areas of the shelf.

5.3.2 Annual Shelf-Wide Fluxes and the Impacts of Ice Cover

Integrating F_{CO_2}rates over time (one season = 91.25 days) and area of each grid cell allowed us to determine the annual F_{CO_2}. When taken together, shelf-wide average annual F_{CO_2} exhibited a sampling bias towards sub-regional areas with more occupied grid cells (e.g., southern middle shelf). To eliminate this error, we isolated fluxes across each of six previously observed biogeochemical domains in the Bering Sea [*Coachman,* 1986; *Stabeno et al.,* 1999; *Kachel et al.,* 2002; *Mathis et al.,* 2010, 2011; *Lomas et al.,*

2012; *Ortiz et al.,* 2012] (three along-shelf domains split into northern and southern portions; see Figure 5.1) and averaged them over these areas (resulting error was listed as one standard deviation from the mean). Because these domains tend to exhibit uniform biogeochemical processes, the average flux within each domain exhibits a lower standard deviation than fluxes averaged across the entire shelf. Consequently, the annual sum of these regional fluxes provides a more precise estimation of the total F_{CO_2} for the SEBS.

The resulting seasonal F_{CO_2} patterns show well-documented seasonal physical and biogeochemical cycles, both before and after accounting for ice cover (first and second series of bars, respectively, Figure 5.3). CO_2 invasion occurred during ice retreat, driven by ice-edge and spring bloom productivity (-11.1 ± 2.2 Tg C yr^{-1}). Minimum ice cover caused a small perturbation, preventing the influx of ~1.6 Tg C yr^{-1}. Some CO_2 invasion continued into the summer open water season (-5.6 ± 2.7 Tg C yr^{-1}), but slower production rates and surface layer warming reduced the overall amount of influx. During ice advance, respiration overwhelmed the start of water column cooling, generating CO_2 efflux (+10.3 ± 3.6 Tg C yr^{-1}). During this season, ice cover caused the greatest impact, preventing ~3 Tg C yr^{-1}, or ~29%, of the overall potential efflux. Both influx and efflux occurred during maximum ice extent but were largely balanced, producing a near-zero potential flux during this season (-0.5 ± 3.7 Tg C yr^{-1}). However, almost all potential CO_2 efflux was again inhibited during this season, causing a three-fold increase in the size of the Febrary – April CO_2 sink although the total growth was small (~1.1 Tg C yr^{-1}).

Overall, ice cover acts to inhibit efflux rather than influx of CO_2 and increases the size of the annual Bering Sea CO_2 sink by ~2.5 Tg C yr^{-1} to a total size of -9.4 ± 5.0 Tg C yr^{-1}. Scaling to match the total area of the SEBS as given by Ortiz *et al*. [2012], we calculate that the corresponding annual Bering Sea sinks published by Walsh and Dieterle [1994] and Takahashi *et al*. [2009] are approximately twice as large as our estimates (20.6 and 16.7 Tg C yr^{-1}, respectively). However, these estimates only account for growing season data (i.e., March – October) and completely neglect late-season respiration. The total potential size of the Bering Sea CO_2 sink, completely neglecting any net regional respiration (adding all regions < 0, Figure 5.3), is close to these literature

values (-20.1 ± 3.7 Tg C yr^{-1}). Accounting for late-season gas exchange, even when partially inhibited by ice cover, reduces the size of the total potential sink by nearly half (~44%) of the total potential influx of CO_2.

On a regional scale, these ice-driven perturbations occur primarily over the ice-dominated northern shelf, and result from large ΔpCO_2 observed in the Middle Domain (50-100 m isobaths; light blue boxes, Figure 5.3). In this region alone, nearly 2.5 Tg C yr^{-1} of potential CO_2 outgassing are suppressed by ice cover (although some influx is also prevented during ice retreat). Recent work has shown some evidence that high CO_2 concentrations in the northern Middle Domain are causing the dissolution of calcium carbonate ($CaCO_3$) minerals [Chapter 4; Appendix B]. While several mechanisms were hypothesized to control this $CaCO_3$ mineral dissolution by causing seasonal accumulation of CO_2, the data presented in this study suggest that the inhibition of outgassing by ice cover may also be a contributing process. By forcing CO_2 retention, it is possible that ice cover contributes to an overall higher inventory of CO_2 in this area, and that fewer subsequent perturbations are needed to produce conditions favoring $CaCO_3$ dissolution.

5.3.3 Implications of Decreasing Seasonal Ice Cover

Some thermodynamic constraints, models, and observational data suggest that seasonal ice will continue to form in the northern Bering Sea [*Stabeno et al.,* 2012a, b], although periods of ice cover may become shorter due to later freezing and earlier melting and presence of ice over the southern shelf may diminish. Delaying the onset of ice cover over the northern shelf could allow temporarily unchecked CO_2 efflux during November – January and uninhibited influx during May – July, resulting in near-neutral net F_{CO_2}. If SSTs over the southern shelf continue to warm in the coming decades, as has been projected [*Stabeno et al.,* 2012a], periods of stronger CO_2 efflux from November – April and weaker CO_2 influx from May – October could also reduce net annual CO_2 uptake. In a warmer, ice-reduced scenario, these combined effects could substantially reduce the size of the SEBS CO_2 sink.

5.3.4 CO_2 Invasion on Alaskan Coastal Shelves

Given the vast spatial extent and the high rates of primary production typical of the SEBS, it is often assumed that the region must be a strong sink for atmospheric CO_2 [*Bates et al.,* 2011]. We have shown here that late-season outgassing partially counteracts spring and summer CO_2 influxes, shrinking the size of the potential sink by about half. The resulting total CO_2 influx is weak despite the overall area of the Bering Sea, accounting for less than 15% of the total CO_2 invasion occurring on the Alaskan coastal shelves (see Table 5.1).

Although similar methods to those employed here were used to generate the net Gulf of Alaska CO_2 flux [*Evans and Mathis*, 2013], potential late-season outgassing was neglected in the calculation of the Chukchi Sea flux [*Bates and Mathis*, 2009]. Given the shallow nature of the Chukchi Sea shelf, it is likely that some outgassing should result from late season respiration processes despite ice cover, as we observed here. Although recent studies have identified mechanisms for open-water outgassing events in the Beaufort Sea, the contribution of these events to the total annual flux was not well constrained [*Mathis et al.,* 2012].

A better comparison of each of the shelves and the calculation of a net Alaskan shelf CO_2 sink would require a uniform synthesis of direct measurements, over matching time and space scales sufficient to resolve regional variability. While this is difficult to achieve using solely direct measurements, a synthetic approach that enlists satellite data [i.e., *Hales et al.,* 2012] blended with direct measurements may hold promise as an avenue for generating basin-scale CO_2 flux products.

5.4 Conclusions

A synthesis of spatially resolved underway and observational data for 2008–2012 provided a unique opportunity to assess late season sea-air CO_2 fluxes and the impact of sea ice on gas exchange over the SEBS. While some influence of temperature on sea-air flux was observed, biological processes dominated most variability in sea-air exchange. In particular, late-season respiration was observed to have a substantial impact on annual

CO_2 fluxes even when partially blocked by ice, balancing nearly half of the potential annual CO_2 sink.

Ice cover reduced sea-air CO_2 efflux, and resulted in the increase of the overall magnitude of the sink from -6.9 Tg C yr^{-1} to -9.4 Tg C yr^{-1}. Regionally, the greatest impact of ice was observed over the northern middle shelf, where nearly 2.5 Tg C yr^{-1} of CO_2 efflux is inhibited. The retention of this CO_2 may enhance the undersaturated conditions for calcium carbonate minerals previously observed in this region. Southern shelf effluxes were relatively uninhibited by ice cover and counteracted nearly half of the total potential influx. While mechanical reduction of sea-air gas fluxes does increase the Bering Sea CO_2 sink by the prevention of some outgassing, quantification of late-season, open water CO_2 fluxes overall decreases this sink relative to previous estimates.

While an extensive comparison to other Pacific Arctic shelves is not presently possible given the different scaling and flux calculation methods employed in the literature, it seems likely that other shallow shelves might experience a similar late-season outgassing resulting from net respiration. Quantification of winter outgassing could therefore reduce the overall size of the Pacific Arctic sink for CO_2 by a substantial amount, even when some inhibition of fluxes by ice cover occurs. If future warming causes significant ice losses over the next several decades, inhibition of respiration-driven CO_2 outgassing may decrease, reducing the magnitude of the Bering Sea sink and causing a significant slowing of carbon uptake in the Pacific Arctic region.

5.5 Tables

Table 5.1 Annual F_{CO_2} of Alaskan continental shelves. Areas and annual fluxes from Evans and Mathis [2013] (Gulf of Alaska; GoA); this study (Bering Sea); Bates and Mathis [2009] (Chukchi Sea); and Mathis *et al*. [2012] (Beaufort Sea).

Shelf	Total Annual Flux		Total Area	
	Tg C yr^{-1}	*%*	*km^2*	*%*
GoA	-14	*19.61*	800000	*34.9*
Bering	-9.4	*13.17*	694355	*30.29*
Chukchi	-46	*64.43*	620000	*27.05*
Beaufort	-2 – 0	*2.8*	178000	*7.76*
Total AK Shelves	-71.4	*100*	2292355	*100*

5.6 Figures

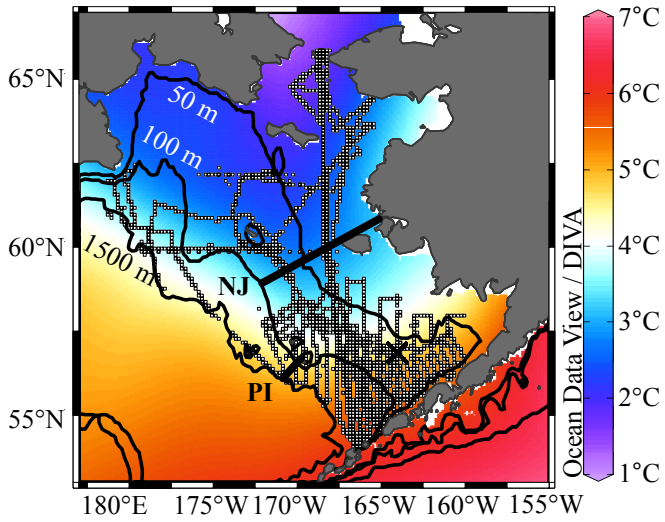

Figure 5.1 Map of the southeastern Bering Sea shelf. Color shading indicates the five-year (2008–2012) mean annual sea surface temperature. Also shown are populated grid cells (white squares) and the location of the M2 mooring (X). The isobathic contours shown approximate the boundaries of the Coastal (0-50 m), Middle (50-100 m), and Outer (100-1500 m) Domains. North-south boundaries across domains are designated by bold black lines at the Nunivak Jet (NJ) and near the Pribilof Islands (PI).

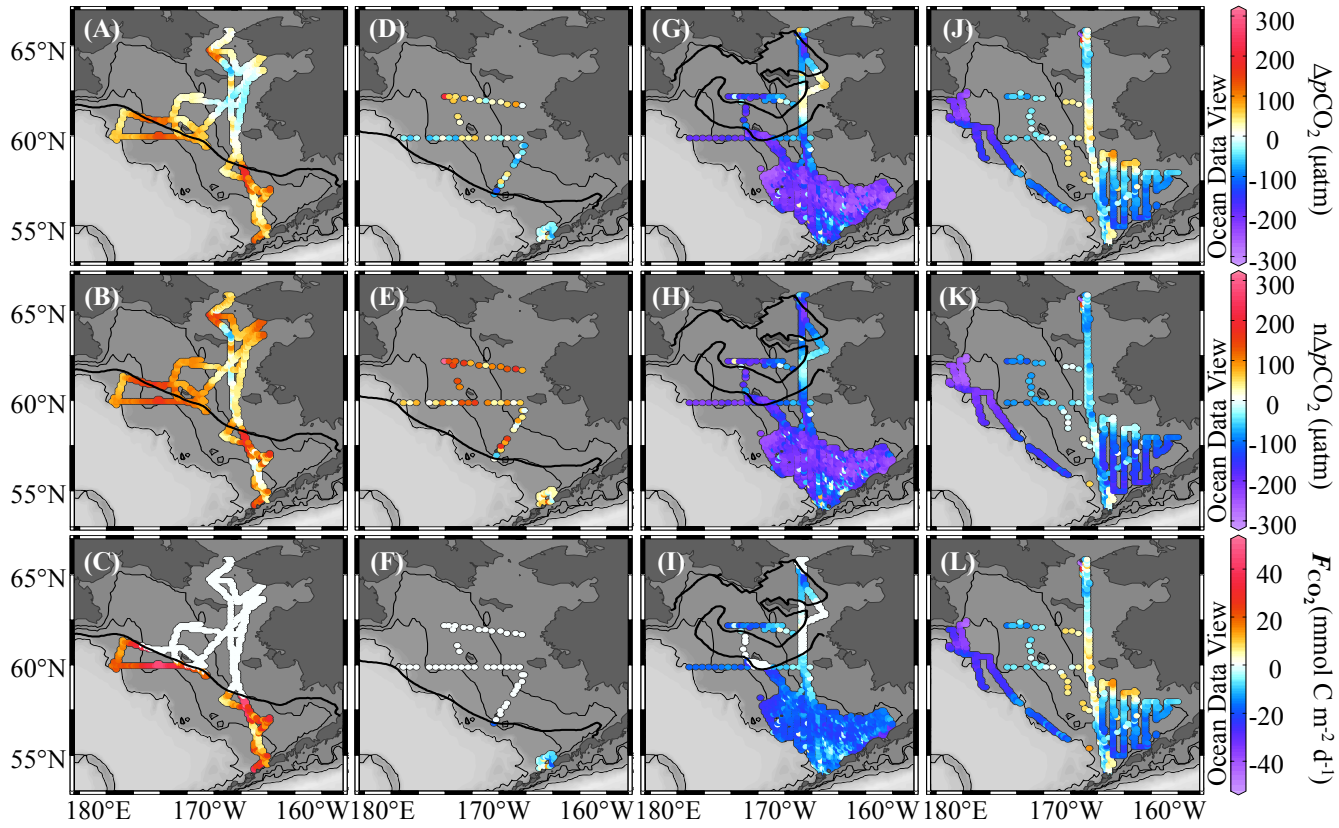

Figure 5.2 Seasonal surface ΔpCO_2, $n\Delta pCO_2$, and F_{CO_2} (2008 – 2012). (A-C) Ice advance (Nov. – Jan.). (D-F) Maximum ice extent (Feb. – Apr.). (G-I) Ice retreat (May – Jul.). (J-L) Open water (Aug. – Oct.). ΔpCO_2 (µatm) appears in the top row (A, D, G, J) $n\Delta pCO_2$ (µatm) in the middle row (B, E, H, K), and F_{CO_2} (mmoles C m^{-2} d^{-1}) appears in the bottom row (C, F, I, L). The seasonal ice edge is indicated by the thick black lines.

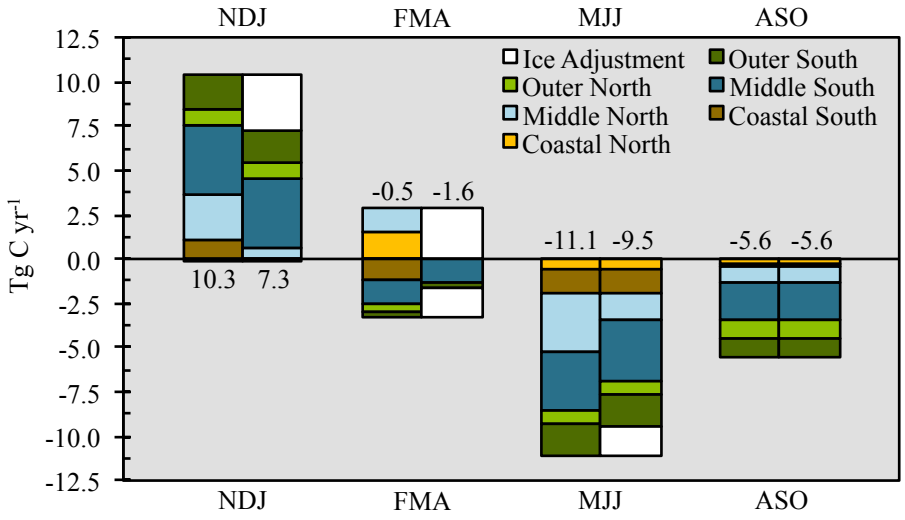

Figure 5.3 Seasonal fluxes and ice cover corrections by region (2008 – 2012). Seasonal fluxes were calculated both without (first series) and with (second series) a correction for ice cover for comparison, given that NDJ: November – December – January. FMA: February – March – April. MJJ: May – June – July. ASO: August – September – October. The total seasonal flux in Tg C yr^{-1} (i.e., sum of all series in a single bar) is given above each bar.

5.7 Acknowledgements

The authors thank the officers and crew of USCGC *Healy*, R/V *Knorr*, and NOAA ships *Miller Freeman* and *Oscar Dyson* for their work in supporting our science during multiple cruises. We also thank our colleagues from the NSIDC, LDEO, NOAA Eco-FOCI group and the Bering Sea Project. This manuscript is BEST-BSIERP contribution no. XX. This synthesis effort was supported by the National Science Foundation (PLR-1107997). Statement of Work: Cross, J.N., synthesized the available pCO_2 datasets, performed upper level analysis, and prepared the manuscript for publication. Mathis, J.T., Frey, K.E., Cosca, C.E., Danielson, S.L. amd Takahashi, T. all contributed data to this synthesis effort and provided guidance during manuscript preparation. Bates, N.R., and

Feely, R.A., provided guidance during manuscript publication. Evans, W., designed the method for and preformed sea-air CO_2 flux calculations.

5.8 References

Bates, N. R., and J. T. Mathis (2009), The Arctic Ocean marine carbon cycle: evaluation of air-sea CO_2 exchanges, ocean acidification impacts and potential feedbacks, Biogeosci, 6, 2433−2459, doi: 10.5194/bg-6-2433-2009.

Bates, N. R., J. T. Mathis, and M. A. Jeffries (2011), Air-sea CO_2 fluxes on the Bering Sea shelf, Biogeosci., 8, 1237−1253, doi: 10.5194/bg-8-1237-2011.

Cavalieri, D. J., C. L. Parkinson, P. Gloersen, and H. Zwally, (2013), Sea ice concentrations from Nimbus-7 SMMR and DMSP SSM/I-SSMIS Passive Microwave Data, NASA DAAC–NSIDC, Boulder, CO.

Coachman, L. K. (1986), Circulation, water masses, and fluxes on the southeastern Bering Sea shelf, Cont. Shelf Res., 51(1-2), 23−108, doi: 10.1016/0278-4343(86)90011-7.

Cooper, L., M. G. Sexson, J. M. Grebmeier, R. Gradinger, C. W. Mordy, and J. R. Lovvorn (2013), Linkages between sea-ice coverage, pelagic-benthic coupling, and the distribution of spectacled eiders: Observations in March 2008, 2009, and 2010, Deep Sea Res. II., 94, 31−43, doi: 10.1016/j.dsr2.2013.03.009.

Delille, B., B. Jourdain, A. V. Borges, J.-L. Tison, and D. Delille (2007), Biogas (CO_2, O_2, dimethylsulfide) dynamics in spring Antarctic fast ice, Limnol. Oceanogr., 52(4), 1367−1379, doi: 10.1016/j.marchem.2013.05.012.

Else, B. G. T., T.N. Papakyriakou, M. A. Granskog, and J. J. Yackel (2008), Observations of sea surface fCO_2 distributions and estimated air-sea CO_2 fluxes in the Hudson Bay region (Canada) during the open water season, J. Geophys. Res., 113, C08026, doi: 10.1029/2007JC004389.

Else, B. G. T., T. N. Papakyriakou, R. J. Galley, W. M. Drennan, L. A. Miller, and H. Thomas (2011), Wintertime CO_2 fluxes in an Arctic polynya using eddy covariance: Evidence for enhanced air-sea gas transfer during ice formation, J. Geophys. Res., 116, C00G03, doi: 10.1029/2010JC006760.

Evans, W., and J. T. Mathis (2013), The Gulf of Alaska coastal ocean as an atmospheric CO_2 sink, Cont. Shelf Res., 65, 52−63, doi: 10.1016/j.csr.2013.06.2013.

Gradinger, R. (2009), Sea-ice algae: Major contributors to primary production and algal biomass in the Chukchi and Beaufort Seas during May/June 2002, Deep Sea Res. II., 56(17), 1201−1212, doi: 10.1016/j.dsr2.2008.10.016.

Hales, B., P. G. Strutton, M. Saraceno, R. Letelier, T. Takahashi, R. A. Feely, *et al*. (2012), Satellite-based prediction of pCO_2 in coastal waters of the eastern North Pacific, Prog. Oceanogr., 103, 1−15, doi: 10.1016/j.pocean.2012.03.001.

Harlay, J., L. Chou, C. De Bodt, N. Van Oostende, J. Piontek, K. Suykens, *et al.* (2011), Biogeochemistry and carbon mass balance of a coccolithophore bloom in the northern Bay of Biscay (June 2006), Deep Sea Res. II., 58, 111−127, doi: 10.1016/j.dsr.2010.11.005.

Ho, D. T., R. Wanninkhof, P. Schlosser, D. S. Ullman, D. Hebert, and K. F. Sullivan (2011), Toward a universal relationship between wind speed and gas exchange: gas transfer velocities measured with $^3He/SF_6$ during the Southern Ocean Gas Exchange Experiment, J. Geophys. Res., 116(C4), C00F04, doi: 10.1029/2010JC006854.

Hunt Jr., G. L., P. J. Stabeno, G. Walters, E. Sinclair, R. D. Brodeur, J. M. Napp, and N. A. Bond (2002), Climate change and control of the southeastern Bering Sea pelagic ecosystem, Deep Sea Res. II., 49, 5821−5853, doi: 10.1016/S0967-0645(02)00321-1.

Hunt Jr., G. L., K. O. Coyle, L. B. Eisner, E. V. Farley, R. A. Heintz, F. Mueter, *et al.*, (2011), Climate impacts on eastern Bering Sea foodwebs: a synthesis of new data and an assessment of the Oscillating Control Hypothesis, ICES J. Mar. Sci., 68(6), 1230−1243, doi: 10.1093/icesjms/fsr036.

Iida, T., K. Mizobata, and S.-I. Saitoh (2012), Interannual variability of coccolithophore *Emiliania huxleyi* blooms in response to changes in water column stability in the eastern Bering Sea, Cont. Shelf Res., 34, 7−17, doi: 10.1016/j.csr.2011.11.007.

Jin, M., C. Deal, J. Wang, V. Alexander, R. Gradinger, S.-I. Saitoh, *et al.*, (2007), Ice-associated phytoplankton blooms in the southeastern Bering Sea, Geophys. Res. Lett., 34(6), L06612, doi: 10.1029/2006GL028849.

Kachel, N. B., G. L. Hunt Jr., S. A. Salo, J. D. Schumacher, P. J. Stabeno, and T. E. Whitledge (2002), Characteristics and variability of the inner front of the southeastern Bering Sea, Deep Sea Res. II., 49, 5889−5909, doi: 10.1016/S0967-0645(02)00324-7.

Lauvset, S. K., W. R. McGillis, L. Bariteau, C. W. Fairall, T. Johannessen, A. Olsen, and C. J. Zappa (2011), Direct measurements of CO_2 flux in the Greenland Sea, Gephys. Res. Lett., 38, L12603, doi: 10.1029/2011GL047722.

Lomas, M. W., S. B. Moran, J. R. Casey, D. W. Bell, M. Tiahlo, J. Whitefield, *et al*., (2012), Spatial and seasonal variability of primary production on the Eastern Bering Sea shelf, Deep Sea Res. II., 65-70, 126−140, doi: 10.1016/j.dsr2.2012.02.010.

Mathis, J. T., J. N. Cross, N. R. Bates, S. B. Moran, M. W. Lomas, C. W. Mordy, and P. J. Stabeno (2010), Seasonal distribution of dissolved inorganic carbon and net

community production on the Bering Sea shelf, Biogeosci., 7, 1769−1787, doi: 10.5194/bgd-7-251-2010.

Mathis, J. T., J. N. Cross, and N. R. Bates (2011), The role of ocean acidification in systemic carbon mineral suppression in the Bering Sea, Gephys. Res. Lett., 38, L19602, doi: 10.1029/2011GL048884.

Mathis, J. T., R. S. Pickart, R. H. Byrne, C. L. McNeil, G. W. K. Moore, L. W. Juranek, *et al*. (2012), Storm-induced upwelling of high pCO_2 waters onto the continental shelf of the western Arctic Ocean and implications for carbonate mineral saturation states, Geophys. Res. Lett., 39(7), L07606, doi: 10.1029/2012GL51574.

Miksis-Olds, J. L., P. J. Stabeno, J. M. Napp, A. I. Pinchuk, J. A. Nystuen, J. D. Warren, *et al.* (2013), Ecosystem response to a temporary sea ice retreat in the Bering Sea: Winter 2009, Prog. Oceaongr., 111, 38−51, doi: 10.1016/j.pocean.2012.10.010.

Miller, L. A., T. N. Papakyriakou, R. E. Collins, J. W. Deming, J. K. Ehn, R. W. Macdonald, *et al.* (2011), Carbon dynamics in sea ice: A winter flux time series, J. Geophys. Res., 116(C2), C02028, doi: 10.1029/2009JC006058.

Mucci, A., B. Lansard, L. A. Miller, and T. N. Papakyriakou (2010), CO_2 fluxes across the air-sea interface in the southeastern Beaufort Sea: Ice-free period, J. Geophys. Res., 115(C4), C04003, doi: 10.1029/2009JC005330.

Niebauer, H. J., V. Alexander, and S. Henrichs (1990), Physical and biological oceanographic interaction in the spring bloom at the Bering Sea marginal ice edge zone, J. Geophys. Res., 95(C12), 22229−22241, doi: 10.1029/JC095iC12p22229.

Nomura, D., H. Eicken, R. Gradinger, and K. Shirasawa (2010), Rapid physically driven inversion of the air-sea ice CO_2 flux in the seasonal landfast ice off Barrow, Alaska after onset of surface melt, Cont. Shelf Res., 30, 1998−2004, doi: 10.1016/j.csr.2010.09.014.

Ortiz, I., F. Wiese, and A. Grieg (2012), Marine regions of the eastern Bering Sea shelf. Accessed June 2012. Available from: http://bsierp.nprb.org/documents/BSIERP_Regions.doc.

Pease, C. (1980), Eastern Bering Sea ice processes, Month. Weath. Rev., 108(12), 2015−2023, doi: 10.1175/1520-0493(1980)108<2015:EBSIP>2.0.CO;2.

Risien, C., and D. Chelton (2008), A global climatology of surface wind and wind stress fields from eight years of QuickSCAT scatterometer data, J. Phys. Oceangr., 38, 2379−2413, doi: 10.1175/2008JPO3881.1.

Rysgaard, S., J. Bendtsen, B. Delille, G. S. Dieckmann, R. N. Glud, H. Kennedy, *et al*., (2011), Sea ice contribution to the air-sea CO_2 exchange in the Arctic and Southern Oceans, Tellus 63(B), 823−830, doi: 10.1111/j.1600-0889.2011.00571.x.

Sambrotto, R. H., H. J. Niebauer, J. J. Goering, and R. L. Iverson (1986), Relationships among vertical mixing, nitrate uptake, and phytoplankton growth during the spring bloom in the southeast Bering Sea middle shelf, Cont. Shelf Res., 5(1-2), 161−198, doi: 10.1016/0278-4343(86)90014-2.

Semiletov, I. P. (1999), Aquatic sources and sinks of CO_2 and CH_4 in the polar regions, J. Atmos. Sci., 56, 286−306, doi: 10.1175/1520-0469(1999)056<0286:ASASOC>2.0.CO;2.

Semiletov, I., A. Makshtas, and S.-I. Akasofu (2004), Atmospheric CO_2 balance: the role of Arctic sea ice, Geophys. Res. Lett., 31, L05121, doi: 10.1029/2003GL017996.

Springer, A. M., C. P. McRoy, and M. V. Flint (1996), The Bering Sea Green Belt: shelf-edge processes and ecosystem production, Fish. Oceangr., 5(3-4), 205−223, doi: 10.1111/j.1365-2419.1996.tb00118.x.

Stabeno, P. J., J. D. Schumacher, and K. Ohtani (1999), The physical oceanography of the Bering Sea, in *Dynamics of the Bering Sea: A summary of physical, chemical, and biological characteristics, and a synopsis of research on the Bering Sea*, edited by T. Louglin and K. Ohtani, pp. 1-28, North Pac. Mar. Sci. Org. (PICES) and Univ. of Alaska Sea Grant, Fairbanks, AK.

Stabeno, P. J., N. B. Kachel, M. Sullivan, and T. E. Whitledge (2002), Variability of physical and chemical characteristics along the 70-m isobath of the southeastern Bering Sea, Deep Sea Res. II., 49, 5931−5943, doi: 10.1016/S0967-0645(02)00327-2.

Stabeno, P. J., N. A. Bond, and S. A. Salo (2007), On the recent warming of the southeastern Bering Sea shelf, Deep Sea Res. II., 54, 2599−2618, doi: 10.1016/j.dsr2.2007.08.023.

Stabeno, P. J., J. M. Napp, C. W. Mordy, and T. E. Whitledge (2010), Factors influencing physical structure and lower trophic levels of the eastern Bering Sea shelf in 2005: Sea ice, tides and winds, Prog. Oceanogr., 85(3-4), 180−196, doi: 10.1016/j.pocean.2010.02.010.

Stabeno, P. J., E. V. Farley Jr., N. B. Kachel, S. Moore, C. W. Mordy, J. M. Napp, *et al*. (2012a), A comparison of the physics of the northern and southern shelves of the eastern Bering Sea and some implications for the ecosystem, Deep Sea Res. II., 65-70, 14−20, doi: 10.1016/j.dsr2.2012.02.019.

Stabeno, P. J., N. B. Kachel, S. E. Moore, J. M. Napp, M. Sigler, A. Yamaguchi, *et al*. (2012b), Comparison of warm and cold years on the southeastern Bering Sea shelf and some implications for the ecosystem, Deep Sea Res. II., 65-70, 31−45, doi: 10.1016/j.dsr2.2012.02.020.

Takahashi, T., S. C. Sutherland, C. Sweeney, A. Poisson, N. Metzl, B. Tilbrook, *et al*., (2002), Global sea-air CO_2 flux based on climatological surface ocean pCO_2, and

seasonal biological and temperature effects, Deep Sea Res. II., 49, 1601−1622, doi: 10.1016/S0967-0645(02)00003-6.

Takahashi, T., S.C. Sutherland, R. Wanninkhof, C. Sweeney, R. A. Feely, D. W. Chipman, *et al*. (2009), Climatological mean and decadal change in surface ocean pCO_2, and net sea-air CO_2 flux over the global oceans, Deep Sea Res. II., 56(8-10), 554−577, doi: doi:10.1016/j.dsr2.2008.12.009.

Vancoppenolle, M., K. M. Meiners, C. Michel, L. Bopp, F. Brabant, G. Carnat, et al., (2013), Role of sea ice in global biogeochemical cycles: emerging views and challenges, Quat. Sci. Rev., 79, 207−230, doi: 10.1016/j.quascirev.2013.04.011.

Walsh J., and C. Johnson (1979), An analysis of Arctic sea ice fluctuations, 1953 – 1977, J. Phys. Oceanogr., 9(3), 580−591, doi: 10.1175/1520-0485(1979)009<0580:AAOASI>2.0.CO;2.

Walsh, J., and D. W. Dieterle (1994), CO_2 cycling in the coastal ocean I–A numerical analysis of the southeastern Bering Sea with applications to the Chukchi Sea and the northern Gulf of Mexico, Progr. Oceanogr., 34, 335−392, doi: 10.1016/0079-6611(94)90019-1

Weiss, R. F. (1974), Carbon dioxide in water and seawater: the solubility of a non-ideal gas, Mar. Chem., 2, 203−215, doi: 10.1016/0304-4203(74)90015-2.

Chapter 6:
Conclusions

6.1 Summary of Results

The work presented in this dissertation investigated new observations of spatiotemporal carbon biogeochemical cycles collected during the Bering Ecosystem Study (BEST) and Bering Sea Integrated Ecosystem Research Program (BSIERP) Bering Sea Project (bsierp.nprb.org; Harvey and Sigler, 2013). This data set was used to present seasonal analyses of both the organic and inorganic carbon systems in an effort to quantify the seasonal accumulation of CO_2, identify natural physico-biogeochemical mechanisms controlling this accumulation, and to determine the effects of natural accumulation in conjunction with the gradual and continuous accumulation of anthropogenic carbon in the environment. New mechanisms of natural CO_2 accumulation were identified, augmenting the potential impacts of ocean acidification processes in two key areas: the Coastal Domain and the northern Middle Domain.

Chapter 2 focused on the spatiotemporal distributions of dissolved organic and inorganic carbon (DOC and DIC, respectively), which revealed net seasonal accumulation of carbon in coastal surface waters. A synthesis of these data and other carbon records collected during the Bering Sea Project was then used to construct a carbon budget to determine the origin of the excess organic matter in this region in Chapter 3. While this chapter showed that coastal surface waters are likely net-autotrophic on the annual scale, imbalances between surface layer production and bottom layer carbon sinks showed that allochthonous organic carbon must accumulate at the coast. While the source of this organic matter was unclear, it was indicated that laterally advected marine organic matter produced over the central shelf could be a likely candidate. This synthesis effort provided the first evidence for focused deposition in the region, a process that has significant biogeochemical implications. Previous work has shown the Phytoplankton-Carbonate Mineral Saturation State (PhyCaSS) interaction produces vertically coupled divergent trajectories of carbonate mineral ($CaCO_3$)

saturation states (Ω) between bottom and surface waters as a result of vertical separation of production and remineralization (Bates and Mathis, 2009). Resultantly, PhyCaSS enhances $CaCO_3$ corrosivity in bottom waters (lowers Ω) at a rate directly coupled to surface layer production. However, the focused deposition of allochthonous marine organic matter and its subsequent remineralization enhances this effect in bottom waters, leading to greater $CaCO_3$ corrosivity than would be expected based solely on the vertically-coupled PhyCaSS Interaction.

In order to understand the implications of this corrosivity for the carbonate system, the first thorough description of conservative and non-conservative variations in total alkalinity (TA) was developed in Chapter 4. This detailed analysis identified an area where enhanced $CaCO_3$ corrosivity from natural CO_2 accumulation in conjunction with anthropogenic CO_2 produced ambient conditions sufficient to dissolve soluble $CaCO_3$ on the northern middle shelf. It was hypothesized that this effect resulted partially from regionally unique physical conditions favoring efficient vertical export of organic matter and local retention of respiration products. The analysis of sedimentary respiration rates indicates that this process is fairly continuous throughout the year. Efficient retention of respiration products would thus cause a continuous accumulation of CO_2 through the growing season. Correspondingly, in Chapter 4 the most corrosive conditions were produced in autumn months.

From these results, it was apparent that little-studied late-season respiration processes were integral to understanding the carbon system as a whole. New underway data sets allowed for the first analysis of late-season sea-air CO_2 fluxes at high spatial and temporal resolution in the region. The analysis of winter conditions presented in Chapter 5 indicated that the mechanical inhibition of air-sea exchange of CO_2 gas by sea ice also caused the accumulation of CO_2 in winter, raising the regional baseline concentration of CO_2 for the remainder of the year.

While CO_2 accumulation is enhanced at the coast due to the respiration of focused marine organic matter deposits, the combination of multiple factors enhancing the respiration signal in the northern Middle Domain indicate that this region is highly

vulnerable to acidification processes. Given the long tradition of multidisciplinary research in the Bering Sea, the obvious next step in this region is to understand the links between these processes and commercially valuable upper trophic levels.

6.2 Future Projections

Accurate prediction of the effects of acidification processes on the Bering Sea ecosystem is dependent both on a thorough understanding of the physiology of Bering Sea organisms and on an understanding of the process of acidification from a chemical perspective. Specifically, the impacts of acidification on biology are typically understood through four key factors: increases in the intensity, duration, and spatial extent of undersaturation events and organismal response. While a physiological or ecosystem level assessment of the biological response to acidification is beyond the scope of this work, it is possible to make preliminary projections of each of these parameters in the Bering Sea.

To illustrate the effects of accumulating anthropogenic CO_2, Figures 6.1 and 6.2 show first-order estimates of the future progression of Ω in surface waters and bottom waters, respectively. Assuming that the rate of anthropogenic CO_2 accumulation in surface waters increases by 0.02 ppm yr^{-1} from 2 ppm yr^{-1} in 2009 (NOAA-ESRL, 2013), surface waters over most of the shelf will likely become perennially undersaturated with respect to aragonite between 2130 and 2200, depending on the degree of surface water warming (Figure 6.1, Table 6.1). Based on thermodynamic constraints and projected sea ice persistence in the coming decades (Stabeno et al., 2012), the northern Bering Sea will likely follow the P2-T0 scenario, with seasonal aragonite undersaturations occurring as early as 2060 in the absence of surface layer warming. By contrast, surface water temperatures over the southern Bering Sea shelf will likely follow the extreme warming scenario (P2-T2; SST increases by 0.042 °C yr^{-1}; Hansen et al., 2010), with seasonal undersaturations of aragonite absent on average ~25 years later than over the northern shelf. Figure 6.2 imposes the P2-T0 scenario on observed seasonal Ω_A in bottom waters. Under this projection, bottom water aragonite undersaturations observed in 2009 (A-C)

expand to cover most of the shelf in each season by 2050 (Figure 6.2D-F), and persistent undersaturations of aragonite cover the entire shelf by 2100 (bottom row, Figure 6.2G-I).

These projections indicate that the intensity, duration, and spatial extent of $CaCO_3$ undersaturations will expand dramatically through the next 100 years, eventually resulting in widespread and persistent undersaturated conditions. Some studies of both present and future CO_2 levels on calcifying Bering Sea species are currently underway (e.g., King and Tanner crab; Long et al., 2013a, b). In order to guide these future studies, the work presented here has identified particularly vulnerable areas and indicated how acidification processes will progress. However, the biogeochemical data presented here may also provide a basis for early detection of net $CaCO_3$ dissolution, and present impacts of acidification on marine calcifying species.

In Chapter 4, observed total alkalinity concentrations in excess of those that should have resulted from conservative mixing processes were used as a proxy for identifying dissolution of present marine carbonates. In discussing this excess alkalinity, it was determined that undersaturated conditions of sufficient intensity and duration were present to dissolve most aragonitic minerals over the shelf. However, the estimates of the e-folding timescale of dissolution were based on a dissolution rate calculated from pure, reagent-grade lithogenic calcite. Biogenic calcite may not dissolve as quickly. This is a function of the surface area to volume ratio (SA/V). The higher this ratio, the faster the particle will dissolve, and vice-versa. Studies utilizing biogenic calcite aggregate an "observed" SA/V for biogenic carbonates that is more accurate than artificial minerals or mineral powders.

Dissolution rate constants based on $CaCO_3$ dissolution observed in the field also have a second advantage, other than implying a real average particle size: some factors like refractory biofilms (Dreybrodt et al., 1996; Hales and Emerson, 1997; Morse and Arvidson, 2002) and "protection" mechanisms utilized by live organisms (e.g., Long et al., 2013a, b; Feely and Bednarsek, unpublished data) can inhibit the rate dissolution processes relative to theoretical values. An "average" inhibition effect is also an emergent value of using rate constants derived from *in-situ* dissolution experiments.

As a result of varying particle size and solubility, dissolution rate constants based on biogenic carbonates are slower than those calculated for the laboratory. For example, in an unpublished data set Feely and Bednarsek calculate dissolution rate constants between $5d^{-1}$ and $15d^{-1}$ using live pteropods, with evidence of active mechanisms to counteract dissolution. Similarly, Gehlen et al. (2007) calculated an average dissolution rate value for sinking biogenic calcite particles of $\sim 10.9d^{-1}$. Both of these values are slower compared to the $3.8d^{-1}$ implied by Hales and Emerson (1997), as was used in Chapter 4.

While dissolution studies of biogenic carbonates continue, major uncertainties still exist concerning these reactions. Some experiments indicate that dissolution of biogenic carbonates (particularly aragonite) exhibits a higher reaction order (e.g., Keir, 1980, Gehlen et al., 2005a, b), implying a non-linear dependence of the dissolution rate on Ω (that is to say, the dissolution rate increases exponentially with decreasing Ω). Because these reaction orders are often quite variable, many studies continue to use a linear reaction order. Another common assumption is that dissolution is only dependent on Ω in undersaturated conditions, while some studies indicate that dissolution of extremely soluble particles can occur when $\Omega > 1$ (Betzer et al., 1984; Feely and Bednaršek, unpublished data.) Further resolution of the reaction order and the period of dependence of dissolution rates on Ω will help to more accurately model and predict biogenic carbonate dissolution.

Dissolution rate constants for calcite are better resolved both in pure laboratory settings and *in-situ* studies (as reviewed by Gangstø et al., 2008). As a result, many present models utilize calcite dissolution rates to model aragonite dissolution. Adopting both of the assumptions above and using the observed biogenic calcite dissolution rate constant from Gehlen et al. 2007, the e-folding time for dissolution (τ) is approximately three times slower than was estimated using the Hales and Emerson dissolution rate constant in Chapter 4 (τ = 18 d and τ = 5 d, respectively). However, relative to the extended period of undersaturations in the Bering Sea (three months at Ω_A = 0.5 observed, Chapter 4 and Appendix B), there is still sufficient time to dissolve 99% of the

original stock of biogenic aragonite (i.e., 5τ). At the observed calcite undersaturations (Ω_C = 0.8), τ = 45 d and τ = 13 d for the Gehlen and Hales and Emerson constants, respectively. At 90 days of persistent calcite undersaturation at this level, ~85-99% calcite species can be expected to dissolve.

These data imply that significant energetic and calcification costs are presently impacting bottom-dwelling Bering Sea species in the northern Middle Domain. However, the extent of the organismal response to these pressures is presently unknown. Future research efforts should focus on resolving this important issue. By contrast, surface waters are not affected to a lesser degree, as supersaturated conditions persist in most of these domains throughout the year (Chapter 4).

6.3 Cascading Impacts Through the Pacific Arctic Region (PAR)

Waters over the Bering Sea shelf are transported northward through Bering Strait into the Chukchi Sea after three months (Coachman, 1986), and eventually impact most of the upper water masses in the Pacific Arctic (Macdonald et al., 2002; Kadko and Swart, 2004; Cooper et al., 2008), an important region for global carbon storage (e.g., Sabine et al., 2004; Bates and Mathis, 2009; Tanhua et al., 2009). The biogeochemical preconditioning that occurs over the subarctic shelf regions is likely propagated into the waters of the Canada Basin, where it can have critical downstream effects (Mathis et al., 2012). Given that many drivers are expected to cause enhanced $CaCO_3$ Ω suppression in the Arctic Ocean in coming decades (e.g., increased ice melt and river discharge: McClelland et al., 2006; White et al., 2007; enhanced production and biological pump: Arrigo et al., 2008), additional suppression from the transport of pre-conditioned, undersaturated waters from the Bering and Chukchi Shelves could further exacerbate this processes.

In Figure 6.3, fecent observations show the flow of undersaturated water through Barrow Canyon (Figure 6.3A) into the Canada Basin halocline layer (Figure 6.3B) before they are upwelled onto the Beaufort Shelf (Figure 6.3C). However, the biogeochemical link between the Bering and Chukchi Seas, and between the Chukchi Sea shelf and

Barrow Canyon are less well understood. Whereas seasonal undersaturations in the Bering and Chukchi Seas (Bates and Mathis, 2009; Bates et al., 2009; Anderson et al., 2010; Mathis et al., 2011; Appendix A) are already apparent, the transport of undersaturated waters between these regions has yet to be observed. Understanding the transport of seasonal carbon accumulations and undersaturated conditions through Bering Strait and Barrow Canyon will be critical to understanding the progression of ocean acidification in the Chukchi Sea and Arctic Ocean.

Direct flow of seasonally undersaturated waters between the Bering Sea shelf and the Chukchi Sea shelf could have profound impacts on the Chukchi Sea ecosystem. The Chukchi Sea sustains a rich and diverse benthic ecosystem, supporting several varieties of calcifying biota (Grebmeier et al., 2006; Feder et al., 2007) vulnerable to ocean acidification processes (Gazeau et al., 2007; Kuffner et al., 2008; Ries et al., 2009; Ries, 2011). Additional seasonal suppression of Ω by mixing with pre-conditioned Bering Shelf bottom waters beyond that already experienced in the Chukchi Sea could result in strongly corrosive fall and winter conditions in this region. While undersaturations with respect to the soluble minerals aragonite and high-magnesium calcite have already been observed, these mounting drivers may eventually result in calcite undersaturations, affecting a broader variety of organisms.

On longer timescales, the Bering Sea shelf and basin could have the opposite impact on downstream waters in the Pacific Arctic region. Chen (1993) predicted that acidification would eventually induce dissolution of carbonate solids in the Bering Sea, which would then cause a negative feedback on ocean acidification processes both within the Bering Sea basin and in downstream Chukchi and Arctic areas. Negative feedback of $CaCO_3$ dissolution on acidification has since been modeled on a global scale (e.g., broadly reviewed by Gehlen et al., 2011). While the effects are small on short-term timescales, they can be very broad on longer-term timescales.

It is presently possible that these effects may already be observable in the Bering Sea. As discussed at length in Chapter 4 and the above discussion, shallow-water dissolution of $CaCO_3$ is already occurring. It was also briefly noted that the calcite

saturation horizon has shoaled by ~150 m in the Bering Sea basin, perhaps due to the penetration of anthropogenic CO_2. The estimate of the average concentration of dissolved carbonates in this water mass calculated in Chapter 4 was similar to Chen (1993), although Chapter 4 indicated that a larger volume of water exhibited these dissolved carbonates. If the shoaling described in Chapter 4 has resulted from acidification processes, then the difference in dissolved carbonates would also represent the start of this negative feedback on acidification. Figure 6.3 indicates that the dominant signal propagated into the Canada Basin at present is likely carbonate mineral suppression. However, over time the dissolution of Bering Sea carbonates will continue to erode this signal. Depending on the concentration of carbonates in the Bering Sea and immediate source waters, it is possible that this negative feedback may eventually induce supersaturation.

6.4 Final Thoughts

The interdisciplinary tradition of research in the Bering Sea has allowed for the rapid advancement of knowledge concerning ecosystem function in the Bering Sea. The benefit of concurrent research with a variety of other investigators specifically enabled the synthesis effort in Chapter 3. As the analysis of the field data collected during the Bering Sea Project continues, new data have brought to light additional questions concerning carbon biogeochemical interactions in the area, particularly relevant given the results also presented here.

A new and seasonal variable circulation model for the shelf has recently been published, implying that flows over the shelf may not be as consistent or as sluggish as previously thought (Danielson et al., 2012). Through the newly hypothesized Nunivak Jet, focused deposition, accumulating carbon and seasonal $CaCO_3$ undersaturation in southern shelf coastal waters could eventually influence the middle and northern shelf. However, coastal biogeochemical processes may be even more complex than indicated here. The paucity of data for the Kuskokwim River and Kuskokwim and Bristol Bays represents a large gap in the present understanding of the Bering Sea carbon cycle,

despite the knowledge that these regions produce the largest salmon runs in the world. These new circulation processes also indicate that upwelling could be episodically relevant to the Bering Sea shelf, in areas and times outside the scope of this study. The penetration of naturally corrosive deep waters onto the shelf and the propagation of these waters northward could represent a new mechanism for $CaCO_3$ Ω suppression.

As measurement techniques, infrastructure, theoretical understanding and technology continues to improve, it will be critical to continually build on previous knowledge to develop robust interpretations of spatiotemporal carbon cycling over the Bering Sea shelf, and to monitor potential perturbations caused by global change. Recent advancements in moored and mobile autonomous sensors and continuous underway measurement systems have the capacity to dramatically increase the temporal and spatial resolution in hard to reach areas like the Bering Sea. Application of these techniques in hotspots where dissolution of soluble minerals has already been observed and to understudied areas already represents a unique opportunity to resolve some of these critical questions in the present. Utilization of these resources should be a strong research priority for the scientific community in the near term.

6.5 Tables

Table 6.1 Years of surface water Ω_A thresholds under warming scenarios. The two thresholds given are the envelope of average variability in the Bering Sea (See also Figure 6.1) and the saturation horizon ($\Omega_A = 1$), below which dissolution of soluble carbonate minerals is expected. Each scenario represents a different degree of expected warming, combined with a linearly growing rate of surface layer CO_2 accumulation (0.02 ppm yr^{-1} from 2 ppm yr^{-1} in 2009; NOAA-ESRL, 2013). P2-T0 indicates no warming; P2-T1 indicates 0.02°C yr^{-1}, the global average surface warming; and P2-T1 indicates 0.042°C yr^{-1}, the lower bound of surface warming for the Arctic Ocean (Hansen et al., 2010).

Scen.	**Ω_A < NVE**	**Ω_A < 1**		
		Spring	*Summer*	*Mean*
P2-T0	2095	2060	2138	2100
P2-T1	2109	2069	2162	2115
P2-T2	2131	2085	2200	2145

6.6 Figures

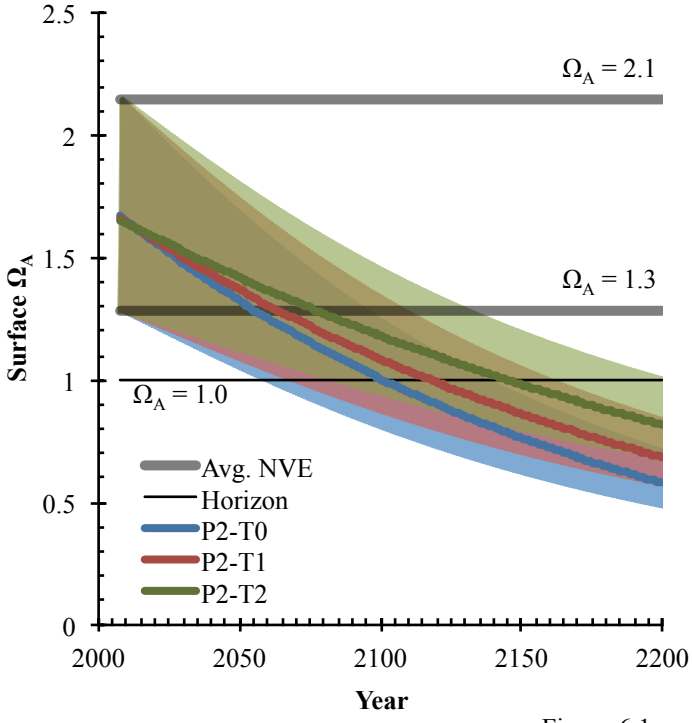

Figure 6.1

Figure 6.1 Surface water progression of Ω_A between 2009 and 2200. Shaded areas indicate the seasonal oscillation of Ω_A for each respective warming scenario and the accumulation of anthropogenic CO_2 as described in Table 6.1 and bold lines indicate the progression of the mean. The natural variability envelope (NVE; average shelf-wide surface Ω_A in spring (bottom) and summer (top), respectively) is indicated by thick grey lines. The saturation horizon (Ω_A = 1) is indicated by a thin black line.

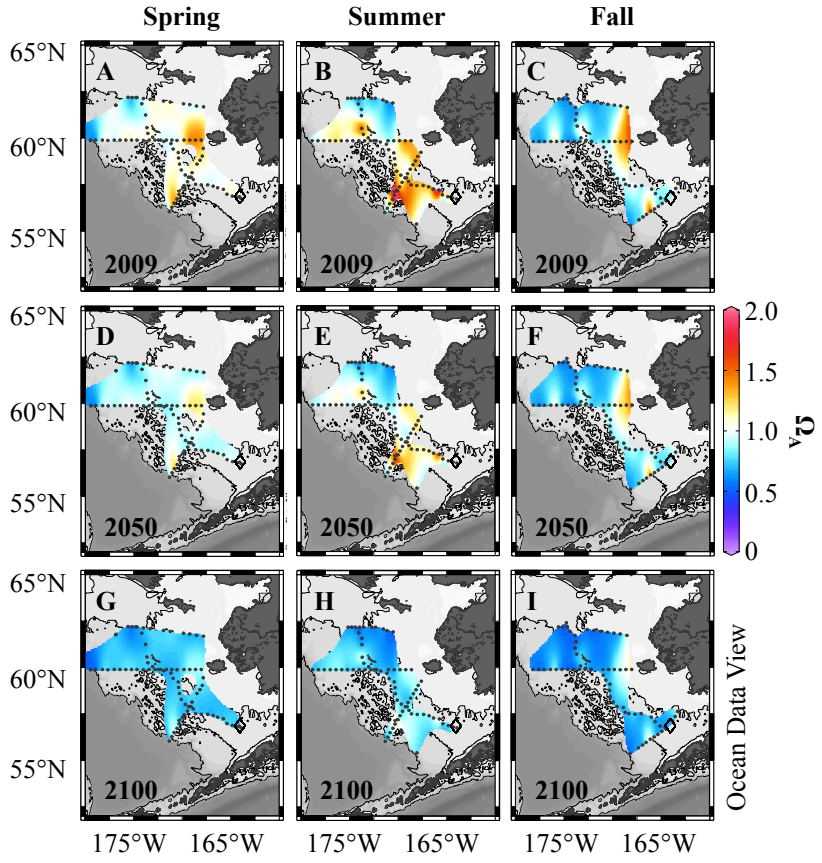

Figure 6.2 Bottom water Ω_A in 2009, 2050, and 2100 under scenario P2-T0. (A-C) Observed bottom water Ω_A. (D-F) Projected bottom water Ω_A in 2050. (G-I) Projected bottom water Ω_A in 2100. Projections in D-I were based on the accumulation of anthropogenic CO_2 over time, starting with the observed conditions in A-C. Cool colors indicate undersaturated conditions ($\Omega_A < 1$), white colors indicate the saturation horizon ($\Omega_A = 1$), and warm colors indicate supersaturated conditions ($\Omega_A > 1$). Some seasonal supersaturations of Ω_A remain in 2050, although these conditions are completely absent by 2100.

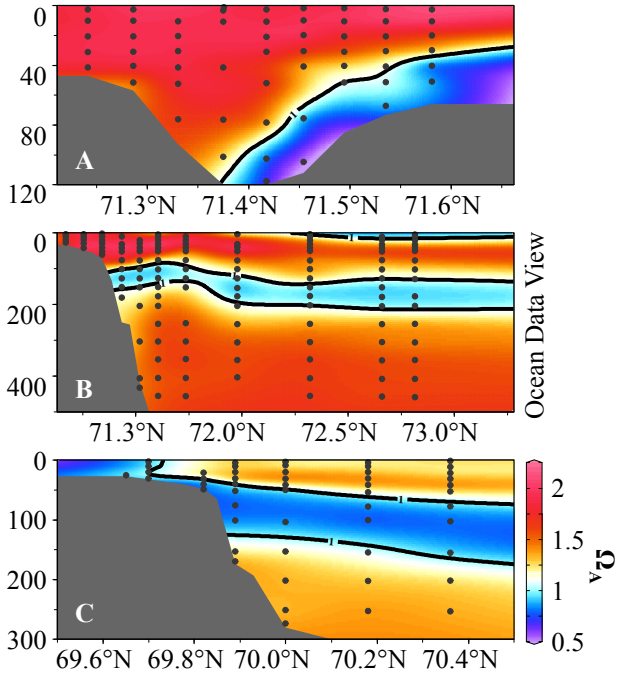

Figure 6.3 Water layers showing aragonite undersaturations in the Pacific Arctic. (A) Barrow Canyon. (B) Canada Basin. (C) Beaufort Sea shelf. Undersaturations (Ω_A < 1) are indicated by cool colors. The saturation horizon (Ω_A = 1) is indicated by thick black contour lines. Aragonite undersaturations are apparent on the northwest side of Barrow Canyon, in the halocline layer of the Canada Basin, and on the Beaufort Sea shelf.

6.7 References

Anderson, L., Tanhua, T., Björk, G., Hjalmarsson, S., Jones, E.P., Jutterström, S., et al., 2010. Arctic ocean shelf-basin interaction: An active continental shelf CO_2 pump and its impact on the degree of calcium carbonate solubility. Deep Sea Res. II. 57, 869−879.

Arrigo, K.R., van Dijken, G., Pabi, S., 2008. Impact of a shrinking Arctic ice cover on marine primary production. Geophys. Res. Lett. 35, L19603.

Bates, N.R., Mathis, J.T., 2009. The Arctic Ocean marine carbon cycle: evaluation of air-sea CO_2 exchanges, ocean acidification impacts, and potential feedbacks. Biogeosci. 6, 2433−2459.

Bates, N.R., Mathis, J.T., Cooper, L.W., 2009. Ocean acidification and biologically induced seasonality of carbonate mineral saturation states in the western Arctic Ocean. J. Geophys. Res. 114, C11007.

Betzer, P.R., Byrne, R.H., Acker, J.G., Lewis, C.S., Jolley, R.R., Feely, R.A., 1984. The oceanic carbonate system: a reassessment of biogenic controls. Science. 226, 1074−1077.

Chen, C.-T.A., 1993. Carbonate chemistry of the wintertime Bering Sea marginal ice zone. Cont. Shelf Res. 13(1), 67−87.

Coachman, L.K., 1986. Circulation, water masses, and fluxes on the southeastern Bering Sea shelf. Cont. Shelf Res. 5(1-2), 23−108.

Cooper, L.W., McClelland, J.W., Holmes, R.M., Raymond, P.A., Gibson, J.J., Guay, C.K., et al., 2008. Flow-weighted values of runoff tracers ($\delta^{18}O$, DOC, Ba, alkalinity) from the six largest Arctic rivers. Geophys. Res. Lett. 35, L18606.

Danielson, S., Hedstrom, K., Aagaard, K., Weingartner, T., Curchister, E., 2012. Wind-induced reorganization of the Bering Shelf circulation. Geophys. Res. Lett. 39, L08601.

Dreybrodt, W., Lauckner, J., Zaihua, L., Svensson, U., and Buhmann, D., 1996. The kinetics of the reaction $CO_2 + H_2O \rightarrow H^+ + HCO_3^-$ as one of the rate limiting steps for the dissolution of calcite in the system H_2O-CO_2-$CaCO_3$. Geochim. Cosmochim. Acta. 60(18), 3375−3381.

Feder, H.M., Jewett, S.C., Blanchard, A., 2007. Southeastern Chukchi Sea (Alaska) macrobenthos. Pol. Biol. 30, 261−275.

Gangstø, R., Gehlen, M., Schneider, B., Bopp, L., Aumont, O., Joos, F., 2008. Modeling the marine aragonite cycle: changes under rising carbon dioxide and its role in shallow water $CaCO_3$ dissolution. Biogeosci. 5, 1057−1072.

Gazeau, F., Quiblier, C., Jansen, J.M., Gattuso, J.-P., Middelburg, J.J., Heip, C.H.R., 2007. Impact of elevated CO_2 on shellfish calcification. Geophys. Res. Lett. 35, L22502.

Gehlen, M., Bassinot, F.C., Chou, L., McCorkle, D., 2005a. Reassessing the dissolution of marine carbonates I. Solubility. Deep Sea Res. I. 52(8), 1445−1460.

Gehlen, M., Bassinot, F.C., Chou, L., McCorkle, D., 2005b. Reassessing the dissolution of marine carbonates II: Reaction kinetics. Deep Sea Res. I. 52(8), 1461−1476.

Gehlen, M., Gangstø, R., Schneider, B., Bopp, L., Aumont, O., Ethe, C., 2007. The fate of pelagic $CaCO_3$ production in a high CO_2 ocean: a model study. Biogeosci. 4, 505−519.

Gehlen, M., Gruber, N., Gangstø, R., Bopp, L., Oschlies, A., 2011. Biogeochemical consequences of ocean acidification and feedbacks to the earth system, in:

Gattuso, J., Hansson, L. (Eds.), Ocean Acidification. Oxford University Press, New York, NY, pp. 230−248.

Grebmeier, J.M., Cooper, L.W., Feder, H.M., Sirenko, B.I., 2006. Ecosystem dynamics of the Pacific-influenced northern Bering and Chukchi seas in the Amerasian Arctic. Prog. Oceanogr. 61(2-4), 31−361.

Hales, B., Emerson, S., 1997. Evidence in support of first-order dissolution kinetics of calcite in seawater. Earth Planet. Sci. Lett. 148, 317−327.

Hansen, J., Ruedy, R., Sato, M., Lo, K., 2010. Global surface temperature change. Rev. Geophys. 48(4), RG4004.

Harvey, H.R., Sigler, M.F., 2013. An introduction to the Bering Sea Project: Volume II. Deep Sea Res. II. 94, 2−6.

Kadko, D., Swart, P., 2004. The source of the high heat and freshwater content of the upper ocean at the SHEBA site in the Beaufort Sea in 1997. J. Geophys. Res. 109, C01022.

Keir, R.S., 1980. The dissolution kinetics of biogenic carbonate in seawater. Geochim. Cosmochim. Acta. 44, 241−252.

Kuffner, I.B., Andersson, A.J., Jokiel, P.L., Rodgers, K.S., Mackenzie, F.T., 2008. Decreased abundance of crustose coralline algae due to ocean acidification. Nat. Geosci. 1(2), 114−117.

Long, C.W., Swiney, K.M., Foy, R.J., 2013a. Effects of ocean acidification on the embryos and larvae of red king crab, *Paralithodes camtschaticus*. Mar. Poll. Bull. 69(1-2), 38−47.

Long, C.W., Swiney, K.M., Harris, C., Page, H.N., Foy, R.J., 2013b. Effects of ocean acidification on juvenile Red King Crab (*Paralithodes camtschaticus)* and Tanner Crab (*Chionoecetes bairdi*) growth, condition, calcification, and survival. PLoS ONE. 8(4), e60959.

MacDonald, R.W., Anderson, L.G., Christensen, J.P., Miller, L.A., Semiletov, I.P., Stein, R., 2009. The Arctic Ocean, in: Liu, K. (Ed.), Carbon and Nutrient Fluxes in Continental Margins: a Global Synthesis. Springer, New York, NY, pp. 291−303.

Mathis, J.T., Cross, J.N., Bates, N.R., 2011. The role of ocean acidification in systemic carbonate mineral suppression in the Bering Sea. Geophy. Res. Lett. 38, L19602.

Mathis, J.T., Pickart, R.S., Byrne, R.H., McNeil, C.L., Moore, G.W.K., Juranek, L.W., et al., 2012. Storm-induced upwelling of high pCO_2 waters onto the continental shelf of the western Arctic Ocean and implications for carbonate mineral saturation states. Geophys. Res. Lett. 39, L07606.

Mathis, J.T., Cooley, S.R., Lucey, N., Hauri, C., Ekstrom, J., Hurst, T., et al., 2013. Ocean acidification risk assessment for Alaska's fisheries sector. Progr. Oceanogr. Submitted.

McClelland, J.W., Déry, S.J., Peterson, B.J., Holmes, R.M., Wood, E.F., 2006. A pan-arctic evaluation of changes in river discharge during the latter half of the 20th century. Geophys. Res. Lett. 33, L06715.

Morse, J.W., Arvidson, R.S., 2002. The dissolution kinetics of major sedimentary carbonate minerals. Earth Sci. Rev. 58, 51−84.

Ries, J.B., 2011. Skeletal mineralogy in a high-CO_2 world. J. Exp. Mar. Biol. Ecol. 403, 54−64.

Ries, J.B., Cohen, A.L., McCorkle, D.C., 2009. Marine calcifiers exhibit mixed responses to CO_2-induced ocean acidification. Geol. 27, 1131−1134.

Sabine, C.L., Feely, R.A., Gruber, N., Key, R.M., Lee, K., Bullister, J.L., et al., 2004. The oceanic sink for anthropogenic CO_2. Science. 305(5682), 367−371.

Stabeno, P.J., Farley Jr., E.V., Kachel, N.B., Moore, S., Mordy, C.W., Napp, J.M., et al., 2012. A comparison of the physics of the northern and southern shelves of the eastern Bering Sea and some implications for the ecosystem. Deep Sea Res. II. 65-70, 14−30.

Tanhua, T., Jones, E.P., Jeansson, E., Justterstrom, S., Smethie, W.M., Wallace, D.W.R., Anderson, L.G., 2009. Ventilation of the Arctic Ocean: Mean ages and inventories of anthropogenic CO_2 and CFC-11. J. Geophys. Res. 114(C1), C01002.

White, D., Hinzman, L., Alessa, L., Cassano, J., Chambers, M., Falkner, K., et al., 2007. The arctic freshwater system: changes and impacts. J. Geophys. Res. 112, G04S54.

Appendix A:

Coupling primary production and terrestrial runoff to ocean acidification and carbonate mineral suppression in the eastern Bering Sea[5]

A.0 Abstract

Water column pH and carbonate mineral saturation states were calculated from dissolved inorganic carbon (DIC) and total alkalinity (TA) data collected over the eastern Bering Sea shelf in spring and summer of 2008. The saturation states (Ω) of the two most important carbonate minerals, calcite (Ω_C) and aragonite (Ω_A) were strongly coupled to terrestrial runoff from the Yukon and Kuskokwim Rivers, primary production in the surface waters, and remineralization of organic matter at depth over the shelf. In spring, before ice melt occurred, pH over the shelf was largely confined to a range of 7.9 to 8.1 and Ω_C and Ω_A ranged from 1.5 to 3.0 and 0.8 to 2.0, respectively. At stations closest to river outflows, aragonite was undersaturated in the water column from the surface to the bottom. During the summer sea ice retreat, high rates of primary production consumed DIC in the mixed layer, which increased pH, Ω_C and Ω_A. However, Ω_C and Ω_A decreased by ~0.3 in the bottom waters over the middle and outer shelf. Over the northern shelf, where export production is highest, Ω_A decreased by ~0.35 and became highly undersaturated. The observed suppression and undersaturation of Ω_C and Ω_A in the eastern Bering Sea are correlated with anthropogenic CO_2 uptake into the ocean and will likely be exacerbated under business-as-usual emission scenarios. Therefore, ocean acidification could threaten some benthic and pelagic calcifying organisms across the Bering Sea shelf in the coming decades.

---

[5]Mathis, J. T., J. N. Cross, and N. R. Bates (2011), Coupling primary production and terrestrial runoff to ocean acidification and carbonate mineral suppression in the eastern Bering Sea, J. Geophys. Res., 116, C02030, doi: 10.1029/2010JC006453.

A.1 Introduction.

Since pre-industrial times, the oceans have absorbed approximately 127 Pg (Pg $=10^{15}$ g C) of anthropogenically produced carbon dioxide (CO_2) from the atmosphere [*Sabine and Feely,* 2007]. While this has mitigated the increase in atmospheric CO_2 concentrations by ~55% [*Sabine et al.*, 2004; *Sabine and Feely*, 2007], it has changed the carbonate chemistry of seawater chemical speciation [e.g., *Caldiera and Wickett*, 2003; *Andersson and Mackenzie*, 2004; *Feely et al.*, 2004; *Orr et al.*, 2005; *Millero*, 2007] with potentially significant impacts to current and future ocean biota [*Fabry et al.*, 2008; *Cooley and Doney*, 2009; *Fabry et al*., 2009]. Most notably, the absorption of atmospheric CO_2 by the ocean has resulted in a lowering of pH, especially over the last few decades [e.g., *Bates*, 2007; *Byrne et al.*, 2010], with a subsequent decrease in the availability of carbonate ions ($[CO_3^{2-}]$) and a suppression of the saturation states (Ω) of calcium carbonate minerals ($CaCO_3$) which could result in a reduction of suitable habitat for marine calcifiers. These processes, collectively termed ocean acidification (OA), have occurred naturally over geologic time scales [e.g. *Zachos et al.*, 2005] but have been accelerated due to anthropogenic emissions from industrial processes and changes in land use [*Feely et al.*, 2004; *Sabine et al.* 2004; *Caldiera and Wickett*, 2005; *Orr et al.*, 2005].

As CO_2 levels rise in the atmosphere, the increased partial pressure of carbon dioxide (pCO_2) in seawater contributes to OA and the suppression of biologically important carbonate mineral concentrations, such as calcite and aragonite, through a series of well-known reactions:

$$CO_2(g) \leftrightarrow CO_2(aq) \qquad \text{(Eq. A-1)}$$

$$CO_2(aq) + H_2O \leftrightarrow H_2CO_3 \qquad \text{(Eq. A-2)}$$

$$H_2CO_3 \leftrightarrow H^+ + HCO_3^- \qquad \text{(Eq. A-3)}$$

$$H^+ + HCO_3^- \leftrightarrow 2H^+ + CO_3^{2-} \qquad \text{(Eq. A-4)}$$

$$CO_3^{2-} + Ca^{2+} \leftrightarrow CaCO_3(s) \qquad \text{(Eq. A-5)}$$

Following dissolution (Eq. A-1), dissolved CO_2 undergoes hydration reactions to form carbonic acid (Eq. A-2), which rapidly dissociates to form carbonate and releases hydrogen ions (Eqs. A-3, A-4). Almost all of the produced carbonate ions react with calcium to form mineral solids (Eq. A-5), preventing this reaction from contributing to dissolved alkalinity. Further, most of the free hydrogen ions produced react with the naturally dissolved alkalinity in seawater, reducing carbonate ion concentrations. The remaining hydrogen ions contribute to the lowering of pH. Carbonate mineral saturation states are dependent on the concentration of free carbonate ions according to the following equations, such that a reduction in available CO_3^{2-} (Eq. A-5) decreases the saturation states of both aragonite and calcite:

$$\Omega_{aragonite} = \frac{[Ca^{2+}][CO_3^{2-}]}{K^*_{sp_{aragonite}}} \qquad \text{(Eq. A-6)}$$

$$\Omega_{calcite} = \frac{[Ca^{2+}][CO_3^{2-}]}{K^*_{sp_{calcite}}} \qquad \text{(Eq. A-7)}$$

Cold ocean temperatures increase the solubility of CO_2 and precondition the seawater to have lower calcium carbonate concentrations and saturation states compared to more temperate ocean environments, leaving polar and subpolar shelves particularly vulnerable to OA [*Orr et al.*, 2005; *Bates and Mathis*, 2009; *Fabry et al*., 2009; *Steinacher et al.*, 2009]. In addition to this temperature effect, several other processes affect the carbonate system and can contribute to the intensification of OA in polar and subpolar regions, including seasonally high rates of primary production, river runoff, and sea ice formation and melt processes [e.g. *Bates and Mathis*, 2009; *Bates et al*., 2009]. For example, seasonally intense periods of primary production are uncoupled from grazing in most polar environments [e.g., *Springer et al.*, 1996; *Macdonald et al.*, 2009] leading to high rates of organic matter export from the surface layer [e.g. *Mathis et al*., 2007]. While this export production supports the biologically diverse benthic communities in these regions it leads to elevated rates of remineralization in bottom

waters and sediments [*Grebmeier and McRoy*, 1989; *Devol and Christensen,* 1993; *Alonso-Saez et al.*, 2008; *Christensen*, 2008; *Garneau et al.*, 2009]. Thus, ocean biology tends to drive seasonally divergent trajectories for seawater chemistry, with primary production in the euphotic zone increasing Ω in the mixed layer while an accumulation of DIC in subsurface waters through remineralization suppresses Ω [*Bates et al*., 2009].

The reduction and undersaturation of carbonate minerals, particularly in bottom waters of polar and subpolar seas could have profound implications for benthic ecosystems. The subpolar continental shelf of the eastern Bering Sea (Figure A-1) sustains a vast and commercially valuable benthic fishery [*Cooley and Doney*, 2009; *Cooley et al.*, 2009] that produces approximately 47% of the U.S. fish catch by weight. This fishery is critical to both the regional and national economy and subsistence communities in Alaska with some species already potentially at risk (e.g., walleye pollock, pink salmon, king crab, tanner crab, ribbon seals) [*Boveng et al*., 2008; *Fabry et al*., 2008, 2009; *Chilton et al*., 2011]. Further decreases in pH and Ω could have significant consequences for the benthic and pelagic ecosystems in a region where organisms are already struggling to adapt to changing environmental conditions [*Løvvorn et al.*, 2003; *Moore et al.*, 2003; *Overland and Stabeno*, 2004; *Grebmeier et al.*, 2006]. Given the importance of the Bering Sea fishery, we must determine the controls and extent of OA and carbonate mineral saturation states in this region.

Here, we describe the seasonal variability of the seawater carbonate system over the eastern Bering Sea shelf in spring and summer of 2008 and investigate the impacts that primary production, sea ice processes, and terrestrial inputs have on carbonate mineral saturation states.

A.2 Background

The eastern Bering Sea contains a wide, shallow shelf covering over 500,000 km^2 [*Askren*, 1972; *Coachman*, 1986] from the Aleutian Islands to Bering Strait (Figure A-1). Semi-permanent frontal structures associated with wind, tidal mixing and bottom topography naturally divide the shelf into three along-shelf domains [*Askren*, 1972;

Muench, 1976; *Coachman*, 1986; *Stabeno et al*., 1999; *Kachel et al.*, 2002; *Stabeno et al.*, 2006] with differing vertical and horizontal structure largely controlled by the penetration of atmospheric forcing and tidal mixing. The Coastal Domain extends from the western shores of Alaska to the 50 m isobath. Within this region, wind and tidal currents vertically mix the water column to the bottom, although some stratification occurs in spring as the result of freshwater input from river runoff (Figure A-1) and sea ice melt. The Inner Front constitutes the boundary between the Coastal Domain and Middle Domain and approximately follows the 50 m isobath [*Kachel et al.*, 2002]. A well-stratified, two-layer system exists in the Middle Domain, where wind mixes the surface waters over a denser, tidally mixed bottom layer. The Central Front generally follows along the 100 m isobath, marking a gradual transition from the Middle Domain to the Outer Domain. A two-layer system is also present in the Outer Domain, although the transition between the surface and bottom layers is more gradual than in the Middle Domain. The Outer Domain is divided from the Bering Sea basin at the shelf break.

Large-scale circulation on the Bering Sea shelf is dominated by the advection of Pacific Ocean water from the Alaskan Stream and tidal energy dominates most of the shelf circulation, although some along-shelf flow following the bathymetry to the northwest is evident in the Coastal and Outer Domains [*Coachman*, 1986, *Overland and Roach*, 1987, *Coachman et al*., 1993; *Stabeno et al*., 1999]. In addition, there is some seasonal cross-shelf flow directed onshore in the Outer Domain during spring as a result of eddies and the funneling of water through submarine canyons [*Coachman*, 1982, 1986; *Schumacher and Stabeno*, 1998; *Stabeno and Van Meurs*, 1999; *Mizobata and Saitoh*, 2004]. Upwelling of deep Bering Sea water can occur over the northern shelf as a result of shoaling topography [*Nihoul et al.*, 1993]. On-shelf flow contributes nutrients to the shelf [*Nihoul et al.*, 1993; *Stabeno et al.*, 1999; *Stabeno et al.*, 2006], while tidal mixing transports coastally derived iron offshore towards the deep Bering Sea [e.g. *Aguilar-Islas et al.*, 2007]. The highest concentrations of iron and macronutrients tend to coincide at the Central Front, producing a region of elevated phytoplankton production known as the "Green Belt" [e.g. *Springer et al.*, 1996; *Aguilar-Islas et al.*, 2007; *Mathis et al.*, 2010].

The physical environment of the Bering Sea shelf is seasonally dominated by sea ice advance and retreat [*Walsh and Johnson*, 1979; *Luchin et al.*, 2002]. Sea ice is produced in the northern Bering Sea and advected southward by winds [*Stabeno et al.,* 2007]. Large-scale atmospheric forcing manifested in winter storm tracks generally dictates the extent of sea ice cover and the timing of sea ice retreat for a particular year, causing large interannual variations [*Neibauer*, 1998; *Wyllie-Escheveria*, 1995]. Over the long-term, maximum sea ice extent coincides with the negative phase of the Pacific Decadal Oscillation (PDO), although changes in the Arctic Oscillation (AO) and annual oscillations of the Aleutian Low are also causally related to recent changes in sea ice extent [*Stabeno et al.*, 1998, *Stabeno and Overland*, 2001; *Staebno et al*., 2001]. Because of the relatively long flushing time (> three months) [*Coachman*, 1986] of the Middle Domain, the formation and melting of sea ice usually results in the formation of a cold pool of bottom water isolated to the Middle Domain [*Wyllie-Escheveria and Wooster*, 1998; *Kachel et al.*, 2002].

Sea ice melt is the primary source of freshwater that influences the Central and Outer Domains [*Aguilar-Islas et al.*, 2008]. However, like most other arctic and subarctic shelves, the eastern Bering Sea receives a disproportionately large volume of freshwater input from rivers along the coast [*Opsahl and Benner*, 1997; *Wheeler et al.*, 1997; *Opsahl et al.*, 1999; *Peterson et al.*, 2002; *Hansell et al.*, 2004]. The principle sources of terrestrial runoff onto the Bering Sea shelf are the Yukon and Kuskokwim Rivers [*Lisitsyn*, 1969] (Figure A-1). The Yukon River Basin spans 853,300 km^2. In conjunction with this expansive area, the Yukon is the fifth largest drainage basin in North America in terms of average annual discharge [*Schumm and Winkley*, 1994; *Brabets et al.*, 2000], delivering ~200 km^3 water into the northern Bering Sea annually [*Brabets et al.*, 2000; *Striegl et al.*, 2005; *Stabeno et al.*, 2006]. The Kuskokwim River Basin is somewhat smaller (130,000 km^2) and contributes a smaller amount of runoff to shelf (34 km^3 annually), but has a greater impact over the southern and central parts of the eastern Bering Sea [*Feely et al.*, 1981]. Seasonal discharge peaks during May and June for both rivers, in conjunction with peak snowmelt [*Brabets et al.*, 2000; *Dornblaser and Striegl*,

2007]. A secondary pulse of increased discharge occurs in August due to peak glacial melt in the Yukon River Basin [*Dornblaser and Striegl*, 2007].

Shelf circulation of river discharge is primarily restricted to the coast by a series of persistent near-shore fronts. The runoff from the Kuskokwim River enters Kuskokwim Bay and flows along the shelf to the north, directed by tidal and wind driven currents [*Feely and Cline*, 1976] (Figure A-1). A semi-permanent front at the mouth of Kuskokwim Bay restricts cross-shelf flow south of Nunivak Island [*Belkin and Cornillon*, 2005; *Danielson et al.*, 2006]. At Nunivak Island, a portion of the flow breaks away from the coast and passes along the western side of the island as it travels north. In contrast, flow from the Yukon River is less restricted to the coast. Although most Yukon River discharge is directed into Norton Sound, a front at the mouth of the sound directs some flow directly towards Bering Strait (Figure A-1).

Overall, river runoff is mostly isolated to the Coastal Domain by the Inner Front. Its influence is extensive enough to significantly impact the vertical structure in the Coastal Domain [*Coachman*, 1986; *Kachel et al.*, 2002], especially during seasonal periods of increased discharge (May-June) [*Brabets et al.*, 2000]. Mixing of this water with Bering Shelf water produces a unique, low-salinity water mass known as Alaskan Coastal Water (ACW) [*Coachman*, 1986] and limited westward penetration of discharge from both rivers can occur under certain wind forcings [*Amos and Coachman*, 1992; *Coachman and Shigaev*, 1992; *Danielson and Kowalik*, 2005].

A.3 Methods

A.3.1 Cruise Information and Water Column Sampling

Physical, chemical and biological measurements were made from the *USCGC Healy* during spring (April/May) and summer (July) cruises to the eastern Bering Sea in 2008 as part of the Bering Ecosystem Study (BEST) project. Stations were occupied on three east-west transect (SL, MN and NP lines) lines and one north-south transect along the 70 m isobath (Figure A-1). The SL line was the northernmost line extending from near shore across the broad northern part of the shelf to a depth of ~90 m. The central line

(MN) extended roughly from the southern tip of Nunivak Island, across the shelf south of St. Matthew Island and terminated at the shelf break (2000 m deep). The southern line (NP) extended from the southern tip of Nunivak Island southwest past the 150 m isobath. The north-south line followed the 70 m isobath (70M) down the length of the shelf from the SL line and ended southeast of the NP line. At the beginning of the spring cruise, sea ice cover was near 100% at all stations with the exception of stations at the southern end of the 70M line and some minor leads, particularly around the islands. Towards the end of the spring cruise, sea ice had diminished and the southern stations of the 70M line were ice-free when sampled. During summer, the entire Bering Sea shelf was ice-free.

At each CTD/hydrocast station, water samples were collected for salinity, inorganic nutrients (ammonium, nitrate, nitrite, phosphate, reactive silicon, and urea), DIC, total alkalinity (TA) and dissolved oxygen (DO). Seawater samples for DIC/TA were drawn from Niskin bottles into pre-cleaned ~300 mL borosilicate bottles. These samples were subsequently poisoned with mercuric chloride ($HgCl_2$) to halt biological activity, sealed, and returned to the laboratory for analysis. Sea ice cores were collected at seven locations across the Bering Sea shelf during the spring cruise. Cores were partitioned into 10 cm sections and kept frozen until analysis. Cores were allowed to thaw and the melt water was transferred into borosilicate bottles, poisoned with $HgCl_2$ and analyzed for DIC and TA. All sampling and analysis was performed in compliance with the guide to best practices for ocean acidification research and reporting [*Riebesell et al.*, 2010].

A.3.2 Laboratory Analysis and Calculation of Carbonate Parameters

DIC and TA samples were analyzed using a highly precise and accurate gas extraction/coulometric detection system [*Bates*, 2001]. The analytical system consists of a VINDTA 3C (Versatile Instrument for the Detection of Total Alkalinity; http://www.marianda.com) coupled to a CO_2 coulometer (model 5012; UIC Coulometrics). TA samples were also determined by potentiometric titration using the VINDTA 3C. Routine analyses of Certified Reference Materials (CRMs, provided by

A.G. Dickson, Scripps Institution of Oceanography) ensured that the accuracy of the DIC and TA measurements were within 0.05% (~1 μmoles kg^{-1}) and stable over time.

Seawater pH and $CaCO_3$ saturation states for calcite (Ω_C) and aragonite (Ω_A) were calculated from DIC, TA, temperature, salinity, phosphate, and silicate data using the thermodynamic model of Lewis and Wallace [1995]. The carbonic acid dissociation constants of Mehrbach *et al*. [1973; as refit by *Dickson and Millero*, 1987; i.e., pK_1 and pK_2] were used to determine the carbonate parameters. The CO_2 solubility equations of Weiss [1974], and dissociation constants for borate [*Dickson*, 1990], silicate and phosphate [*Dickson and Goyet*, 1994] were used as part of the calculations. Uncertainty in the calculation of Ω_C and Ω_A were ~0.02.

A.4 Results

A.4.1 Seasonal Variability in Seawater Carbonate Parameters

TA in spring across the shelf and throughout the water column ranged from ~2150 μmoles kg^{-1} to ~2440 μmoles kg^{-1} over a salinity range of 31 to 34.5 (Figure A-2). In summer, TA was reduced by as much as 100 μmoles kg^{-1} in the surface layer (salinity 29.5-31; Figure A-2). In general, TA was higher over the northern regions of the shelf (> 60°N) and offshore in spring (Figure A-3A). TA decreased the most between spring and summer over the northern part of the shelf (Figure A-3B) and was higher over the southern shelf in summer. A similar trend was observed in DIC, where the highest drawdown between spring and summer occurred over the northern shelf [*Mathis et al.*, 2010].

In spring, pH ranged from ~7.87 to 8.30 over the shelf, with most values falling between 8.0 and 8.1. In summer, pH increased in the surface waters by as much as 0.2. However, pH decreased in bottom waters by as much as 0.3. In surface waters, there was a gradient with pH increasing along all three transect lines moving offshore in spring (Figure A-4A). Between spring and summer, pH increased in surface waters at all stations (Figure A-4B).

Increasing pH in surface waters over the shelf between spring and summer caused an average increase in Ω (Table A-3; Figures A-5A and B) for both Ω_C and Ω_A. In spring, Ω_C and Ω_A ranged from 1.5 to 3.0 and 0.8 to 2.0, respectively. For Ω_A, nearly the entire water column exhibited Ω near the saturation horizon. Average Ω_A was 1.25, although undersaturation was evident at the surface in some areas (Figure A-5A). In summer, Ω_C and Ω_A ranged more widely, from 1.1 to 4.5 and 0.65 to 3.2 (Figure A-5B). Increasing saturation states were particularly pronounced in the surface waters. In the upper 30 m of the water column, Ω_C and Ω_A increased by ~1.5 and ~1 between spring and summer, respectively (Table A-3). Bottom water saturation states decreased by ~0.20, in comparison.

In spring, along the northern most transect line (SL, Figure A-1), bottom waters were undersaturated with respect to aragonite ($\Omega_A < 1$) from the Coastal Domain to the Inner Front (Figure A-6A). At the Central Front (SL 10 and 11), the water column was undersaturated with respect to aragonite from the surface to the bottom (Figure A-6A). During this time, the water column was vertically stratified at the Central Front, which likely resulted in mixing of remineralized DIC from the bottom waters and the sediment. High silicate concentrations throughout the water column at the Central Front compared to the surrounding water masses indicated a strong benthic remineralization signature. Along the SL Line in summer, aragonite saturation states increased at the inshore stations with the exception of SL 1, where the water was undersaturated from the surface to the bottom. On either side of the Central Front (SL 7-14) the bottom waters (40-85 m) were undersaturated ($\Omega_A < 0.7$) in aragonite. However, in the surface waters above this feature, Ω_A values had increased ($\Omega_A < 2.5$) relative to spring values (Figure A-6B).

In spring, along the central transect line (MN), the water column was also vertically stratified. At the inshore stations (MN1 and 2), the water column was undersaturated with respect to aragonite from the surface to the bottom. Saturation states increased offshore with the highest values ($\Omega_A > 1.5$) present in the surface waters of the Outer Domain (Figure A-6C). In summer, the entire water column of the Coastal and Middle Domains were saturated with respect to aragonite likely due to the drawdown of

DIC throughout the water column (nitrate was depleted from the surface to the bottom in this region). Ω_A in the surface waters of the Outer Domain had also increased ($\Omega_A > 2.5$). However, the saturation states in the bottom waters at the Central Front (MN 13) and in the Outer Domain decreased ($\Omega_A = 1$ at 80 m; Figure A-6D).

The water column along the NP line in spring was supersaturated with respect to aragonite (Figure A-6E). These saturations states increased during summer throughout the entire water column from the coast to the Central Front. However, the saturation horizon for aragonite outcropped to within 40 m of the surface (NP 14-16), likely due to upwelling of deep Bering Sea water along this part of the shelf (Figure A-6F).

An analysis of saturation states from north to south along the 70 m isobath (70M) showed that there was a gradient between the northern and southern parts of the shelf. Ω_A were lower north for 60°N, with undersaturated conditions present in the bottom waters at stations 70M 50-58. Ω_A undersaturations were also observed in the southern part of the shelf in the bottom waters at stations 4 and 8, but these conditions were less prevalent than those in the north (Figure A-6G). In summer, saturations states increased, with the exception of persistent undersaturations at station 58. The increase was greatest ($\Omega_A >$ 2.5) in the surface waters of the northern shelf (Figure A-6H).

A.4.2 Carbonate Parameters in Sea Ice

Sea ice cores were collected across the shelf in spring of 2008 and analyzed for DIC and TA. Both DIC and TA increased with increasing salinity in these cores (Figure A-7A) with the lowest concentrations found closest to the sea ice/atmosphere interface and the highest concentrations observed near the ice-water interface, where brine concentration is highest. DIC and TA were tightly correlated at all locations, exhibiting consistent TA : DIC ratios of ~1.14, similar to the ratios obtained by Rysgaard *et al.* (2007; Figure A-7B). This indicates that in-ice productivity was at a minimum, while brine rejection had a substantial effect on the DIC/TA concentrations in the ice. These DIC and TA data were used to calculate the saturation states in the melt water. Ω values were low for both aragonite and calcite, ranging from 0.05 to 1.35 and 0.08 to 2.25,

respectively (Figure A-7C). All of the cores exhibited both calcite and aragonite undersaturation, except near the ice-water interface. The degree of undersaturation was not correlated to sampling location.

A.5 Discussion

Using the data collected in 2008 and historical observations from the Yukon and Kuskokwim Rivers, we can describe the influence of phytoplankton primary production, river runoff, and sea ice processes on pH and $CaCO_3$ mineral saturation states across the shelf. The controls and impacts on the carbonate system in surface waters are described in Section A.5.1, and the processes driving saturation states of subsurface waters are discussed in Section A.5.2. The unique processes controlling carbonate chemistry in the nearshore environment are discussed in Section A.5.3. Finally, we discuss how the conditioning of waters over the Bering Sea shelf might influence seawater carbonate chemistry in the western Arctic Ocean in Section A.5.4.

A.5.1 Carbonate Chemistry of the Surface Waters

In early summer, the combination of nutrient-rich slope waters, winter-renewed iron concentrations, nearly continuous solar irradiance, and consistent stratification over the eastern shelf of the Bering Sea creates one of the world's most productive environments [*Walsh et al.*, 1989]. In spring of 2008, DIC concentrations ranged from 1900 to 2400 μmoles kg^{-1} [*Mathis et al.*, 2010] but were drawn down in the mixed layer by as much as 150 μmoles kg^{-1} in summer. Meanwhile, DIC concentrations increased in bottom waters likely due to the remineralization of exported organic matter [*Mathis et al.*, 2010]. From this seasonal change in DIC concentrations, shelf-wide average net community production (NCP) was estimated at 28 ± 10 mmoles C m^{-2} d^{-1} in 2008 with the highest rates observed in the "Green Belt" at the Central Front (40-47 mmoles C m^{-2} d^{-1}), where micro- and macronutrient inputs as well as stratification are usually at their peak during late spring and summer [*Springer et al.*, 1996; *Mathis et al.*, 2010]. In contrast to these highly productive regions, phytoplankton blooms in the Coastal Domain

tend to rapidly deplete all available nitrate shortly after ice retreat [*Walsh et al.*, 1989], thereby limiting total production. NCP [*Mathis et al*., 2010] in the Outer Domain is also limited, due to low micronutrient concentrations [i.e., iron: *Aguilar-Islas et al.*, 2007]. In 2008, there was a north-west gradient in productivity, with higher NCP trending towards northern regions in the Outer and Middle Domains, and towards southern regions in the Coastal Domain [*Mathis et al.*, 2010]. A summary of domain-specific rates of productivity is given in Table A-3.

Large phytoplankton blooms consume DIC in the surface layer, thereby raising pH and increasing Ω. Figure A-8 shows the changes in aragonite saturation states between spring and summer along the four transect lines. Increases in Ω can be seen in the surface waters along each line, and were particularly pronounced above the Central Front and in the northern regions of the 70M line, where our previous work indicated the highest NCP [*Mathis et al*., 2010]. The greatest increases in Ω between spring and summer corresponded to regions where dissolved oxygen (DO) concentrations were highest in summer, further indicating the coupling between productivity and increased Ω.

Table A-3 shows a comparison between the rates of net community production and the change in saturation states in the upper 30 m. A loose trend between the rate of productivity and the increase in surface layer saturation states is obvious. The lowest change in saturation states (~0.1) is coincident with the lowest rate of productivity on the shelf in the northern Outer Domain, and the greatest change in mixed layer saturation states occurs in the southern Outer Domain, in conjunction with the second-highest rate of production in the southern Outer Domain. However, the drastically low change in saturation state in the northern Coastal Domain seems too great to be completely due to low rates of production, and the inconsistent relationship between higher rates of productivity and greater increases in saturation states indicate that other factors must be influencing saturation states in the surface waters.

Warming sea surface temperatures between spring and summer may also be contributing to the increases in saturation states. Increased temperatures raise the partial pressure of carbon dioxide, promoting outgassing events that decrease the concentration

of carbon dioxide in the surface layer, in turn increasing saturation states. These effects are particularly dominant in the southern Outer and Middle Domains [*Bates, et al.,* 2010], which may contribute to the particularly high increases in surface layer saturation states in these regions.

These effects may be mitigated in some regions by the influence of ice melt [e.g. *Bates et al.*, 2009; *Yamamoto-Kawai et al.*, 2009]. Both DIC and TA are rejected with brine during the formation of sea ice [*Glud et al.*, 2002; *Papadimitriou et al.*, 2003; *Delille et al.*, 2007; *Rysgaard et al.*, 2007] and contribute substantially to the high latitude carbon pump [*Kelley*, 1968; *Gibson and Trull*, 1999; *Anderson et al.*, 2004; *Semiletov et al.*, 2004; *Omar et al.*, 2005; *Rysgaard et al.*, 2007]. As the ice ages throughout the winter, in-ice productivity [*Gleitz et al.*, 1995; *Glud et al.*, 2002] and brine rejection can substantially alter the carbonate parameters in sea ice [*Gleitz et al.*, 1995]. Together, nutrient exhaustion and brine rejection precondition melt waters to have particularly low DIC and TA concentrations (Table A-2), which leads to suppression and undersaturation of Ω_A and Ω_C in the ice (Figure A-7). During the melt period, the mixing of melt waters with low Ω_A and Ω_C with the surface layer likely created a divergent trajectory for Ω in the surface waters as NCP increased Ω_A and Ω_C. The increases in Ω_A observed in the surface layer in 2008 (Figure A-8) were likely moderated by melt water. Unlike the Arctic, there is no perennial sea ice in the Bering Sea so there will not be an expansion of the influence of the low Ω_A and Ω_C melt water in response to decreases in seasonal sea ice cover. However, as surface waters continue to absorb CO_2 from the atmosphere the seasonal levels of Ω_A and Ω_C prior to water column productivity will continue to decrease. Because this is a macro- and micro- nutrient-limited system, the removal of DIC through NCP each year will not compensate for the anthropogenically induced increases in seawater pCO_2. Therefore, as OA continues to decrease Ω_A and Ω_C, the onset of ice melt each year could cause Ω_A to become undersaturated. This effect may be particularly apparent over the inner and outer shelf where NCP is reduced, much like the undersaturations observed in the oligotrophic Canada Basin in the Arctic Ocean [*Yamamoto-Kawai et al*., 2009].

A.5.2 Carbonate System of the Subsurface Waters

In response to high export production, the remineralization of organic matter increases the concentration of DIC and pCO_2 in bottom waters and suppresses carbonate mineral saturation states to a varying degree across the shelf. Over the northern part of the shelf and through the Central Front, where bottom temperatures are lowest and export production is highest, we observed the strongest seasonal suppression of aragonite (~ -0.35; Figures A-8A and B) in subsurface water. This suppression of Ω_A corresponded to high Apparent Oxygen Utilization (AOU) values and elevated silicate in the bottom waters indicating both pelagic and benthic remineralization. The subsurface effects of remineralization can be especially significant during periods of intense production when Ω increases at the surface. These biologically driven, seasonally divergent trajectories of Ω, or the Phytoplankton-Carbonate Saturation State (PhyCaSS) interaction, have been observed in the Chukchi Sea [*Bates et al.*, 2009; *Bates and Mathis*, 2009], and are likely typical of highly productive polar and subpolar shelves.

The PhyCaSS interaction could be particularly influential on benthic calcifiers (i.e. crabs) in the Bering Sea because the lowest Ω coincide with areas of highest export production and the bottom water cold pool. It appears that the export production, which provides the food source at the bottom, is causing the undersaturation that could inhibit shell and test growth in calcifying organisms. However, because the Bering Sea has been highly productive since well before industrial times, we must quantify whether the observed undersaturations are a natural phenomenon or due to the absorption of anthropogenic CO_2 emissions.

Ideally, the amount of anthropogenic CO_2 in a given system can be estimated by directly calculating the age of the water mass, but a paucity of data in this region prevents this approach. However, based on the origin of the water on the Bering Sea shelf and the observed density constraints, we can approximate anthropogenic CO_2 inventories to evaluate the pre-industrial state of the carbon cycle in the Bering Sea. Sabine *et al.* [2004] estimated that ~35 μmoles kg^{-1} anthropogenic CO_2 has penetrated into waters of the

North Pacific Ocean to the 26 kg m^{-3} isopycnal surface. Because the source waters for the Bering Sea shelf are derived from the North Pacific Ocean and the density of waters we sampled ranged from 23.6 kg m^{-3} to 27.71 kg m^{-3}, and averaged ~25.5 kg m^{-3} for both spring and summer, we assume that the concentrations of anthropogenic CO_2 in this region is ~35 μmoles kg^{-1}

To determine the impact of OA due to the uptake of anthropogenic CO_2, we subtracted 35 μmoles kg^{-1} from our DIC observations while keeping the remaining parameters constant (TA, salinity, etc.) and recalculated the seawater Ω_A and Ω_C using the thermodynamic model of Lewis and Wallace [1995]. In this scenario, the entire water column over the shelf was supersaturated with respect to aragonite in both spring and summer. The only aragonite undersaturations present were below 100 m at the shelf break of the NP line. While there are a number of weaknesses associated with this first order approximation, the calculation suggests that OA has resulted in persistent aragonite undersaturation in northern domain bottom waters and within the Coastal Domain and a suppression of Ω_C across the shelf. As atmospheric CO_2 concentrations increase, it is likely that these undersaturations will spread across the bottom waters of the shelf for at least part of the year.

The timing of sea ice retreat may also have a substantial effect on Ω in subsurface waters. Ice retreat exerts a significant control on the fate of the organic matter produced during the phytoplankton blooms [*Hunt et al*., 2002]. Zooplankton grazing of seasonal production is minimal during blooms associated with colder surface water temperatures favoring the benthic ecosystem [*Coyle and Pinchuk*, 2002]. In contrast, warmer years increase zooplankton production by up to 50% [*Coyle and Pinchuk*, 2002]. Thus, colder waters are expected to be associated with higher export production to the benthos, and large remineralization signals will be generated at depth, corresponding to increases in pCO_2 and decreases in Ω. Warmer water blooms will retain carbon in the mixed layer and contribute to increased pelagic production and reduced bottom water remineralization.

Variation in the timing of sea ice retreat could change the mode of production over the shelf. The earlier retreat of sea ice in recent years [*Overland and Stabeno*, 2004;

Grebmeier et al., 2006; *Moore and Laidre*, 2006] indicates that the blooms have been occurring in colder water, favoring export production. The biological effects of this retreat have been documented in the benthos of the southern shelf, although the effect may be impacting the northern shelf as well [*Grebmeier et al.,* 2006]. If ice continues to retreat earlier in the spring it could lead to a dichotomy for benthic scavengers such as crabs. On the one hand, higher rates of export production should lead to increased food supply and an expansion of biomass. However, if high rates of export production coupled to increasing anthropogenic CO_2 inventories over the shelf cause expanded aragonite undersaturations, a reduction in habitat could result.

A.5.3 The Carbonate System of the Near Shore Waters of the Bering Sea Shelf

The near shore waters of the Bering Sea shelf are seasonally dominated by terrestrial runoff from both the Yukon and the Kuskokwim Rivers (Figure A-1), and it is likely that the complete aragonite undersaturation of the inner stations along the MN and SL lines is the result of freshwater influence. Chemical processes occurring in both rivers precondition runoff waters to have low pH and Ω. Furthermore, the influence of productivity indicated by the divergent trajectories of Ω and AOU in the waters of the middle and outer shelf are absent in the inshore region (Table A-3; Figure A-8) leading us to conclude that biology is not the dominant control on Ω in the near shore environment.

In 2008, pH values in the Coastal Domain closely matched the pH values of river discharge (Figure A-4A and B) during both spring and summer, indicating that even minimum rates of discharge (Dec-Apr) [*Brabets et al*., 2000] have a significant impact on the pH in the Coastal Domain. Seasonal variability in the rates of discharge exert some control over the carbonate parameters within the river (Table A-1) [*Striegl et al.*, 2005]. During spring, seasonal peaks in glacial melt and precipitation significantly dilute TA and DIC values. This dilution of DIC is minimally balanced through summer and autumn through the remineralization of peak dissolved organic carbon (DOC) concentrations resulting from increased soil drainage [*Streigl et al.,* 2005, 2007]. Increased soil drainage

in summer does not increase TA significantly as the drainage basin for both rivers is relatively carbonate-poor [*Brabets et al.*, 2000; *Dai and Trenberth*, 2002; *Cai et al.*, 2008; *Cooper et al.*, 2008], with the exception of the White River, which is carbonate-rich but only accounts for ~10% of the total Yukon River discharge [*Brabets et al.,* 2000; *Eberl*, 2004]. DIC concentrations reach a maximum during winter, when ice cover over the river reduces air-sea exchange causing high concentrations of pCO_2 and low pH (Table A-1).

Although there is a paucity of carbonate data in the Kuskokwim River, basin lithology links the Yukon and the Kuskokwim drainage areas [*Gallant et al.*, 1995] and processes occurring during downstream transport should be similar. However, the shorter length of the Kuskokwim limits the amount of preconditioning that waters can undergo. For example, summer pH, TA and organic carbon are higher in the Kuskokwim River (Table A-2), suggesting less remineralization occurs during downstream flow. In the Yukon, nearly all organic carbon that reaches the coastal margin is non-labile, as is typical in other high latitude shelves [*Fahl and Stein*, 1997; *Neumann*, 1999; *Boucsein and Stein*, 2000; *Fernandes and Sicre*, 2000; *Krishnamurthy et al.*, 2001; *Dittmar and Kattner*, 2003]. However, because of the shorter length of the Kuskokwim River, some labile organic carbon may reach the coastal margin, where it is likely remineralized in near shore estuaries rather than during downstream transport. While the mouth of the Kuskokwim River may exhibit higher pH and lower DIC values, we expect that coastal modification processes, such as primary productivity and remineralization, will balance these differences, and the net effect of Kuskokwim waters discharged to the inner shelf should be comparable to that of the Yukon River.

Overall, these processes precondition the freshwater discharge of the Yukon and Kuskokwim Rivers to have particularly low Ω for two different reasons: (1) When river discharge rates are relatively low, DIC concentrations are highest and the shelf is covered with sea ice, [*Makkaveev*, 1994] and outgassing of high pCO_2 water is prevented at the air-sea interface, maintaining supersaturation with respect to carbon dioxide. (2) When

river discharge rates are highest, the low alkalinity of river waters effectively causes the greatest dilution of shelf alkalinity [*Salisbury et al.*, 2008].

Complete undersaturation of MN 1 and 2 (Figure A-6C) occurs in spring, and may indicate the influence of peak concentrations of high pCO_2 water in Kuskokwim River outflow beneath the sea ice over the shelf. Primary productivity occurring in the Coastal Domain draws down DIC values in summer, mitigating the springtime undersaturation caused by river discharge. In contrast, undersaturation at SL 1 (Figure A-6B) occurs during summer, indicating that primary productivity cannot balance the carbonate mineral suppression caused by the dilution of alkalinity through river discharge (Table A-3). Therefore, we can assume that peak river discharge exerts the greatest influence over shelf carbonate parameters in summer, and that the dilution of alkalinity is the primary driver of riverine carbonate mineral suppression on the inner Bering Sea shelf. Based on these observations, it is likely that the coastal waters from Kuskokwim Bay to Bering Strait, including Norton Sound, are undersaturated in aragonite at least part of the year due to the direct influence of river discharge.

A.5.4 Preconditioning Surface Waters of the Western Arctic Ocean

Model predictions indicate that the Arctic Ocean will experience the impacts of OA before other areas due to colder water temperatures, the loss of sea ice, and high volumes of terrestrial runoff [*Orr et al.*, 2005; *Salisbury et al.*, 2008]. Our observations in the Bering Sea show that biogeochemical preconditioning of Pacific Ocean inflow that occurs during transport to the Arctic could also contribute significantly to OA. The seasonal drawdown of DIC in the mixed layer, coupled with terrestrial runoff and remineralization processes, has a major impact on the carbonate chemistry of the Bering Sea shelf and may strongly influence the Arctic Ocean. Bering Sea shelf waters flow through Bering Strait, where they are then transported northward over the shallow Chukchi Sea shelf [*Coachman and Barnes*, 1961; *Overland and Roach*, 1987; *Roach et al.*, 1995; *Woodgate and Aagaard*, 2005; *Woodgate et al.*, 2005a, 2005b] where the

PhyCaSS interaction further suppresses bottom water Ω by as much as 0.34 on a seasonal basis [*Bates and Mathis*, 2009; *Bates et al.*, 2009].

Pacific Ocean waters and freshwater inputs biogeochemically modified over these shelves make up the majority of the upper water masses in the western Arctic Ocean [*Macdonald et al.*, 2002; *Kadko and Swart*, 2004; *Cooper et al.*, 2008]. Furthermore, the suppression of Ω is expected to continue to increase, especially due to the increasing phytoplankton primary production observed in the western Arctic Ocean resulting from reduced sea ice cover and a lengthened production season [*Arrigo et al.*, 2008]. Additionally, carbonate-poor river discharge typical of the Arctic Ocean is also increasing [*McClelland et al*., 2006; *White et al*., 2007], further diluting TA. These mounting drivers of OA may have negative consequences for benthic calcifying biota in the region [*Buddemeier et al*., 2008; *Fabry et al*., 2008; *Kuffner et al.*, 2008; *Fabry et al.*, 2009; *Bates and Mathis*, 2009; *Bates et al.*, 2009; *Doney et al.*, 2009]. Aragonite undersaturation has already been observed in the Canada Basin halocline [e.g., *Jutterström and Anderson*, 2005; *Bates et al.*, 2009]. However, as mentioned in Section A.5.1, these effects may be mitigated by reduced sea ice cover and warmer sea surface temperatures. Near the Aleutian Islands, surface temperatures have been high enough to induce outgassing of carbon dioxide, which raises saturation states in these isolated areas [*Bates et al*., 2010]. Further, evidence of northward penetration of warmer sea surface temperatures within the Bering Sea has already been documented [*Overland and Stabeno,* 2004; *Grebmeier et al.*, 2006]. As sea surface temperatures in the Arctic and subarctic continue to warm, it is possible that temperature effects on carbon dioxide and calcium carbonate saturation states may be significant further and further northward. Due these and similar complex feedbacks in the region, estimation of future changes in saturation states is at best uncertain.

A.6 Conclusions

Our observations have shown that freshwater inputs from the Kuskokwim and Yukon Rivers seasonally suppress Ω in the coastal waters of the eastern Bering Sea while

remineralization of organic matter in bottom waters across the shelf reduces Ω_A and Ω_C by ~0.20 and pH by ~0.25 causing areas of aragonite undersaturation. In spring, when the water column under the ice was vertically stratified aragonite undersaturations reached all the way to the surface in an area where NCP is the highest. In summer, primary production in surface waters significantly raises Ω_A, Ω_C and pH, particularly in the highly productive "Green Belt." Our analysis shows that both persistent and seasonal undersaturations are likely a result of the uptake of anthropogenic CO_2 in the region. Under business-as-usual projections for CO_2 emissions [*IPCC*, 2007], it has been estimated that the surface ocean will absorb an additional 50-100 μmoles kg^{-1} of anthropogenic CO_2 over the next 100 years resulting in further suppression of carbonate mineral saturation states. As this happens, seasonal processes like the suppression of Ω from sea ice melt could have a more substantial impact on the surface waters of the Bering Sea.

Current and future reductions in pH and Ω could have significant effects on the Bering Sea and its associated economy and subsistence inhabitants. In addition to impacting the ability of calcifying organisms to maintain and form shells and tests, reductions in pH could elicit physiological responses from non-calcifying organisms through less obvious pathways. Of great concern is that climate forcing and the uptake of anthropogenic CO_2 could result in an ecosystem wide shift in speciation which could be less economically viable for current fisheries. Although several current estimates of the effects of ocean acidification on economic systems have been published [*Cesar et al.*, 2002; *Burke et al.*, 2004; *Stern*, 2006; *Cooley and Doney*, 2009], predictions of the future effects of changing climate and biogeochemistry on the Bering Sea shelf ecosystem and economy remain unclear. However, we should not wait until a major shift occurs to prioritize this region for expanded study.

A.7 Tables

Table A-1 Seasonal variation of Yukon River carbon parameters. DIC, DOC, and pCO_2 data are taken from Striegl *et al.*, 2007. pH and TA estimates are taken from the PARTNERS provisional online data set (Accessed June 2009; available at: http://ecosystems.mbl.edu/partners/data.html). DIC and pCO_2 concentrations peak in winter due to ice cover and continuous remineralization, creating a pH minimum.

Reference			Spring	Summer-Autumn	Winter
Striegl *et al*., 2007	**DOC**	µmoles kg^{-1}	900 ± 7.0	430 ± 10	220 ± 2.7
	DIC	µmoles kg^{-1}	1480 ± 4.2	1890 ± 3.0	4100 ± 1.9
	pCO_2	µatm	1530 ± 9.5	1650 ± 24.0	8280 ± 3.6
PARTNERS	**pH**		7.8	7.9	7.0
	TA	µmoles kg^{-1}	619.4	898.6	1300.8

Table A-2 Carbon parameters for the Yukon and Kuskokwim Rivers and sea ice. DOC and pH in the Kuskokwim River are higher than in the Yukon while DIC concentrations are lower, indicating a shorter time for remineralization to occur. Due to near shore estuarine modification, the net effect of the discharge of both rivers should be similar despite these differences. Comparatively, the freshwater input from ice melt to the shelf has a much lower DIC and TA.

		Yukon	Kuskokwim	Sea Ice
		Striegl et al*., 2007*	*Wang, 1999*	*This Study*
DOC	µmoles kg^{-1}	900 ± 7.0	199.8	-
DIC	µmoles kg^{-1}	1480 ± 4.2	-	384.8
pCO_2	µatm	1530 ± 9.5	-	-
pH		7.8	8.1	-
TA	µmoles kg^{-1}	619.4	639.4	424.6

Table A-3 NCP and seasonal changes in $CaCO_3$ saturation states (2008). A comparison of the rate of average net community production and the average changes in aragonite and calcite saturation states between spring and summer of 2008 in the upper 30 m of the water column. The greatest changes in saturation states occur in conjunction with high rates of net community production and warm sea surface temperatures. The lowest changes in saturation state are seen in the northern Coastal Domain, near the outlet of the carbonate-poor discharge of the Yukon River.

Domain		**NCP Rate**	**$\Delta\ \Omega_A$**	**$\Delta\ \Omega_C$**
		mmoles C m^{-2} d^{-1}	*Summer – Spring*	*Summer – Spring*
N	**C**	19	0.08	0.12
S	**C**	23	0.74	1.17
N	**M**	37	0.97	1.55
S	**M**	26	0.94	1.49
S	**O**	34	1.38	2.20

A.8 Figures

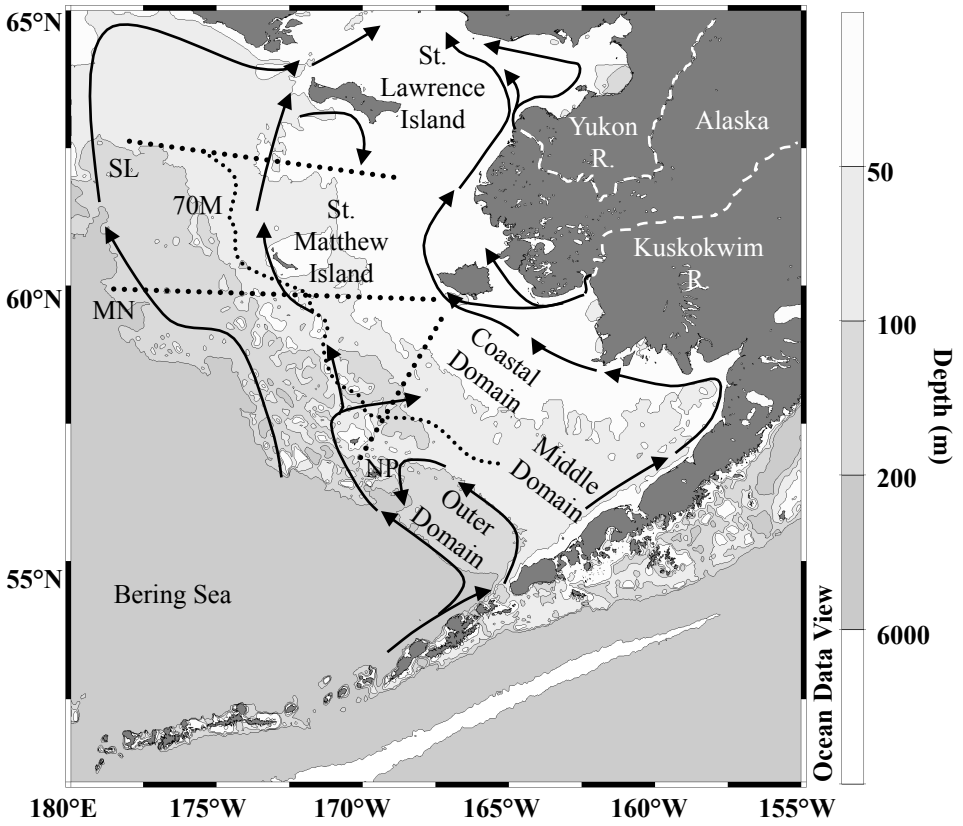

Figure A-1 Map of the eastern shelf of the Bering Sea. Shown with generalized circulation in solid arrows, the location of the Yukon and Kuskokwim Rivers in dashed lines, and the four transect lines (SL, MN, NP, 70M) occupied in spring and summer of 2008 in dotted lines. The Coastal, Middle, and Outer Domains are labeled.

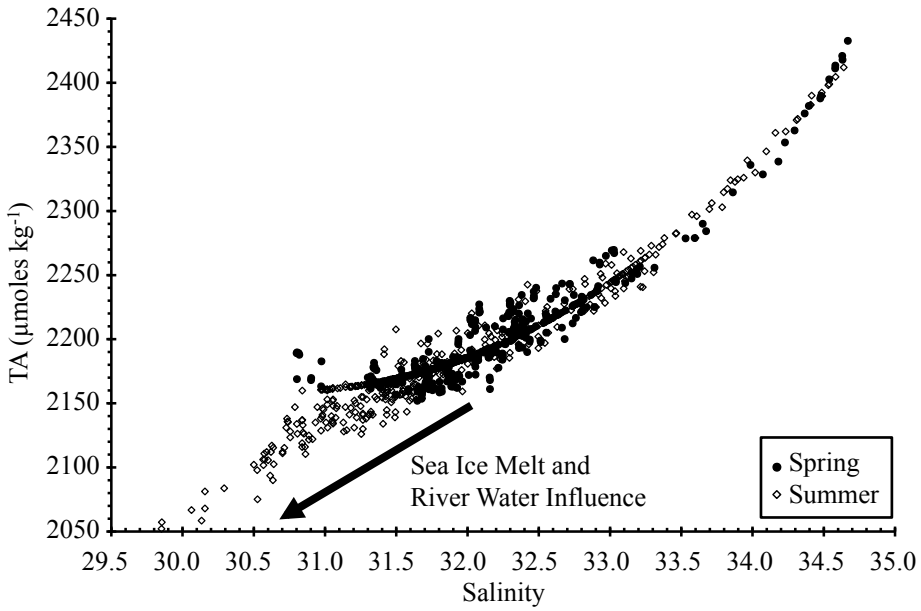

Figure A-2 Relationship of TA and salinity (Spring, Summer 2008). Distribution of TA (µmoles kg^{-1}) plotted against salinity for spring and summer of 2008. The black arrow shows the impact that ice melt and freshwater inputs have on TA, particularly in the upper water column.

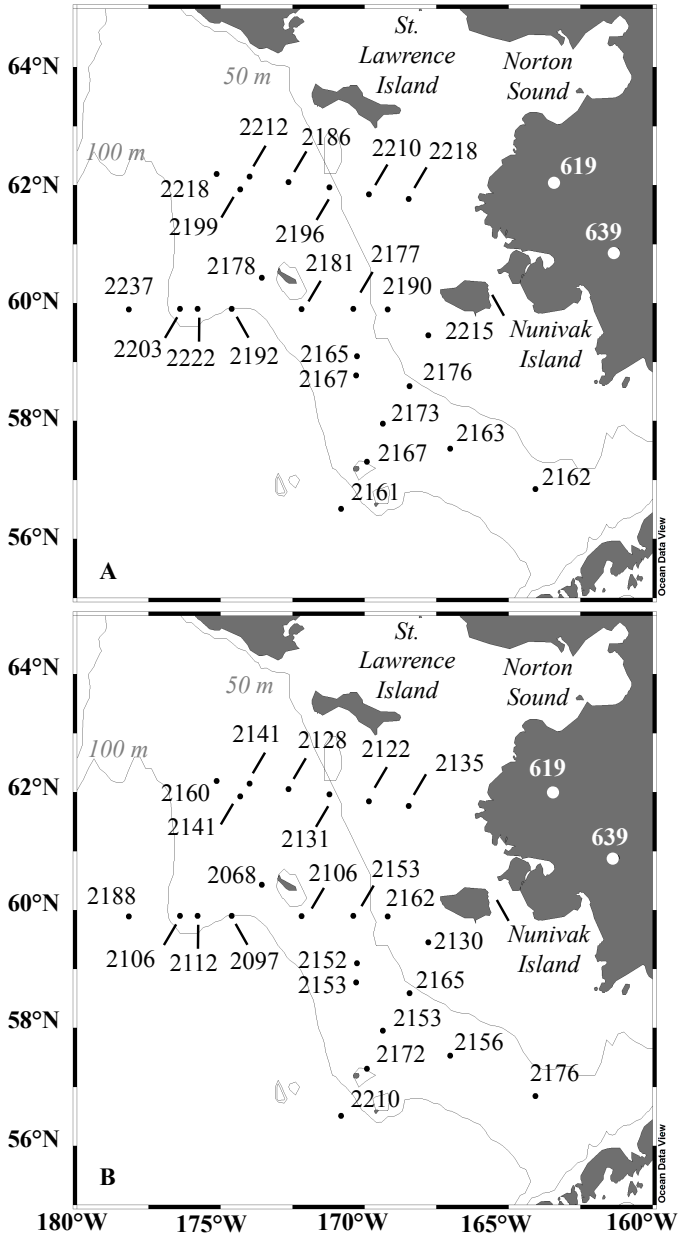

Figure A-3 Spatial variation of surface TA (Spring, Summer 2008). Surface (upper 20 m) distribution of TA (μmoles kg^{-1}) across the shelf and in the Yukon (PARTNERS provisional online data set; Accessed June 2009; available at: http://ecosystems.mbl.edu/partners/data.html) and Kuskokwim [*Wang*, 1999] Rivers (see Tables A-1 and A-2) for (A) Spring and (B) Summer of 2008.

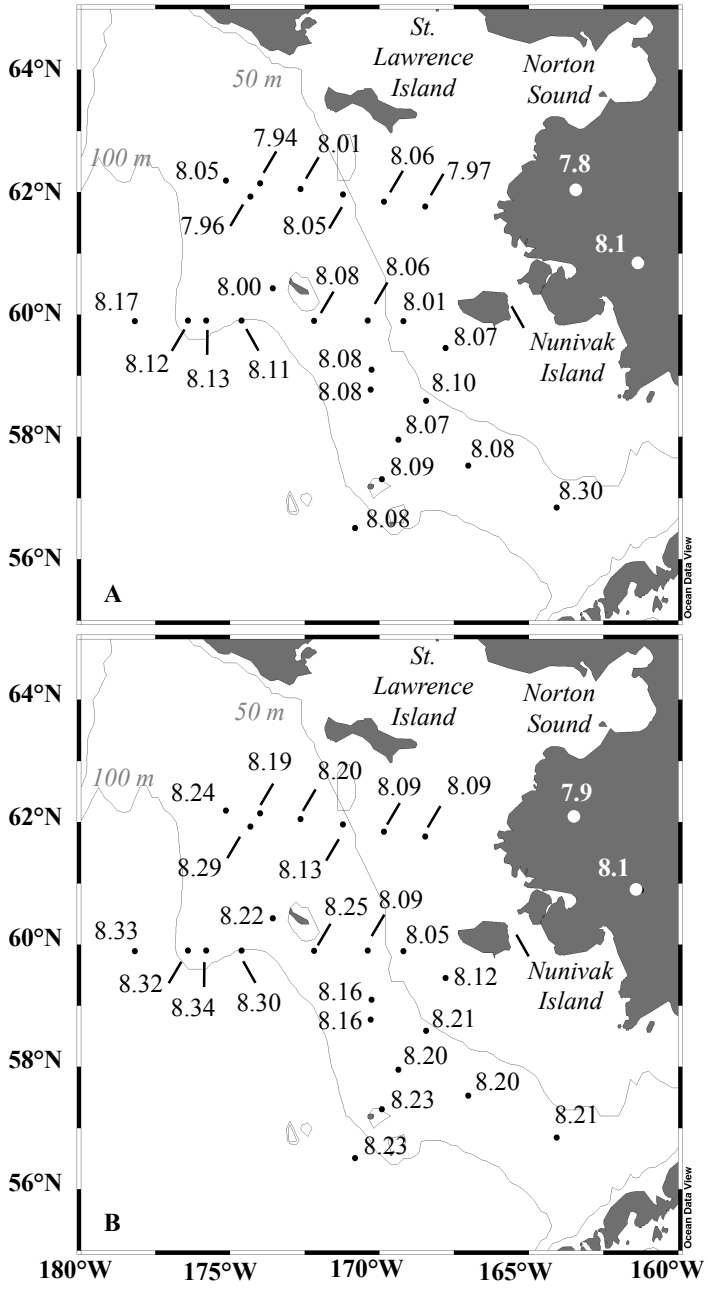

Figure A-4 Spatial variation of surface pH (Spring, Summer 2008). Surface (upper 20 m) distribution of pH across the shelf and in the Yukon (PARTNERS provisional online data set; Accessed June 2009; available at: http://ecosystems.mbl.edu/partners/data.html). and Kuskokwim [*Wang*, 1999] rivers (see Tables A-1 and A-2) for (A) Spring and (B) Summer of 2008.

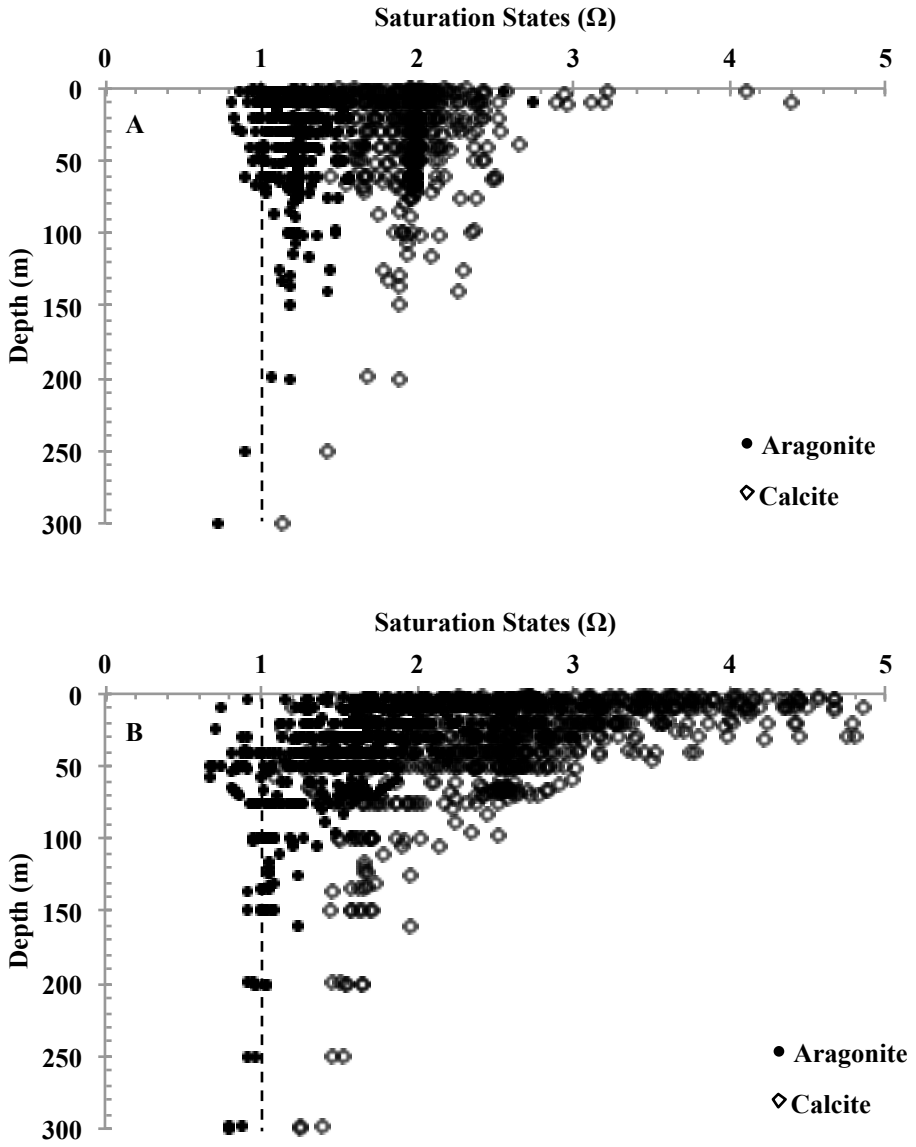

Figure A-5 Depth variation of $CaCO_3$ saturation states (Spring, Summer 2008).
Calcite and aragonite saturation states (Ω_C and Ω_A) plotted against depth (m) in the upper 300 m over the shelf of the Bering Sea in (A) Spring and (B) Summer of 2008.

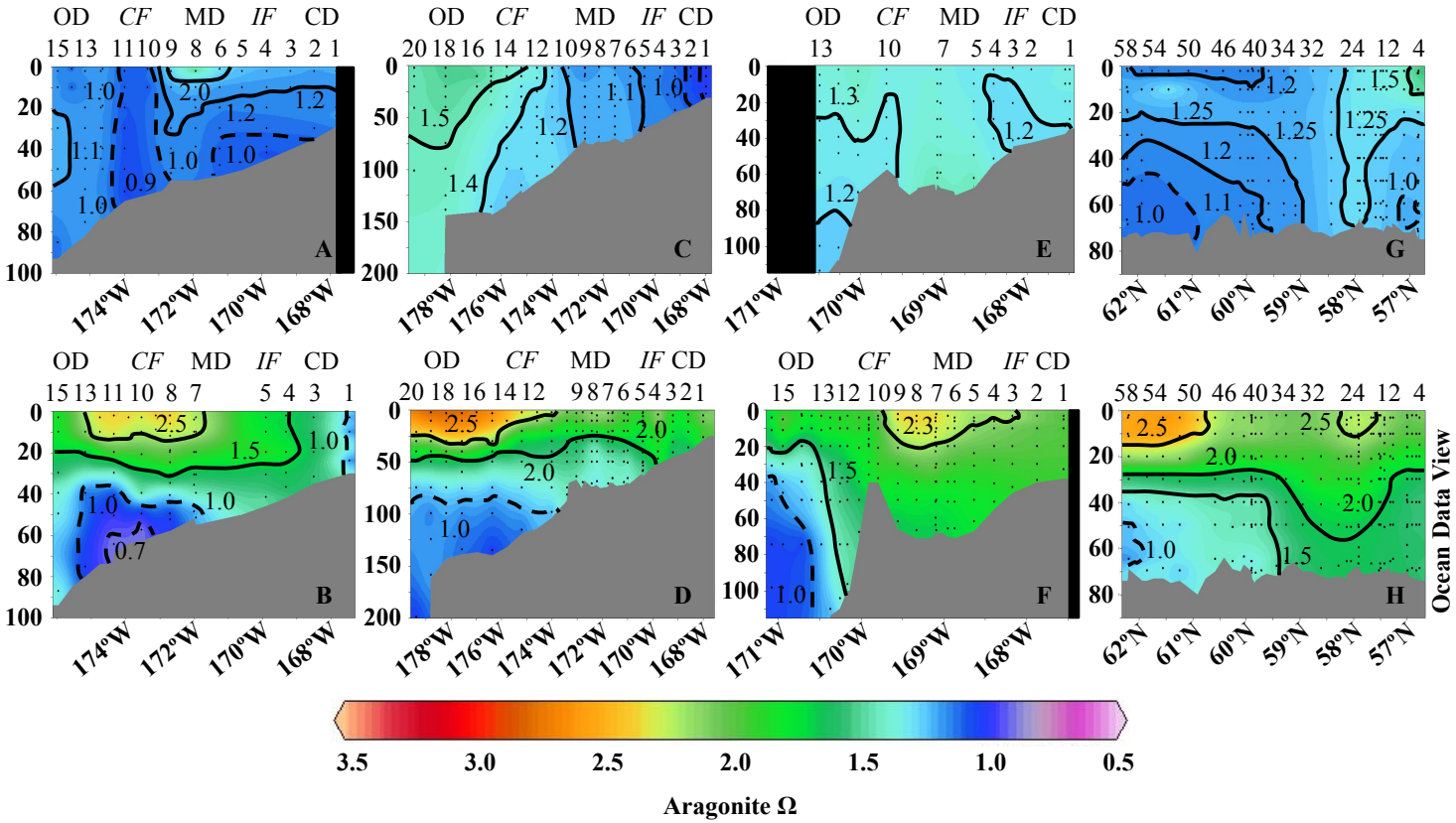

Figure A-6 Seasonal variation of aragonite saturation states (2008). Contoured section plots (depth in m) of aragonite saturation states (Ω_A) along the SL transect line (A, B), MN transect line (C, D), NP transect line (E, F) and 70M transect line (G, H) in spring (A, C, E, G) and summer (B, D, F, H) of 2008. The dashed contour lines represent locations where the observed saturation states were below 1.0. The major domains, fronts, and station numbers are identified at the top.

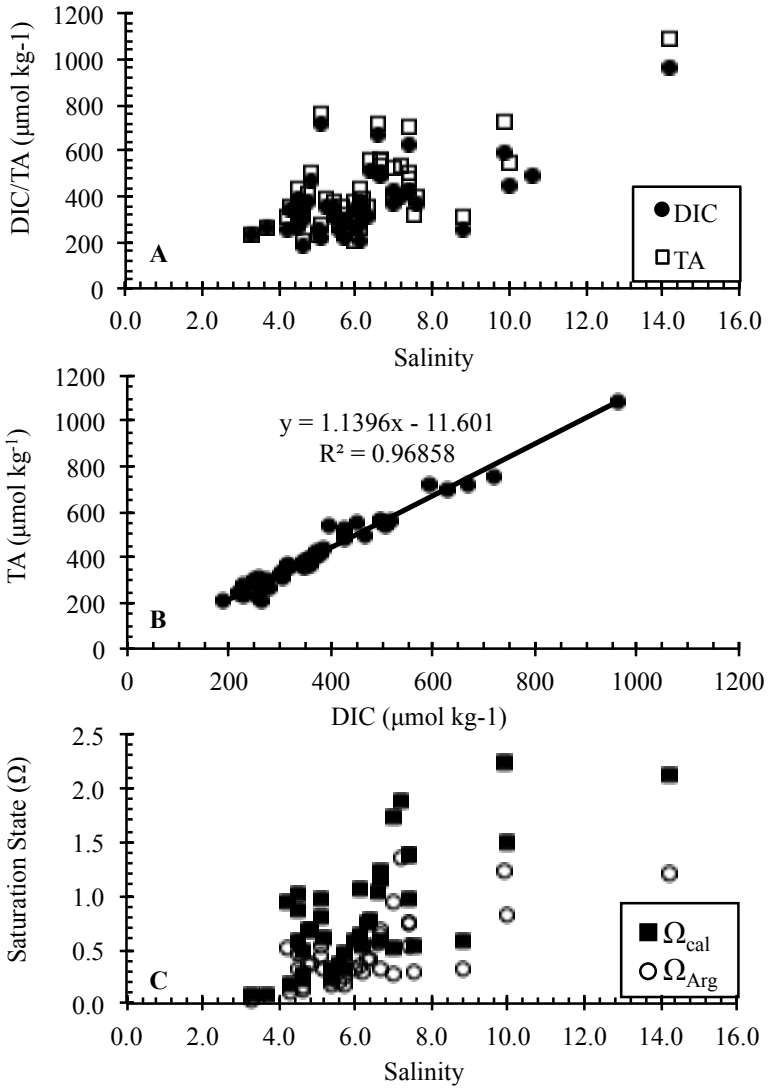

Figure A-7 Carbonate parameters of seven Bering Sea ice cores (Spring, 2008). Geographically and vertically integrated carbonate parameters of seven ice cores collected across the Bering Sea shelf in spring 2008 showing (A) concentrations of DIC and TA (µmoles kg^{-1}) plotted against salinity. Both parameters consistently decrease with increasing salinity. (B) concentrations of DIC (µmoles kg^{-1}) plotted against TA (µmoles kg^{-1}), showing a strong correlation between these two parameters ($R^2 = 0.97$). (C) Saturation states for calcite (Ω_C) and aragonite (Ω_A) plotted against salinity. The dotted line indicates the saturation horizon ($\Omega = 1$).

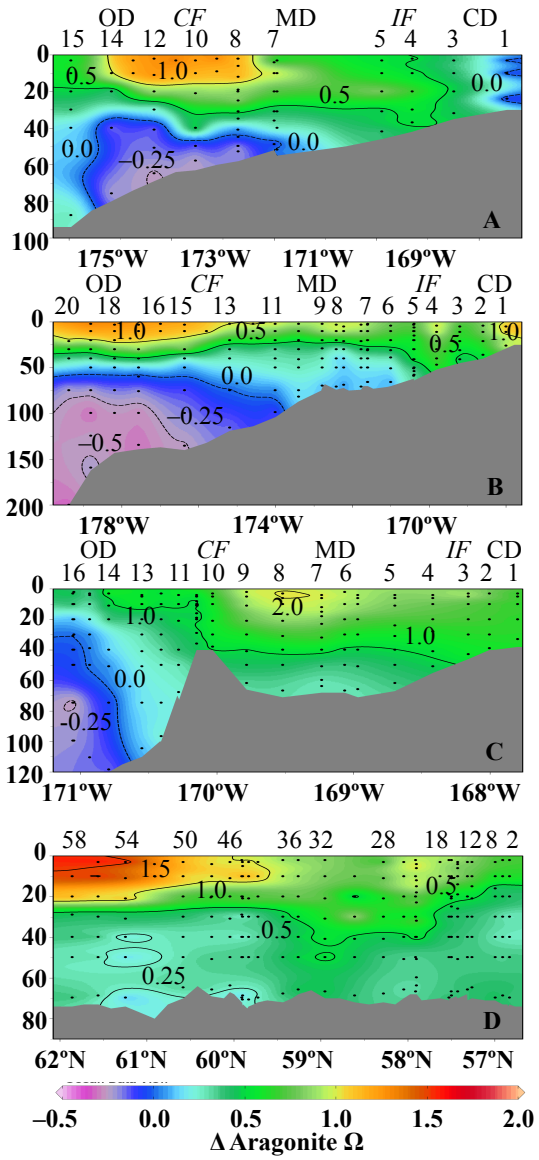

Figure A-8 Seasonal change in aragonite saturation states (2008). Contoured sectional plots (depth in m) of the difference in aragonite saturation states (Ω_A) between spring and summer. (A) SL transect line. (B) MN transect line. (C) NP transect line. (D) 70M transect line. The dashed contour lines represent locations where the observed saturation states were negative, indicating a suppression of Ω. The major domains, fronts, and station numbers are identified at the top of each panel.

A.9 Acknowledgements

The authors thank the officers and crew of the *USCGC Healy* for their tireless efforts in supporting our work. Without their commitment, none of the science would be possible. We also thank the hydrographic team from NOAA-PMEL for providing data and helping in sample collection. Finally, we thank our colleagues in the BEST-BSIERP Project, supported by NSF and NPRB. The work presented in this paper was supported by the U.S. Minerals Management Service, Alaska OCS Region and the Coastal Marine Institute at the University of Alaska Fairbanks under Agreement M08AC12645. Statement of Work: Mathis, J.T. collected samples in 2008, performed the analysis, and prepared the manuscript for publication. Cross, J.N., assisted in analysis procedures and prepared manuscript for publication. Bates, N.R., provided guidance through manuscript preparation.

A.10 References

Aguilar-Islas, A. M., M. P. Hurst, K. N. Buck, B. Sohst, G. J. Smith, M. C. Lohan, et al. (2007), Micro- and macronutrients in the southeastern Bering Sea: Insight into iron-replete and iron-depleted regimes, Prog. Oceanogr., 73, 99–126, doi: 10.1016/j.pocean.2006.12.002.

Aguilar-Islas, A. M., R. D. Rember, C. W. Mordy, and J. Wu (2008), Sea ice-derived dissolved iron and its potential influence on the algal bloom in the Bering Sea, Geophys. Res. Lett., 35, L24601, doi: 10.1029/2008GL035736.

Alonso-Sáez, L., O. Sanches, J. M. Gasol, V. Balague, and C. Pedros-Alio (2008), Winter-to-summer changes in the composition and single-cell activity of near-surface Arctic prokaryotes. Env. Microbiol., 10(9), 2444–2454, doi: 10.1111/j.1462-2920.2008.01674.x.

Amos, A. F., and L. K. Coachman (1992). Water mass modification from the Bering into the Chukchi Sea, in *Results of the Third Joint U.S.-U.S.S.R. Bering & Chukchi Seas Expedition (BERPAC), Summer 1988*, edited by P.A. Nagel, pp. 27–35, U.S. Fish and Wildlife Service, Washington, D.C.

Anderson, L. G., E. Falck, E. P. Jones, S. Jutterström, and J. H. Swift (2004), Enhanced uptake of atmospheric CO_2 during freezing of seawater: a field study in Storfjorden, Svalbard, J. Geophys. Res., 109, C06004, doi: 10.1029/2003JC002120.

Andersson, A. J., and F. T. Mackenzie (2004), Shallow-water oceans: a source or sink for atmospheric CO_2?, Front. Ecol. Env., 2(7), 348–353, doi: 10.2307/3868359.

Andersson, A. J., N. R. Bates, and F. T. Mackenzie (2007), Dissolution of carbonate sediments under rising pCO_2 and Ocean Acidification: Observations from Devil's Hole, Bermuda, Aqu. Geochem., 13, 237–264, doi: 10.1007/s10498-007-9018-8.

Arrigo, K. R., G. van Dijken, and S. Pabis (2008). Impact of a shrinking Arctic ice cover on marine primary production, Geophys. Res. Lett., 35, doi: L19603, 10.1029/2008GL035028.

Askren, D. R. (1972), Holocene Stratigraphic Framework—Southern Bering Sea Continental Shelf, M.S. thesis, University of Washington, Seattle, Washington.

Bates, N. R. (2001), Interannual variability of oceanic CO_2 and biogeochemical properties in the Western North Atlantic subtropical gyre, Deep Sea Res. II., 48, 1507–1528, doi: 10.1016/S0967-0645(00)00151-X.

Bates, N. R. (2007), Interannual variability of the oceanic CO_2 sink in the subtropical gyre of the North Atlantic Ocean over the last two decades, J. Geophys. Res., 112(C9), C09013, doi: 10.1029/2006JC003759.

Bates, N. R., and J. T. Mathis (2009), The Arctic Ocean marine carbon cycle: evaluation of air-sea CO_2 exchanges, ocean acidification impacts and potential feedbacks, Biogeosci., 6, 2433–2459, doi: 10.5194/bg-6-2433-2009.

Bates, N. R., J. T. Mathis, and L. W. Cooper (2009), Ocean acidification and biologically induced seasonality of carbonate mineral saturation states in the Arctic Ocean, J. Geophys. Res., 114, C11007, doi: 10.1029/2008JC004862.

Bates, N. R., J. T. Mathis, and M. A. Jeffries, (2010), Air-sea CO_2 fluxes on the Bering Sea shelf, Biogeosci. Disc., 7, 7271−7314, doi: 10.5194/bg-8-1237-2011.

Belkin, I. M., and P. C. Cornillon (2005), Bering Sea thermal fronts from Pathfinder data: seasonal and interannual variability. Pacif. Oceanogr., 3(1), 6–20. [doi not avail.]

Boucsein, B., and R. Stein, (2000), Particulate organic matter in surface sediments of the Laptev Sea (Arctic Ocean): application of maceral analysis as organic-carbon-source indicator, Mar. Geol., 162, 573–586, doi: 10.1016/S0025-3227(99)00066-3.

Boveng, P. L., J. L. Bengtson, T. W. Buckley, M. F. Cameron, S. P. Dahle, B. A. Megrey, *et al*. (2008), Status review of the Ribbon Seal (*Histriophoca fasciata*). *NOAA Tech. Mem. NMFS-AFSC-191*. U.S. Dept. of Comm., Seattle, WA.

Brabets, T. P., B. Wang, and R. H. Meade (2000). Environmental and hydrologic overview of the Yukon River Basin, Alaska and Canada. *Water-Re. Inv. Rep. 99-4204*. USGS, Anchorage, AK.

Buddemeier, R. W., J. A. Kleypas, and R. B. Aronson (2004), *Coral Reefs and Global Climate Change: Potential Contributions of Climate Change to Stresses on Coral Reef Ecosystems*, Pew Center on Climate Change, Arlington, VA.

Burke, L., and J. Maidens (Eds.) (2004), *Reefs at risk in the Caribbean*, World Resources Institute, Washington, D.C.

Byrne, R. H., S. Mecking, R. A. Feely, and Z. Liu (2010), Direct observations of basin-wide acidification of the North Pacific Ocean, Geophys. Res. Lett., 37, L02601, doi: 10.1029/2009GL040999.

Cai, W. J., X. Guo, C.-T. A. Chen, M. Dai, L. Zhang, W. Zhai, *et al*. (2008). A comparative overview of weather intensity and HCO_3^- flux in the world's major rivers with emphasis on the Changjiang, Huanghe, Zhujiang (Pearl) and Mississippi Rivers, Cont. Shelf Res. 28, 1538–1549, doi: 10.1016/j.csr.2007.10.014.

Caldeira, K. and M. E. Wickett, (2003), Anthropogenic carbon and ocean pH, Nature, 425(6956), 365, doi: 10.1038/425365a

Caldeira, K., and M. E. Wickett (2005), Ocean model predictions of chemistry changes from carbon dioxide emissions to the atmosphere and ocean, J. Geophys. Res. 110(C9), C09S04, doi: 10.1029/2004JC002671.

Cesar, H., P. van Beaukering, S. Plintz, and J. Dierking (2002), Economic valuation of the coral reefs of Hawaii, *Final Report,* NOAA, Cesar Env. Econ. Consul., Netherlands.

Chilton, E.A., K. Swiney, E. Munk, and R. J. Foy (2011), 2010 Ecosystem consideration indicators for Bering Sea and Aleutian Islands tanner and king crab species, *NMFS-AFSC-Ecosystem Crab SAFE-May 2011*, U.S. Dept. of Comm., NOAA, Nat. Mar. Fish. Svc., AK Fish. Sci. Ctr., Kodiak, AK.

Christensen, J. P. (2008), Sedimentary carbon oxidation and denitrification on the shelf break of the Alaskan Beaufort and Chukchi Seas, Op. Oceanogr. J., 2, 6–17, doi: 10.2174/1874252100802010006.

Coachman, L. K. (1982), Flow convergence over a broad, flat continental shelf, Cont. Shelf Res., 1, 1–14, doi: 10.1016/0278-4343(82)90029-2.

Coachman, L. K. (1986), Circulation, water masses, and fluxes on the southeastern Bering Sea shelf, Cont. Shelf Res. 5, 23–108, doi: 10.1016/0278-4343(86)90011-7.

Coachman, L. K. (1993), On the flow field in the Chirikov basin, Cont. Shelf Res. 13, 481–508, doi: 10.1016/0278-4343(93)90092-C.

Coachman, L. K., and C. A. Barnes (1961), The contribution of Bering Sea water to the Arctic Ocean, Arctic, 147–161, doi: jstor.org/stable/40506914.

Coachman, L. K., and V. V. Shigaev (1992), Northern Bering-Chukchi ecosystem: the physical basis, in *Results of the Third Joint U.S.-U.S.S.R. Bering & Chukchi Seas Expedition (BERPAC), Summer 1988*, edited by P. A. Nagel, pp. 17–27, U.S. Fish and Wildlife Service, Washington, D.C.

Cooley, S. R., and S. C. Doney (2009), Anticipating ocean acidification's economic consequences for commercial fisheries, Env. Res. Lett., 4, 024007, doi: 10.1088/1748-9326/4/2/024007.

Cooley, S. R., H. L. Kite-Powell, and S. C. Doney (2009), Ocean acidification's potential to alter global marine ecosystem services, Oceanogr., 22(4), 172–181, doi: 10.5670/oceang.2009.106.

Cooper, L. W., J. W. McClelland, R. M. Holmes, P. A. Raymond, J. J. Gibson, C. K. Guay, *et al*. (2008), Flow-weighted values of runoff tracers ($\delta^{18}O$, DOC, Ba, alkalinity) from the six largest Arctic rivers, Geophys. Res. Lett., 35, L18606, doi: 10.1029/2008GL035007.

Coyle, K. O., and A. I. Pinchuk (2002), Climate-related differences in zooplankton density and growth on the inner shelf of the southeastern Bering Sea, Prog. Oceanogr., 55(1-2), 177–194, doi: 10.1016/S0079-6611(02)00077-0.

Dai, A. G., and K. E. Trenberth (2002), Estimates of freshwater discharge from continents: latitudinal and seasonal variations, J. Hydrometerol., 3, 660–687, doi: 10.1175/1525-7541(2002)003<0660:EOFDFC>2.0.CO;2.

Danielson, S., and Z. Kowalik (2005), Tidal currents in the St. Lawrence Island region, J. Geophys. Res., 110, C10004, doi: 10.1029/2004JC002463.

Danielson, S., K. Aagaard, T. Weingartner, S. Martin, P. Winsor, G. Gawarkiewicz, *et al*. (2006), The St. Lawrence polynya and the Bering shelf circulation: New observations and a model comparison, J. Geophys. Res., 111, C09023, doi: 10.1029/2005JC003268.

Delille, B., B. Jourdain, V. Borges, J.-L. Tison, and D. Delille (2007), Biogas (CO_2, O_2, dimethylsulfide) dynamics in spring Antarctic fast ice, Limnol. Oceanogr., 52(4), 1367–1379, doi: 10.4319/lo/2007.52.4.1367.

Devol, A. H., and J. P. Christensen (1993), Benthic fluxes and nitrogen cycling in sediments of the continental margin of the eastern North Pacific, J. Mar. Res., 51, 345–372, doi: 10.1357/0022240933223765.

Dickson, A. G. (1990) Thermodynamics of the dissolution of boric acid in synthetic seawater from 273.15°K 318.15°K, Deep Sea Res. A., 37(5), 755−766, doi: 10.1016/0198-0149(90)90004-F.

Dickson, A. G., and F. J. Millero (1987), A comparison of the equilibrium constants for the dissociation of carbonic acid in seawater media, Deep Sea Res. I., 34(10), 1733–1743, doi: 10.1016/0198-0149(87)90021-5.

Dickson, A. G., and C. Goyet (Eds.) (1994), Handbook of methods for the analysis of various parameters of the carbon dioxide system in seawater, Ver. 2.0, *ORNL/CDIAC-74,* U.S. Dept. of En., Washington, D.C.

Dittmar, T., and G. Kattner (2003), The biogeochemistry of the river and shelf ecosystem of the Arctic Ocean; a review, Mar. Chem., 83, 103–120, doi: 10.1016/S0304-4203(03)00105-1.

Doney, S. C., V. J. Fabry, R. A. Feely, and J. A. Kleypas (2009), Ocean acidification: The other CO_2 problem, Ann Rev. Mar. Sci., 1, 169–192, doi: 0.1146/annurev.marine.010908.163834.

Dornblaser, M. M., and R. G. Striegl (2007), Nutrient (N, P) loads and yields at multiple scales and subbasin types in the Yukon River Basin, Alaska, J. Geophys. Res. 112, G04S57, doi: 10.1029/2006JG000366.

Eberl, D. D. (2004), Quantitative mineralogy of the Yukon River system: Changes with reach and season and determining sediment provenance, Am Minerol., 89, 1784–1794, doi: 0003-004X/04/1112–1784.

Fabry, V. J., B. A. Seibel, R. A. Feely, and J. C. Orr (2008), Impacts of ocean acidification on marine fauna and ecosystem processes, ICES J. Mar. Sci., 65, 414–432, doi: 10.1093/icesjms/fsn048.

Fabry, V. J., J. B. McClintock, J. T. Mathis, and J. M. Grebmeier (2009), Ocean acidification at high latitudes: the bellwether, Oceanogr., 22(4), 160–171, doi: 10.5670/oceanog.2009.105.

Fahl, K., and R. Stein (1997), Modern organic carbon deposition in the Laptev Sea and the adjacent continental slope: surface water productivity vs. terrigenous input, Org. Geochem., 26, 379–390, doi: 10.1016/S0146-6380(97)00007-7.

Feely, R. A., and J. D. Cline (1976), Distribution, composition and transport of suspended particulate matter in the Gulf of Alaska and southeastern Bering Shelf, in *Environmental Assessment of the Alaskan Continental Shelf, Vol. 12*. pp. 467–484. NOAA, Boulder, CO.

Feely, R. A., G. J. Massoth, and A. J. Paulson (1981), The distribution and elemental composition of suspended particulate matter in Norton Sound and the Northeastern Bering Sea Shelf: Implications for Mn and Zn recycling in coastal waters, in *The Eastern Bering Sea Shelf: Oceanography and Resources, Vol. 1*, edited by D. W. Hood and J. A. Calder, pp. 321–337, U.S. Dept. of Comm., NOAA, Washington, D.C.

Feely, R. A., C. L. Sabine, K. Lee, W. Berelson, J. Kleypas, V. J. Fabry, *et al*. (2004), Impact of anthropogenic CO_2 on the $CaCO_3$ system in the oceans, Science, 305(5682), 362–266, doi: 10.1126/science.1097329.

Feely, R. A., S. C. Doney, and S. R. Cooley (2009), Ocean acidification: Present conditions and future changes in a high-CO_2 world, Oceanogr. 22(4), 36–47, doi: 10.5670/oceang.2009.95.

Fernandes, M. B., and M.-A. Sicre (2000), The importance of terrestrial organic carbon inputs on Kara Sea shelves as revealed by *n*-alkanes, OC, and $\delta^{13}C$ values, Org. Geochem., 31, 363–374, doi: 10.1016/S0146-6380(00)00006-1.

Gallant, A. L., E. F. Binnian, J. M. Omernik, and M. B. Shasby (1995), Ecoregions of Alaska, *USGS Prof. Pa. 1567*, U.S. Govt. Pr. Off., Washington, D.C.

Garneau, M. E., W. F. Vincent, R. Terrado, and C. Lovejoy (2009), Importance of particle-associated bacterial heterotrophy in a coastal Arctic ecosystem, J. Mar. Syst., 75(1-2) 185–197, doi: 10.1016/j.jmarsys.2008.09.002.

Gibson, J. A. E., and T. W. Trull (1999), Annual cycle of fCO_2 under sea ice and in open water in Prydz Bay, East Antarctica, Mar. Chem., 66, 187–200, doi: 10.1016/S0304-4203(99)00040-7.

Gleitz, M., M. R. R. von der Loeff, D. N. Thomas, G. S. Dieckmann, and F. J. Millero (1995), Comparison of summer and winter inorganic carbon, oxygen, and nutrient concentrations in Antarctic sea ice brine, Mar. Chem., 51, 81–91, doi: 10.1016/0304-4203(95)00053-T.

Glud, R. N., S. Rysgaard, and M. Kuhl (2002), A laboratory study on O_2 dynamics and photosynthesis in ice algal communities: Quantification by microsensors, O_2 exchange rates, ^{14}C incubations and a PAM-fluorometer, Aqu. Microb. Ecol., 27, 117–133, doi: 10.3354/ame027301.

Grebmeier, J. M., and C. P. McRoy (1989), Pelagic-benthic coupling on the shelf of the northern Bering and Chukchi Seas III: Benthic food supply and carbon cycling, Mar. Ecol. Prog. Ser., 53, 79–91, doi: 10.3354/meps/048057.

Grebmeier, J. M., J. E. Overland, S. E. Moore, E. V. Farley, E. C. Carmack, L. W. Cooper, *et al*. (2006), A major ecosystem shift in the Northern Bering Sea, Science, 311(5766)**,** 1461–1464, doi: 10.1126/science.1121365.

Hansell, D. A., D. Kadko, and N. R. Bates (2004), Degradation of terrigenous dissolved organic carbon in the western Arctic Ocean, Science, 304(5672), 858–861, doi: 10.1126/science.1096175.

Hunt Jr., G. L., and P. J. Stabeno (2002), Climate change and the control of energy flow in the southeastern Bering Sea, Prog. Oceanogr., 55, 5–22, doi: 10.1016/S0079-6611(02)00067-8.

Hunt Jr., G. L., P. J. Stabeno, G. Walters, E. Sinclair, R. D. Brodeur, J. M. Napp, *et al*. (2002), Climate change and control of the southeastern Bering Sea pelagic ecosystem, Deep Sea Res. II., 49(26), 5821–5853, doi: 10.1016/S0967-0645(02)00321-1.

Intergovernmental Panel on Climate Change (IPCC) (2007), *Climate change 2007: The physical science basis, contribution of working group I to the fourth assessment report of the Intergovernmental Panel on Climate Change*, edited by S. Solomon *et al*., Cambridge University Press, Cambridge, U.K.

Kachel, N. B., G. L. Hunt Jr., S. A. Salo, J. D. Schumacher, P. J. Stabeno, and T. E. Whitledge (2002), Characteristics of the Inner Front of the Southeastern Bering Sea, Deep Sea Res. II., 49, 5889–5909, doi: 10.1016/S0967-0645(02)00324-7.

Kadko, D., and P. Swart (2004), The source of the high heat and freshwater content of the upper ocean at the SHEBA site in the Beaufort Sea in 1997, J. Geophys. Res., 109, C01022, doi: 10.1029/2002JC001734.

Kelley, J. J. (1968), Carbon dioxide in the seawater under the Arctic Sea Ice, Nature, 218(5144), 862–864, doi: 10.1038/218862a0.

Krishnamurthy, R. V., M. Machavaram, M. Baskaran, J. M. Brooks, and M. A. Champ (2001), Organic carbon flow in the Ob, Yenisey rivers and Kara Sea of the Arctic region, Mar. Poll. Bull. 42, 726–732, doi: 10.1016/S0025-326X(00)00202-2.

Kuffner, I. B., A. J. Andersson, P. L. Jokiel, K. S. Rodgers, and F. T. Mackenzie (2008), Decreased abundance of crustose coralline algae due to ocean acidification, Nat. Geosci., 1, 114–117, doi: 10.1038/ngeo100.

Lewis, E. R., and D. W. R. Wallace (1995), Basic programs for the CO_2 system in seawater, *BNL-61827*, U.S. Dept. of En., Oak Ridge Nat. Lab., Carbon Dioxide Inf. Anal. Ctr., Oak Ridge, TN.

Lisitsyn, A. P., 1969. *Recent Sedimentation in the Bering Sea*. Bezrukov, P.L. (Transl.) Israel Program for Scientific Translations, Jerusalem, Israel.

Løvvorn, J. R., S. E. Richman, J. M. Grebmeier, and L. W. Cooper (2003), Diet and body condition of Spectacled Eiders wintering in pack ice of the Bering Sea, Pol. Biol., 26, 259–267, doi: 10.1007/s00300-003-0477-0.

Luchin, V. A., I. P. Semiletov, and G. E. Weller (2002), Changes in the Bering Sea region: atmosphere-ice-water system in the second half of the twentieth century, Prog. Oceanogr., 55(1-2), 23–44, doi: 10.1016/S0079-6611(02)00068-X.

Macdonald, R.W., McLaughlin, F.A., and Carmack, E.C., 2002. Fresh water and its sources during the SHEBA drift in the Canada Basin of the Arctic Ocean. *Deep Sea Research I*, **49**(10), 1769–1785.

Macdonald, R. W., L. G. Anderson, J. P. Christensen, L. A. Miller, I. P. Semiletov, and R. Stein, (2009), The Arctic Ocean, in *Carbon and Nutrient Fluxes in Continental Margins: A Global Synthesis*, edited by K. K. Liu, L. Atkinson, R. Quiñones, and L. Talaue-McManus, pp. 291–303, Springer, New York, NY.

Makkaveev, P. N. (1994), The dissolved inorganic carbon in the Kara Sea and in the mouths of the Ob and Yenisei Rivers, Oceanol. Engl. Transl., 34(5), 668–672, doi: 0001-4370/95/3405-0004.

Mathis, J. T., D. A. Hansell, D. Kadko, N. R. Bates, and L. W. Cooper (2007), Determining net dissolved organic carbon production in the hydrographically complex western Arctic Ocean, Limnol. Oceanogr., 52(5), 1789–1799, doi: 10.4319/lo.2007.52.5.1789.

Mathis, J. T., J. N. Cross, N. R. Bates, S. B. Moran, M. W. Lomas, and P. J. Stabeno (2010), Seasonal distribution of dissolved inorganic carbon and net community production on the Bering Sea shelf, Biogeosci., **7**, 1769-1787, doi: 10.5194/bg-7-1769-2010.

McClelland, J. W., S. J. Déry, B. J. Peterson, R. M. Holmes, and E. F. Wood (2006), A pan-Arctic evaluation of changes in river discharge during the latter half of the 20th century, Geophys. Res. Lett., 33, L06715, doi: 10.1029/2006GL025753.

Mehrbach, C., C. H. Culberson, J. E. Hawley, and R. M. Pytkowicz (1973), Measurement of the apparent dissociation constants of carbonic acid in seawater at atmospheric pressure. Limnol. Oceanogr., 18, 897–907. [doi not avail.]

Millero, F. J. (2007), The marine inorganic carbon cycle, Chem. Rev., 107(2), 308–341, doi: 10.1021/cr0503557.

Mizobata, K., and S. Saitoh (2004), Variability of Bering Sea eddies and primary productivity along the shelf edge during 1998 – 2000 using satellite multisensor remote sensing, J. Mar. Syst., 50, 101–111, doi: 10.1016/j.jmarsys.2003.09.014

Moore, S. E., and K. L. Laidre (2006), Trends in sea ice cover within habitats used by bowhead whales in the western Arctic, Ecol Appl., 16, 932–944, doi: 10.1890/1051-0761(2006)016[0932:TISICW]2.0.CO;2.

Moore, S. E., J. M. Grebmeier, and J. R. Davis (2003), Gray whale distribution relative to forage habitat in the northern Bering Sea: Current conditions and retrospective summary, Can. J. Zool., 81, 734–742, doi: 10.1139/z03-043.

Muench, R. D. (1976), A note on eastern Bering Sea shelf hydrographic structure: August 1974, Deep Sea Res., 23, 245–247, doi: 10.1016/0011-7471(76)91329-2.

Neumann, K. (1999), Nitrogenous organic matter in surface sediments in the estuaries of the Ob and Yenisei rivers, Rep. Pol. Res., 300, 110–114. [doi not avail.]

Niebauer, H. J., 1998. Variability in Bering Sea ice cover as affected by a “regime shift” in the north Pacific in the period 1947 – 1996, J. Geophys. Res., 103, 27717–27737, doi: 10.1029/98JC02499.

Nihoul, J. C. J., P. Adam, P. Brasseur, E. Deleersnijder, S. Djenidi, and J. Haus (1993), Three-dimensional general circulation model of the Bering-Chukchi Shelf. Cont. Shelf Res., 13, 509–542, doi: 10.1016/0278-4343(93)90093-D.

Omar, A., T. Johannessen, R. G. J. Bellerby, A. Olsen, L. G. Anderson, and C. Kivimae (2005), Sea ice and brine formation in Storfjorden: Implications for the Arctic wintertime air-sea CO_2 flux, in *The Nordic Seas: An Integrated Perspective: Oceanography, Climatology, biogeochemistry, and modeling*, Geophys. Monogr. Ser., vol. 158, edited by H. Drange, T. Dokken, T. Furevik, R. Gerdes, and W. Berger, pp. 177−187, AGU, Washington, D.C., doi: 10.1029/158GM12.

Opsahl, S., and R. Benner (1997), Distribution and cycling of terrigenous dissolved organic matter in the ocean, Nature, 386, 480−482, doi: 10.1038/386480a0.

Opsahl, S., R. Benner, and R. W. Amon (1999), Major flux of terrigenous dissolved organic matter through the Arctic Ocean, Limnol. Oceanogr., 44(8), 2017−2023, doi: 10.4319/lo.1999.44.8.2017.

Orr, J. C., V. J. Fabry, O. Aumont, L. Bopp, S. C. Doney, R. A. Feely, *et al*. (2005), Anthropogenic ocean acidification over the twenty-first century and its impact on calcifying organisms, Nature, 437(7059), 681–686, doi: 10.1038/nature04095.

Overland, J. E., and A. T. Roach, (1987), Northward flow in the Bering and Chukchi Seas, J. Geophys. Res., 92(C7), 7097–7105, doi: 10.1029/JC092iC07p07097.

Overland, J. E., and P. J. Stabeno (2004), Is the climate of the Bering Sea warming and affecting the ecosystem? Eos Trans. Am. Geophys. Un. 85(33), 309, doi: 10.1029/2004EO330001.

Papadimitriou, S., H. Kennedy, G. Kattner, G. S. Dieckmann, and D. N. Thomas (2003), Experimental evidence for carbonate precipitation and CO_2 degassing during sea ice formation, Geochim. Cosmochim. Acta., 68, 1749–1761, doi: 10.1016/j.gca.2003.07.004.

Peterson, B. J., R. M. Holmes, J. W. McClelland, C. J. Vorosmart, R. B. Lammers, A. Shiklomanov, *et al*. (2002), Increasing river discharge to the Arctic Ocean, Science, 298, 2171–2173, doi: 10.1126/science.1077445.

Riebesell U., V. J. Fabry, L. Hansson, and J. P. Gattuso (Eds.) (2010), *Guide to Best Practices for Ocean Acidification Research and Data Reporting*, Publica. Off. of the EU, Luxembourg.

Roach, A. T., K. Aagaard, G. H. Pease, S. A. Salo, T. E. Weingartner, V. Pavlov, *et al*. (1995), Direct measurements of transport and water properties through Bering Strait, J. Geophys. Res., 100, 18443−18457, doi: 10.1029/95JC01673.

Rysgaard, S., R. N. Glud, M. K. Sejr, J. Bendtsen, and P. B. Christensen (2007), Inorganic carbon transport during sea ice growth and decay: A carbon pump in polar seas. J. Geophys. Res., 112, C03016, doi: 10.1029/2006JC003572.

Sabine, C. L., R. A. Feely, N. Gruber, R. M. Key, K. Lee, J. L. Bullister, *et al*. (2004). The oceanic sink for anthropogenic CO_2, Science, 305(5682), 367–371, doi: 10.1126/science.1097403.

Sabine, C. L. and R. A. Feely (2007), The oceanic sink for carbon dioxide, in *Greenhouse Gas Sinks*, edited by D. Reay, N. Hewitt, J. Grace and K. Smith, pp. 31–49, CABI Publ., Oxfordshire, U.K.

Salisbury, J. E., M. Green, C. Hunt, and J. Campbell (2008), Coastal acidification by rivers: A threat to shellfish? Eos Trans. Am. Geophys. Un. 89(50), 513−528, doi: 10.1029/2008EO500001.

Schumacher, J. D., and P. J. Stabeno (1998), The continental shelf of the Bering Sea, in *The Sea: Vol. 11—The Global Coastal Ocean: Regional Studies and Synthesis*. pp. 789–822, John Wiley and Sons, Inc., New York, NY.

Schumm, S. A., and B. R. Winkley (1994), The character of large alluvial rivers, in *The Variability of Large Alluvial Rivers*, edited by S.A. Schumm and B.R. Winkley, pp. 1–9, Am. Soc. Civ. Eng. Press, New York, NY.

Semiletov, I., A. Makshtas, S.-I. Akasofu, and E. Andreas (2004), Atmospheric CO_2 balance: The role of Arctic sea ice, Geophys. Res. Lett., 31, L05212, doi: 10.1029/2003GL017996.

Springer, A. M., C. P. McRoy, and M. V. Flint (1996), The Bering Sea green belt: shelf-edge processes and ecosystem production, Fish Oceanogr., 5(3-4), 205–223, doi: 10.1111/j.1365-2419.1996.tb00118.x.

Stabeno, P. J., and P. van Meurs (1999), Evidence of episodic on-shelf flow in the southeastern Bering Sea, J. Geophys. Res., 104(29), 715–729, doi: 10.1029/1999JC900242.

Stabeno, P. J., and J. E. Overland (2001), Bering Sea shifts toward an earlier spring transition, Eos Trans. Am. Geophys. Un., 29, 317–321, doi: 10.1029/01EO00185.

Stabeno, P. J., J. D. Schumacher, R. F. Davis, and J. M. Napp (1998), Under-ice observations of water column temperature, salinity, and spring phytoplankton dynamics: Eastern Bering Sea shelf, 1995, J. Mar. Res., 56, 239–255, doi: 10.1357/002224098321836172.

Stabeno, P. J., J. D. Schumacher, and K. Ohtani (1999), The physical oceanography of the Bering Sea, in *Dynamics of the Bering Sea: A Summary of Physical, Chemical, and Biological Characteristics, and a Synopsis of Research on the Bering Sea*, edited by T. R. Loughlin and K. Ohtani, pp. 1–28, North Pac. Mar. Sci. Org. (PICES), Univ. of Alaska Sea Grant, Fairbanks, AK.

Stabeno, P. J., N. A. Bond, N. B. Kachel, S. A. Salo, and J. D. Schumacher (2001), On the temporal variability of the physical environment over the southeastern Bering Sea, Fish. Oceanogr., 10(1), 81–98, doi: 10.1046/j.1365-2419.2001.00157.x.

Stabeno, P. J., G. L. Hunt Jr., J. M. Napp, and J. D. Schumacher (2006), Physical forcing of ecosystem dynamics on the Bering Sea shelf, in *The Sea. Vol. 14*, edited by A.

R. Robinson and K. H. Brink, pp. 1177−1212, John Wiley and Sons, New York, NY.

Stabeno, P. J., N. A. Bond, and S. A. Salo (2007), On the recent warming of the Bering Sea Shelf, Deep Sea Res. II., 54(23-26), 2599–2618, doi: 10.1016/j.dsr2.2007.08.023

Steinacher, M., F. Joos, T. L. Frölicher, G.-K. Plattner, and S. C. Doney (2009), Imminent ocean acidification of the Arctic projected with the NCAR global coupled carbon-cycle climate model, Biogeosci, 6, 515–533, doi: 10.5194/bg-6-515-2009.

Stern, N., 2006. *The Economics of Climate Change: The Stern Review*. Cambridge Univ. Press, Cambridge, U.K.

Striegl, R. G., G. R. Aiken, M. M. Dornblaser, P. A. Raymond, and K. P. Wickland (2005), A decrease in discharge-normalized DOC export by the Yukon River during summer through autumn, Geophys. Res. Lett., 32, L21413, doi: 10.1029/2005GL024413.

Striegl, R. G., M. M. Dornblaser, G. R. Aiken, K. P. Wickland, and P. A. Raymond (2007), Carbon export and cycling by the Yukon, Tanana, and Porcupine rivers, Alaska, 2001 – 2005, Wat. Resour. Res., 43, W02411, doi: 10.1029/2006WR005201.

Takahashi, T., S. C. Sutherland, R. Wanninkhof, C. Sweeney, R. A. Feely, D. W. Chipman, *et al*. (2009), Climatological mean and decadal change in surface ocean pCO_2, and net sea-air CO_2 flux over the global oceans, Deep Sea Res. II., 56(8-10), 554−577, doi: 10.1016/j.dsr2.2008.12.009.

Walsh, J. E., and C. M. Johnson (1979), An analysis of Arctic sea ice fluctuations, 1953 – 1977, J. Phys. Oceangr., 9, 580–591, doi: 10.1175/1520-0485(1979)009<0580:AAOASI>2.0.CO;2.

Walsh, J. J., C. P. McRoy, L. K. Coachman, J. J. Goering, J. J. Nihoul, T. E. Whitledge, *et al*. (1989), Carbon and nitrogen recycling with the Bering/Chukchi Seas: source regions for organic matter affecting AOU demands of the Arctic Ocean, Prog. Oceanogr., 22, 277–359, doi: 10.1016/0079-6611(89)90006-2.

Wang, B. (1999), Spatial distribution of chemical constituents in the Kuskokwim River, Alaska, *Water-Res. Inv. Rep. No. 99-4177*, USGS, Anchorage, AK.

Weiss, R. F. (1974), Carbon dioxide in water and seawater: The solubility of a non-ideal gas, Mar. Chem., 2, 203–215, doi: 10.1016/0304-4203(74)90015-2.

Wheeler, P. A., H. M. Watkins, and R. L. Hansing (1997), Nutrients, organic carbon, and organic nitrogen in the upper water column of the Arctic Ocean: implications for the sources of dissolved organic carbon, Deep Sea Res. II., 44, 1571–1592, doi: 10.1016/S0967-0645(97)00051-9.

White, D., L. Hinzmann, L. Slessa, J. Cassano, M. Chambers, K. Falkner, *et al*. (2007), The arctic freshwater system: Changes and impacts, J. Geophys. Res., 112, G04S54, doi: 10.1029/2006JG000353.

Woodgate, R. A., and K. Aagaard (2005), Revising the Bering Straight freshwater flux into the Arctic Ocean, Geophys. Res. Lett., 32, L02602, doi: 10.1029/2004GL021747.

Woodgate, R. A., K. Aagaard, and T. J. Weingartner (2005a), A year in the physical oceanography of the Chukchi Sea: Moored measurements from autumn 1990 – 1991, Deep Sea Res. II., 52, 3116–3149, doi: 10.1016/j.dsr2.2005.10.016.

Woodgate, R. A., K. Aagaard, and T. J. Weingartner (2005b), Monthly temperature, salinity and transport variability of the Bering Straight through flow, Gephys. Res. Lett., 32, L04601, doi: 10.1029/2004GL021880.

Wyllie-Escheveria, T., 1995. Seasonal Sea Ice, the Cold Pool and Gadid Distribution on the Bering Sea Shelf, Ph.D. dissertation, Univ. of Alaska, Fairbanks, Fairbanks, AK.

Wyllie-Escheveria, T., and W. S. Wooster (1998), Year-to-year variations in Bering Sea ice cover and some consequences for fish distributions, Fish. Oceangr., 7(2), 159–170, doi: 10.1046/j.1365-2419.1998.00058.x

Yamamoto-Kawai, M., F. A. McLaughlin, E. C. Carmack, S. Nishino, and K. Shimada (2009), Aragonite undersaturation in the Arctic Ocean: Effects of ocean acidification and sea ice melt, Science, 326(5956), 1098–1100, doi: 10.1126/science.1174190.

Zachos, J. C., U. Röhl, S. A. Schellenberg, A. Sluijs, D. A. Hodell, D. C. Kelly, *et al*. (2005), Rapid acidification of the ocean during the Paleocene-Eocene Thermal Maximum, Science, 308(5728), 1611–1615, doi: 10.1126/science.1109004.

Zhuravlev, A. Y., and R. A. Wood (2009), Controls on carbonate skeletal mineralogy: Global CO_2 evolution and mass extinctions, Geology, 37(12), 1123–1126, doi: 10.1130/G30204A.1.

Appendix B:

Evidence of prolonged aragonite undersaturations in the bottom waters of the southern Bering Sea shelf from autonomous sensors[6]

B.0 Abstract

The southeastern shelf of the Bering Sea is a dynamic area that experiences seasonal variability in primary production and remineralization of organic matter that largely controls the carbon biogeochemistry of the water column. Surface water partial pressure of carbon dioxide (pCO_2) is greatly reduced in summer by biological production, which increases carbonate mineral saturation states (Ω). In contrast, the export of large quantities of organic matter from surface blooms drives an active remineralization loop that sharply increases pCO_2 near the bottom, while lowering pH and suppressing Ω. New observations from moored biogeochemical sensors showed that seasonal net community production lowers surface water pCO_2, causing large gradients between the ocean and atmosphere that are sustained throughout the summer, confirming that these waters likely remain supersaturated with respect to aragonite throughout the open water season. On the other hand, moored sensors deployed near the bottom showed that pCO_2 levels exceed 500 μatm by early June and remain at these high levels well into the autumn months indicating that the bottom waters are likely continuously undersaturated in aragonite for at least several months during each year. However, only a small fraction of the increased pCO_2 can currently be attributed to the intrusion of anthropogenic CO_2 from the atmosphere, while the majority is due to natural respiration processes. Therefore, the timing and duration of these undersaturation events are likely critical in the development of larval and juvenile calcifiers in the region and will change as anthropogenic CO_2 concentrations continue to rise.

---

[6]Mathis, J.T., Cross, J.N., Monacci, N.M., Feely, R.A., and Stabeno, P.J., 2013. Evidence of prolonged aragonite undersaturations in the bottom waters of the southern Bering Sea shelf from autonomous sensors. Deep Sea Res. II. Submitted.

B.1 Introduction

The southeastern continental shelf of the Bering Sea is a region that has demonstrated remarkable variability in recent decades in response to climate forcing (Stabeno et al., 2007) and the areas of the Bering Sea that are being affected by these changes are expanding, with unknown consequences to higher trophic level organisms and commercial fisheries (Grebmeier et al., 2006; Mathis et al., 2013). Many of the anthropogenically-induced changes that have garnered international attention in recent years, such as ocean acidification (OA; e.g., Caldeira and Wickett, 2003) are exacerbated in the Bering Sea due to its unique physical and biogeochemical processes (Mathis et al., 2011). One area of particular concern is the intensity and duration of events that lead to the suppression and undersaturation of carbonate minerals that are critical for the production and maintenance of shells and tests in both pelagic and benthic calcifying organisms (e.g. Feely et al., 2008; Hauri et al., 2009; Reis et al., 2009; Barton et al., 2012; Bednarŝek et al., 2012).

While the average pH of the global ocean has decreased by ~0.1 over the two and a half centuries since the Industrial Revolution due mostly to human emission of carbon dioxide (CO_2) (Feely et al., 2009), more rapid and seasonally intensified changes in pH have occurred in the Bering Sea due to unique circulation patterns in the north Pacific (Byrne et al., 2010) and natural seasonal variations in fresh water inputs from rivers and ice melt and coupling between pelagic and benthic carbon production and remineralization (Mathis et al., 2011; Appendix A). It is likely that these factors make the Bering Sea both more sensitive and susceptible to short-term future changes brought on by OA than many other coastal margins (Fabry et al., 2009).

Natural seasonal changes in carbonate mineral saturation states are driven by the region's intense cycle of organic matter production and export. Each spring, the retreat of sea ice northward from the Bering Sea shelf stimulates extensive ice algae and phytoplankton blooms that are driven by the onset of stratification (Ladd and Stabeno, 2012). These blooms consume dissolved inorganic carbon (DIC) in the surface mixed layer (Mathis et al., 2010; Chapter 2) and produce vast quantities of organic matter during

photosynthesis. However, some uncoupling between the seasonally intense periods of primary production and pelagic grazing can occur (e.g., Springer et al., 1996; Appendix A), leading to high rates of organic matter export from the surface (e.g., Moran et al., 2013; Chapter 2; Chapter 4). The removal of DIC from the surface mixed layer causes a sharp increase in pH and carbonate mineral saturation states (Ω), while the export production that supports the biologically diverse benthic communities in the southern Bering Sea leads to elevated rates of remineralization in bottom waters and sediments (Grebmeier and McRoy, 1989; Devol and Christensen, 1993). The resulting accumulation of DIC at depth in summer and fall causes a broad reduction in pH and suppresses Ω for both calcite and aragonite (Mathis et al., 2011). Thus, ocean biology tends to drive seasonally divergent trajectories for seawater chemistry (Bates et al., 2009), with primary production in the euphotic zone increasing Ω in the mixed layer while an accumulation of DIC in subsurface waters through remineralization suppresses Ω (Appendix A).

Coupled with the natural seasonal variability exhibited by the system, anthropogenic CO_2 provides the additional suppression necessary to cause carbonate mineral undersaturations (Mathis et al., 2011), leading to concerns about the commercial, economic, and subsistence viability of this ecosystem in response to rising CO_2 levels and increasing OA (Mathis et al., 2013). Unlike much of the west coast of North America, where seasonal upwelling is the dominant driver of OA events (Feely et al., 2008; Gruber et al., 2012; Hauri et al., 2012), the eastern Bering Sea seems to behave more like an estuarine system (e.g. Feely et al., 2010), where stratification and the biological pump are the dominant drivers of Ω.

Given the coarse temporal resolution of carbonate observations in the southeastern Bering Sea, it has been impossible to quantify the timing of onset, the period of duration, and the peak intensity of these carbonate mineral undersaturation events until now. Here, we describe new data collected at the M2 mooring site (Figure B-1) in 2011 that provide new insights into the seasonal progression of CO_2 concentrations and carbonate biogeochemistry at the surface and near the bottom in this region.

B.2 Background

The southeastern Bering Sea sustains one of the most productive marine ecosystems in the ocean and supports an extraordinarily rich fishery that generates more the 40% of all finfish and shellfish landings in the United States. It directly or indirectly provides over 20 million pounds of subsistence foods used by nearly 55,000 Alaska natives (Stabeno et al., 2012), particularly in small coastal communities that have very low resiliency for responding to disruptions in their food supply (Mathis et al., 2013).

The southeastern continental shelf is relatively wide (> 500 km) compared to other coastal regions along the west coast of North America and is heavily influenced by the seasonal advance and retreat of sea ice, terrestrial discharge and interannual variability in the wind fields (Stabeno et al., 2010). Semi-permanent temperature fronts naturally divide the shelf into three along-shelf domains (Coachman, 1986; Kachel et al., 2002; Stabeno et al., 2012; Chapter 4), each with differing vertical and horizontal structure largely controlled by the penetration of atmospheric forcing and tidal mixing, the seasonal advance and retreat of sea ice, terrestrial discharge, and bottom topography. The Coastal Domain extends from the western shores of Alaska to the 50 m isobath with the Inner Front constituting the boundary between the Coastal Domain and Middle Domain, which is the focus of this paper. A well-stratified, two-layer system exists in the Middle Domain during the ice-free months (April – October), where wind mixes the surface waters over a denser, tidally mixed bottom layer. A two-layer system is also present in the Outer Domain, although the transition between the surface and bottom layers is more gradual than in the Middle Domain.

The M2 mooring lies about half way through the Middle Domain, several hundred kilometers southwest of Bristol Bay (Figure B-1). Here, the water depth ranges from approximately 50 m to 100 m, gradually deepening from east to west. In winter, the water column is generally well mixed with little to no gradient in temperature and salinity (Stafford et al., 2010). However, in summer the onset of seasonal ice melt and large volumes of riverine discharge create a well-defined two-layer structure. The surface layer

is typically 20-30 m thick, with bottom waters underlying sharp gradients in temperature, salinity, inorganic nutrient and DIC concentrations (Mathis et al., 2010).

In spring, DIC concentrations in the Middle Domain near the M2 mooring range from ~2000-2050 μmoles kg^{-1} and are fairly uniform from the surface to the bottom (Mathis et al., 2010; Chapter 2). In summer, as rates of net primary production (NPP) reach as high as 13 g C m^{-2} d^{-1} (Niebauer et al., 1995; Lomas et al., 2012; Chapter 2) there is a pronounced gradient in DIC concentrations between the surface and bottom, with DIC accumulating at depth in response to remineralization of exported organic carbon produced at the surface. This remineralization increases the partial pressure of CO_2 (pCO_2) in bottom waters, which suppresses carbonate mineral saturation states to a varying degree across the shelf. Over the northern part of the shelf, where bottom temperatures are lowest and export production is highest, an intense seasonal suppression of aragonite has been observed in bottom waters, while Ω at the surface increase (Mathis et al., 2011; Appendix A). The bottom water suppression of Ω_A corresponds to high apparent oxygen utilization (AOU) values and elevated silicate in the bottom waters, probably the result of both water column and sedimentary remineralization. The subsurface effects of remineralization can be especially significant during periods of peak production. These biologically driven, seasonally divergent trajectories of Ω, or the Phytoplankton-Carbonate Saturation State (PhyCaSS) interaction, has also been observed in the Chukchi Sea (Bates and Mathis, 2009; Bates et al., 2009), and is likely a typical feature of highly productive polar and subpolar shelves.

Using data from seasonal, repeat hydrographic cruises in the Bering Sea from 2008 – 2010, Mathis et al., (2011) determined that anthropogenic CO_2 (~35 μmoles kg^{-1}) in the bottom waters were responsible for some of the carbonate mineral suppression and undersaturations that were observed. However, the paucity of fully resolved temporal data limited our understanding of how this process evolved with time. Several questions remained regarding when pCO_2 levels reach a point where carbonate mineral undersaturation would occur, how long these levels of undersaturation would remain, and ultimately how intense these undersaturations become. To fill this data gap, we deployed

OA sensors on the M2 mooring to better constrain the carbonate chemistry at the surface and at depth.

B.3 Methods

B.3.1 M2 Mooring Site

The Pacific Marine Environmental Laboratory (PMEL) and the Fisheries Oceanography Coordinated Investigations (FOCI) group began continuous monitoring at the M2 (Figure B-1) mooring site on the southeastern Bering Sea shelf in 1995. M2 is located on the 70m isobath (Stabeno et al. 2010) southwest of Bristol Bay. During the ice-free season (April/May – September/October), the M2 mooring array includes a surface toroid buoy with an aluminum tower. A subsurface mooring line is deployed during the winter season (November – March). Past instrumentation at the M2 site is documented in Ladd and Stabeno (2012) and Stabeno et al. (2007) and includes measurements of temperature, salinity, fluorescence, currents, and nitrate.

B.3.2 OA Instrumentation at M2

From May 2011 to October 2011, ocean acidification (OA) instrumentation was deployed at the surface buoy and approximately 3 m from the bottom at the M2 site. A Seabird Electronics package at a depth of 1 m sampled every three hours to obtain measurements of temperature (°C), salinity, dissolved oxygen (μmoles kg^{-1}), florescence (μg l^{-1}), and turbidity (% transmission). A Sunburst Sensors Submersible Autonomous Moored Instrument for CO_2 (SAMI-CO_2) was also deployed at 1 m. The SAMI-CO_2 (DeGrandpre et al., 1995) was calibrated over a range of 100-1500 μatm with a reported ±1 μatm precision, with all observed data falling within this range. At a three-hour sampling interval, the SAMI-CO_2 runs blanks every 28 cycles or every three days to test for instrument drift over the course of the deployment. A Sunburst Sensors Submersible Autonomous Moored Instrument for pH (SAMI-pH) was deployed at 1 m and near the bottom, but both sensors failed during the deployment and no pH data were recovered.

From May 2011 to October 2011, a bottom cage was deployed at a depth of 67 m, or roughly 3 m off the bottom. The cage included a Seabird Electronics package measuring temperature (°C), salinity, and dissolved oxygen (μmoles kg^{-1}) as well as a SAMI-CO_2 programmed to sample at longer intervals (18 hours) than the surface instrument to conserve battery life in the colder water waters. The bottom SAMI-CO_2 sensor also ran routine blanks and was calibrated over a range of 100-1500 μatm with a reported ±1 μatm precision, with all recorded data falling within this range. Calibration casts, using a profiling, Seabird Electronics 911-plus CTD, were made during the mooring deployment (May 16th, 2011) and retrieval (October 3rd, 2011), aboard the NOAA Ship Dyson.

Calibration samples for pCO_2 and dissolved oxygen were taken at the moored sensor depths at the surface and near the bottom. A modified version of the Winkler Titration method (Langdon 2010) was used to calibrate the DO sensors on the Seabird Electronics packages. pCO_2 was calculated from dissolved inorganic carbon (DIC), total alkalinity (TA), temperature, and salinity using CO2SYS (version 1.05) and the thermodynamic model of Lewis and Wallace (1995). DIC and TA samples were collected as suggested by the guide to best practices for ocean CO_2 measurements (Dickson and Goyet, 1994). DIC/TA samples were analyzed using a highly precise and accurate gas extraction/coulometric detection system (~0.02%, < 2 μmoles kg^{-1}). The analytical system consists of a VINDTA 3C (Versatile Instrument for the Detection of Total Alkalinity) coupled to a CO_2 coulometer (model 5012; UIC Coulometrics). Routine analyses of Certified Reference Materials (CRMs, provided by A.G. Dickson, Scripps Institution of Oceanography) and repeat sampling ensured that the accuracy of the DIC/TA measurements was within 0.05% and was stable over time.

The complete seawater carbonic acid system (i.e., CO_2, $H_2CO_3^-$, HCO_3^-, CO_3^{2-}, H^+) can be calculated from two of five measureable carbonate system parameters (i.e., DIC, TA, pCO_2, pH, and more recently CO_3^{2-}), along with temperature and salinity (Zeebe and Wolf-Gladrow, 2001; Dickson et al., 2007). The carbonic acid dissociation constants (pK1 and pK2) of Mehrbach et al. (1973), as refit by Dickson and Millero

(1997), were used to calculate seawater pCO_2 and other carbonate parameters, using the equations of Zeebe and Wolf-Gladrow (2001). In addition, the CO_2 solubility equations of Weiss (1974), and dissociation constants for borate and phosphate (Dickson et al., 2007) were used.

B.3.3 Empirical Relationship Between pCO_2 *and* Ω_A

In order to fully constrain the carbonate system, two of the five parameters must be measured although currently, only two of these parameters (pCO_2 and pH) can be measured autonomously on moorings with any reliability. Unfortunately, during the M2 deployment in 2011, only the pCO_2 sensors returned good data, leaving us with only one of the two needed carbonate parameters. However, given our extensive sampling over the shelf in the preceding years we can estimate an approximate seasonal relationship between the carbonate mineral saturation state for aragonite (Ω_A) and pCO_2 and to a lesser extent dissolved oxygen concentrations. Similar approaches have been employed along the west coast of North America and the Gulf of Alaska (Juranek et al., 2009; Alin et al., 2012; Evans et al., 2013), where multiple linear regressions (MLRs) have been used to determine Ω_A from non-carbonate parameters (i.e. temperature, salinity, nitrate and dissolved oxygen), but here we use direct empirical relationships, rather than MLRs to estimate seasonal changes in Ω_A.

In order to develop empirical relationships between pCO_2/O_2 and Ω_A for the southeastern Bering Sea, we synthesized data (over 1,000 measurements) from seven Bering Sea Ecosystem Study (BEST) cruises (MN, NP and 70M lines in Figure B-1) over the southern shelf where discrete carbonate measurements were made (Tables B-1 and B-2; Figure B-2). In addition to looking at the entire water column, we also developed empirical equations for just the surface mixed layer (0-30 m) and the subsurface layer (30 m to the bottom) in each season to determine if there were any biases. In the three years before the mooring deployment, pCO_2 ranged from < 200 μatm at the surface to ~1,500 μatm at depth over the course of the open water season (observations were made in May – September). Dissolved oxygen concentrations ranged from > 50 μmoles kg^{-1} near the

bottom to > 450 μmoles kg^{-1} at the surface. These data show that when pCO_2 values reach approximately 500 μatm (Table B-1), Ω_A is at or below the saturation horizon (Ω_A = 1.0; horizontal dashed lines in Figure B-2A, B). Although the relationships are not as robust, particularly at the surface, the threshold for aragonite undersaturation with respect to dissolved oxygen was ~225-260 μmoles kg^{-1} (Table B-2; Figure B-2C, D). When pCO_2 values were less than 500 μatm and dissolved oxygen was greater than 260 μmoles kg^{-1}, the data show that Ω_A is above the saturation horizon. These empirical relationships (Tables B-1 and B-2) were used to relate the moored observations of pCO_2/O_2 to Ω_A to better understand the impacts of primary production and remineralization on the carbonate chemistry.

One caveat to our $pCO_2 - \Omega_A$ relationships is that we have to assume that the relationship between total alkalinity (TA) and DIC did not change between the 2008 – 2010 ship-based measurements and our mooring observations in 2011. A robust explanation of the conservative and non-conservative behavior of TA is given in Chapter 4 but it was shown that a number of factors such as sea ice melt, riverine inputs, carbonate mineral dissolution and coccolith production can cause anomalies in TA concentrations relative to salinity over the shelf. However, all of these drivers for the non-conservative behavior of TA were observed during our 2008 – 2011 measurements and are therefore captured in the calculated pCO_2 and Ω_A values. Therefore, we feel confident that the $pCO_2 - \Omega_A$ relationship is valid for the discussion presented here.

B.4 Results and Discussion

B.4.1 Surface Observations

When the M2 mooring was deployed in mid-May 2011 sea ice had already retreated from the area and the ice edge was several hundred miles to the north. Surface water temperatures were still relatively cold (~2.5°C), but some warming had occurred since the onset of ice melt. During the deployment of the mooring, surface water temperatures warmed considerably and reach a peak of 11°C in mid-August before cooling began (Figure B-3). At the time of deployment, surface salinity was ~31.3, but

increased to a maximum of ~31.9 a few weeks later likely due to flushing of ice melt waters out of the area. Starting in early July, salinity began to steadily decline, dropping to a minimum value of 31.1 in early September, likely due to the influence of freshwater discharge from the coast (Figure B-3).

Because the mooring was deployed in water that had been ice-free for at least a few weeks, the onset of the ice edge bloom was not observed. Chlorophyll concentrations ranged from 0-1.2 μl^{-1} in the first few weeks of deployment, but later spiked to over 5.0 $\mu g\ L^{-1}$ (early June; Figure B-3) with transmissivity dropping by 15% (Figure B-3). The increase in chlorophyll coincided with a period of increasing temperature and near constant salinity, which likely indicated the onset of temperature stratification often necessary to support significant late spring open water phytoplankton blooms. Dissolved oxygen (DO) concentrations were elevated (> 400 μmoles kg^{-1}) and oxygen was supersaturated at the surface at the time of the deployment, also indicating primary production had already begun (Figure B-3). After the early June bloom, chlorophyll concentrations dropped quickly and remained fairly constant (~0-0.5 μL^{-1}) until mid-August when a more gradual, less intense increase in chlorophyll occurred in conjunction with an increase in DO concentrations, indicating a late-season bloom. The increase in chlorophyll coincided with an increase in salinity, which could indicate that a pulse of high-salinity, nutrient-replete, basin-influenced water moved into the area and stimulated a surge of primary production.

As with DO concentrations, surface pCO_2 values at the time of deployment indicated that biological production had already occurred. Bates et al., 2011 showed that pCO_2 values under the sea ice of the eastern Bering Sea were near atmospheric concentrations (~390 μatm), which was certainly not the case at the time of the mooring deployment. In mid-May, pCO_2 values at the surface at M2 were ~150 μatm (red data in Figure B-4) or roughly 240 μatm lower than atmospheric values (black data in Figure B-4). This differential in air-sea pCO_2 (ΔpCO_2) values indicated the removal of several hundred μmoles kg^{-1} of DIC from the surface layer, which is consistent with previous observations of DIC drawdown (Mathis et al., 2010; Chapter 2) in the region. pCO_2

values increased fairly consistently at the surface throughout the deployment, with the exception of slight drawdowns occurring with the increases in chlorophyll values in early June and September (Figure B-3). The near constant increase in the pCO_2 is due to surface warming (Figure B-3) and air-sea gas exchange that occurred over the course of the deployment, although values remained below atmospheric CO_2 concentrations for nearly all of the deployment confirming that this part of the shelf provides a strong seasonal sink for atmospheric CO_2 (Bates et al., 2011; Chapter 4) throughout the spring and summer.

Individual seasonal estimates from ship observations collected in 2008 showed that CO_2 fluxes into the surface layer ranged from -30 to 53 mmoles C m^{-2} d^{-1} during spring and between -7 and -113 mmoles C m^{-2} d^{-1} during summer (Bates et al., 2011). In general, fluxes were similar between the southern Middle and southern Coastal Domains during spring (~20 mmoles C m^{-2} d^{-1}). During summer, influx of CO_2 to the surface layer increased strongly in the southern Coastal Domain (~59 mmoles C $m^{-2}d^{-1}$) while influxes remained similar (16.5 mmoles C m^{-2} d^{-1}) in the southern Middle Domain where M2 is located.

We used the ΔpCO_2 data along with daily averaged wind speed data from the M2 mooring to calculate air-sea exchange (F_{CO_2}; mmoles m^{-2} d^{-1}) in 2011 using the following formula:

$$F_{CO_2} = K_{SST} \times K_{CO_2} + \Delta pCO_2 \quad \text{(Eq. B-1)}$$

where K_{SST} is the gas transfer velocity (cm hr^{-1}), K_{CO_2} is the solubility of CO_2 (mmoles m^{-3} μatm^{-1}) estimated by Weiss (1974), and ΔpCO_2 is the air-sea pCO_2 difference (μatm) between the atmosphere and surface water values at M2. Values of K_{SST} were determined from the quadratic wind speed dependency from Ho et al. (2011), such that:

$$K_{SST} = (0.277 \times U^2) \times (Sc/600)^{-0.5} \quad \text{(Eq. B-2)}$$

where U is the daily averaged wind speed above the sea surface, and Sc is the Schmidt number for CO_2 at the *in situ* temperature. Wind speed was measured from sensors

mounted on the tower of the M2 mooring approximately 3 m from the surface of the water.

During the first few weeks of the M2 deployment, F_{CO_2} was fairly high (-15 to -125 mmoles C m^{-2} d^{-1}) and consistent with seasonal ship-based estimates over this part of the shelf due to the large disequilibrium between the atmosphere and surface water pCO_2 values (Figure B-4) and relatively high, but variable wind speeds (2-12 m s^{-1}). However, by July, F_{CO_2} had decreased by -5 to -50 mmoles C m^{-2} d^{-1} as surface pCO_2 values quickly increased and winds diminished. Both of these factors sharply diminish air-sea gas exchange. Near the end of the deployment, surface water pCO_2 values exceeded atmospheric values (Figure B-4), even though surface temperatures had been decreasing for several weeks, which would have lowered surface water pCO_2. In late September, the surface waters at M2 became a weak source of CO_2 (+5 mmoles C m^{-2} d^{-1}) to the atmosphere. This pattern has been previously observed over the northern shelf, resulting from the remineralization of allochthonous organic matter, likely derived from river discharge (Chapter 2). While the trajectory of surface water pCO_2 values was still increasing at the time of the mooring recovery, it is unclear how high these values reached before the onset of sea ice and how much outgassing occurred.

B.4.2 Bottom Water Observations

Measurements from near the bottom of the M2 mooring site showed that temperature and salinity were much more uniform than at the surface during the duration of the deployment. Temperatures near the bottom warmed slightly from ~0.5°C in mid-May to a maximum of 3°C in early October (Figure B-5). Salinity showed very little variability ranging from only 31.8 to 32.1 (Figure B-5). There was no chlorophyll sensor on the Seabird Electronics package near the bottom, but transmissometer data showed a steep decrease in light transmission starting roughly at the same time as the sharp chlorophyll increase was observed at the surface (Figure B-5). The low light transmission continued from mid-June through the end of the deployment likely due to particle export from the surface (Moran et al., 2013) and sediment resuspension.

DO concentrations near the bottom started at ~310 μmoleses kg^{-1}, but decreased sharply and consistently during the deployment reaching a minimum value of ~200 μmoles kg^{-1} in September. pCO_2 values showed an inverse trend, starting at ~400 μatm and rising quickly to over 1,400 μatm by the beginning of July, which was consistent with ship-based observations in 2008 − 2011. The combination of oxygen consumption and increased pCO_2 values is a clear indication of the remineralization of exported organic matter near the bottom. Although temperatures did warm slightly during the deployment, this would have only accounted for a ~50 μatm increase in pCO_2. The remaining increase (~950 μatm) had to have come from remineralization processes in the water column and underlying sediments, assuming that TA stayed relatively constant throughout the deployment. This seems likely given that salinity remained fairly constant and Chapter 4 showed that most of the non-conservative processes that impact TA occur in the surface mixed layer. The only process that could have caused a non-conservative increase in TA is carbonate mineral dissolution, which was evident in some locations over the shelf in summer and fall of 2008 − 2010 (Chapter 4) where pCO_2 were above 1,250 μatm.

B.4.3 Assessing the Carbonate Chemistry

Using the $pCO_2/O_2 – \Omega_A$ relationships we can show that the surface waters at M2 likely remained supersaturated with respect to aragonite throughout the spring and summer months. When pCO_2 ranged from 150-400 μatm and DO concentrations were > 260 μmoles kg^{-1} in 2008 – 2010, Ω_A was between 3.5 and 1.2, which was likely what occurred during the M2 deployment as Ω_A steadily decreased as air-sea gas exchange increased pCO_2 at the surface (Figure B-4) and DO concentrations returned to pre-bloom levels (Figure B-3). The only locations where aragonite was undersaturated at the surface in 2008 – 2010 was where there was a high concentration of sea ice melt or river runoff, both of which are low in TA (Appendix A) relative to marine waters. These locations all had salinities less than 30, which was not the case during the deployment at M2, although observations were not made at the time of ice retreat.

Although the 2011 results showed that Ω_A is currently supersaturated in the surface waters near M2 this will likely not be the case by the end of this century. Anthropogenic CO_2 is accumulating in the ocean at rate of ~1.5-3.0 ppm yr^{-1} (Feely et al., 2009) so even as biological productivity lowers pCO_2 each spring, baseline levels of CO_2 in the surface waters of the Bering Sea will continue to rise. Because primary production in the eastern Bering Sea is nutrient limited, there will likely be no significant increase in productivity to offset the increasing CO_2 levels and increased stratification due to warming surface temperatures and increased freshwater discharge may actually lead to a reduction in primary production. In 2011, primary production lowered pCO_2 values to ~150 μatm, but with even a decade's worth of CO_2 accumulation at current emission rates minimum, post-bloom values would be closer to 165-180 μatm, excluding any further warming effects, which would also increase pCO_2. Because atmospheric pCO_2 will be increasing in tandem, the driving force for air-sea gas exchange will only increase. We can see from our 2011 observations that by the beginning of August, the surface water pCO_2 values at M2 were close to equilibrium with the atmosphere. By mid-century (2050), pCO_2 values at the surface will likely be greater than 450 μatm at the end of summer and ~500 μatm before the onset of sea ice assuming constant temperature and no change in TA. At that time, it is likely that localized aragonite undersaturation at the surface will begin to occur. By the end of the century (2100), if pCO_2 values exceed 700 μatm, aragonite will likely be undersaturated at the surface for most of the year with only short-term alleviation coming directly after the most intense periods of primary production.

On the other hand, the $pCO_2/O_2 - \Omega_A$ relationships showed that aragonite is already undersaturated near the bottom for at least four months (June – September) in 2011. It is unclear how long pCO_2 values stayed above 500 μatm and DO values stay below 260 μmoles kg^{-1}, although there was a slight downward trend in pCO_2 between mid-August and October and we know that values return to < 500 μatm by the following spring, but it may have taken several more months for the high pCO_2 water to dissipate either through vertical and horizontal mixing or tidal flushing. Although only a relatively

small portion of the current CO_2 loading (~150 ppm) in the bottom waters can be attributed to anthropogenic sources, the inventory will continue to increase as anthropogenic CO_2 concentrations increase, lengthening the duration and intensity of the undersaturation events.

The current bottom water carbonate mineral undersaturations and future surface undersaturations may have detrimental consequences for local calcifying organisms, but direct evidence from the environment is still lacking. Initial results of the experimental studies (Robert Foy, personal communication) indicate that OA may have a substantial negative effect on red king and Tanner crab stocks, particularly at the larval stages. Reduced survival at the larval stage is likely to reduce recruitment and subsequently affect the number of crabs available for commercial harvest (Mathis et al., 2013). However, these early life stages do not currently coincide with undersaturation events, as they happen early in the year (January – June). More research on the effects of OA on other life history stages and the molecular response is necessary to fully understand the effects it will have on crab populations throughout the year as well as other benthic calcifying organisms.

The impacts of OA on pelagic calcifying and non-calcifying organisms in the southern Bering Sea is also unclear, but a new environmental study of pteropods in the Southern Ocean (Bednarŝek et al., 2012) showed extensive shell dissolution when aragonite became undersaturated. Previous work has shown that pteropods make up as much as 40% of the juvenile pink salmon diet (Aydin et al., 2005) so any disruptions to their stocks could have a cascading impact on the commercial salmon fishery, particularly around Bristol Bay. On the other hand, recent studies of pollock show that both juvenile and adult fish have a high tolerance for OA (Hurst et al., 2012) with little to no impact on growth or mortality further reinforcing the idea that there will be winners and losers in a post-OA ecosystem. However, it is unknown how OA will affect the food supply of the pollock.

B.5 Conclusions

Data from moored sensors deployed at the surface and near the bottom in the southeastern Bering Sea during the ice-free season of 2011 provided new insights into the seasonal cycling of carbonate biogeochemistry. Previous synoptic studies have shown that carbonate mineral saturation states are largely controlled by the timing, extent and location of primary production in the water column and the fate of the organic matter produced during these blooms. These findings were confirmed in 2011 as surface pCO_2 data during the open water season showed a substantial disequilibrium between the ocean and the atmosphere, particularly from mid-May to August where fluxes reached as high as -125 mmoles C m^{-2} d^{-1}. Using empirical relationships between pCO_2/O_2 and Ω_A, we determined that Ω_A is likely supersaturated at the surface throughout the year at the M2 site. During the open water months, there was a large range of Ω_A as values peaked at ~3.5, but then quickly begin to decrease as air-sea exchange increased the pCO_2 and reduced Ω_A to a minimum of ~1.2. The highest pCO_2 values (~410 μatm) observed during the mooring deployment correspond to lowest Ω_A values, but they do not currently lead to aragonite undersaturation. However, pCO_2 values at the surface were trending upward at the time of sensor recovery and it is unclear how high surface pCO_2 reached prior to the onset of primary production the following spring. In addition, anthropogenic CO_2 is accumulating in these surface waters and will likely cause Ω_A to become undersaturated at certain times of the year within the next few decades and perennially by the end of the century. This could have important consequences for pteropod populations, which are highly sensitive to Ω_A and are a keystone species in the food web due to their prevalence as a food source for juvenile pink salmon.

Sensor data from near the bottom confirmed that extensive aragonite undersaturations occur over this part of the shelf due to the remineralization of exported organic matter from the surface. In 2011, the onset of aragonite undersaturations began in mid-June and persisted until the sensors were recovered at the beginning of October. This prolonged event was also notable due to its intensity, with pCO_2 rising above 1,400 μatm, which is two times higher than the threshold where aragonite becomes undersaturated. It

is unclear from the current data how long pCO_2 remained at these levels, but it seems safe to assume that aragonite was highly undersaturated for at least four months in 2011.

The sustained aragonite undersaturations could have profound implication for benthic calcifiers in the eastern Bering Sea. Currently, anthropogenic CO_2 is a relatively small contributor to the high pCO_2 values observed over the shelf and the timing of undersaturations is such that sensitive organisms are not exposed to undersaturated waters during critical growth and reproductive stages. However, as anthropogenic CO_2 continues to accumulate, the duration and intensity of undersaturation events will increase, exposing organisms to longer periods of potentially corrosive conditions.

The southeastern Bering Sea is an import area for both the local and U.S. National economy, with hundreds of millions of dollars in commercial species at risk due to increasing OA. Our results have shown that this area needs careful monitoring in the coming decades coupled with laboratory based experiments to determine the sensitivity of commercial organisms and keystone species in this sensitive and rapidly changing region.

B.6 Tables

Table B-1 Empirical relationships between pCO_2 and Ω_A (2008 – 2010). The empirically derived relationships between pCO_2 and Ω_A from observations made over the southeastern Bering Sea shelf in 2008, 2009 and 2010. The regression equations were developed by fitting the data from different cruises in each year shown in Figure B-2A, B. The equation for the complete record was based on all of the available data. The $\Omega = 1$ column indicates the pCO_2 values (μatm) that were determined by solving the regression equations. The R^2 values indicate the fit of the curve for each data set.

$pCO_2 - \Omega_A$ Relationships	Full Water Column			Surface (0 – 30 m)			Bottom (30 m – Bottom)		
	Regression Equations	$\Omega = 1$ *μatm*	R^2	Regression Equations	$\Omega = 1$ *μatm*	R^2	Regression Equations	$\Omega = 1$ *μatm*	R^2
Spring 2008	$101.51x^{-0.752}$	466	0.91	$129.21x^{-0.794}$	456	0.96	$98.31x^{-0.745}$	473	0.89
Summer 2008	$126.70x^{-0.762}$	575	0.88	$79.45x^{-0.667}$	706	0.83	$80.16x^{-0.696}$	544	0.91
Spring 2009	$111.39x^{-0.770}$	455	0.91	$229.34x^{-0.892}$	443	0.96	$98.79x^{-0.749}$	460	0.90
Summer 2009	$262.97x^{-0.896}$	502	0.95	$239.96x^{-0.873}$	533	0.92	$150.73x^{-0.809}$	493	0.93
Fall 2009	$771.61x^{-1.053}$	552	0.93	$503.39x^{-0.977}$	583	0.84	$406.33x^{-0.957}$	532	0.87
Spring 2010	$126.23x^{-0.778}$	502	0.94	$130.45x^{-0.783}$	503	0.91	$101.82x^{-0.744}$	500	0.87
Summer 2010	$340.96x^{-0.942}$	488	0.90	$260.74x^{-0.889}$	522	0.84	$166.18x^{-0.829}$	477	0.85
Complete Record	$187.13x^{-0.840}$	507	0.88	$203.02x^{-0.849}$	522	0.82	$116.59x^{-0.767}$	495	0.89

Table B-2 Empirical relationships between O_2 and Ω_A (2008 – 2010). The empirically derived relationships between O_2 and Ω_A from observations made over the southeastern Bering Sea shelf in 2008, 2009 and 2010. The regression equations were developed by fitting the data from different cruises in each year shown in Figure B-2C, D. The equation for the complete record was based on all of the available data. The $\Omega = 1$ column indicates the O_2 values (μmoles kg^{-1}) that were determined by solving the regression equations. The R^2 values indicate the fit of the curve for each data set.

$O_2 - \Omega_A$ Relationships	Full Water Column			Surface (0-30 m)			Bottom (30 m-Bottom)		
	Regression Equations	$\Omega = 1$ *μmoles* kg^{-1}	R^2	Regression Equations	$\Omega = 1$ *μmoles* kg^{-1}	R^2	Regression Equations	$\Omega = 1$ *μmoles* kg^{-1}	R^2
Spring 2008	$0.5124e^{0.0024x}$	279	0.62	$0.423e^{0.0029x}$	--	0.12	$0.5128e^{0.0024x}$	278	0.82
Summer 2008	$0.5285e^{0.0034x}$	188	0.43	$1.7707e^{0.0002x}$	--	0.00	$0.5286e^{0.0033x}$	213	0.62
Spring 2009	$0.4671e^{0.0023x}$	331	0.57	$0.3118e^{0.0035x}$	--	0.09	$0.4699e^{0.0023x}$	328	0.71
Summer 2009	$0.3521e^{0.0042x}$	249	0.28	$5.377e^{-0.0031x}$	--	0.03	$0.3996e^{0.0032x}$	287	0.42
Fall 2009	$0.2375e^{0.0058x}$	248	0.31	$1.5959e^{-0.0002x}$	--	0.00	$0.446e^{0.0027x}$	299	0.11
Spring 2010	$0.4836e^{0.0033x}$	220	0.62	$0.4815e^{0.0036x}$	--	0.17	$0.5759e^{0.0024x}$	230	0.62
Summer 2010	$0.5183e^{0.0032x}$	205	0.33	$2.3962e^{-0.0009x}$	--	0.01	$0.5286e^{0.0025x}$	255	0.52
Complete Record	$0.5173e^{0.0029x}$	227	0.31	$1.5441e^{0.0001x}$	--	0.00	$0.5069e^{0.0026x}$	261	0.48

B.7 Figures

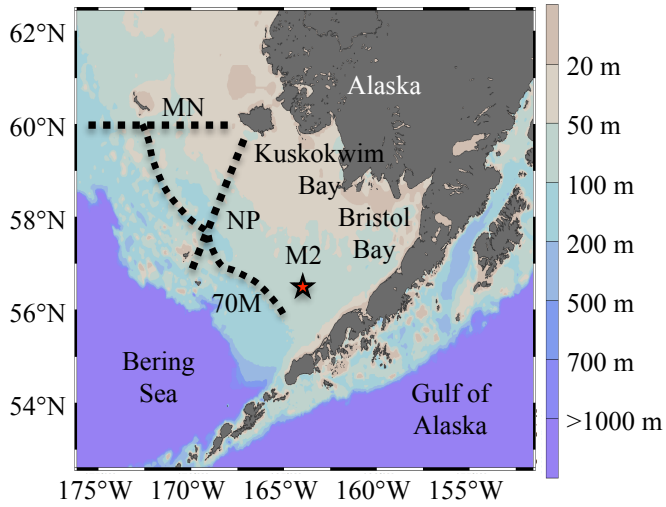

Figure B-1 Map of the southeastern Bering Sea and the M2 mooring. The black dashed lines (MN, NP and 70M) show the location where discrete carbonate measurements were made in the water column in 2008 – 2010 to develop the relationship shown in Figure B-2.

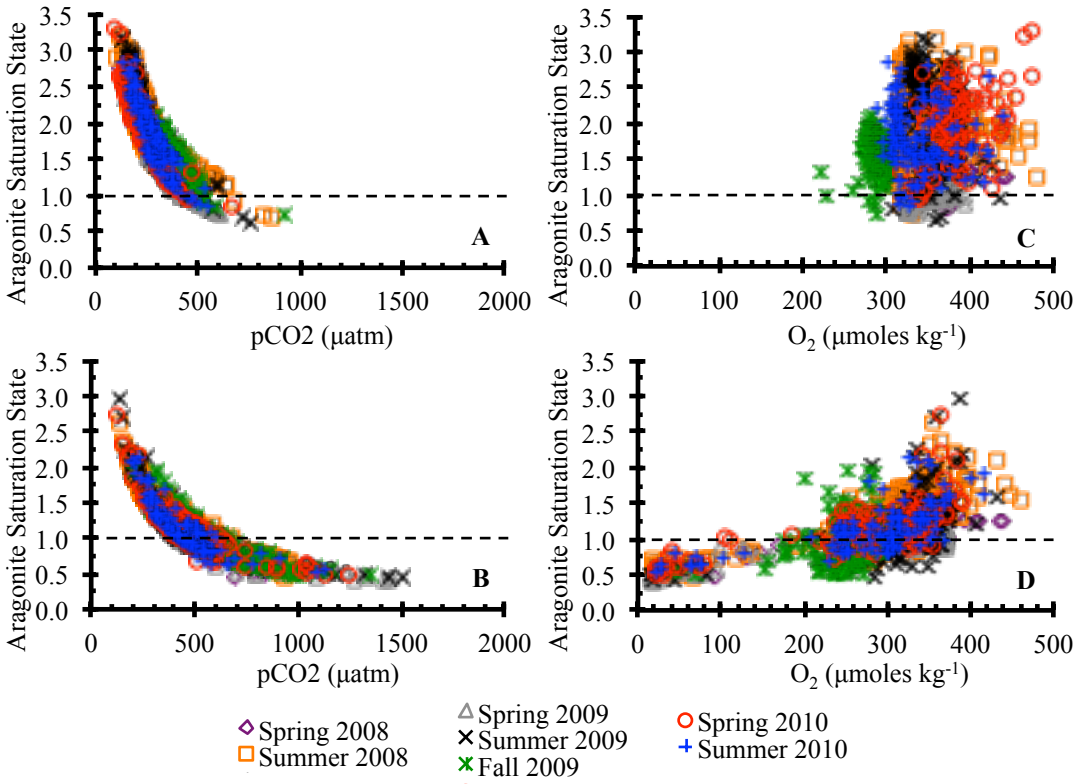

Figure B-2 Empirical relationships between Ω_A, pCO_2 and O_2 (2008 – 2010). (A, B) Empirical relationships between aragonite saturation state (Ω_A) and pCO_2 (µatm). (C, D) Empirical relationships between aragonite saturation state Ω_A and O_2 (µmoles kg^{-1}). These equations were developed for the surface mixed layer (A, C) and subsurface waters (B, D) for the southeastern Bering Sea from discrete data collected in 2008 – 2010. The dashed line indicates the saturation horizon for aragonite ($\Omega_A = 1$). Spring = April/May, Summer = June/July, Fall = September/October. The regression equations for each data set are shown in Tables B-1 and B-2.

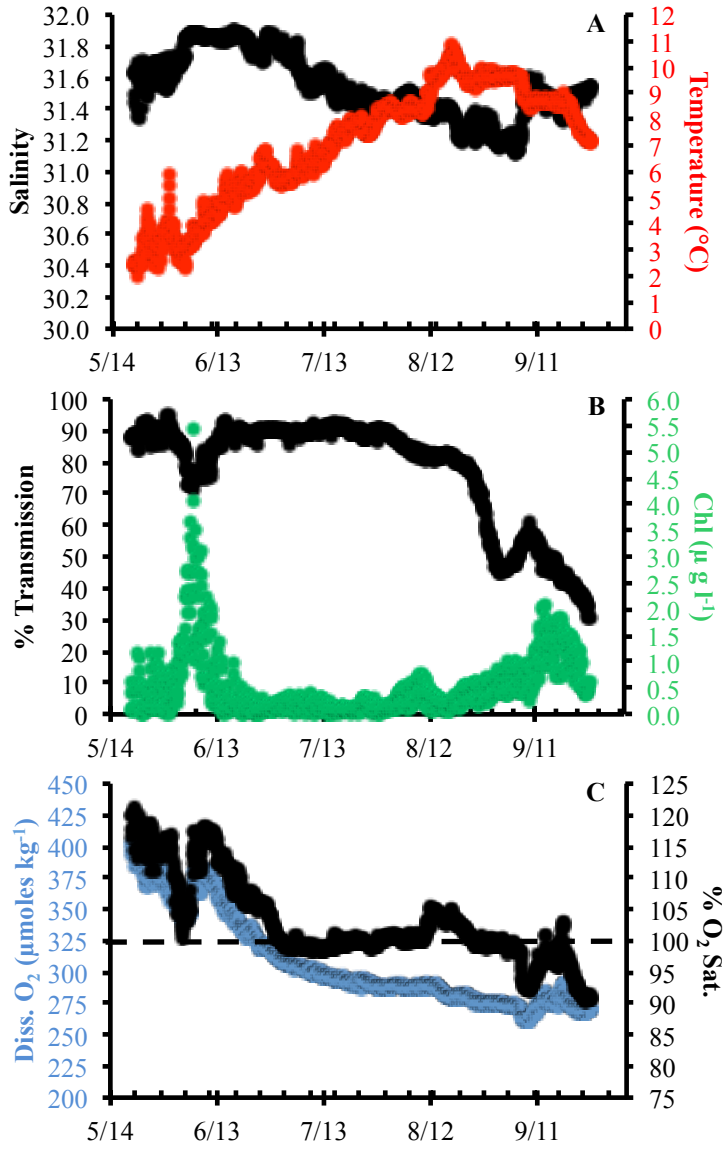

Figure B-3 Surface hydrographic mooring data (Summer, 2011). Hydrographic mooring data from the surface (1 m depth) Seabird Electronics instrument package. (A) Temperature (°C) and salinity. (B) Transmissivity (% light transmission) and fluorescence (µg L^{-1}). (C) Dissolved oxygen concentration (µmoles kg^{-1}) and oxygen saturation (% saturation at *in-situ* temperature).

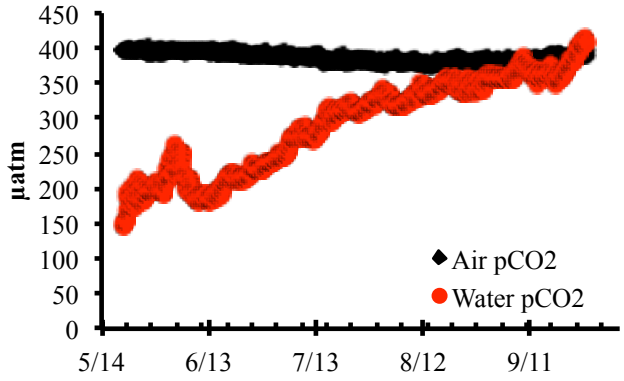

Figure B-4 Surface and atmospheric pCO_2 mooring data (Summer, 2011). Mooring data from the surface (1 m) pCO_2 (µatm) sensor (red points) as well as atmospheric pCO_2 values (black points).

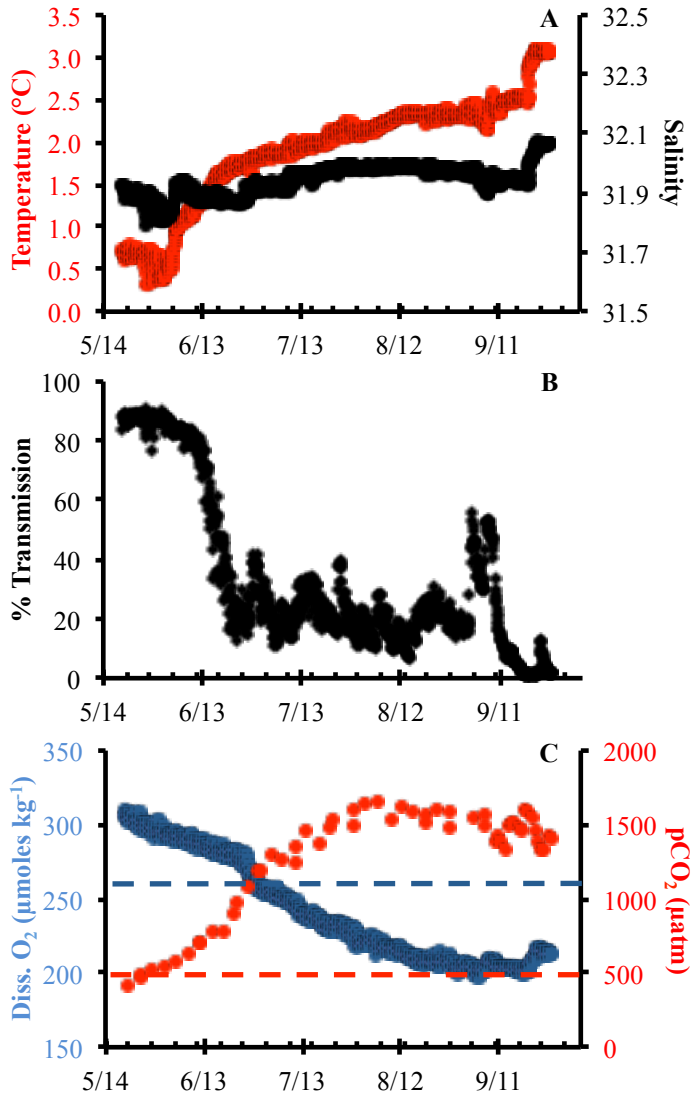

Figure B-5 Bottom hydrographic mooring data (Summer, 2011). Hydrographic mooring data from the near the bottom (67 m depth) Seabird Electronics instrument package. (A) Temperature (°C) and salinity. (B) Transmissivity (% light transmission). (C) Dissolved oxygen (blue) concentration (µmoles kg^{-1}) and pCO_2 (red) (µatm). The red, dashed line shows the threshold of where pCO_2 values exceed 500 µatm (Table B-1) and the blue, dashed line indicates the DO threshold of 260 µmoles kg^{-1} (Table B-2).

B.8 Acknowledgements

The authors thank the officers and crew of the NOAA Research Vessel Oscar Dyson for their efforts in supporting our work. We also thank the ECO-FOCI group, especially Bill Floering from NOAA-PMEL, for their efforts. The work presented in this paper was supported by the Alaska Ocean Observing System under NOAA awards A08NOS4730406 and NA11NOS0120020, the Cooperative Institute for Alaska Research with funds from NOAA under cooperative agreement NA08OAR4320751 with the University of Alaska, and the National Science Foundation through award ARC-1107997 and the NOAA Ocean Acidification Program. Statement of Work: Mathis, J.T., prepared the manuscript for publication. Cross, J.N., performed analytical calculations. Monacci, N.M., performed sample analysis. Feely, R.A., and Stabeno, P.J., provided expertise in moored sensor arrays and advised during manuscript preparation.

B.9 References

Alin, S.R., Feely, R.A., Dickson, A.G., Hernández-Ayón, J.M., Juranek, L.W., Ohman, M.D., et al., 2012. Robust empirical relationships for estimating the carbonate system in the southern California Current System and application to CalCOFI hydrographic cruise data (2005 – 2011). J. Geophys. Res. 117(C5), C05033.

Aydin, K.Y., McFarlane, G.A., King, J.R., Megrey, B.A., Myers, K.W., 2005. Linking oceanic food webs to coastal production and growth rates of Pacific salmon (*Oncorhynchus spp*.), using models on three scales. Deep Sea Res. II. 52(5-6), 757–780.

Barton, A., Hales, B., Waldbusser, G.G., Langdon, C., Feely, R.A., 2012. The Pacific oyster, *Crassostrea gigas*, shows negative correlation to naturally elevated carbon dioxide levels: Implications for near-term ocean acidification effects. Limnol. Oceanogr. 57(3), 698–710.

Bates, N.R., Mathis, J.T., 2009. The Arctic Ocean marine carbon cycle: Evaluation of air-sea CO_2 exchanges, ocean acidification impacts and potential feedbacks. Biogeosci. 6, 2433–2459.

Bates, N.R., Mathis, J.T., Cooper, L.W., 2009. Ocean acidification and biologically induced seasonality of carbonate mineral saturation states in the Arctic Ocean. J. Geophys. Res. 114, C11007.

Bates, N.R., Mathis, J.T., Jefferies, M.A., 2011. Air-sea CO_2 fluxes on the Bering Sea Shelf. Biogeosci. 8, 1237−1253.

Bednarŝek, N., Tarling, G.A., Bakker, D.C.E., Fielding, S., Jones, E.M., Venables, H.J., et al., 2012. Extensive dissolution of live pteropods in the Southern Ocean. Nature Geosci. 5, 881−885.

Brodeur, R.D., Wilson, M.T., Cianelli, L., Doyle, M., Napp, J.M., 2002. Interannual and regional variability in distribution and ecology of juvenile pollock and their prey in frontal structures of the Bering Sea. Deep Sea Res. II. 49(26), 6051−6067.

Byrne, R.H., Meckling, S., Feely, R.A., Liu, Z., 2010. Direct observations of basin-wide acidification of the North Pacific Ocean. Geophys. Res. Lett. 37, L02601.

Caldeira, K., Wickett, M.E., 2003. Anthropogenic carbon and ocean pH, Nature. 425(6956), 365.

Coachman, L.K., 1986. Circulation, water masses, and fluxes on the southeastern Bering Sea shelf. Cont. Shelf Res. 5, 23–108.

Codispoti, L.A., Friederich, G.E., Iverson, R.L., Hood, D.W., 1982. Temporal changes in the inorganic carbon system of the southeastern Bering Sea during spring 1980. Nature. 296, 242−245.

DeGrandpre, M.D., Hammar, T.T., Smith, S.P., Sayles, F.L., 1995. *In-situ* measurements of seawater pCO_2. Limnol. Oceanogr. 40(5), 969−975.

Devol, A.H., Christensen, J.P., 1993. Benthic fluxes and nitrogen cycling in sediments of the continental margin of the eastern North Pacific, J. Mar. Res. 51, 345–372.

Dickson, A.G., Millero, F.J., 1987. A comparison of the equilibrium constants for the dissociation of carbonic acid in seawater media. Deep Sea Res. 34, 1733–1743.

Dickson, A.G., Goyet, C., Eds., 1994. Handbook of Methods for the Analysis of Various Parameters of the Carbon Dioxide System in Seawater, version 2.0. Report No. ORNL/CDIAC-74. U.S. Department of Energy, Washington, D.C., 187 pp.

Dickson, A.G., Sabine, C.L., Christian, J.R., 2007. Guide to best practices for ocean CO_2 measurements [report]. North Pacific Marine Science Organization (PICES), Sidney, British Columbia, 191 pp.

Duffy-Anderson, D.A., Dailey, K.M., Livingston, P.A., 1987. Feeding habits and daily ration of walleye pollock (*Theragra chalcogramma*) in the eastern Bering Sea, with special reference to cannibalism. Can. J. Fish. Aquat. Sci. 44(11), 1972−1984.

Evans, W., Mathis, J.T., Winsor, P., Whitledge, T., Statscewich, H., 2013. A regression modeling approach for studying carbonate saturation states on the northern Gulf of Alaska shelf. J. Geophys. Res. 118(1), 476−489.

Fabry, V.J., Seibel, B.A., Feely, R.A., Orr, J.C., 2008. Impacts of ocean acidification on marine fauna and ecosystem processes. ICES J. Mar. Sci. 65(2), 414−432.

Fabry, V.J., McClintock, J.B., Mathis, J.T., Grebmeier, J.M., 2009. Ocean acidification at high latitudes: the bellwether. Oceanogr. 22(4), 160−171.

Feely, R.A., Sabine, C.L., Hernández-Ayón, J.M., Ianson, D, Hales, B., 2008. Evidence for upwelling of corrosive "acidified" water onto the continental shelf. Science, 320, 1490−1492.

Feely, R.A., Doney, S.C., and Cooley, S.R., 2009. Ocean acidification: Present conditions and future changes in a high-CO_2 world. Oceanogr. 22(4), 36–47.

Feely, R.A., Alin, S.R., Newton, J., Sabine, C.L., Warner, M., Devol, A., et al., 2010. The combined effects of ocean acidification, mixing, and respiration on pH and carbonate saturation in an urbanized estuary. Estuar. Coast. Shelf Sci. 88, 442−449.

Grebmeier, J.M., McRoy, C.P., 1989. Pelagic-benthic coupling on the shelf of the northern Bering and Chukchi seas III. Benthic food supply and carbon cycling. Mar. Ecol. Prog. Ser. 53, 79–91.

Grebmeier, J.M., Cooper, L.W., Feder, H.M., Sirenko, B.I., 2006. Ecosystem dynamics of the Pacific-influenced northern Bering and Chukchi Seas in the Amerasian Arctic. Prog. Oceanogr. 71, 331–361.

Gruber, N., Hauri, C., Lachkar, Z., Loher, D., Frölicher, T.L., Plattner, G.K., 2012. Rapid progression of ocean acidification in the California Current System. Science. 337(6091), 220−223.

Hauri, C., Gruber, N., Plattner, G.-K., Alin, S., Feely, R.A., Hales, B., et al., 2009. Ocean acidification in the California current system. Oceanogr. 22(4), 60−71.

Hauri, C., Gruber, N., Doney, S.C., Feely, R.A., Lachkar, Z., Leinweber, A., et al., 2012. Spatiotemporal variability and long-term trends of ocean acidification in the California Current System. Biogeosci. Discuss. 9, 10371−10428.

Ho, D.T., Wanninkhof, R., Schlosser, P., Ullman, D.S., Hebert, D., Sullivan, K.F., 2011. Toward a universal relationship between wind speed and gas exchange: Gas transfer velocities measured with $^3He/SF_6$ during the Southern Ocean Gas Exchange Experiment. J. Geophys. Res. 116, C00F04.

Hurst, T., Fernandez, E., Mathis, J.T., Miller, J.A., Stinson, C.M., Ahgeak, E.F., 2012. Resiliency of juvenile walleye pollock to projected levels of ocean acidification. Aquat. Biol. 17, 247−259.

Juranek, L.W., Feely, R.A., Peterson, W.T., Alin, S.R., Hales, B., Lee, K., et al., 2009. A novel method for determination of aragonite saturation state on the continental shelf of central Oregon using multi-parameter relationships with hydrographic data. Geophys. Res. Lett. 36, L24601.

Kachel, N.B., Hunt Jr., G., Salo, S.A., Schumacher, J.D., Stabeno, P.J., Whitledge, T.E., 2002. Characteristics of the Inner Front of the southeastern Bering Sea. Deep Sea Res. II. 49, 5889–5909.

Ladd, C., Stabeno, P.J., 2012. Stratification on the Eastern Bering Sea shelf revisited. Deep Sea Res. II. 65-70, 72−83.

Langdon, C., 2010. Determination of dissolved oxygen in seawater by Winkler titration using the amperometric technique, IOCCP Report No. 134. IOC/IOCCP, Paris, 18 pp.

Lewis, E.R., Wallace, D.W.R., 1995. Basic programs for the CO_2 system in seawater. Report No. BNL-61827. U.S. Department of Energy, Oak Ridge National Laboratory, Carbon Dioxide Information Analysis Center, Oak Ridge, TN, 38 pp.

Lomas, M.W., Moran, S.B., Casey, J.R., Bell, D.W., Tiahlo, M., Whitefield, J., et al., 2012. Spatial and seasonal variability of primary production on the Eastern Bering Sea Shelf. Deep Sea Res. II. 65-70, 126–140.

Long, W.C., Swiney, K.M., Foy, R.J., 2013a. Effects of ocean acidification on the embryos and larvae of red king crab, *Paralithodes camtschaticus*. Mar. Poll. Bull. 69, 38−47.

Long, W.C., Swiney, K.M., Harris, C., Page, H.N., Foy, R.J., 2013b. Effects of ocean acidification on juvenile red king crab (*Paralithodes camtschaticus*) and Tanner crab (*Chinoecetes bairdi*) growth, condition, calcification, and survival. PLoS ONE. 8(4), e60959.

Mathis, J.T., Cross, J.N., Bates, N.R., Lomas, M.L., Moran, S.B., Mordy, C.W., et al., 2010. Seasonal distribution of dissolved inorganic carbon and net community production on the Bering Sea shelf. Biogeosci. 7, 1769–1787.

Mathis, J.T., Cross, J.N., Bates, N.R., 2011. The role of ocean acidification in systemic carbonate mineral suppression in the Bering Sea. Geophys. Res. Lett. 38, L19602.

Mathis, J.T., Cooley, S.R., Lucey, N., Hauri, C., Ekstrom, J., Hurst, T., et al., 2013. Ocean acidification risk assessment for Alaska's fisheries sector. Progr. Oceanogr. Submitted.

Mehrbach, C., Culberson, C.H., Hawley, J.E., Pytkowicz, R.M., 1973. Measurement of the apparent dissociation constants of carbonic acid in seawater at atmospheric pressure. Limnol. Oceanogr. 18, 897–907.

Moran, S.B., Lomas, M.L., Kelly, R.P., Iken, K., Gradinger, R., Mathis, J.T., et al., 2013. Sea-ice control of lower trophic carbon partitioning in the eastern Bering Sea. Deep Sea Res. II. In press.

Moss, J.H., Farley, E.V., Feldman, A.M., Ianelli, J.N., 2009. Spatial distribution, energetic status, and food habits of eastern Bering Sea age-0 walleye pollock. Trans. Am. Fish. Soc. 138(3), 497−505.

Napp, J.M., Kendall, A.W., Schumacher, P., 2001. A synthesis of biological and physical processes affecting the feeding environment of larval walleye pollock (*Theragra chalcogramma*) in the eastern Bering Sea. Fish. Oceanogr. 9(2), 147−162.

Niebauer, H.J., Alexander, V., Henrichs, S.M., 1995. A time-series study of the spring bloom at the Bering Sea ice edge I: Physical processes, chlorophyll, and nutrient chemistry. Cont. Shelf Res. 15, 1859–1878.

Ries, J.B., Cohen, A.L., McCorkle, D.C., 2009. Marine calcifiers exhibit mixed responses to CO_2-induced ocean acidification. Geol. 37(12), 1131–1134.

Sigler, M.F., Stabeno, P.J., Eisner, L.B., Napp, J.M., Mueter, F.J., 2012. Spring and fall phytoplankton blooms in a productive subarctic ecosystem, the eastern Bering Sea, during 1995 – 2011. Deep Sea Res. II. In press.

Springer, A.M., McRoy, C.P., Flint, M.V., 1996. The Bering Sea green belt: Shelf-edge processes and ecosystem production. Fish. Oceanogr. 5, 205–223.

Stabeno, P.J., Bond, N.A., Salo, S.A., 2007. On the recent warming of the Southeastern Bering Sea shelf. Deep Sea Res. II. 54, 2599–2618.

Stabeno, P.J., Napp, J., Mordy, C., Whitledge, T., 2010. Factors influencing physical structure and lower trophic levels of the eastern Bering Sea shelf in 2005: sea ice, tides and winds. Prog. Oceanogr. 85(3-4), 180–196.

Stabeno, P.J., Kachel, N.B., Moore, S.E., Napp, J.M., Sigler, M., Yamaguchi, A., et al., 2012. Comparison of warm and cold years on the southeastern Bering Sea shelf and some implications for the ecosystem. Deep Sea Res. II. 65-70, 31−45.

Stafford, K.M., Moore, S.E., Stabeno, P.J., Holliday, D.V., Napp, J.M., Mellinger, D.K., 2010. Biophysical ocean observations in the southeastern Bering Sea. Geophys. Res. Lett. 37, L02606.

Weiss, R.F., 1974. Carbon dioxide in water and seawater: the solubility of a non-ideal gas. Mar. Chem. 2, 203–215.

Zeebe, R., Wolf-Gladrow, D., 2001. CO_2 in Seawater: Equilibrium, Kinetics, Isotopes. Elsevier Oceanography Series, San Diego, CA, 360 pp.